ELECTROSTATIC INTERACTIONS AND

THE pH-DEPENDENT STABILITY AND MECHANISM OF BCX

by

MANISH D. JOSHI

BSc, The University of British Columbia, 1994

A THESIS SUBMITTED IN PARTIAL FULFILLMENT OF

THE REQUIREMENTS FOR THE DEGREE OF

DOCTOR OF PHILOSOPHY

in

THE FACULTY OF GRADUATE STUDIES

(Department of Biochemistry and Molecular Biology)

We accept this thesis as conforming
to the required standard

THE UNIVERSITY OF BRITISH COLUMBIA

November 2000

In presenting this thesis in partial fulfillment of the requirements for an advanced degree at the University of British Columbia, I agree that the Library shall make it freely available for reference and study. I further agree that permission for extensive copying of this thesis for scholarly purposes may be granted by the head of my department or by his or her representatives. It is understood that copying or publication of this thesis for financial gain shall not be allowed without my written permission.

Department of Biochemistry and Molecular Biology

The University of British Columbia
Vancouver, Canada

Date: Friday, October 27, 2000.

ABSTRACT

The pH-dependent activity of *Bacillus circulans* xylanase (BCX) is determined by ionization states of the nucleophile (Glu78, pK_a 4.6) and the acid/base catalyst (Glu172, pK_a 6.7). Inspection of the BCX structure shows that Glu78 and Glu172 are in similar environments and surrounded by equivalent, conserved active-site residues. Hence, there are no obvious reasons as to why their pK_a's are different. To address this question, a mutagenic approach was implemented to determine what features establish the pK_a's (measured by ^{13}C-NMR and pH-dependent activity profiles) of these two catalytic carboxylic acids and give rise to their difference in ionization behaviour. Results indicate that all of the conserved active-site residues act concertedly in establishing the pK_a's of Glu78 and Glu172, with no particular residue being singly more important than any of the others. In general, residues that contribute positive charges and hydrogen-bonds serve to lower the pK_a's of Glu78 and Glu172. In contrast, neighbouring acidic groups can either lower or raise the pK_a's of the catalytic glutamic acids, using direct hydrogen-bonding interactions or reverse-protonation mechanisms. Analysis of several BCX structures indicates that Glu78 is preferentially stabilized over Glu172 in part by stronger hydrogen-bonds donated by rigidly held residues. Furthermore, theoretical calculations show that Glu78 has a lower pK_a than Glu172 due to more favourable local and global electrostatics. Mutating neighbouring residues within the active-site modifies the BCX pH-optimum, achieving greater than wildtype levels of activity in isolated cases. However, activity is usually compromised due to loss of important ground and/or transition-state interactions. The roles that specific acidic groups play in the pH-dependent stability of BCX were also assessed by measuring the pK_a's, using ^{13}C-NMR, of all seven aspartates. The pK_a's of all aspartate residues

are less than corresponding values observed with random coil polypeptides, indicating that their ionization contributes favourably to the stability of the folded enzyme. Residues that were most conserved, most buried and most perturbed in pK_a contributed the most to the pH-dependent stability of the enzyme and were stabilized extensively by either hydrogen-bonds or salt bridges, implicating a role for electrostatics in the protein interior of family 11 xylanases.

TABLE OF CONTENTS

LIST OF TABLES

LIST OF FIGURES

ABBREVIATIONS

β_{1g}	Brønsted coefficient for general acid/base catalysis
BSA	bovine serum albumin
CGTase	cyclodextrin glycosyl transferase
CHES	2-[N-cyclohexylamino] ethanesulphonic acid
$\delta\Delta$	the magnitude and direction of the chemical shift change upon deprotonation of the listed residue
DNP2FXb	2,4-dinitrophenyl 2-deoxy-2-fluoro-β-xylobioside
2,5-DNPX$_2$	2,5-dinitrophenyl β-xylobioside;
3,4-DNPX$_2$	3,4-dinitrophenyl β-xylobioside
ESMS	electrospray mass spectrometry
2FXb	2-fluoro-2-β-xylobioside
HEPES	4-(2-hydroxyethyl)-1-piperazineethanesulfonic acid
HPA	human pancreatic α-amylase
HSQC	heteronuclear shift quantum correlation spectroscopy
IPTG	isopropyl β-D-thioglucopyranoside
LBHB	low barrier hydrogen bond
MES	2-[N-morpholino]ethane-sulfonic acid
ONPX$_2$	orthonitrophenyl β-xylobioside
pH*	the measured pH without correction for isotope effect
PhX$_2$	phenyl β-xylobioside
PPA	pig pancreatic α-amylase

r.m.s.   root mean square

SDS-PAGE   sodium dodecyl sulfphate polyacrylamide gel electrophoresis

WT   wild type

Xb   xylobiose

ACKNOWLEDGMENTS

Firstly, I wish to acknowledge my research supervisor, Dr. Lawrence McIntosh, for all his support throughout my undergraduate and graduate studies. His direction, dedication, and kindness has set an example for me to follow in all of my endeavours. I also wish to sincerely thank the members of my thesis committee, Dr. George Mackie and Dr. Stephen Withers for their outstanding mentorship, professionalism, and advocacy. Collectively, Lawrence, George and Steve have inspired and enlightened me considerably throughout the years.

Many of the results that are presented in this thesis would not have been possible had it not been for the assistance of a number of persons. I wish to thank Isabelle Pot for her important contributions to the N35D BCX studies as well as always being a member of the team that everyone could count on. In the Withers Laboratory, I wish to thank Dr. Sherry Lawson, Timothy Hebert, David Zechel, and Lloyd Mackenzie for their advice on enzymological studies and for synthesizing substrates and covalent inhibitors. In the Brayer Group, I wish to thank Gary Sidhu, Dr. Robert Maurus, Nham Nguyen and Dr. Gary Brayer for helping me patiently with X-ray crystallographic studies. Within the McIntosh lab, I would like to acknowledge past and present members for all their advice and help over the years.

Outside of the laboratory, I wish to thank my family, Dilip, Manjula, Urvi and Jories as well as my dear friends, Wilhelmina, Jimmy, Isa, Michael and Chris, for their encouragement since the beginning.

Chapter 1

General Introduction

1.1 Electrostatic Interactions

Questions to biological problems can be solved in many ways and at many different levels. Where possible, explanations that can be made at fundamental levels are often the most revealing. Structural biology seeks to explain biological phenomena at the most fundamental level—that of the atom. Protein structures can be viewed in different ways, the most common being as a static arrangement of interconnected atoms. However, they can also be viewed from an electrostatic viewpoint as a dynamic and vibrant arrangement of point charges that act concertedly in carrying out and contributing to the maintenance of biological function (Figure 1.1). The predominant sources of electrostatic fields within proteins are ionizable groups such as the side chains of aspartic/glutamic acid, histidine, arginine and lysine to name the most common. The tendency of a group to be ionized or neutral at a given pH is described by its pK_a value ($K_a = ([conjugate\ base\ (A^-)]\ [conjugate\ acid\ (H^+)])\ /\ [acid\ (HA)]$. The importance of characterizing the pK_a values of ionizable groups is emphasized by the widely recognized fact that almost every property of a protein can vary with changes in pH and mobile ion concentration of the solvent (Matthew, 1985).
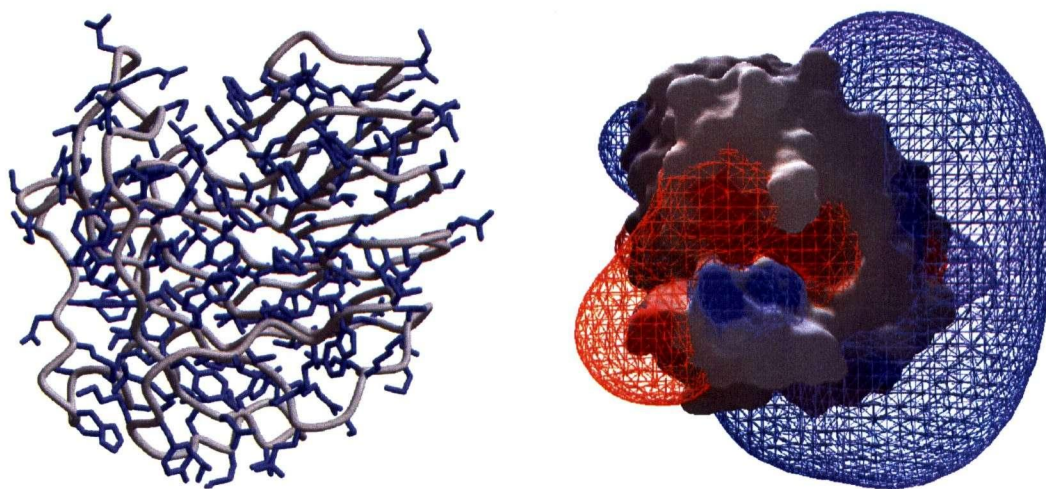
Figure 1.1. Structural and electrostatic representations of *Bacillus circulans* xylanases (BCX). For the structural representation (left), side chains are represented in blue, whereas, the backbone is shown in silver. For the electrostatic representation (right), blue meshed areas indicate an equipotential region of +1.0 k_BT, whereas, regions of red mesh show regions of −1.0 k_BT equipotential. The structural representation was produced using the programs Molscript (Kraulis, 1991) and Raster3D (Merrit and Murphy, 1994), whereas, the electrostatic representation was made using the program GRASP (Nicholls *et al.*, 1991).

1.1.1 pK_a Values of Ionizable Groups

Why do we seek to measure pK_a values of ionizable groups in proteins when we can just estimate their values from those observed in model compounds? The reason is that pK_a values of ionizable residues in proteins can often be quite perturbed relative to their values in model compounds. Furthermore, ionizable groups that function catalytically within active-sites, and thus are the most interesting, often have the most anomalous pK_a values (McIntosh *et al.*, 1996). For example, the pK_a values of the catalytic aspartic acid residues in *Escherichia coli* Ribonuclease HI are quite different from the value of ~ 4 observed in model compounds (Creighton, 1993): Asp10 has a pK_a value of 6.1, whereas Asp70 has a pK_a value of 2.6 (Oda *et al.*, 1994). Ionization constants of histidine residues (model value ~ 6.5) have also been reported to be as high as > 10 in superoxide dismutase (Stoesz *et al.*, 1979), 9.2 in bovine protein tyrosine phosphatase (Tishmack *et al.*, 1997), and as low as < 2 in *Bacillus circulans* xylanase (BCX) (Plesniak *et al.*, 1996a). Furthermore, the pK_a values of glutamic acid residues have been reported to be more than 2 pH units higher than the model compound value of ~ 4.5 (McIntosh *et al.*, 1996). Given this variance, it is therefore important to characterize accurately the pK_a values of ionizable residues within proteins by experimental or theoretical methods. Many factors such as proximity to neighboring full or partial charges, hydrogen bonding, dielectric constant of the protein and medium, solvent accessibility and ionic strength, and conformational fluctuations, to name a few, contribute to establishing the protonation state of an ionizable residue within a protein. Hence, prediction of pK_a values within proteins is a rather complex undertaking in which many different computational approaches have been applied with only modest degrees of success (Antosiewicz *et al.*, 1996; Bashford and Karplus, 1990; Sharp and Honig, 1990).

1.1.2 Electrostatic Interactions and Enzymatic Function

Ionizable groups in enzymes are frequently involved in catalysis as they have the intrinsic ability to serve as nucleophiles or general acid/base catalysts. Frequently, the pH-dependent activities of enzymes follow single or double ionization profiles, implying that only a few key ionizable groups, out of the many present, are directly responsible for this behaviour (Fersht, 1998). Determination of the apparent pK_a values of the groups that are responsible for the pH-dependent activity of an enzyme can yield information about not only mechanism, but also the identities of the putative catalytic residues.

An excellent example of an enzyme that uses a multi-faceted approach in carrying out catalysis is the classic serine protease chymotrypsin (Figure 1.2) (Fersht, 1998). Inactivation studies using the affinity label *tosyl*-L-phenylalanine chloromethyl ketone showed that the activity of chymotrypsin declined at decreasing pH according to a pK_a value of ~ 7 (Schoellman and Shaw, 1963), which is characteristic of a histidine residue. In addition, the labelling also revealed that the residue that was modified was His57, located in the active-site of chymotrypsin. Further NMR measurements confirmed that His57 titrated with a pK_a value of 6.8, while Asp102, adjacent to His57, has a pK_a value of < 2 (Bachovchin *et al.*, 1981). Thus, Asp102 is able to stabilize the positive charge that accumulates on the side chain of His57 as well as position it by hydrogen bonding. According to the mechanism of chymotrypsin, with a pK_a value of ~ 7, His57 is ideally suited to function as either a general acid or a general base at neutral pH. When it functions as a general base, it serves to enhance the nucleophilicity of Ser195 O^γ by abstracting the proton attached to it. On the other hand, when it functions as a general acid, it
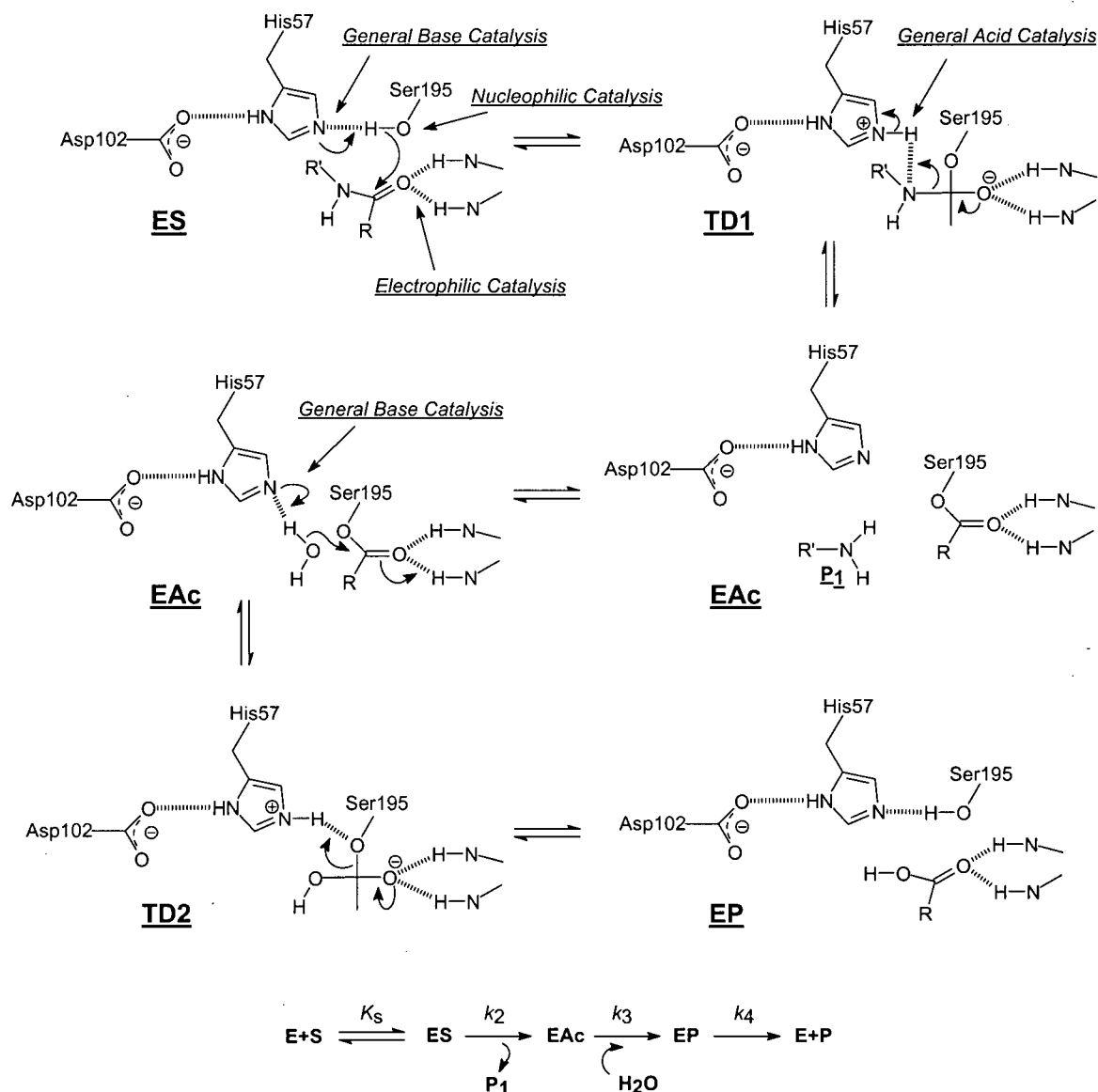
Figure 1.2. Ping-pong mechanism of chymotrypsin for the hydrolysis of esters and amides. In the enzyme-substrate complex (ES), His57, functioning as a general base, enhances the nucleophilicity of Ser195 by abstracting its hydroxyl proton. Ser195 serves as a nucleophile in the acylation step of the reaction (k_2) by attacking the carbonyl carbon of the bound peptide. This process is further enhanced by polarization of the peptide carbonyl by hydrogen bonding backbone amide groups that function as electrophiles. In the first tetrahedral adduct (TD1) His57 now plays the role of a general acid catalyst by donating a proton to the leaving peptide (P_1), thus facilitating its departure and leading to the formation of the acyl-enzyme complex (EAc). The acyl-enzyme intermediate is subsequently hydrolyzed in the deacylation step of the reaction (k_3) by attack of a water molecule whose nucleophilicity is enhanced by His57 functioning again as a general base. In both tetrahedral complexes, an anionic Asp102 serves to stabilize the positive charge developing on the side chain of His57 (Figure was modified from Fersht (1998).

donates a proton to the leaving peptide. Its activity is augmented by other groups, such as backbone amides, that serve as electrophilic catalysts by polarizing the carbonyl of the peptide bond and thereby stabilize the tetrahedral intermediates throughout the hydrolysis reaction. Chymotrypsin, therefore, provides an excellent example of how an enzyme can use many modes of catalysis in carrying out function. Although the mechanism of this enzyme is widely accepted as presented here, there is much debate over issues such as the role of the interaction between Asp102 and His57 in catalysis (Ash *et al.*, 1997; Lin *et al.*, 1998). Clearly, central to these issues is knowledge of the ionization constants of the catalytic residues throughout the reaction cycle. Parenthetically, I will return to the concept of a residue, such as His57, "cycling" between a role as a general acid and general base catalyst, in my discussion of BCX.

1.1.3 Electrostatic Interactions and Protein Stability

The overall stability of a protein in its folded state relative to its unfolded state(s) is the delicate balance of many contributions arising from electrostatic interactions, hydrogen bonding, van der Waals forces, hydrophobic interactions and configurational entropy (Yang and Honig, 1993). The concept that ionizable groups make important contributions to protein stability was initially derived from the phenomenon of acid denaturation. The first plausible explanation for this behaviour was put forth by Linderstorm-Lang, (1924). In this traditional model, acid (and base) denaturation are attributed to the accumulation of a net excess of charge at extremes of pH. At low pH, decreased stability is the result of a net repulsion of positive charges, while at high pH decreased stability results from repulsion of excess negative charges. Although correct in the first approximation, in this model the protein is treated as a sphere of continuous charge

ad distribution, where electrostatic free energy is proportional to the square of the surface charge, and thus the roles of specific electrostatic interactions are neglected (Yang and Honig, 1993).

Of course pioneer biophysicists, such as Linderstorm-Lang, did not know the three-dimensional structures of the proteins that they studied. Currently held theoretical models treat proteins as regions of low dielectric constant embedded with point charges that are immersed in aqueous solvent of high dielectric value (Gilson *et al.*, 1985). In addition, more recent evidence suggests that a small number of groups with unusually shifted pK_a values may contribute significantly to the net electrostatic free energy difference between the folded and unfolded states of a protein (Anderson *et al.*, 1990; Pace *et al.*, 1990). By thermodynamic linkage, the free energy of stabilization of the folded state of a protein relative to its unfolded state, due to the deprotonation of a charged group, is reflected directly by the difference in the pK_a values of that group in these two conformational states (Tanford, 1961). For example, if the pK_a value of an acidic residue such as an Asp or Glu is lowered in the folded state of the protein compared to its pK_a value in the unfolded state, then the folded state of the protein stabilizes the ionized form of the residue and conversely the ionized form of the residue helps to stabilize the folded state of the protein.

The question then arises as to how the protonation of residues within a protein is linked to the unfolding-folding equilibrium. Consider a model where there are *m* binding sites for protons (H) in the folded (F) and unfolded (U) forms of the protein (Scheme 1.1) (Anderson *et al.*, 1990):

$$\begin{array}{ccc}
F & \overset{K}{\rightleftharpoons} & U \\
+ & & + \\
H & & H \\
\updownarrow & & \updownarrow \\
FH & & UH \\
+ & & + \\
\cdot & & \cdot \\
\cdot & & \cdot \\
\cdot & & \cdot \\
+ & & + \\
FH_m & \rightleftharpoons & UH_m
\end{array}$$
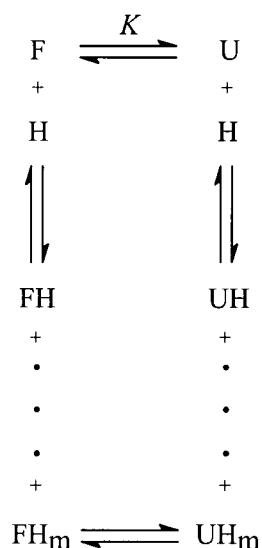
If the unprotonated forms of the folded and unfolded states of the protein are in equilibrium, characterized by the equilibrium constant (K), then an apparent equilibrium (K_{app}) can be defined at any given pH, where φ_{ui} and φ_{fi} represent the phenomenological overall constants that describe the binding of i protons to the unfolded and folded states, respectively (equation 1.1) (Anderson *et al.*, 1990; Anderson *et al.*, 1993).

$$K_{app} = \frac{\displaystyle\sum_{i=0}^{m} UH_i}{\displaystyle\sum_{i=0}^{m} FH_i} = K \frac{\dfrac{\displaystyle\sum_{i=0}^{m} i\varphi_{ui}[H^+]^i}{1+\displaystyle\sum_{i=0}^{m} i\varphi_{ui}[H^+]^i}}{\dfrac{\displaystyle\sum_{i=0}^{m} i\varphi_{fi}[H^+]^i}{1+\displaystyle\sum_{i=0}^{m} i\varphi_{fi}[H^+]^i}} \quad (1.1)$$

For an individual ionizable group, the apparent equilibrium constant can be expressed as (equation 1.2):

$$K_{app} = K\frac{1+K_u[H^+]}{1+K_f[H^+]} \quad (1.2)$$

$$\Delta G^o = -RT\ln K_{app} \quad (1.3)$$

At high pH, K_{app} is reduced to K, whereas at low pH, it can be simplified to $K_{app} = K(K_u/K_f)$, where K_u and K_f are unfolding and folding equilibrium constants. In this case, the difference in stability between low and high pH is given by $\Delta\Delta G^\circ = 2.303RT\Delta pK_a$, where $\Delta pK_a = pK_f - pK_u$. Thus a change of 1 unit in pK_a corresponds to a stabilization of ~ 1.4 kcal mol^{-1}. In this manner, the difference in pK_a of an ionizable group between the folded and unfolded forms is indicative of its contribution to the pH-dependent stability of a protein. Therefore, groups whose pK_a values in the folded protein are unperturbed compared to those of model values (which approximate pK_a values in the unfolded protein) contribute little to the protein's pH-dependent stability whereas those whose values are highly perturbed contribute significantly (Anderson *et al.*, 1993). (Note, however, recent studies suggest that the pK_a values of carboxyl groups in the denatured state are on average 0.4 units lower than those of model compounds (Elcock, 1999; Oliveberg *et al.*, 1995) indicating that, as expected for a polymer, inter-residue electrostatic interactions also exist in the denatured state). An excellent example of direct assessment, using pK_a perturbation comparisons, of the roles that individual ionizable groups confer to the stability of the folded state of a protein is presented in a study of T4 lysozyme (Anderson *et al.*, 1990). The role that acid residues play in determining the pH-dependent stability of BCX is examined using a similar method of pK_a perturbation analysis and is presented in Chapter 2.

1.2 Carbohydrates

Carbohydrates are the most abundant biomolecules on earth and feature in a wide variety of biological roles. Their structures are extremely diverse due to the number of ways and the nature in which their monomeric substituents can be linked together. Further diversity also exists

because they are amenable to linkage with other biomolecules such as peptides, proteins and lipids (Figure 1.3).

Carbohydrates play a role in nutrient storage in animals, plants and bacteria. Glycogen serves as a primary energy source in animal cells and consists of $\alpha(1\rightarrow4)$-linked subunits of D-glucose branched by an $\alpha(1\rightarrow6)$-linkage every 8 to 12 residues. Starch, on the other hand, is a primary metabolite in plants and consists almost exclusively of $\alpha(1\rightarrow4)$-linked subunits of D-glucose without any branching. Plants synthesize starch in the light and degrade it as an energy source in the dark.

Carbohydrates also serve important structural functions in terrestrial organisms. In higher animals, protection is usually conferred by specialized tissue such as skin, while general shape is determined and supported by a skeleton (Ginsberg and Robbins, 1981). In contrast, in arthropods, plants, fungi and bacteria, protection is possible through the use of a cell wall or shell. Polysaccharides are usually the main components of these entities and their relative rigidity, due to their tendency to form higher aggregates by hydrogen bonding in fibers, makes them excellent structural material. Some common structural polysaccharides include cellulose (unbranched $\beta(1\rightarrow4)$-linked subunits of D-glucose), chitin (unbranched $\beta(1\rightarrow4)$-linked subunits of *N*-acetyl-D-glucosamine), and peptidoglycan (alternating $\beta(1\rightarrow4)$-linked repeating subunits of *N*-acetylglucosamine and *N*-acetylmuramic acid cross-linked by short peptides).

There has also been considerable focus on the role of carbohydrates in cellular signaling and cell-mediated interactions. Glycosylation of peptides/proteins occurs by attaching the carbohydrate at the anomeric carbon through a glycosidic bond to the side chain hydroxyl of Ser and Thr residues (an *O*-linkage) or through an *N*-linkage to the side chain amide nitrogen of an Asn residue. For example, CD59 is an erythrocyte surface glycoprotein that binds to complement
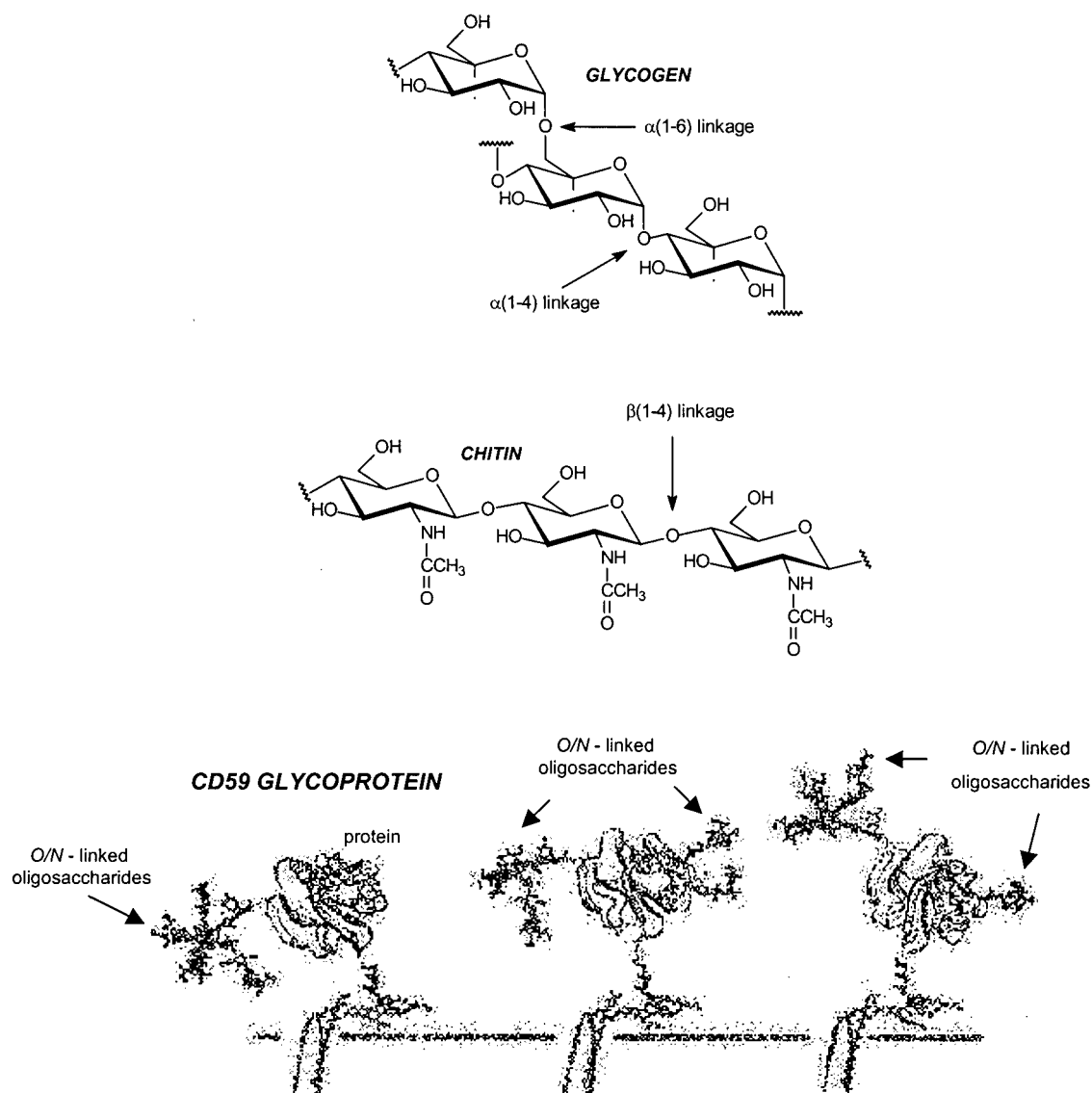
Figure 1.3. Some examples of carbohydrates. Glycogen, containing two types of linkages, is extensively branched and plays a role in energy storage in animals. Chitin is a structural polysaccharide found, for example, in arthropods and, next to cellulose, is the second must abundant carbohydrate on the earth. It is a linear polymer of *N*-acetyl-D-glucosamine units. CD59 is a glycoprotein whose relative orientation on the erythrocyte membrane can be modulated by the presence of *O/N* –linked oligosaccharides (CD59 illustration adapted from Rudd *et al.*, 1997).

proteins C8 and/or C9 in the nascent membrane attack complex. It is believed that the *N* and *O*-linked surface carbohydrates help to orient CD59 on the membrane in the attack complex such that it is well positioned to bind complement proteins (Rudd *et al.*, 1997). In plants, many classes of oligosaccharides are able to exert signalling effects. Carbohydrates that can elicit such a response are termed oligosaccharins (Darvill *et al.*, 1992). For example, oligosaccharides derived from chitin have been shown to signal both defense responses as well as growth responses in certain types of plants (Reviewed in Pome, 1996). Therefore, the roles of carbohydrates in biology are extremely vast and diverse as are the number of known glycosidases that have evolved to selectively hydrolyze them.

1.3 Glycosyl Hydrolases

1.3.1 Classifications of Glycosyl Hydrolases

The ubiquitous occurrence of glycosidases in nature is reflected by the fact that over 1500 sequences of these enzymes are currently known (Henrissat, 1998). These enzymes have been organized into 70 "families" based on amino acid sequence similarities (Henrissat and Bairoch, 1993). Sequence identities within these families can be as low as 10 % provided that recognizable conserved motifs in the catalytic domains can be identified. The proliferation of the number of known three-dimensional structures of glycosyl hydrolases solved has led to the distillation of the seventy families of glycosidases into eight distinct clans (GH-A to H). Clan classifications are based upon fold conservation, catalytic machinery (type of catalytic residue and position in the active-site), catalytic mechanism (inverting *versus* retaining), and stereochemistry of the substrate (axial or equatorial glycosidic bond) (Henrissat and Bairoch, 1993). Further properties of glycosidases also include the position at which the polysaccharide

substrate is cleaved. Those that cleave the substrate towards the terminal ends are noted as exo-acting while those that cleave internally are termed endo-acting. Significant topological features, such as a tunnel or active-site cleft are known to dictate the ability of a glycosidase to function in either an exo- or endo- fashion (Davies and Henrissat, 1995).

1.3.2 Mechanisms of Glycosyl Hydrolases

Although defined by sequence, it is now clear that one invariant property within a family is mechanism (Henrissat, 1998). Glycosidases hydrolyze glycosidic bonds via two main mechanisms and thus are classified as either "inverting" (Figure 1.4) or "retaining" (Figure 1.5) depending on the stereochemical outcome of the reaction (Koshland, 1953; Sinnott, 1990). While both mechanisms hydrolyze glycosidic bonds using general acid/base catalysis, there are pre-requisite structural differences between anomer inverting and anomer retaining enzymes. The most notable factor is the distance between the two catalytic carboxylates (Davies and Henrissat, 1995; McCarter and Withers, 1994). The average distance is ~ 5.5 Å (± 0.5 Å) in retaining glycosidases, whereas it is ~ 10 Å (± 3.0 Å) in inverting glycosidases. The greater distance observed in inverting glycosidases is required to accommodate a water molecule, which serves as the displacing nucleophile in the single step of the reaction. Some examples of retaining glycosidases are β-galactosidase (Jacobson *et al.*, 1994) and BCX (Wakarchuk *et al.*, 1994a) while examples of inverting glycosidases include β-amylase (Mikami *et al.*, 1993) and T4 lysozyme (Kuroki *et al.*, 1995). Interestingly, attempts have been made at converting retainers to inverters by increasing the distance between the catalytic residues but the desired result was not attained (Lawson *et al.*, 1996). Serendipitously, the converse has been successful, however, in
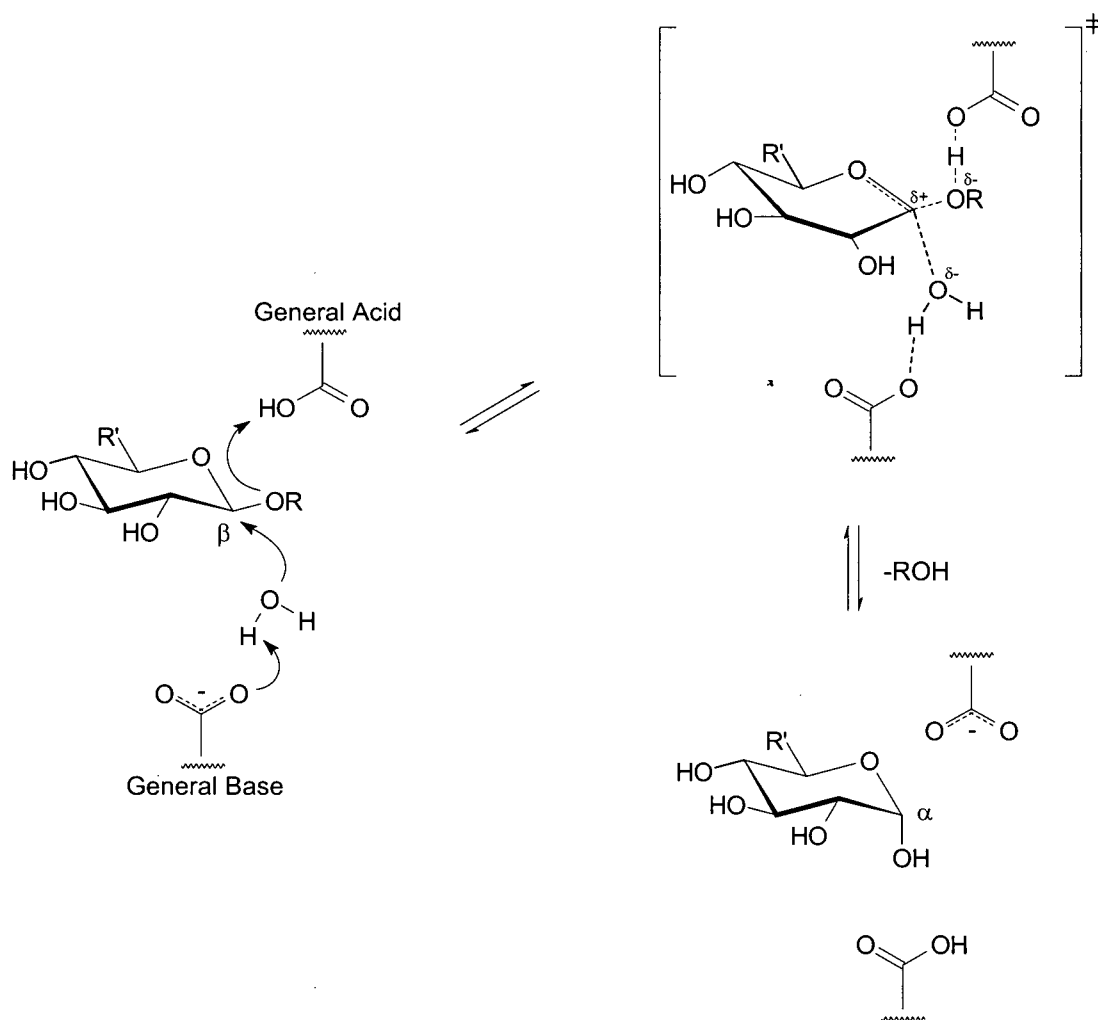
Figure 1.4. Mechanism of inverting glycosidases. This mechanism involves a single chemical step where one of the two catalytic groups functions as a general acid to protonate the departing aglycone while the other functions as a general base by abstracting a proton from a water molecule thus enhancing its nucleophilicity. The reaction proceeds through a single oxocarbenium ion-like transition state and results in net inversion of the anomeric centre ($\alpha \rightarrow \beta$ or $\beta \rightarrow \alpha$) (Koshland, 1953; Sinnott, 1990).
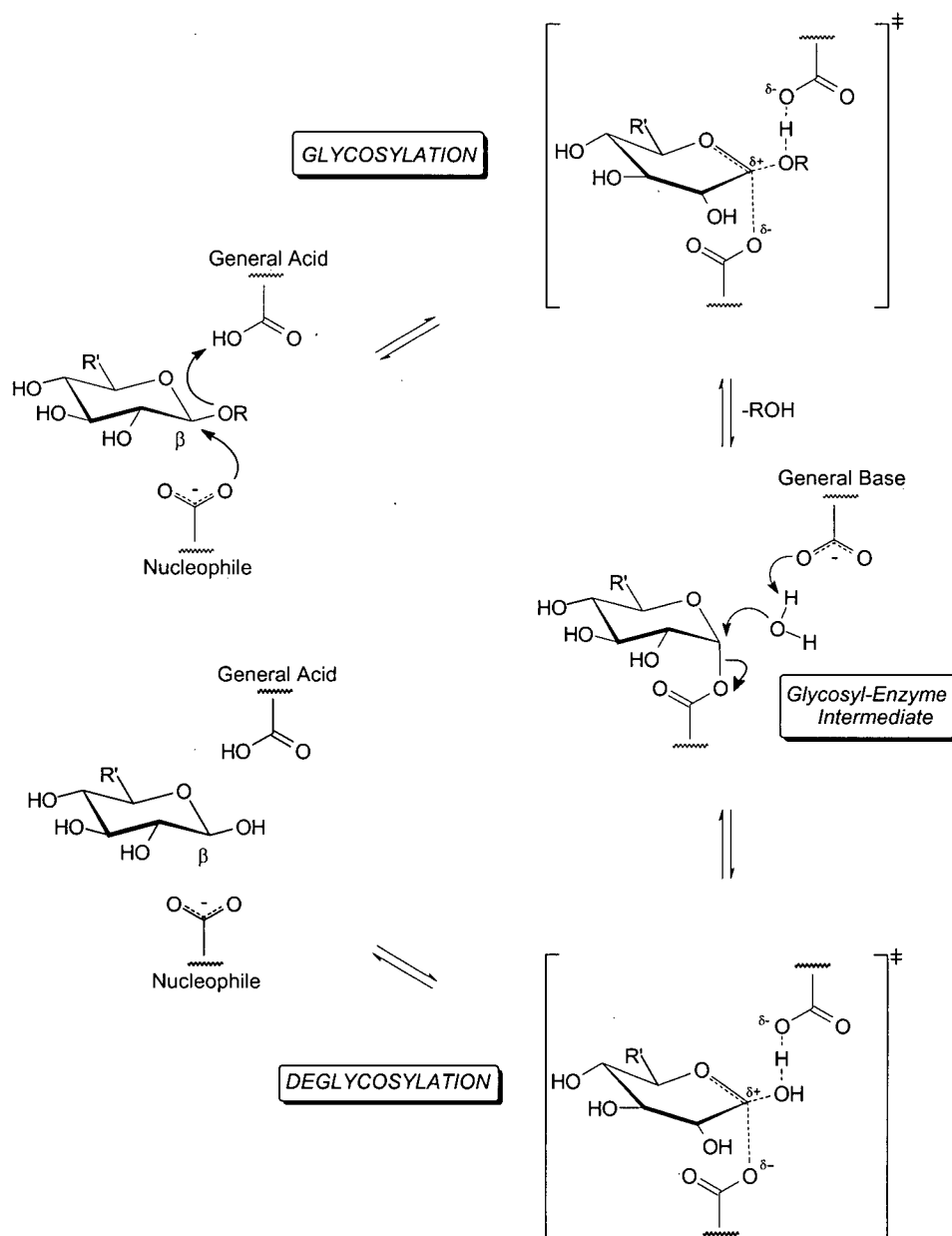
Figure 1.5. Mechanism of retaining glycosidases. The double-displacement retaining mechanism of glycosidases involves two distinct chemical steps: glycosylation and deglycosylation. During the glycosylation step, one catalytic group serves as a nucleophile to attack the anomeric C1 carbon of the saccharide substrate, whereas, the other functions as a general acid and protonates the leaving aglycone. A glycosyl-enzyme intermediate is formed and is subsequently hydrolyzed in the deglycosylation step. In the second step, the group that functioned as a general acid during glycosylation now functions as a general base and removes a proton from an attacking water molecule. The retaining mechanism involves two oxocarbenium ion-like transition states and results in overall retention of anomeric configuration ($\beta \rightarrow \beta$ or $\alpha \rightarrow \alpha$) (Koshland, 1953; Sinnott, 1990).

the case of T4 lysozyme, which was converted from an anomer inverting enzyme to an anomer retaining enzyme (Kuroki *et al.*, 1995) by introduction of a new catalytic nucleophile (His26) in the presence of the original general base catalyst (Asp20).

1.3.4 Xylanases

Xylan is the primary carbohydrate found in the hemicellulosic fraction of plant tissues and accounts for one third of all renewable organic carbon available on earth (Figure 1.6). Hence, xylanases have a variety of applications in the pulp and paper, food processing, textile and other biotechnologically enhanced industries (Prade, 1996). Xylose is slightly different from glucose in that it is a five carbon pentose instead of a six carbon hexose saccharide. Nevertheless, it forms a six-membered pyranose ring in solution with all of the ring substituents lying equatorially. This is similar to glucose, only the CH_2OH at position 6 is not present. A majority of the known xylanases belong to either family 10 (clan GH-A) or 11 (clan GH-C) glycosyl hydrolases and come from a variety of taxonomic ranges including both prokaryotic and eukaryotic sources (Henrissat and Bairoch, 1993).

Bacillus circulans xylanase (BCX) is a low molecular mass xylanase (20.4 kDa) that is a member of the family 11 glycosyl hydrolases (Sung *et al.*, 1993). The structure of the enzyme is characterized by 14 β-strands, arranged in a network of three β-sheets, and a single α-helix. Two of the β-sheets intersect to form a long binding cleft that is bordered by a flexible loop region (Wakarchuk *et al.*, 1994a) (Figure 1.7). This endo-β-(1,4)-glycosidase catalyzes xylan hydrolysis using a retaining mechanism (Gebler *et al.*, 1992) that employs two absolutely conserved catalytic carboxyl groups, namely the nucleophile Glu78 and the acid/base catalayst Glu172, that are embedded in a network composed of other highly conserved active-site residues (Miao *et al.*,

1994; Wakarchuk *et al.*, 1994a) (Figures 1.8 and 1.9). The enzyme has been the focus of numerous studies and is thus extremely well characterized from many points of view: structural (Joshi *et al.*, 2000a; Sidhu *et al.*, 1999; Wakarchuk *et al.*, 1994a), enzymological (Joshi *et al.*, 2000a; Lawson *et al.*, 1996; Lawson *et al.*, 1997; McIntosh *et al.*, 1996; Miao *et al.*, 1994) and biophysical (Connelly and McIntosh, 1998; Connelly *et al.*, 2000; Davoodi *et al.*, 1995; Davoodi *et al.*, 1998; Joshi *et al.*, 1997; Joshi *et al.*, 2000a; McIntosh *et al.*, 1996; Plesniak *et al.*, 1996a; Plesniak *et al.*, 1996b; Wakarchuk *et al.*, 1994b). It is therefore an excellent model system to study glycosidase structure and function.
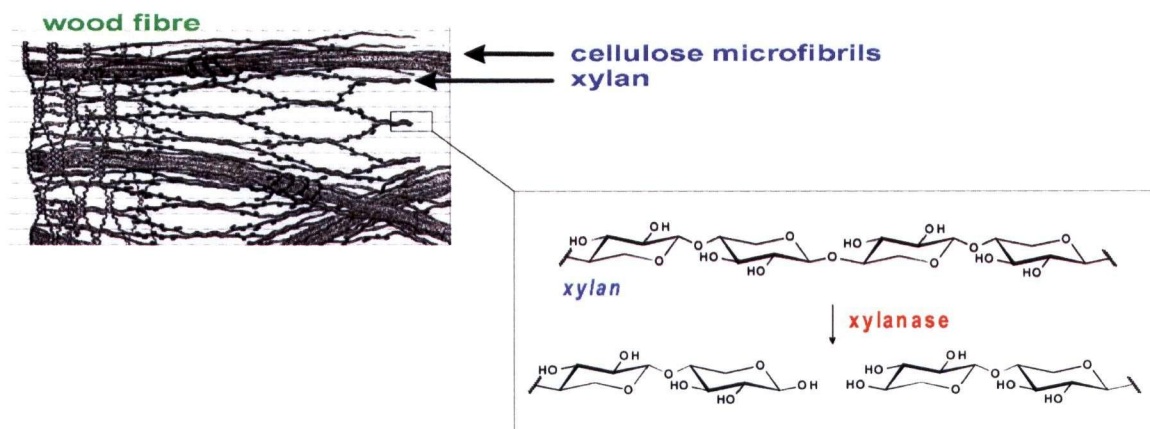
Figure 1.6. Xylans are a major constituent of plant cell walls and consist of a backbone of β-(1,4) linked xylopyranosyl residues that are found to be closely associated with cellulose microfibrils in wood fibre.

Figure 1.7. Ribbon diagram representation of the crystal structure of BCX (Wakarchuk *et al.*, 1994a). BCX has predominantly β-sheet (light green) topology with one α-helix (purple). The two catalytically essential glutamic acid residues, Glu78 and Glu172, are indicated in red.

```
                              35
                              ↓
B.circulans   : ASTDYWQNWTDGGGIVNAVNGSGCNYSVNWS--NTGNFVVGKGWTTGSP-------FRTINYNA
T.reesei II   : NNGYFYSYWNDGHGGVTYTNGPGGQFSVNWS--NSGNFVGGKGWQPGTK-------NKVINFSG
A.niger II    : NNGFYYSFWTDGGGDVTYTNGDAGAYTVEWS--NVGNFVGGKGWNP-GS-------AQDITYSG
T.harzianum   : SNGYYYSYWNDGHAGVTYTNGGGCSFTVNWS--NSGNFVAGKGWQPGTK-------NKVINFSG
S.commune     : DGGYYYSWWTDGAGDATYQNNGGGSYTLTWSG-NNGNLVGGKGWNPCAA-------SRSISYSG
B.pumilus     : HSGYDYELWKDYGNTSMTLN-NGGAFSAGWN--NIGNALFRKGKKFDSTRTHHQLGNISINYNA
T.reesei I    : ASINYDQNYQ-TGGQVSYSP-SNTGFSVNWN--TQDDFVVGVGWTTGSS-------APINFGG
A.niger I     : AGINYVQNYNGNLGDFTYDE-SAGTFSMYWEDGVSSDFVVGLGWTTGSS-------KAITYSA

               69          78 80                                   112
               ↓          ↓  ↓                                     ↓
B.circulans   : GVWAPNGNGYLTLYGWTRSPLIEYYVVDSWGTYRPTG--TYKGTVKSDGGTYDIYTTTRYNAPS
T.reesei II   : SYN-PNGNSYLSVYGWSRNPLIEYYVVENFGTYNPSTGATKLGEVTSDGSVYDIYRTQRVNQPS
A.niger II    : TFT-PSGNGYLSVYGWTDPLIEYYIVESYGTYNPGSGGTYKGTVTSDGSVYDIYTATRTNAAS
T.harzianum   : SYN-PNGNSYLSIYGWSRNPLIEYYIVENFGTYNPSTGATKLGEVTSDGSVYDIYRTQRVNQPS
S.commune     : TYQ-PNGNSYLSVYGWTRSSLIEYYIVESYGSYDPSSAASHKGSVTCNGATYDILSTWRYNAPS
B.pumilus     : SFN-PGGNSYLCVYGWTQSPLAEYYIVDSWGTYRPTG--AYKGSFYADGGTYDIYETTRVNQPS
T.reesei I    : SFSVNSGTGLLSVYGWSTNPLVEYYIMEDNHNYP--AQGTVKGTVTSDGATYTIWENTRVNEPS
A.niger I     : EYSASGSSSYLAVYGWVNYPQAEYYIVEDYGDYNPCSSATSLGTVYSDGSTYQVCTDTRTNEPS

               127                                          172
               ↓                                            ↓
B.circulans   : IDGDRTTFTQYWSVRQSKR-----PTGSNATITFTNHVNAWKSHGMNLGSNWAYQVMATEGYQS
T.reesei II   : IIG-TATFYQYWSVRRNHR-----SSG---SVNTANHFNAWAQQGLTLG-TMDYQIVAVEGYFS
A.niger II    : IQG-TATFYQYWSVRQNK-----RVGG---TVITSNHFNAWAKLGMNLG-THNYQIVATEGYQS
T.harzianum   : IIG-TATFYQYWSVRRNHR-----SSG---SVNTANHFNAWASHGLTLG-TMDYQIVAVEGYFS
S.commune     : IDG-LQTFEQFWSVRNPKKAPGGSISG---TVDVQCHFDAWKGLGMNLGSEHNYQIVATEGYQS
B.pumilus     : IIG-IATFKQYWSVRQTKR-----TSG---TVSVSAHFRKWESLGMPMG-KMYETAFTVEGYQS
T.reesei I    : IQG-TATFNQYISVRNSPR-----TSG---TVTVQNHFNAWASLGLHLG-QMNYQVVAVEGWGG
A.niger I     : ITG-TSTFTQYFSVRESTR-----TSG---TVTVANHFNFWAQHGFGNS-DFNYQVMAVEAWSG


B.circulans   : SGSSNVTVW------
T.reesei II   : SGSASITVS------
A.niger II    : SGSSSITVQ------
T.harzianum   : SGSASITVS------
S.commune     : SGTATITVT------
B.pumilus     : SGSANVMTNQLFIGN
T.reesei I    : SGSASQSVSN-----
A.niger I     : AGSASVTISS-----
```

Figure 1.8. Sequence alignment of representative family 11 xylanases. Completely conserved residues are shaded in black, residues with > 75 % identity in dark grey, and those with > 60 % identity in light grey. Salient active-site residues studied in this thesis are indicated by arrows (BCX numbering). The two invariant catalytic glutamic acid residues, Glu78 and Glu172, are underlined. Sequences were aligned using the program CLUSTAL V (Higgins, 1994). Protein sequences were obtained from the SwissProt database with the following accession numbers: *B.circulans*, P09850; *T.reesei* II, P36217; *A.niger* II, P55330; *T.harzianum*, P48793; *S.commune*, P35809; *B.pumilus*, P00694; *T.reesei* I, P36218; and *A.niger* I, P55329.
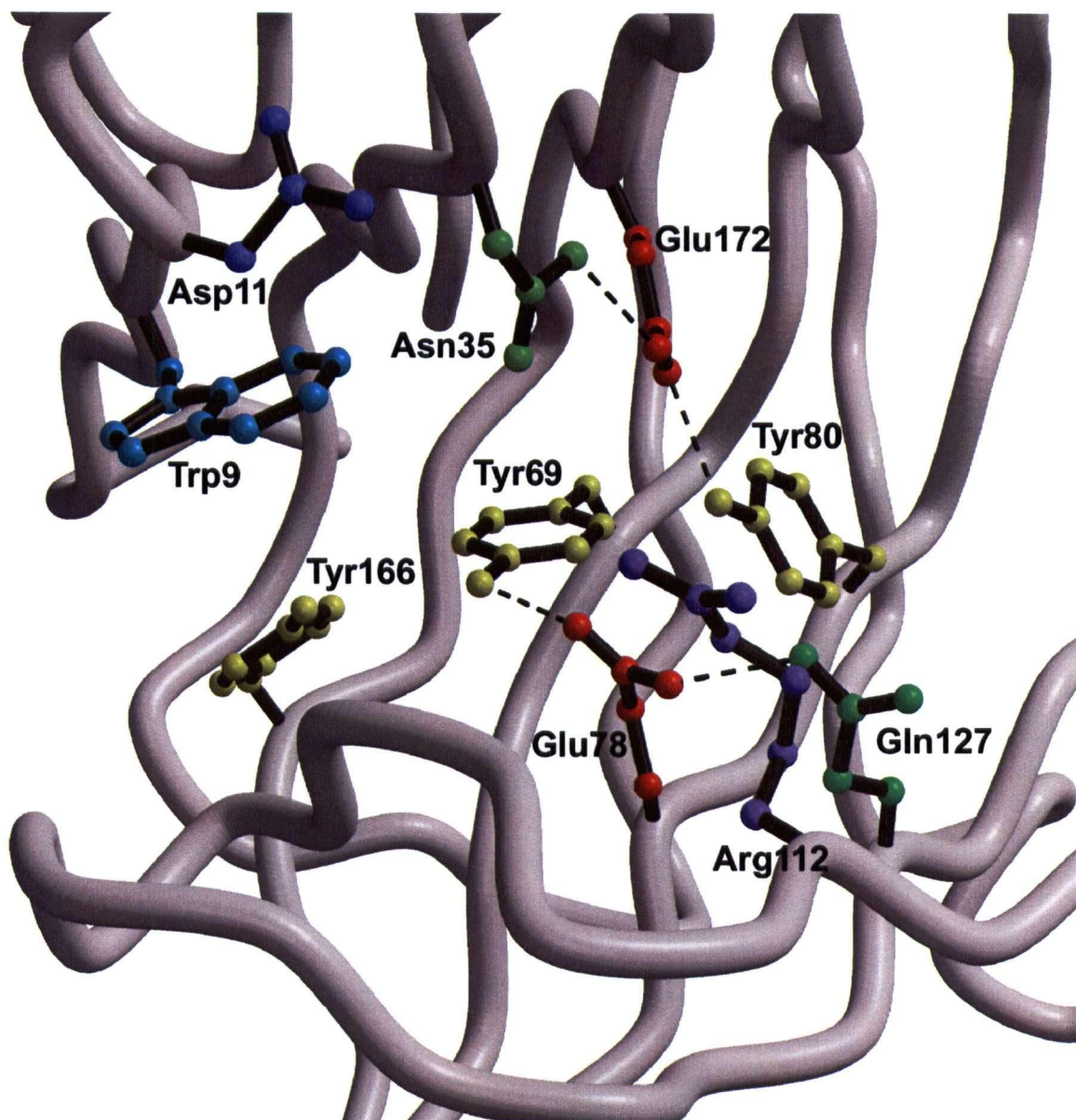
Figure 1.9. A structural representation of the active-site of BCX showing the network of conserved residues and hydrogen bonds (dashed black lines) that surround Glu78 and Glu172. Crystallographically identified bound waters are excluded.

1.4 Thesis Goals, Significance, and Results

This thesis provides one of the most comprehensive accounts of the pH-dependent stability, mechanism, and activity of an enzyme studied to date. Other studies provide selective analyses of particular pH-dependent behaviours but none collectively examines as many aspects of pH-dependence as this study. BCX proved to be an excellent candidate for investigating pH-dependent properties because it was highly amenable to analysis by a number of techniques. A multidisciplinary experimental approach was hence implemented to assess in detail the roles that specific amino acids played in determining the pH-dependent behaviours of this enzyme. NMR was used to site-specifically measure the pK_a values of salient ionizable groups, while X-ray crystallographic techniques were used to determine the structures of various mutant and wild type BCX proteins. These enzymes were further assessed enzymologically with the use of well-characterized synthetic substrates and inhibitors in order to bridge structural and biophysical observations to enzyme activity. A majority of the work presented in this thesis has been published (Joshi *et al.*, 1997; Joshi *et al.*, 2000a; McIntosh *et al.*, 1996) or will soon be submitted for publication in peer-reviewed journals (Joshi *et al.*, 2000b; Joshi *et al.*, 2000c).

Specifically, in Chapter 2, I describe a study that highlights the roles that acidic residues play in determining the pH-dependent stability of BCX. The pK_a values of all of the aspartic and glutamic acid residues were measured in order to identify those that were perturbed relative to values in model compounds. In general, those with the most reduced or perturbed pK_a values were the least solvent accessible and most highly conserved. These results indicate the key role that these buried ionizable groups play in stabilizing the structure of BCX as well as how their energetically unfavourable burial is accommodated and used to the advantage of the enzyme.

In Chapter 3, I provide an account of the dynamic interplay of electrostatic interactions in BCX and their effects on mechanism and activity. NMR measurements of the pK_a values of the catalytic glutamic acid residues, Glu78 and Glu172, showed that their ionizations reflect their catalytic roles and that they are primarily responsible for the pH-dependent activity of the enzyme. Remarkably, pK_a measurements of the acid/base catalyst Glu172 in the free and glycosyl-enzyme intermediate showed that the pK_a of Glu172 changes to match its dual catalytic function as a general acid in the first step of the reaction and as a general base in the second: we termed this presumably general phenomenon of retaining glycosidases as "pK_a cycling". The next challenge was to determine what factors set the pK_a values of Glu78 and Glu172 and hence the pH optimum of BCX. A systematic approach was taken where conserved active-site residues were mutated. Subsequently, the crystal structures, pK_a values of Glu78 and Glu172, and the activities of the resulting enzymes were determined. The results indicated that hydrogen bonding and adjacent charges serve to concertedly establish the ionization constants of residues 78 and 172; however, this is accomplished in a complex manner due to strong structural and electrostatic coupling in the active-site. In general, while the pH optimum of BCX was modified by active-site substitution, this was usually accompanied by a significant reduction in total activity. A number of implications for engineering glycosidases to function under different conditions of pH arose out of these studies. Finally, the experimentally measured pK_a values were compared with those calculated theoretically. These studies highlighted the complexities of electrostatic interactions in proteins and emphasized the need to develop computational methods that adequately predict and account for complex hydrogen bonding networks that surround ionizable residues.

In the final experimental chapter (Chapter 4), I present a lesson learned from nature in changing pH optima. By mimicking a naturally occurring substitution in the family 11 xylanases, we produced a mutant enzyme (N35D BCX) where the pH optimum has been successfully lowered and activity is maintained compared to wild type levels. Through detailed structural, biophysical, and enzymological studies, a novel explanation was discovered, based on a reverse protonation mechanism that highlights the importance of hydrogen bonding interactions in catalysis. This study provides a clear solution to a widely documented enigma and can be applied to explain the pH-dependent activities of numerous glycosidases.

Chapter 2

The pH-Dependent Stability of BCX

ABSTRACT

Electrostatic interactions in proteins can be dissected experimentally by determining the pK_a values of their constituent ionizable amino acids. NMR methods were used to measure the pK_a values of the seven aspartic acids and the C-terminus of *Bacillus circulans* xylanase (BCX). The pK_a values of these carboxyls are all lower than the corresponding values observed with random coil polypeptides, indicating that their ionization contributes favourably to the stability of the folded enzyme. In general, the aspartic acids with the most reduced pK_a values are those with limited exposure to the solvent and a high degree of conservation among homologous xylanases. Most dramatically, Asp83 and Asp101 have pK_a values < 2 and thus remain deprotonated in native BCX under all conditions examined. Asp83 is completely buried, forming a strong salt bridge with Arg136. In contrast, Asp101 is located near the surface of the protein and is stabilized in the deprotonated form by an extensive network of hydrogen bonds involving an internal water molecule and the neutral side chain and main chain atoms of Ser100 and Thr145. Combined with previous studies of the glutamic acid and histidine residues, these data provide a complete experimental database for theoretical studies of the ionization behaviour of xylanase under acidic conditions.

2.1 INTRODUCTION

The ionizable side chains of the acidic and basic amino acids play important roles in establishing the structure, stability, and function of proteins (Creighton, 1993). Electrostatic interactions between charged groups may help stabilize the native conformation of a protein, as well as define the specificity and affinity of ligand or substrate binding and the pH-dependent activity of an enzyme (Discussed in Chapters 3 and 4). To understand the contributions made by these amino acid residues, it is necessary to determine experimentally their pK_a values and hence protonation states within a given protein. These studies provide key insights into the possible catalytic functions of an active-site residue in an enzyme, as well as a direct measure of the contributions made by electrostatic interactions to the stability of a protein.

By thermodynamic linkage, the free energy of stabilization of the native state of a protein relative to its unfolded state, due to the deprotonation of a charged group, is reflected directly by the difference in the pK_a values of that group in these two conformational states (Tanford, 1961) (Discussed in Chapter 1). Accordingly, considerable experimental and theoretical efforts continue to be directed towards understanding the complex factors that dictate the pK_a values of amino acids in proteins and protein-ligand complexes (Yang and Honig, 1993).

The environment of an ionized group that is freely accessible to solvent (e.g. in a model compound or on the surface of a protein) is substantially different from one that is buried within a protein. The dielectric of bulk water is ~ 80, in contrast to that estimated for the interior of a protein (4-10) where the medium is less polarizable (Matthew, 1985). In transferring a charged residue from a region of high dielectric (ionic aqueous solution) to a region of low dielectric (non-polar interior of a protein), an energetic penalty must be paid if the residue is to remain ionized. This energy is known as either the electrical potential "self-energy" or the Born energy

of solvation (van Holde *et al.*, 1998). Within the protein, the charged residue can interact with fixed partial charges of neighboring atoms, as well as other ionizable groups. The pK_a of the residue will reflect the sum of these free energy terms. If a buried charge is not adequately "quenched" by the surrounding protein, it can be extremely destabilizing (Yang and Honig, 1993) and thus will have a pK_a shifted to favour the neutral form. Conversely, formation of strong ion-pairs and charge-stabilizing hydrogen bonds can contribute favourably to the net stability of a protein, as reflected by a shift in pK_a to favour the charged state. For example, ionizable residues that are less solvent accessible have been shown to contribute as much as 3-5 kcal mol^{-1} to overall stability (Anderson *et al.*, 1990). In contrast, charged groups on the surface of the protein often contribute little due to high dielectric constant and charge screening (Dao-pin *et al.*, 1991).

The knowledge of the precise roles that specific ionizable residues play in protein stability has come from a limited number of studies, since comprehensive sets of site-specific pK_a measurements are available for few proteins (Anderson *et al.*, 1990; Forsyth *et al.*, 1998; Oliveberg *et al.*, 1995; van Vlijmen *et al.*, 1998). BCX provides an excellent system for studying the contributions that individual charged residues have upon stability. It is highly amenable to being studied by NMR (Plesniak *et al.*, 1996b) in addition to belonging to a well-represented family of glycosidases from which many homologues are available for sequence comparisons. Furthermore, a high-resolution crystal structure of the WT protein has been solved (Wakarchuk *et al.*, 1994a). One of the less fortunate properties of the enzyme is the absence of thermodynamic data on its stability, due to its irreversible folding curve.

The pK_a values of the glutamic acids, which fortuitously are the two catalytic carboxyls, as well as of the histidines in this protein have been measured. The pK_a of the nucleophile,

Glu78, is 4.6 whereas that of the general acid/base, Glu172, is 6.7 in the free enzyme and 4.2 in a trapped glycosyl-enzyme intermediate (McIntosh *et al.*, 1996). These values agree closely with the apparent pK_a values describing the pH-dependence of the second-order rate constant, k_{cat}/K_m, for BCX towards xylobiosyl substrates (Discussed in Chapter 3). The pK_a of His156, a surface residue, is relatively unperturbed at ~ 6.5. In contrast, His149 has a pK_a value < 2.3, and thus is never ionized significantly within the folded protein (Plesniak *et al.*, 1996a). This histidine is completely buried within the hydrophobic core of BCX and is involved in an extensive network of hydrogen bonding interactions. The structural importance of His149 is confirmed by the destabilizing effect of amino acid substitutions at this position. To complete the characterization of the ionization behaviour of BCX under acidic conditions, I measured the pK_a values of the seven aspartic acid residues.

The work presented in this chapter was published in a peer-reviewed letter in *Protein Science* (Joshi *et al.*, 1997). The original paper was written in collaboration with Dr. Lawrence McIntosh. I carried out all experimental work, except for the measurement of the pK_a of the C-terminal residue, which was done by a summer student, Anders Hedberg.

2.2 MATERIALS AND METHODS

2.2.1 Cloning and Protein Expression

The synthetic gene encoding BCX was cloned into the pCW plasmid system under control of an inducible *tac* promoter, as described previously (McIntosh *et al.*, 1996; Sung *et al.*, 1993; Wakarchuk *et al.*, 1994a). Recombinant DNA procedures, such as plasmid isolation and purification, were performed using a Qiaprep Spin Miniprep Kit (Qiagen Inc., Mississauga ON). Sequences were confirmed by automated DNA sequencing and plasmids were transformed into an appropriate strain of *E. coli* using electroporation.

Proteins were expressed in *E. coli* strain EA1 (*asp⁻, asn⁻, tyr⁻, kan^r*) grown in a synthetic medium (Anderson *et al.*, 1993; McIntosh *et al.*, 1996; Muchmore *et al.*, 1989) containing 275-325 mg/L 99% L-[γ-^{13}C]-aspartate (Tracer Technology, Cambridge, MA). With lesions in the *asnA, asnB, aspC* and *tyrB* genes, this strain does not metabolically convert aspartic acid to asparagine (Anderson *et al.*, 1993). Bacteria were grown at 37 °C until the time of induction (OD$_{600}$ = 0.5 - 0.6) and thereafter at 30 °C until the cells were harvested 16 hours later. Protein expression was induced by addition of IPTG to a final concentration of 0.75 mM. Purification was performed as described previously using SP-Sepharose™ ion-exchange chromatography (Pharmacia Biotech, Inc.) (Sung *et al.*, 1993). The [γ-^{13}C]-Asp enriched xylanases were purified to > 90% homogeneity as verified by SDS-PAGE with Coomassie Blue staining.

2.2.2 NMR

All NMR spectra were recorded using a Varian Unity™ spectrometer operating at 500 MHz for protons.

i) Titration curves

The [γ-^{13}C]-Asp enriched BCX protein was dialyzed or exchanged, using a microconcentration device, into 25 mM sodium phosphate, 10% D$_2$O/90% H$_2$O, at pH* ~ 6.0 with a total sample volume of 2.0 mL. The initial sample concentration was 0.75 mM. One-dimensional ^{13}C-NMR spectra were recorded as a function of pH* at 25 °C and processed as described previously (McIntosh *et al.*, 1996). Chemical shifts were referenced to an external sample of DSS at 0.00 ppm.

Titration curves were generated by recording ^{13}C-NMR spectra of [δ-^{13}C]-Asp labelled xylanases as a function of pH* at 25 °C. Proteins were titrated using microlitre aliquots of either 0.25-0.50 M HCl or NaOH. The pH* of the sample was determined using a Corning G-P Micro Combo™ electrode. After measuring the acidic limb of the titration curve, the protein was exchanged into neutral buffer using a micro concentrating device to remove any excess salt and to avoid aggregation resulting from the addition of a large quantity of base. Titration of the basic limb was then carried out in a similar manner to that used for the acidic limb. The sample was also centrifuged periodically to remove any precipitate that formed during the titration. The assignments of the γ-^{13}C resonances were obtained from a variation of the 3D CBCACO(CA)HA experiment that provides correlations between the C$^{\alpha}$/C$^{\beta}$, C$^{\gamma}$, and H$^{\beta}$/$^{\beta'}$ of each Asp residue in a uniformly ^{13}C/^{15}N labelled sample of BCX (Plesniak *et al.*, 1996b). pK_a values were determined by nonlinear least squares fitting of the observed data to models involving one or two sequential ionizations (equations 2.1 and 2.2) (Shrager *et al.*, 1972) using the program, PlotData (TRIUMF,

University of British Columbia). The inherent error of the pH measurements is estimated to be $\pm$ 0.1 pH unit.

NMR-derived titration curves characterized by one or two apparent or macroscopic pK_a values (Appendix I) are described by equations 2.1 and 2.2, respectively. δ_{obs} is the chemical shift of the residue being monitored, and δ_i represents the chemical shift of the residue in each macroscopic ionization state of the enzyme:

$$\delta_{obs} = \frac{\delta_a 10^{-pH} + \delta_b 10^{-pK_a}}{10^{-pH} + 10^{-pK_a}} \quad (2.1)$$

$$\delta_{obs} = \frac{\delta_a 10^{-2pH} + \delta_b 10^{-(pH+pK_{a1})} + \delta_c 10^{-(pK_{a1}+pK_{a2})}}{10^{-2pH} + 10^{-(pH+pK_{a1})} + 10^{-(pK_{a1}+pK_{a2})}} \quad (2.2)$$

Selection of the appropriate model was based on the criteria of using the minimal number of ionization events to adequately fit the observed titration data.

2.3 RESULTS

Shown in Figure 2.1 is the pH-dependence of the chemical shifts of the γ-^{13}C nuclei from the seven aspartic acids in BCX at 25 °C. The upfield change of ~ 3 ppm with decreasing pH observed for five of these residues is consistent with that expected for the protonation of a carboxyl group (Gu *et al.*, 1994). The pK_a values of these side chains were determined by fitting of the NMR data to standard equations describing titrations involving one (Asp11, 106, and 121) or two ionizable groups (Asp4 and 119) (Shrager *et al.*, 1972). In the latter case, the apparent or macroscopic pK_a associated with the aspartic acid is taken to correspond to the major change in chemical shift occurring near pH 3. Minor changes near neutral pH are attributed to perturbations of these residues due to the titrations of other ionizable groups in BCX.

In striking contrast to five of the aspartic acid residues in BCX, Asp83 and Asp101 have essentially constant γ-^{13}C chemical shifts between pH 2.1 to 9.4 and thus do not titrate over this measured pH range. The pK_a value of these side chains must either be < 2 or > 9. The downfield chemical shift (184.3 ppm) of Asp101 is indicative of a deprotonated carboxylate, while the upfield chemical shift (176.8 ppm) of Asp83 is characteristic of a protonated carboxylic acid. However, as is evident by the dispersion of aspartic acid γ-^{13}C chemical shifts observed in BCX, the ionization states of these residues cannot be determined reliably based only on the data presented in Figure 2.1. To resolve this critical question, we also recorded the spectrum of the selectively labelled protein in 90% D$_2$O/10% H$_2$O buffer at pH* 6.1. Whereas the ^{13}C resonance of a neutral carboxylic acid experiences a two-bond isotope shift of ~ -0.25 ppm upon deuteration, that of an ionized carboxylate remains unaffected (Ladner *et al.*, 1975; Yamazaki *et al.*, 1994). The absence of such a readily measurable isotope shift for either Asp83 or Asp101 unambiguously demonstrates that both residues exist in the *deprotonated* form within BCX, and thus must have pK_a values < 2.0 (data not shown). Indeed, if we assume that changes in chemical
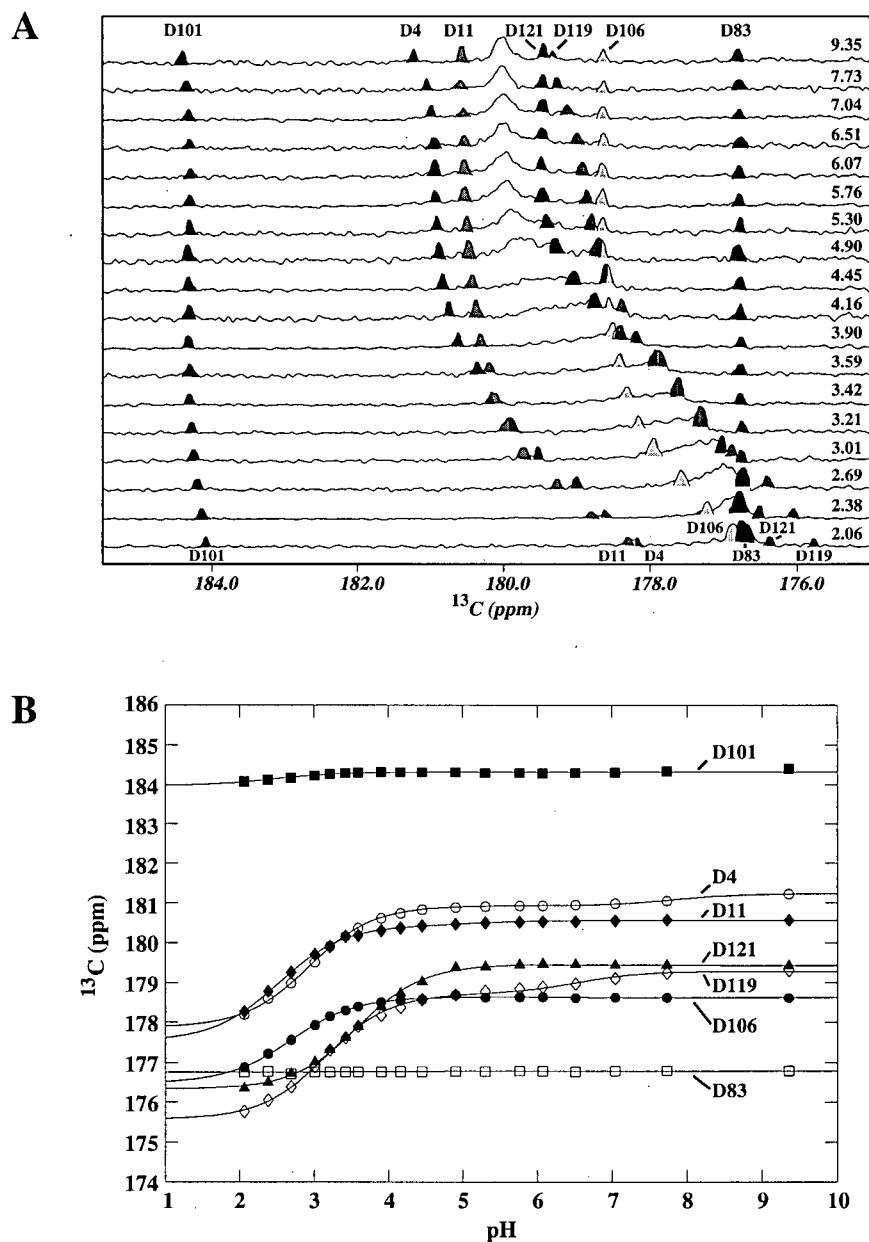
Figure 2.1 (A) ^{13}C-NMR spectra of BCX recorded as a function of pH at 25 °C. The peaks corresponding to the Asp residues are shaded for emphasis. Spectral assignments were based on previous analysis of BCX (Plesniak *et al.*, 1996b) and pH values are listed above each spectrum. (B) Apparent pK_a values were determined by fitting the data for Asp101 (■), Asp4 (○), Asp11 (◆), Asp121 (▲), Asp119 (◇), Asp106 (●) and Asp83 (□) to an equation describing the pH-dependence of the chemical shift of a residue to one or two sequential ionization events.

shift are detectable at pH values within a unit of the pK_a of a carboxyl group, then estimates for the upper bounds for the pK_a values of Asp83 and Asp101 can be set at ~ 1.0.

Finally, based upon the pH-dependence of the amide ^{15}N chemical shift of Trp185 determined using a 2D [1]H-^{15}N heteronuclear correlation experiment, the pK_a of the α-carboxyl group of this C-terminal residue is assigned tentatively to ~ 2.7 (data not shown; Bundi and Wuthrich, 1979). A summary of the measured pK_a values of all the carboxyl and imidazole groups in BCX is presented in Table 2.1.

Table 2.1. Measured pK_a values and structural characteristics of the carboxyl and imidazole groups in BCX.

Residue	pK_a[a]	Hydrogen Bonding Partner[b]	Fractional Solvent Accessible Surface Area[c]	Conservation[d]
Asp4	3.0	Thr43 (N, O^η)	0.35	15 %
Asp11	2.5	Gly13 (N), Asn35 (N), H_2O (244)	0.25	70 %
Asp83	< 2.0	Tyr53 (O^η), Tyr105 (O^η), Arg136 ($N^{\eta 1}$)	0.00	100 %
Asp101	< 2.0	Ser100 (O^γ), Thr145 (N, $O^{\gamma 1}$), H_2O (200)	0.08	90 %
Asp106	2.7	Arg89 ($N^{\eta 2}$)	0.15	80 %
Asp119	3.2	Arg73 (N^ε, $N^{\eta 2}$)	0.43	50 %
Asp121	3.6		0.97	15 %
Glu78	4.6	Tyr69 (O^η), Gln127 ($N^{\varepsilon 2}$)	0.12	100 %
Glu172	6.7	Asn35 ($N^{\delta 2}$), Tyr80 (O^η)	0.13	100 %
His149	< 2.3	Ser130 (O^γ), H_2O (200)	0.00	100 %
His156	~ 6.5	Ala152 (O)	0.33	35 %
W185 (α-C)	~ 2.7	Ala1 (α-N), Asn52 (N)	0.00	-

[a] Apparent pK_a values of the aspartic acid residues are determined from the data in Figure 2.1, while those of the glutamic acids were taken from McIntosh *et al.*, (1996). Histidine pK_a values are from Plesniak *et al.*, (1996a), while that of the C-terminus is from a HSQC-titration of ^{15}N-labelled BCX. Errors are estimated to be ±0.1 units.

[b] Hydrogen bonds were determined from the crystal structure of BCX (RCSB PDB file 1XNB (Wakarchuk *et al.*, 1994a)) by visual inspection and by using the programs HBPLUS (McDonald and Thornton, 1994) and VADAR (Wishart *et al.*, 1995). Only internal water molecules are listed. Positively charged groups are underlined.

[c] Solvent accessible surface areas are reported for selected atoms of the aspartic acid (C^γ, $O^{\gamma 1}$, $O^{\gamma 2}$), glutamic acid (C^δ, $O^{\delta 1}$, $O^{\delta 2}$), and histidine (C^γ, C^δ, $N^{\delta 1}$, $C^{\varepsilon 2}$, $N^{\varepsilon 2}$) side chains in the PDB file 1XNB relative to those calculated for the same atoms in a fully extended Gly-X-Gly tripeptide. Calculations were performed with the program SURFCV using a probe radius of 1.4 Å (Sridharan *et al.*, 1995).

[d] Residue conservation is based on the aligned sequences of 14 family 11 xylanases (Wakarchuk *et al.*, 1994a). Aspartic acid and glutamic acid residues are considered equivalent.

2.4 DISCUSSION

The pK_a values of an aspartic acid side chain and a C-terminal α-carboxyl group in an unstructured polypeptide are approximately 4.0 and 3.3 - 3.8, respectively (Creighton, 1993; Richarz and Wuthrich, 1978). The pK_a values of all the aspartic acids and the C-terminus of BCX are less than these reference values, indicating that the environment of each in the native protein favours its deprotonation (Figure 2.2). Stated equivalently, the ionization of these acidic groups contributes to the stability of the folded protein relative to its unfolded state. Quantitatively, each decrease in the pK_a of a given residue compared to its value in the unfolded state by one unit corresponds to ~ 1.4 kcal mol^{-1} in free energy of stabilization of the native protein at 25 °C (Anderson *et al.*, 1990; Tanford, 1961). The reduced pK_a value of the carboxyl groups may result from global electrostatic effects, due to the net positive charge of BCX under acidic conditions, combined with local electrostatic interactions including opposite charge pairing and hydrogen bonding. BCX displays a very interesting electrostatic surface. The enzyme has a computed pI of 9.1 (Joshi *et al.*, 2000a) and is a net basic protein with 2 Glu, 7 Asp, 2 His, 7 Arg, and 5 Lys residues. The profile of the electrostatic surface shows a rather asymmetric charge distribution (Figure 2.3). The front-side of the molecule, where the active-site is located, is dominated by regions of negative potential (5/9 acidic residues are located on the front face), whereas, the back-side is marked by substantially positive regions of potential (9/12 basic residues are located on the rear face). Nevertheless, offsetting the favourable effects of buried negative charges in a net positively charged molecule is the screening of exposed charged groups by solvent counterions and the destabilization of ionizable groups upon burial within the low dielectric medium of the protein core. To help in the evaluation of these complex factors, a summary of the
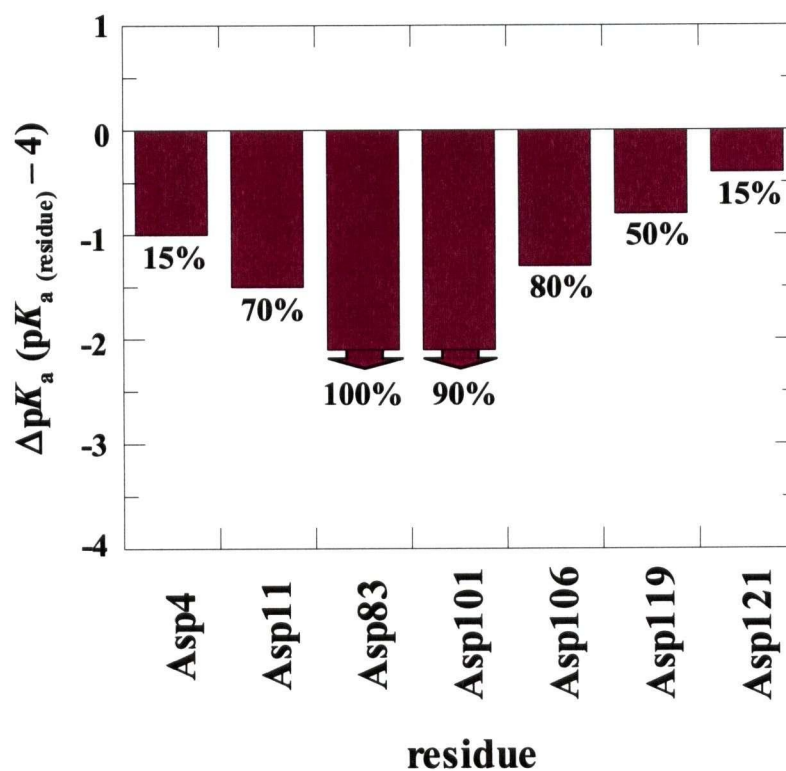
Figure 2.2. Aspartic acid pK_a shift associated with the folded state. The pK_a values of all the Asp residues in BCX were compared to the pK_a value of an Asp residue in an unstructured polypeptide (p$K_a \sim 4$). The % conservation of the Asp residue amongst the family 11 xylanases is indicated on the plot. Asp83 and Asp101 have the lowest pK_a values (< 2) and are also the most highly conserved.
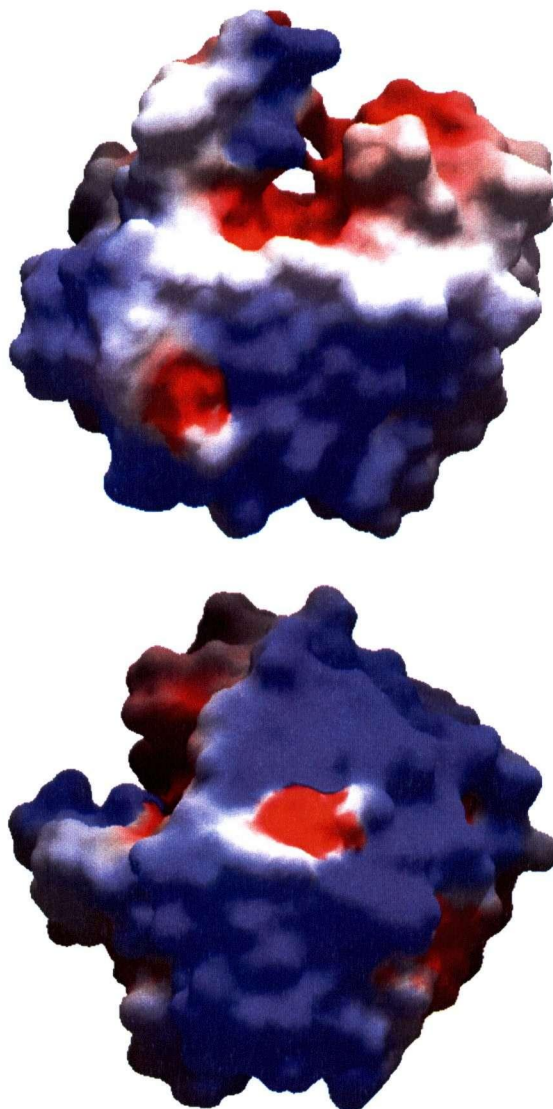
Figure 2.3. Electrostatic represenation of the potential surface of BCX. Regions of negative potential are shown in red (active-site) while regions of positive potential (a majority of the molecular surface of BCX) are shown in blue. At the top is the front-side of the molecule, which shows the active-site, and below is the back-side of the molecule. Figure was generated using the coordinates of WT (wild type) BCX (Wakarchuk *et al.*, 1994a) (RCSB PDB ID: 1XNB) and the program GRASP (Nicholls *et al.*, 1991).

environments of the Asp, Glu, and His residues observed in the crystal structure of BCX is also given in Table 2.1.

With pK_a values below 2.0, Asp83 and Asp101 contribute most significantly to the stabilization of BCX. Indeed, since the stability of BCX decreases with pH such that the protein unfolds readily under strongly acidic conditions (Davoodi *et al.*, 1995), we conclude that these two aspartate groups are always ionized within the context of the native enzyme. Based on the crystal structure of BCX (Wakarchuk *et al.*, 1994a), Asp83 is buried entirely in the interior of the protein, forming hydrogen bonds with the positively-charged δ-guanido group of Arg136 and the phenolic O^η atoms of Tyr53 and Tyr105 (Figure 2.4). The structural importance of this ion pair is highlighted by the strict conservation of positions 83 and 136 as Asp/Glu and Arg/Lys residues, respectively, in all family 11 xylanases. It is intriguing to note that, in bacteriophage T4 lysozyme, Asp10 has a pK_a value < 2 yet also shows an unusual upfield γ-^{13}C shift characteristic of a protonated carboxyl. This aspartate is buried within the protein, interacting with the side chains of two arginines and a tyrosine (Anderson *et al.*, 1993). It is plausible that a strongly electron-withdrawing ionic hydrogen bond or an electric field effect from an adjacent charged guanido group leads to the upfield changes in the γ-^{13}C chemical shifts of these two aspartates (Batchelor *et al.*, 1975; Gu *et al.*, 1994). In support of this suggestion, the second and third most upfield carboxylate resonances in Figure 2.1 arise from Asp106 and Asp119, both of which also contact arginine side chains in BCX (Table 2.1).

Asp101 is also a strong acid in this xylanase, yet in contrast to Asp83, it is not adjacent to any positively charged groups. The carboxyl of Asp101 is positioned near the surface of BCX, neither buried within its hydrophobic core nor exposed fully to the solvent. The charge of this side chain appears to be stabilized by hydrogen bonding to the amide of Thr145, the hydroxyl of

Ser100, and an internal water molecule (Figure. 2.4). Consistent with this interaction, the amide H^N resonance of Thr145 is shifted strongly downfield to 10.58 ppm (Plesniak *et al.*, 1996b). Furthermore, Asp101, Ser100, and the buried water are well conserved in homologous xylanases of known structure. Somewhat surprisingly, Asp101 is hydrogen bonded to the same internal water molecule as is the buried, neutral His149. This histidine has a pK_a value < 2.3, and thus is never positively charged in native BCX, despite the presence of the adjacent negatively-charged aspartate (Plesniak *et al.*, 1996a). Buried ion pairs consistently appear in proteins in low number and have distinct roles in maintaining structure and providing stability. Furthermore, isolated charged groups can also be buried in spite of the aforementioned energetic penalty of desolvation; however, they must be stabilized by hydrogen bonding or salt-bridges. This emphasizes the complex balance between charge stabilizing and destabilizing interactions within a folded protein.

Of the five aspartic acids in BCX that show measurable pH titrations, those that are well conserved in family 11 xylanases (Asp 11 and 106) have pK_a value < 3, while those that are not (Asp 4, 119, and 121) have pK_a values ≥ 3. The latter three also have the most exposed carboxyls of all the aspartic acids in BCX. This is not unexpected as residues involved in stabilizing the native fold of a protein are often maintained across a family of related proteins and often form the core of their structures. Both Asp106 and Asp119 are hydrogen bonded to arginine guanido groups in the crystal structure of BCX. However, the more exposed of these, Asp119, has a pK_a of 3.2, suggesting that solvent screening may reduce the stabilizing effect of this salt bridge. In contrast, neither Asp4 nor Asp11 is located in the immediate proximity of a charged side chain. The depressed pK_a values of these two residues are attributed to hydrogen bonding interactions with neutral polar atoms. The side chain of Asp121 is entirely exposed to the solvent, accounting
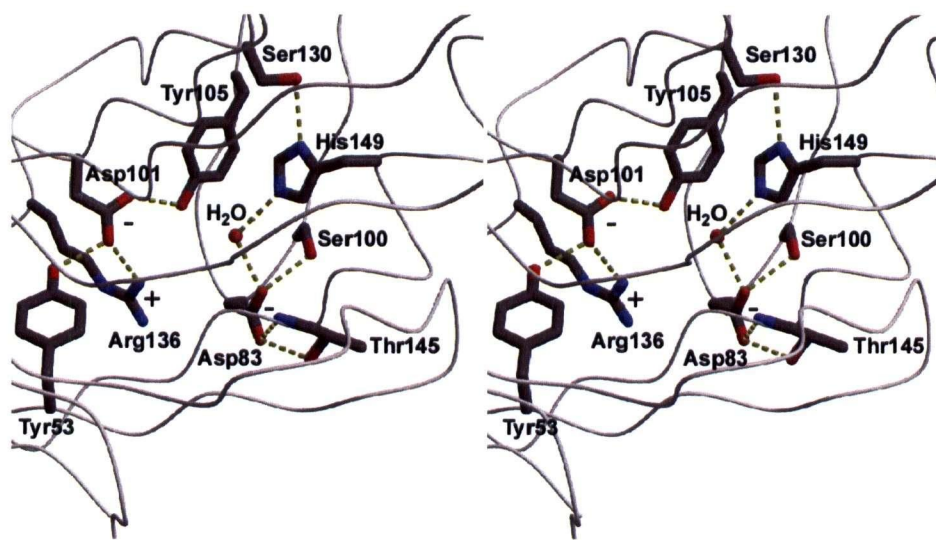
Figure 2.4. A stereo-view of the structural environment of Asp83 and Asp101 in BCX. Selected side chains are shown in dark gray, with potential hydrogen bonds indicated by broken yellow lines, protein and water oxygen atoms in red, nitrogen atoms in blue and the protein backbone trace in silver. Both Asp83 and Asp101 have pK_a values < 2.0 and thus are negatively charged under all conditions examined. Asp83 is buried, yet stabilized by a salt bridge with Arg136. Asp101 is nearby on the surface of BCX, forming hydrogen bonds to Ser100, Thr145 and an internal water molecule. His149, which is also hydrogen bonded to this water molecule, has a pK_a value < 2.3 and thus is neutral within the folded protein. The figure was generated from the RCSB Protein Databank (Bernstein *et al.*, 1977) coordinate file 1XNB (Wakarchuk *et al.*, 1994a) using the programs Molscript (Kraulis, 1991) and Raster3D (Merrit and Murphy, 1994).

for its relatively unperturbed pK_a of 3.6. Lastly, in the crystal structure of BCX, the α-carboxyl of Trp185 forms a salt bridge to the α-amino group of Ala1, presumably leading to its reduced pK_a of 2.7. Consistent with this interaction, heteronuclear relaxation studies reveal that the termini of BCX are well ordered in solution and do not display rapid local motion typical of residues near the ends of many proteins (Connelly *et al.*, 2000).

2.5 CONCLUSION

In summary, the pK_a values of all the carboxyl and imidazole groups in BCX have been measured and this study serves to further define the roles that each plays in establishing the pH-dependent stability of this protein. Conserved charged groups were found to have the most perturbed pK_a values and contributed the most to stability as expected. However, what was not expected was the observation that the most buried (least solvent accessible) groups had the lowest pK_a values. Definitely, exposed residues have "normal" pK_a values, but what about those that are buried? Traditional texts imply that burying charges is unfavourable, but we see that this is not the case. Indeed, in a low dielectric medium, a charge pair can interact very strongly and easily offset the Born energy term. This study therefore provides a database for future experimental and theoretical studies (Chapter 3) aimed at understanding the factors that determine the precise pK_a values of these residues within the folded and unfolded states of xylanases and proteins in general.

Measurements of the pK_a values of the acidic residues in BCX have provided insight into the pH-dependent stability of this enzyme. The focus of the next chapter will be on the two catalytic glutamic acid resides, Glu78 and Glu172, in order to define what factors set their pK_a values and hence the activity and pH optimum of the enzyme.

Chapter 3

The pH-Dependent Activity and Mechanism of BCX

ABSTRACT

The double-displacement reaction mechanism of retaining glycosidases necessitates that the ionization state of the catalytic nucleophile (lower pK_a) and the general acid/base catalyst (higher pK_a) be different such that they match their catalytic roles. The difference in ionization states between the catalytic groups is essential for function and gives rise to the bell-shaped pH-dependent activity profile of these enzymes. Previous studies of the low molecular mass family 11 xylanase from *Bacillus circulans* (BCX) show that the ionization state of the nucleophile (Glu78, pK_a 4.6) and the acid/base catalyst (Glu172, pK_a 6.7) gives rise to its pH-dependent activity profile. Inspection of the crystal structure of BCX shows that Glu78 and Glu172 are in very similar environments and are surrounded by several equivalent highly conserved active-site residues. Hence, there are no obvious reasons as to why their pK_a values are different. To address this question, a mutagenic approach was implemented to determine what features establish the pK_a values (measured directly by ^{13}C-NMR and indirectly by pH-dependent activity profiles) of these two catalytic carboxylic acids and give rise to their difference in ionization behaviour. The results indicate that all of the conserved active-site residues act concertedly in establishing the pK_a values of Glu78 and Glu172, with no particular residue being singly more important than any of the others. In general, residues that contribute positive charges and hydrogen bonds serve to lower the pK_a values of Glu78 and Glu172. The degree to which a hydrogen bond lowers a

pK_a value is largely dependent on the length of the hydrogen bond (shorter bonds lower pK_a values more) and the chemical nature of the donor (COOH > OH > NH_2). In contrast, neighbouring acidic groups can either lower or raise the pK_a values of the catalytic glutamic acids. The mechanism that they use to modulate pK_a values is complex and depends upon the electrostatic linkage of the ionization constants of the residues involved in the interaction. Analysis of several BCX structures indicates that Glu78 is preferentially stabilized over Glu172 in part by stronger hydrogen bonds contributed by two well-seated residues, namely Tyr69 and Gln127. In addition, theoretical pK_a calculations show that Glu78 has a lower pK_a value than Glu172 due to a lower desolvation energy and more favourable background interactions with permanent partial charges and ionizable groups within the protein. While the pH optimum of BCX can be modified (from -1.0 to +0.6 pH units) by mutating neighboring residues within the active-site, activity is usually compromised due to the loss of important ground and or transition state interactions. These results suggest that the pH optimum of an enzyme might be best engineered by making strategic amino acid substitutions at positions outside of the "core" active-site that electrostatically influence catalytic residues without perturbing their structures.

3.1   INTRODUCTION

Enzymes catalyze virtually all biochemical reactions in a bewildering array of organisms, and often under extremes of environmental conditions. Remarkably, this can be carried out using a rather limited repertoire of amino acids that serve as nucleophiles, electrophiles, and general acids and bases. Clearly, enzyme structures have evolved in part to modulate the physicochemical properties of these amino acids, as required for catalysis of a particular reaction under a given set of conditions. Since these catalytic amino acids generally have ionizable side chains, one critical property is their precise pK_a value within the context of the native enzyme. For example, all low-molecular weight xylanases use the same configuration of two catalytic glutamic acids to hydrolyze xylan. The pK_a values of these two residues must, however, differ considerably within a given enyzme as one must be deprotonated and serve as a nucleophile while the other must be protonated and function as a general acid. In addition, the relative pK_a values of these catalytic residues must be shifted between individual members of this family as some xylanases function optimally under acidic conditions, whereas others function under more alkaline pH values. Accordingly, a major challenge in the field of enzymology is to delineate experimentally the parameters that establish the pK_a values of ionizable groups in proteins and protein complexes. Knowledge of these factors can be applied to engineer rationally the pH optima of enzymes for use in biotechnology, as well as to improve their pH-dependent stability. Furthermore, studies that provide direct experimental information about structural and functional electrostatic interactions in proteins will also aid in the development and refinement of suitable algorithms for the theoretical prediction of the pK_a values of their constituent ionizable groups.

The low molecular mass endo-β-(1,4)-xylanase from *Bacillus circulans* (BCX) (Sung *et al.*, 1993; Wakarchuk *et al.*, 1992) provides an excellent model system to study the pH-

dependent activity of retaining glycosidases. This 20.4 kDa enzyme has been extensively characterized kinetically (Joshi *et al.*, 2000; Lawson *et al.*, 1996; Lawson *et al.*, 1997; McIntosh *et al.*, 1996) and structurally (Joshi et al., 2000; Sidhu *et al.*, 1999; Wakarchuk *et al.*, 1994) in both its free and covalent glycosyl enzyme-intermediate states. In addition, the NMR spectrum of BCX has been assigned (Plesniak *et al.*, 1996b) and the pK_a values of all of its carboxyl (Chapter 2; Joshi *et al.*, 1997; McIntosh et al., 1996) and imidazole (Plesniak et al., 1996a) groups have been determined.

BCX, like all family 11 glycosidase members (Gilkes *et al.*, 1991), hydrolyzes xylosidic substrates with net retention of anomeric configuration. This proceeds via a double-displacement mechanism involving two sequential S_N2 reactions (Gebler *et al.*, 1992; Koshland, 1953; Sinnott, 1990) (Figure 3.1). A covalent intermediate is formed in the glycosylation step and subsequently hydrolyzed in the following deglycosylation step. Previous studies have determined that, during the glycosylation reaction, Glu78 serves as a nucleophile and thus must initially be negatively charged, whereas Glu172 functions as a general acid and hence must be protonated (McIntosh *et al.*, 1996; Miao *et al.*, 1994; Sidhu *et al.*, 1999). Consistent with their catalytic roles, the pK_a values of Glu78 and Glu172, measured directly using ^{13}C-NMR spectroscopy, are 4.6 and 6.7, respectively. These values are in close agreement with those determined from the bell-shaped pH-activity profile of this enzyme and show that the ionization states of Glu78 and Glu172 determine that BCX functions optimally at pH 5.7 (McIntosh *et al.*, 1996).

The double-displacement mechanism of BCX requires that Glu172 plays a dual catalytic role as a general acid in the first step and as a general base in the second. This requirement places specific demands on the ionization state of Glu172. Remarkably, when the pK_a of Glu172 is measured in a trapped covalent glycosyl-enzyme intermediate, its pK_a drops to 4.2, where, at the
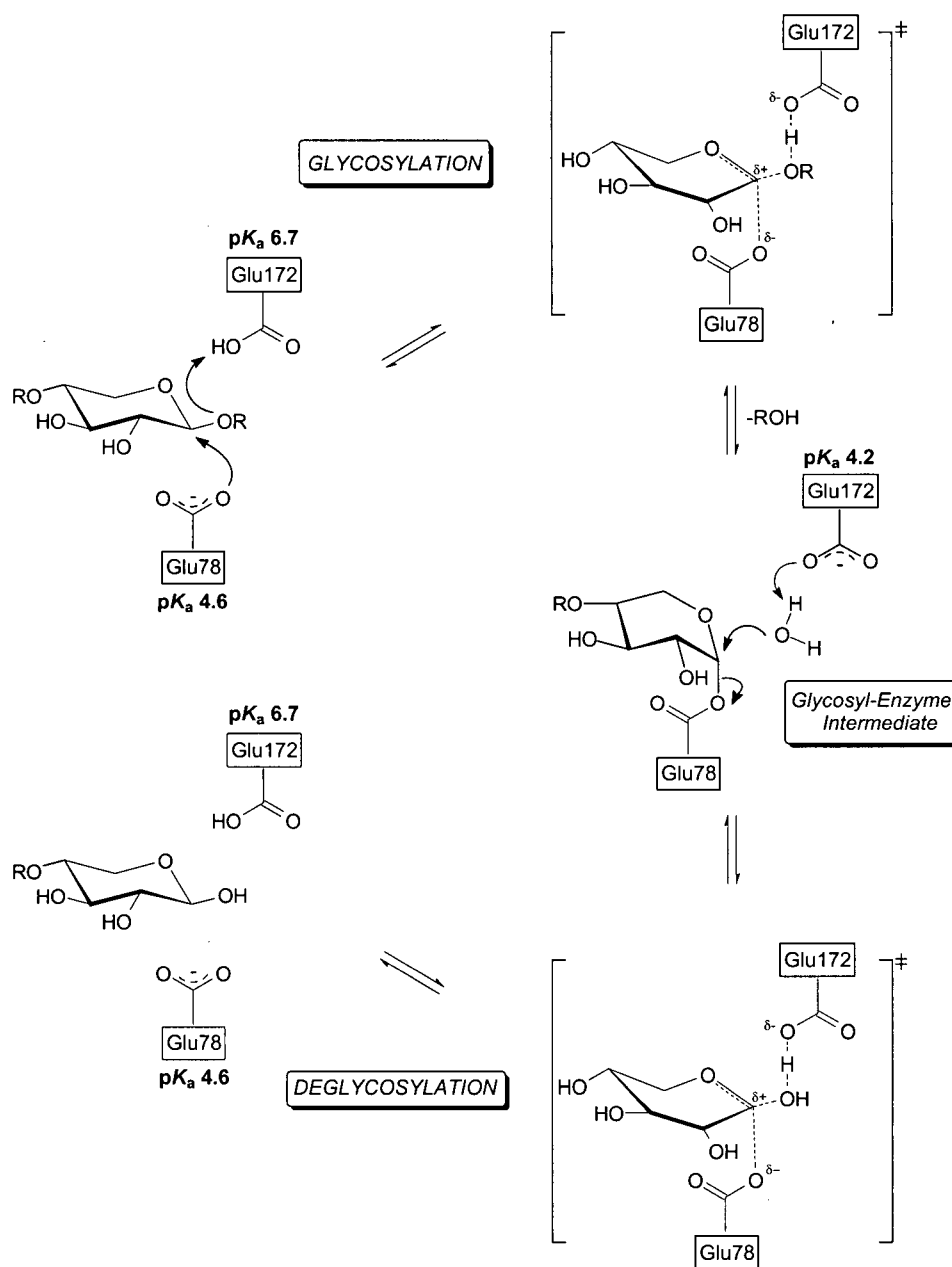
Figure 3.1. The double-displacement anomer-retaining mechanism employed by BCX involves two distinict steps. In the glycosylation step, Glu78 functions as a nucleophile (pK_a 4.6) and attacks the glycosidic bond of the β-(1,4)-linked xylose polymer while Glu172 functions as a general acid (pK_a 6.7) and donates a proton to the departing aglycone. In the subsequent deglycosylation step, the glycosyl-enzyme intermediate (with the proximal saccharide distorted in the $^{2,5}B$ conformation) is hydrolysed with the assistance of Glu172 (pK_a 4.2), which now functions as a general base. (R = xylose).

pH optimum, can function as a general base. The pK_a of Glu172 thus "cycles" to match its dual catalytic role (McIntosh *et al.*, 1996). A similar pK_a (4.2) was measured for Glu172 in a protein where Glu78 was substituted with a glutamine. This large decrease in pK_a of ~ 2.5 units is consistent with the role of Glu172 as a general base catalyst in the deglycosylation step and appears to be a consequence of both reduced electrostatic repulsion due to neutralization of Glu78 and subtle conformational changes in the protein. Therefore, the predominant driving force for pK_a cycling is the change in ionization state of Glu78 from a negatively charged nucleophile to a neutral glycosylated residue during the double-displacement reaction. Hence, this phenomenon is intrinsic to the retaining mechanism of glycosidases.

A major goal of this study of BCX was to delineate the factors that establish the exact pK_a values of these two catalytic glutamic acid residues. As expected, crystallographic studies of BCX reveal that Glu78 and Glu172 are surrounded by several highly conserved residues within the active-site of the enzyme (Wakarchuk *et al.*, 1994a). However, upon closer inspection, Glu78 and Glu172 are both found to be hydrogen bonded to primary amides (Gln127 and Asn35, respectively) and phenolic oxygens (Tyr69 and Tyr80, respectively) and are approximately equidistant from the same positively charged arginine (Arg112). Furthermore, both catalytic residues are in similar environments of secondary structure and exhibit comparable accessibilities to the solvent (Joshi *et al.*, 1997). Thus, there is no obvious reason as to why the pK_a values of these two glutamic acids differ by 2.1 units. To help answer this question, a systematic mutagenesis study was undertaken in order to determine the effects that specific hydrogen bonding and electrostatic interactions, contributed by conserved neighboring residues, have upon the pK_a values of Glu78 and Glu172 and hence the pH-dependent activity of BCX.

In this chapter, I report the kinetic, NMR spectroscopic, and X-ray crystallographic analyses of several BCX variants containing substitutions of active-site residues. Proteins were characterized kinetically in both the pre-steady state and steady state phases of hydrolysis. In particular, the second-order rate constants k_{cat}/K_m for hydrolysis of a xylobiosyl derivative were measured for all of the proteins as a function of pH. From the resultant bell-shaped activity profiles, the pH optimum of each variant, as well as the apparent pK_a values of Glu78 and Glu172, could be extracted and compared to those of the wild type enzyme. In parallel, NMR spectroscopy was utilized to measure directly the pK_a values of these two catalytic residues in each mutant protein. Where possible, X-ray crystallographic structures of mutant xylanases were solved to provide additional structural information. The structure of WT BCX was also determined under acidic conditions to assess the extent of pH-dependent conformational changes, which may influence the activity of the enzyme. Finally, the pK_a values of the catalytic glutamic acids were calculated theoretically in order to help dissect the factors contributing to the differences observed between the WT and mutant enzymes.

A survey of the literature suggests that this work represents one of the most extensive and detailed accounts of the pH-dependence of activity of any enzyme performed to date. BCX is highly amenable to being studied by a multitude of biophysical, structural and enzymological techniques and thus affords us this unique opportunity to examine its pH-dependent activity in detail. The vast majority of work presented in this chapter was performed by me. Some of the plasmids (Y69F, Y80F, R112N and Q127A) were created by Dr. Warren W. Wakarchuk, who also cloned the original synthetic BCX gene. However, in some cases I had to regenerate the plasmid DNA due to problems with the expression system (not discussed in this thesis). The synthetic substrates were made in the laboratory of Dr. Stephen Withers by Timothy Hiebert, Dr.

Spencer Williams and Dr. Lothar Ziser. Finally, the pK_a calculations were performed by my supervisor, Dr. Lawrence McIntosh, while on sabbatical leave at the European Molecular Biology Laboratory in Heidelberg, Germany in collaboration with a graduate student, Jens E. Nielsen. A manuscript describing this work is currently in preparation for submission to *Biochemistry* (Joshi *et al.*, 2000b).

3.2 MATERIALS AND METHODS

3.2.1 Cloning, Mutagenesis and Protein Expression

The synthetic gene encoding BCX was cloned into the pCW plasmid system under control of an inducible *tac* promoter, as described previously (McIntosh *et al.*, 1996; Sung *et al.*, 1993; Wakarchuk *et al.*, 1994a). To create the genes encoding the N35A, Y69F, Y80F, R112N and Q127A variants of BCX, site-directed mutagenesis was carried out as described previously (Wakarchuk *et al.*, 1994a) using the Kunkel method (Kunkel *et al.*, 1983). The QuickChange™ Site-Directed Mutagenesis Kit (Stratagene Cloning Systems, La Jolla, CA) was used to create the gene encoding Q127E BCX. All other recombinant DNA procedures, such as plasmid isolation and purification, were performed as recommended by the manufacturers. After the sequences were confirmed by automated DNA sequencing, the mutated plasmids were transformed into an appropriate bacterial *E. coli* strain using electroporation or calcium chloride-heat shock.

Proteins used for kinetic studies were expressed in *E. coli* strain BL21 (λDE3) or 594 grown in TYP medium at 37 °C until the time of induction (OD_{600} = 0.5 - 0.6) and thereafter at 30 °C until the cells were harvested 16 hours later. Protein expression was induced by addition of IPTG to a final concentration of 0.75 mM. Purification was performed as described previously using SP-Sepharose™ ion-exchange chromatography followed by Sephacryl S-100™ HR size exclusion chromatography (Pharmacia Biotech, Inc.) (Sung *et al.*, 1993). Fresh column material was used for different proteins to prevent any possible cross contamination. Proteins were purified to > 95% homogeneity as judged by SDS-PAGE with Coomassie Blue staining. Further characterization was performed using a Perkin Elmer Sciex API III electrospray mass spectrometer with the following results: N35A, observed 20 358 ± 3.5 Da (expected 20 353 Da); Y69F, observed 20 385 ± 4.5 Da (expected 20 380 Da); Y80F, observed 20 385 ± 4.5 Da

(expected 20 380 Da); R112N, 20 359 ± 3.5 Da observed (expected 20 354 Da); Q127A, 20 344 ± 4.0 Da observed (expected 20 339 Da); and Q127E, 20 400 ± 3.5 Da observed (expected 20 402 Da).

BCX mutant proteins, ^{13}C-enriched in the side chain δ-carbonyl of the glutamate and glutamine residues, were prepared as described previously (McIntosh *et al.*, 1996). Bacteria were grown in a synthetic medium (Anderson *et al.*, 1993; McIntosh *et al.*, 1996; Muchmore *et al.*, 1989) containing 275-325 mg/L 99% L-[δ-^{13}C]-glutamate (Tracer Technology, Cambridge, MA). The isotopically labelled proteins were expressed and purified as above, except that the size-exclusion chromatography step was not performed in order to maximize yield. The [δ-^{13}C]-Glu and -Gln enriched xylanases were purified to > 90% homogeneity as judged by SDS-PAGE and Coomassie Blue staining. Further characterization was performed using electrospray mass spectrometry, yielding the following values: N35A, observed 20 351 ± 3.5 Da (expected 20 360 Da); Y69F, observed 20 391 ± 2.0 Da (expected 20 387 Da); Y80F, observed 20 387 ± 2.0 Da (expected 20 387 Da); R112N, observed 20 362 ± 2.4 Da (expected, 20 361 Da); Q127A, observed 20 346 ± 3.6 Da (expected 20 346); and Q127E observed 20 408 ± 3.2 Da (expected 20 409). The expected mass value was calculated assuming 100% ^{13}C enrichment of seven residues. Deviations from observed and expected molecular masses reflects isotopic dilution of the [δ-^{13}C]-glutamate.

3.2.2 Enzyme Kinetics

(i) Steady State Kinetics

Two aryl β-xylobiosides were used as substrates in the assays described below: 2,5-dinitrophenyl β-xylobioside (2,5-DNPX$_2$), $\Delta\varepsilon_{440nm} = 3.57$ mM^{-1} cm^{-1} (where $\Delta\varepsilon$ is the difference

in molar absorptivity between the phenol and its corresponding xylobioside at pH 6.0); and orthonitrophenyl β-xylobioside (ONPX$_2$), $\Delta\epsilon_{400nm} = 1.07$ mM^{-1} cm^{-1}. All substrates were synthesized and characterized according to previously published procedures (Lawson *et al.*, 1997; Ziser *et al.*, 1995). All other materials, unless otherwise stated, were obtained from the Sigma Chemical Company. Spectrophotometric assays were performed on either a Pye Unicam 8700 or UV4 UV/Vis spectrophotometer, both equipped with a circulating water bath for temperature control. Assays were carried out in 200 μL micro black-walled quartz cuvettes with a 1 cm path length, according to methods described previously (Lawson *et al.*, 1997). The pH values of assay solutions were measured using a Corning G-P Micro Combo™ electrode. Steady-state kinetic data were fitted using the programs PlotData (TRIUMF, University of British Columbia) and GraFit (Leatherbarrow, 1998).

Assays to determine the Michaelis-Menten steady state parameters, k_{cat} and K_m, utilized the appropriate aryl β-xylobioside substrate in 20 mM MES, 50 mM NaCl, 0.1 % BSA buffer (pH 6.0). Typically, substrate concentrations were varied from $0.2K_m$ to $5K_m$. After a 15 minute preincubation time at 40 °C, 10 μL of enzyme at an appropriate concentration (2.0×10^{-4} mM to 7.0×10^{-2} mM final) was added to 190 μL of the assay solution. The initial rates of enzymatic hydrolysis of the aryl β-xylobiosides, v, were determined by monitoring the rate of phenol release at the appropriate wavelength in a continuous assay at 40 °C. Enzyme concentrations and reaction times were chosen such that less than 10 % of the total substrate was hydrolyzed over the course of the measurement. Experimental rates measured at each given substrate concentration were fitted by a non-linear least squares method to the standard Michaelis-Menten expression (Scheme 3.1 and equation 3.1) to obtain the parameters k_{cat} and K_m. Values of k_{cat}/K_m were determined from the slope of a Lineweaver-Burke plot.

Scheme 3.1: Standard Michaels-Menten scheme used to describe the hydrolysis of xylo-oligosaccharides by BCX proteins (k_2 and k_3 represent the glycosylation and deglycosylation steps respectively).

$$E + S \underset{k_{-1}}{\overset{k_1}{\rightleftharpoons}} ES \xrightarrow{k_2} ES' \xrightarrow{k_3} E+P$$
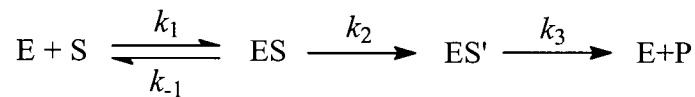
$$v_0 = \frac{k_{cat}[E_T][S]}{K_m + [S]} \quad (3.1)$$

where,

$$k_{cat} = \frac{k_2 k_3}{k_2 + k_3} \quad (3.2)$$

$$K_m = \left(\frac{k_{-1} + k_2}{k_1}\right)\left(\frac{k_3}{k_2 + k_3}\right) \quad (3.3)$$

and

$$K_d = \left(\frac{k_{-1}}{k_1}\right) \quad (3.4)$$

Assays used to determine the pH-dependence of k_{cat}/K_m employed low concentrations of ONPX$_2$ substrate (0.35 mM), 50 mM NaCl, 0.1 % BSA, and the appropriate buffer for a given pH range (pH 2-5: 20 mM succinate; pH 5-7: 20 mM MES; pH 7-8: 20 mM HEPES; pH 8-11: 20 mM CHES). After a 15 minute preincubation time at 25 °C, the enzymatic reaction was initiated by addition of 10 µL of enzyme (3.0×10^{-3} mM final) to 190 µL of the assay solution. Progress curves were followed by measuring the release of *o*-nitrophenolate at 400 nm *versus*

time until at least 80 % substrate depletion was observed. The pH of each assay solution was

measured after completion of the reaction. An aliquot of the assay mix was then re-assayed at pH

6.0 to confirm the stability of the enzyme compared to an aliquot of unassayed enzyme which

had not been exposed to assay conditions. Experimental data were fitted to a pseudo-first-order

expression, which upon division by the enzyme concentration yielded k_{cat}/K_m values. This

method obviated the need to correct for the variation of extinction coefficient of $ONPX_2$ with pH

and eliminated any errors associated with the determination of substrate concentrations. The

k_{cat}/K_m data were then plotted as a function of pH and fitted to a bell-shaped activity profile,

described in equation 3.5, from which apparent pK_a values corresponding to the acidic and basic

limbs were determined.

$$\left(\frac{k_{cat}}{K_m}\right)_{obs} = \left(\frac{k_{cat}}{K_m}\right)_{max}\left(\frac{1}{1+\dfrac{10^{-pH}}{10^{-pK_{a1}}}+\dfrac{10^{-pK_{a2}}}{10^{-pH}}}\right) \quad (3.5)$$

(ii) Pre-Steady State Kinetics

Pre-steady state kinetic measurements were taken for mutant BCX proteins using a

stopped-flow spectrophotometer (Olis RSM-1000) with a 2 cm cell path length and a circulating

water bath, as described previously (Zechel *et al.*, 1998). The dead-time of the instrument was

2.5 ms. Assays consisted of various amounts of 2,5-$DNPX_2$ substrate (0.30 mM to 2.20 mM) and

enzyme (1.0×10^{-3} mM to 2.0×10^{-3} mM) in 10 mM MES, 25 mM NaCl, buffer (pH 6.0) at 25

°C. The limited solubility of 2,5-$DNPX_2$ under the conditions described precluded assays

containing higher concentrations of substrate. Phenolate release was monitored at 440 nm by

collecting data at a rate of 1000 spectra/s over a 10 s time period. Pre-steady state bursts were

observed only for Y80F BCX. For this protein, the resulting time courses were fitted to an expression with an exponential term (pre-steady state phase) and a linear term (steady state phase) (equation 3.6).

$$A_{440}(t) = A(1 - e^{k_{obs}t}) + Bt + C \quad (3.6)$$

First-order rate constants for the exponential pre-steady state phase (k_{obs}) were then fitted to a linearized form of equation 3.7 that is valid in the absence of saturating conditions ($[S] < K_d$) (equation 3.8) (Hiromi, 1979; Namchuk and Withers, 1995; Zechel *et al.*, 1998). The slope of this plot yielded subsequent values of k_2/K_d.

$$k_{obs} = k_3 + \frac{k_2[S]}{K_d + [S]} \quad (3.7)$$

$$k_{obs} = k_3 + \frac{k_2[S]}{K_d} \quad (3.8)$$

3.2.3 NMR

All NMR spectra were recorded using a Varian Unity™ spectrometer operating at 500 MHz for protons.

(i) Titration curves

The [δ-^{13}C]-Glu and -Gln enriched BCX proteins were dialyzed or exchanged, using a microconcentration device, into 10 mM sodium phosphate, 10% D_2O/90% H_2O, at pH* ~ 6.0 with a total sample volume of 2.0 mL. Initial sample concentrations were: N35A, 1.27 mM; Y69F, 1.20 mM; Y80F, 1.45 mM; R112N, 0.75 mM; Q127A, 0.37 mM; and Q127E, 0.42 mM. One-dimensional ^{13}C-NMR spectra were recorded as a function of pH* at 25 °C and processed as described previously (McIntosh *et al.*, 1996). Chemical shifts were referenced to an external sample of DSS at 0.00 ppm. Titration curves were generated by recording ^{13}C-NMR spectra of

[δ-^{13}C]-Glu and -Gln labelled xylanases as a function of pH* at 25 °C. Proteins were titrated using microlitre aliquots of either 0.25-0.50 M HCl or NaOH. The pH* of the sample was determined using a Corning G-P Micro Combo™ electrode. After measuring the acidic limb of the titration curve, the protein was exchanged into neutral buffer using a micro concentrating device to remove any excess salt and to avoid aggregation resulting from the addition of a large quantity of base. Titration of the basic limb was then carried out in a similar manner to that used for the acidic limb. The sample was also centrifuged periodically to remove any precipitate that formed over the course of the titration. Individual δ-carbon resonances of glutamate and glutamine side chains of mutant xylanase proteins were assigned based on previous analysis of the WT spectra (McIntosh *et al.*, 1996; Plesniak *et al.*, 1996b). Macroscopic pK_a values were determined by nonlinear least squares fitting of the observed data to models involving one, two, or three sequential ionizations (equations 3.9-3.11) (Shrager *et al.*, 1972) using the program, PlotData (TRIUMF, University of British Columbia) (Appendix I).

$$\delta_{obs} = \frac{\delta_a 10^{-pH} + \delta_b 10^{-pK_a}}{10^{-pH} + 10^{-pK_a}} \quad (3.9)$$

$$\delta_{obs} = \frac{\delta_a 10^{-2pH} + \delta_b 10^{-(pH+pK_{a1})} + \delta_c 10^{-(pK_{a1}+pK_{a2})}}{10^{-2pH} + 10^{-(pH+pK_{a1})} + 10^{-(pK_{a1}+pK_{a2})}} \quad (3.10)$$

$$\delta_{obs} = \frac{\delta_a 10^{-(3pH)} + \delta_b 10^{-(pK_{a3}+2pH)} + \delta_c 10^{-(pK_{a2}+pK_{a3}+pH)} + \delta_d 10^{-(pK_{a1}+pK_{a2}+pK_{a3})}}{10^{-(3pH)} + 10^{-(pK_{a3}+2pH)} + 10^{-(pK_{a2}+pK_{a3}+pH)} + 10^{-(pK_{a1}+pK_{a2}+pK_{a3})}} \quad (3.11)$$

Here, δ_{obs} is the chemical shift of the residue being monitored, and δ_i represents its chemical shift in each ionization state of the enzyme. Selection of the appropriate model was based on the criterion of using the minimal number of ionization events to adequately fit the observed titration data as judged by a visual comparison of the observed and calculated plots of δ_{obs} versus pH*. The error of the pH measurements is estimated to be $\pm$ 0.1 units.

3.2.4 X-ray Crystallography

Crystals of mutant BCX proteins were grown at pH 7.5 in 17-20 % $(NH_4)_2SO_4$, 10 mM NaCl and 40 mM Tris HCl as previously described for the WT enzyme (Sidhu *et al.*, 1999). The crystals of WT BCX at acidic pH values were prepared by further soaking those grown at pH 7.5 in 1.0 M sodium citrate buffer at pH 5.5 or pH 4.0 for approximately four hours. Diffraction data for each mutant were collected from a single crystal on a Rigaku R-AXIS IIC imaging plate area detector system using CuK_α radiation supplied by a Rigaku RU300 rotating anode generator operating at 50 kV and 100 mA. Each diffraction data frame was exposed for 20 minutes during which time the crystal was oscillated through 1.2°. Intensity data were integrated, scaled, and reduced to structure factor amplitudes with the HKL suite of programs (Otwinowski and Minor, 1997) (Table 3.1). Because all types of crystals retained unit cells isomorphous to WT BCX, the published structure of the parent enzyme (RCSB PDB ID: 1XNB), with the residue at the site of mutation truncated to alanine, was used as the starting model in each case. These models were subjected to rigid body, simulated annealing, positional, and individual isotropic thermal factor refinement using X-PLOR (Brunger, 1992) and the CCP4 Suite (Collaborative Computational Project Number 4, 1994). At this point F_o-F_c difference electron density maps were calculated and the mutated residue was built into observed density with the program

Table 3.1. X-ray crystallographic data collection parameters.

Parameters	Y80F	Q127A	WT pH 5.5	WT pH 4.0
Space group	$P2_12_12_1$	$P2_12_12_1$	$P2_12_12_1$	$P2_12_12_1$
Cell dimensions (Å)				
a	44.0	43.9	43.8	44.0
b	52.6	52.7	52.7	52.7
c	78.5	78.2	78.3	78.6
Number of measurements	157188	157188	157414	121149
Number of unique reflections	24862	17548	24859	15032
Mean I/σI[†]	28.0 (7.5)	21.8 (6.6)	24.9 (5.4)	30.0 (9.1)
Merging R-factor (%)[a,b]	4.8 (16.2)	5.4 (11.5)	4.8 (21.0)	3.0 (11.0)
Resolution range (Å)	∞ - 1.6	∞ - 1.8	∞ - 1.6	∞ - 1.9

[a]Values in parentheses are for data in the highest resolution shell (1.66 – 1.60 Å for Y80F BCX, 1.88 – 1.80 for Q127A BCX, 1.66 – 1.60 for pH 5.5 WT pH 5.5 BCX and 1.97 – 1.90 for WT pH 4.0 BCX).

$$[b]R_{merge} = \frac{\sum_{hkl}\sum_{i=0}^{n}\left|I_i - \bar{I}_{hkl}\right|}{\sum_{hkl}\sum_{i=0}^{n}I_{hkl}}$$

O (Jones *et al.*, 1991). The models were then refined further with X-PLOR, with manual adjustments made periodically during refinement using F_o-F_c, $2F_o$-F_c, and fragment-deleted difference electron density maps. The validity of solvent molecules was assessed based on both hydrogen bonding potential to appropriate protein atoms and refinement of a thermal factor of less than 75 Å^2 (Table 3.2). The r.m.s coordinate errors estimated from Luzzati plots (Luzzati, 1952) are: 0.20 Å for Y80F BCX, 0.18 Å for Q127A BCX, 0.20 Å for WT pH 5.5 BCX, and 0.20 Å for WT pH 4.0 BCX (Figure 3.2).

Atomic coordinates and related structure factors will be deposited in the RCSB Protein Data Bank (Bernstein *et al.*, 1977). Structural illustrations using atomic coordinates were generated using the programs Bobscript (Kraulis, 1991) and Raster3d (Merrit and Murphy, 1994). Potential hydrogen bonds were identified using the programs HBPLUS (McDonald and Thornton, 1994) and WHAT IF (Hooft *et al.*, 1996), combined with manual inspection of the structures.

3.2.5 Theoretical pK$_a$ Calculations

pK$_a$ values for the ionizable groups in the WT and mutant forms of BCX were calculated essentially as described previously (Nielsen *et al.*, 1999; Nielsen *et al.*, 2000). Briefly, this involved the use of: (i) a combination of automated and manual scripts implemented in WHAT IF to construct optimized hydrogen bonding networks for each ionization state of a given residue, as well as to allow flipping of asparagine, glutamine, and histidine side chains by 180° about their χ_2, χ_3, or χ_2 dihedral angles, respectively (Hooft *et al.*, 1996); (ii) DELPHI to solve the finite-difference Poisson-Boltzman equation, with uniform dielectric constants of 8 and 80 for the protein and bulk solvent, respectively, an ionic strength of 0.05 M, and a temperature of

Table 3.2. X-ray crystallographic refinement statistics.

Parameters	Y80F	Q127A	WT pH 5.5	WT pH 4.0
Number of reflections	24156	15042	23836	13847
Resolution range (Å)	10 – 1.6	10 – 1.8	10 – 1.6	10 – 1.9
Completeness within range (%)	95.0	95.0	96.6	93.2
Number of non-hydrogen protein atoms	1447	1444	1448	1448
Number of solvent atoms	196	176	196	129
Average thermal factors ($Å^2$)				
Protein	10.9	9.6	10.4	10.2
Solvent	14.1	13.5	13.4	12.9
Final refinement R-factor (%)[a]	18.1	16.4	18.5	18.0
Stereochemistry		r.m.s deviations		
bonds	0.006	0.009	0.006	0.007
angles	1.150	0.911	0.721	1.144

[a]R-factor $= \dfrac{\sum_{hkl}|F_{o,hkl} - F_{c,hkl}|}{\sum_{hkl}|F_{o,hkl}|}$
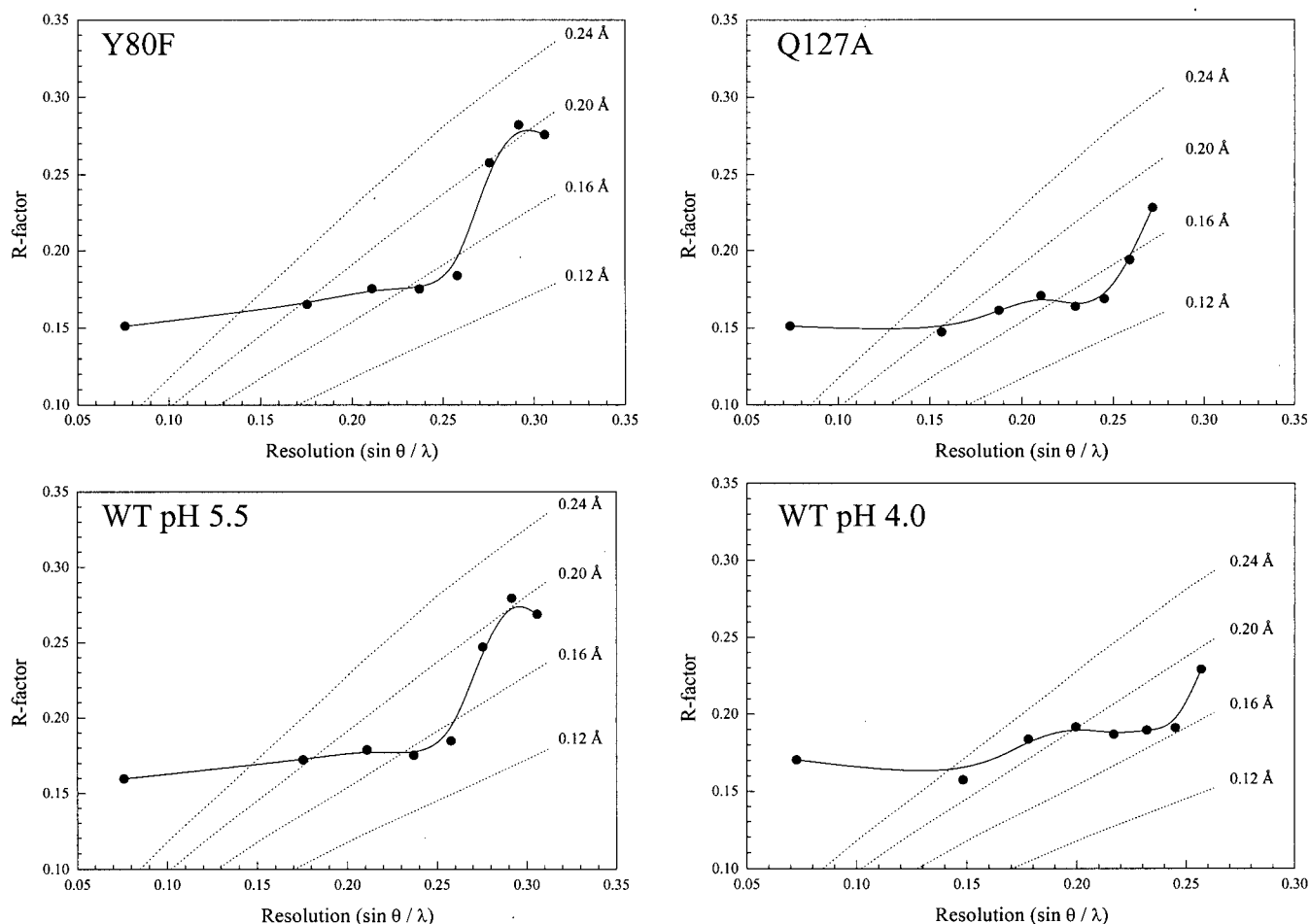
Figure 3.2. Luzzati plots of the crystallographic R-factor as a function of resolution for the structures of BCX proteins. The theoretical dependence of R-factor on resolution for various levels of coordinate error (indicated on plot) is shown with broken lines. The r.m.s. coordinate errors are estimated to be 0.20 Å for Y80F BCX, 0.18 Å for Q127A BCX, 0.20 Å for WT "pH 5.5" BCX, and 0.20 Å for WT "pH 4.0" BCX.

25 °C (Yang and Honig, 1993); and (iii) a Monte-Carlo sampling of the Boltzman distribution describing the interaction of all ionizable groups in order to calculate the fractional protonation of each as a function of pH. The pK_a value of a group is defined as the pH at which it is half-protonated. Pertinent model pK_a values were Asp (4.0), Glu (4.4), C-terminus (3.8), and His (6.3).

In the cases of WT BCX, as well as N35D, Y69F, Y80F, Q127A, and the covalently modified WT-2FXb and N35D-2FXb variants, the crystallographic coordinates determined at pH 7.5 were utilized directly, without explicit inclusion of bound waters. Generally, the side chains of Asn54, Asn63, Asn114, Gln133, Asn148, and Asn159 (surface residues, distant from the catalytic glutamic acids) were flipped relative to their orientations in the published coordinate files. In the remaining cases of N35A, E78Q, Q127E, R112N, and E172Q BCX, models were constructed by direct amino acid replacements into the WT template. Using WHAT IF to select for the appropriate orientation of the glutamine side chain amides, Gln78 was positioned to hydrogen bond to Tyr69 via its $N^{\varepsilon 2}H$ and Q127 via its $O^{\varepsilon 2}$ in E78Q, and Gln172 positioned to hydrogen bond to Asn35 via its $O^{\varepsilon 2}$ and Tyr80 via its $N^{\varepsilon 2}H$ in E172Q BCX.

3.3 RESULTS

3.3.1 Kinetic Studies

i) Determination of k_{cat} and K_m at pH 6.0

The Michaelis-Menten steady-state kinetic parameters, k_{cat} and K_m, were determined at 40 °C and pH 6.0 for the series of BCX mutants using ONPX$_2$ as a substrate (Figure 3.3 and Table 3.3). N35A BCX was the most active mutant with k_{cat}/K_m values for hydrolysis of ONPX$_2$ double that exhibited by the WT protein. Although k_{cat} was reduced by almost 3-fold for this mutant, its overall activity was increased as a result of a greater apparent affinity for the ONPX$_2$ substrate. A similar, albeit smaller, increase in activity results from the substitution of Asn35 with Asp (Chapter 4; Joshi *et al.*, 2000a). Other mutants, such as Y80F, R112N, Q127A and Q127E BCX were still active, but showed significantly impaired catalysis relative to the parental WT enzyme. Y80F and R112N BCX had k_{cat}/K_m values that were reduced by > 95 % compared to WT BCX, mainly due to decreases in k_{cat} by approximately two orders of magnitude. Substitutions at position 127 with an Ala (Q127A) and a Glu (Q127E) led to similar reductions in k_{cat}/K_m to about 10% of that of WT BCX. The parameter k_{cat} was reduced to a greater extent in Q127E, yet this was compensated by a favourable change in K_m, yielding an overall activity comparable to Q127A. On the far end of the spectrum of mutants was Y69F BCX, with the substitution of a Phe for Tyr69 resulting in virtual abolition of activity. Thus, with one exception, the overall activities (based on values of k_{cat}/K_m) of the xylanases with active-site mutations were reduced significantly when compared to WT BCX, primarily due to reductions in their k_{cat} constants.
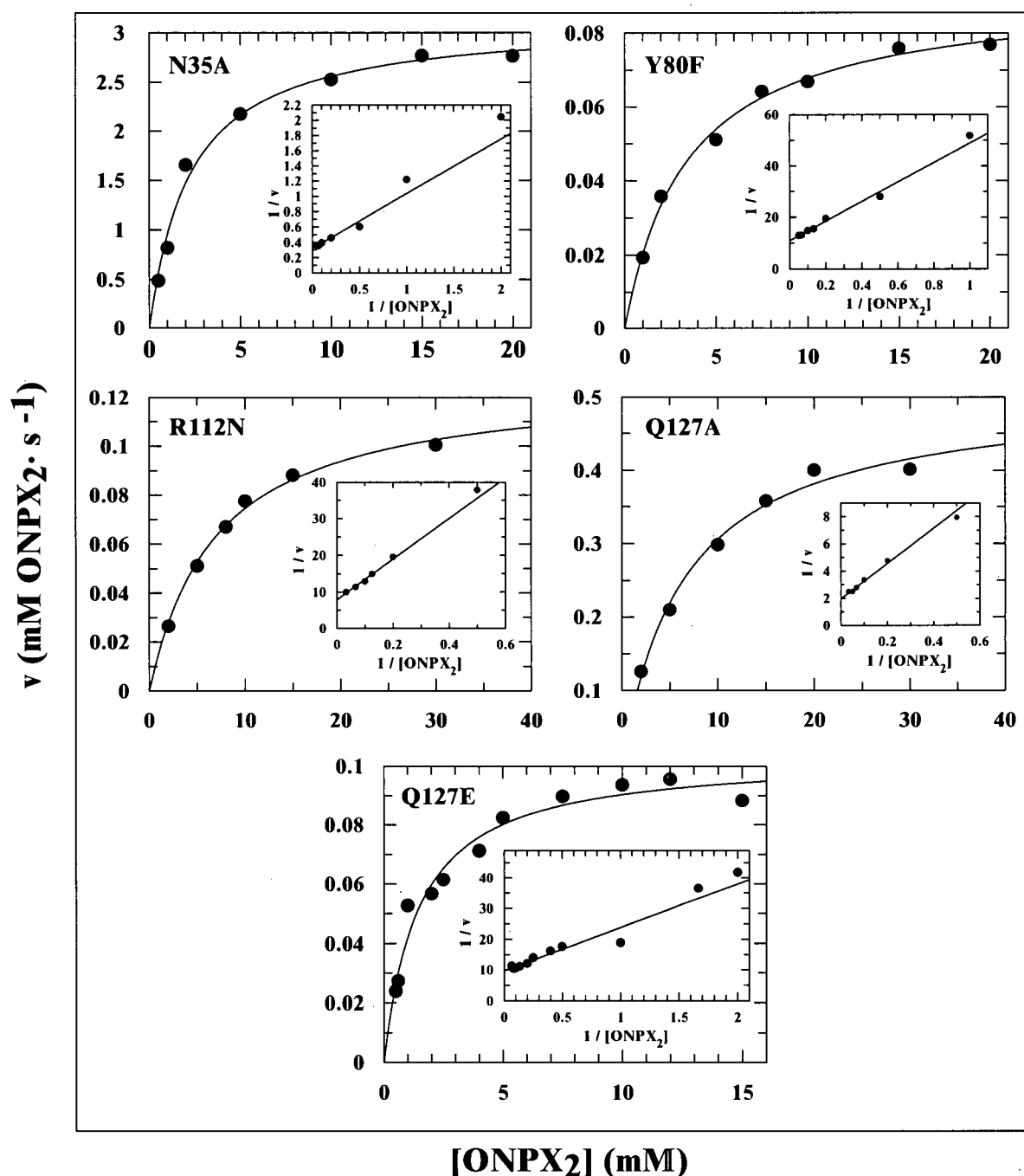
Figure 3.3. Michaelis-Menten plots for BCX mutant proteins at 40 °C and pH 6.0 reveals that each enzyme exhibits saturation kinetics towards the synthetic substrate ONPX$_2$. Furthermore, Lineweaver-Burke plots (inserted) are linear, indicating a lack of significant transglycosylation activity at elevated substrate concentrations. For each mutant, k_{cat} and K_m were extracted by nonlinear least squares fitting of the initial rates, v, to a standard Michaelis-Menten expression, whereas the value of k_{cat}/K_m was determined from the slope of the Lineweaver-Burke plot. These kinetic parameters are summarized in Table 3.3.

Table 3.3. Steady state kinetic parameters for the hydrolysis of ONPX$_2$ by WT and mutant BCX proteins[a].

Protein	k_{cat}[b] (s^{-1})	K_m[b] (mM^{-1})	k_{cat}/K_m[b] (s^{-1} mM^{-1})	Activity[c] (% of WT)	pK_{aGlu78}[d]	p$K_{aGlu172}$[d]	pH$_{optimum}$[e]
WT[f]	9.58	14.2	0.70	100 (103)	4.6 (4.6)	6.8 (6.7)	5.7
N35A	3.13	2.2	1.40	200 (207)	4.4 (4.5)	6.9 (6.9)	5.7
Y69F[g]	-	-	-	-	- (4.9)	- (8.3)	-
Y80F	0.09	3.5	0.03	4 (4)	4.8 (5.0)	7.7 (7.9)	6.3
R112N	0.13	7.0	0.02	3 (3)	4.5 (5.0)	7.8 (7.6)	6.2
Q127A	0.51	6.7	0.08	11 (11)	4.1 (4.2)	7.3 (7.3)	5.7
Q127E	0.10	1.5	0.07	10 (12)	3.6 (3.8)	6.5 (6.5)	5.1
N35D[h]	14.5	25.6	0.56	85 (190)	3.5 (5.7)[i]	5.8 (8.4)[i]	4.7
N35D/E172Q[h]	0.72	33.3	0.021	4	[j]	[j]	[j]
N35D/E78Q[g,h]	-	-	-	-	-	-	-
E172Q[f]	0.62	8.3	0.075	11	(5.1)[j]	-	[j]
E172C[f]	0.40	2.5	0.16	23	4.0[j]	[j,k]	[k]
E172D[f]	0.25	7.2	0.03	4	4.2	8.0	6.1
E78Q[l]	-	-	-	-	-	(4.2)[j]	-
E78C[l]	-	-	-	-	-	-	-
E78D[l]	0.005	14.0	0.0004	-	-	-	-

[a]Assays were carried out at pH 6.0 and 40 °C.

[b]Values of k_{cat}/K_m were taken from the slope of the Lineweaver-Burk plot, whereas values of k_{cat} and K_m were determined from a non-linear fit of the Michaelis-Menten equation. The differences between the measured k_{cat}/K_m and those calculated from the latter two parameters are small, reflecting the precision of the data fitting and the lack of significant transglycosylation activity at elevated substrate concentrations.

[c]Based on relative k_{cat}/K_m values, determined at pH 6.0 and 40 °C. Values in brackets are the ratios of the values of k_{cat}/K_m interpolated to the pH optimum of each enzyme.

[d]Apparent pK_a values were determined by fitting the data to the bell-shaped activity profiles shown in Figure 3.4. The pK_a of the acidic limb is attributed to Glu78 and that of the basic limb to Glu172. Corresponding pK_a values measured by NMR, and listed in Table 3.4, are indicated in parenthesis.

[e]pH$_{optimum}$ = (pK_{aGlu78} + p$K_{aGlu172}$) / 2.

[f]Data were taken from Lawson *et al.*, (1996) and/or McIntosh *et al.*, (1996).

[g]No detectable enzymatic hydrolysis.

[h]Data were taken from Chapter 4 and Joshi *et al.*, (2000a).

[i]N35D BCX follows a reverse protonation mechanism. See Chapter 4 and Joshi *et al.*, (2000a) for an extensive discussion.

[j]NMR and/or kinetic data are unavailable.

[k]The pH-dependent activity profile showed that the basic limb was invariant up to the limit of the assay conditions (pH 9) and hence the pK_a of Cys172 was undeterminable.

[l]Data were taken from Lawson *et al.*, (1996).

For comparison, Table 3.3 also summarizes kinetic data published previously for variants

of BCX with substitutions at positions 35, 78, and 172 (Joshi *et al.*, 2000a; Lawson *et al.*, 1996;

Lawson *et al.*, 1997; McIntosh *et al.*, 1996). As expected, mutation of the nucleophile Glu78 to

glutamine or cysteine abolishes the activity of BCX, while substitution with aspartic acid allows

a very small degree of hydrolysis to occur. In the case of activated substrates with better leaving

groups, such as $ONPX_2$, general acid catalysis is not absolutely required, and thus the same

substitutions at position 172 have less dramatic effects.

ii) pH-Dependence of Activity

To characterize further the mutant xylanases, their k_{cat}/K_m values for the hydrolysis of

$ONPX_2$ were measured as a function of pH at 40° C. There are several advantages for monitoring

this kinetic parameter rather than k_{cat} or K_m alone. First, since k_{cat}/K_m is the second-order rate

constant for the reaction of free enzyme and substrate, we are able to interpret its pH-dependence

in terms of ionization events related specifically to the unbound enzyme. This allows for a direct

comparison of the apparent pK_a values, extracted from bell-shaped k_{cat}/K_m versus pH activity

profiles, with those measured site-specifically for Glu78 and Glu172 by ^{13}C-NMR. The use of

k_{cat} would not have allowed for this comparison, as this first-order rate constant reflects bound

species including the enzyme-substrate, -intermediate and -product complexes. Parenthetically,

however, previous studies have shown that the k_{cat} and k_{cat}/K_m values of the WT enzyme towards

this neutral substrate have similar pH-dependencies due to K_m being essentially constant.

Second, since k_{cat}/K_m always reflects the events up to and including the first *irreversible* step in

the mechanism (in this case the initial C-O bond cleavage), its value will not be influenced by

potential changes in the *rate-determining* step (e.g. from glycosylation to deglycosylation) that

may result from active-site mutation. Third, and perhaps experimentally most important, it is also difficult to interpret K_m and k_{cat} values individually when competing transglycosylation reactions can potentially occur at elevated substrate concentrations. In contrast, the ratio of these kinetic constants, given by k_{cat}/K_m, may be accurately measured and interpreted from a pseudo-first order analysis of the reaction velocity under conditions of limited substrate.

Data summarizing the pH-dependence of k_{cat}/K_m for the hydrolysis of ONPX$_2$ by the mutant xylanases with measurable activity is presented in Table 3.3 and Figure 3.4. As readily seen in this figure, each of these enzymes exhibited a classical bell-shaped activity versus pH profile. Previous studies of WT BCX have shown that deprotonation of the nucleophile, Glu78 (pK_a 4.6), leads to the increase in activity on the acidic limb of this curve, while ionization of the general acid catalyst, Glu172 (pK_a 6.7), causes the loss in activity on the basic limb (McIntosh *et al.*, 1996; Miao *et al.*, 1994; Wakarchuk *et al.*, 1994a). As confirmed below using NMR methods, this assignment of kinetically-determined apparent pK_a values to the two catalytic residues remains valid for each BCX mutant studied herein. Replacement of an Ala for Asn in N35A BCX resulted in minimal changes in the pK_a values controlling both limbs of its activity profile (pK_a Glu78 = 4.4, pK_a Glu172 = 6.9). Thus, while the overall activity of N35A was doubled relative to WT BCX, its pH optimum remained unchanged at 5.7. The activity profile of Y80F BCX followed apparent pK_a values of 4.8 and 7.7 for the acidic and basic limbs, respectively. This resulted in a change in pH optimum of Y80F from 5.7 to 6.3, due mainly to the increase in the apparent pK_a value of Glu172 by one unit. Similarly, the pH optimum of R112N BCX shifted from 5.7 in the WT to a more basic value of 6.2. This was also due mainly to an elevation of the
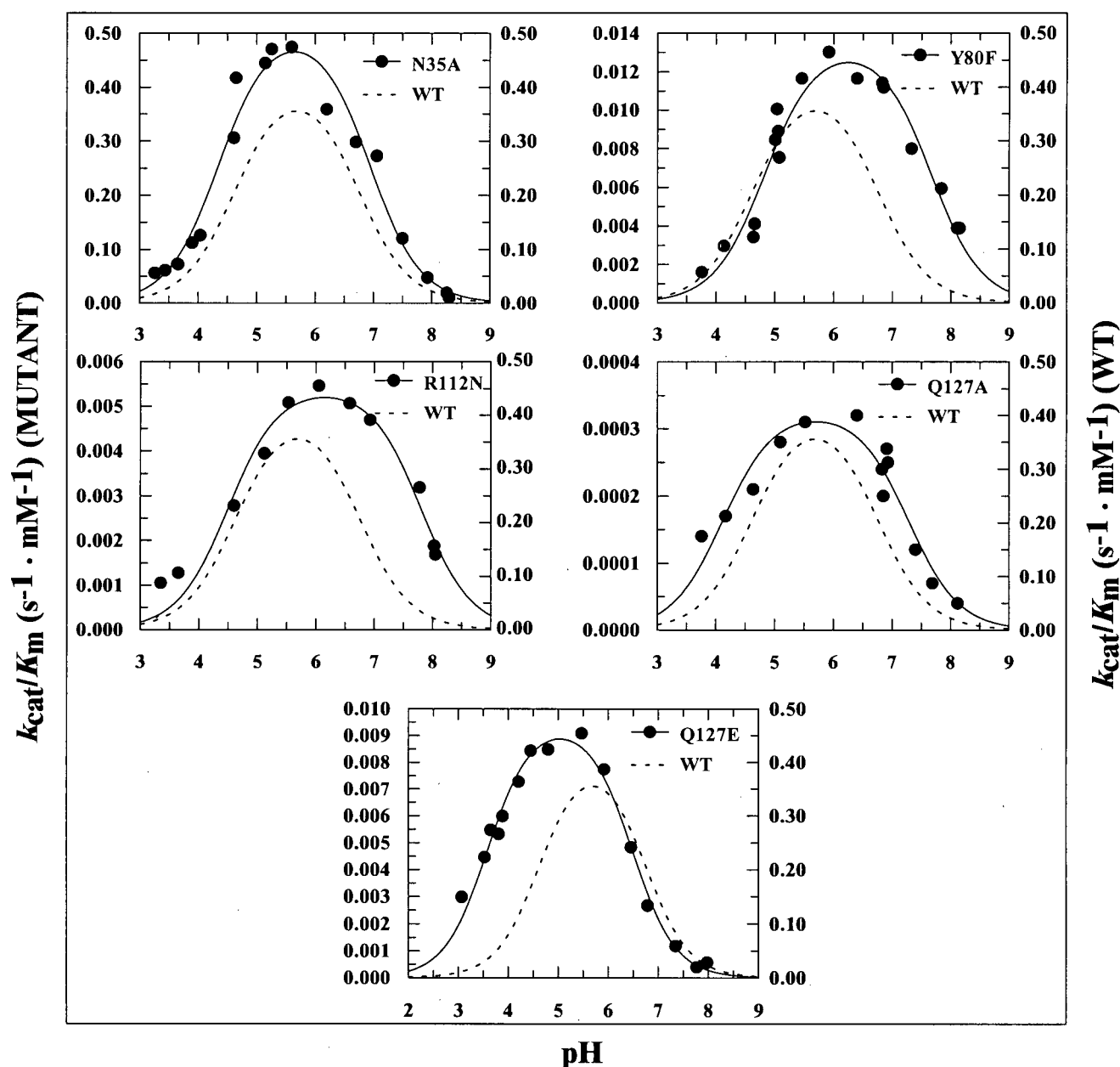
Figure 3.4. pH-dependence of k_{cat}/K_m for BCX mutant proteins ($\bullet$) at 25 °C towards the substrate ONPX$_2$. As confirmed by NMR spectroscopic studies, the acidic and basic limbs of the activity profiles follow the ionizations of Glu78 and Glu172, respectively. The pH optima of N35A and Q127A BCX remained unchanged at the WT value of 5.7 with an approximate doubling of relative activity of N35A BCX compared to WT. R112N and Y80F BCX functioned optimally under slightly more basic conditions with pH optima of 6.3 and 6.2 respectively while Q127E BCX showed optimal activity under more acidic conditions and had an optimum of 5.1. The data points, shown only for the mutant BCX proteins, were fitted (solid line) as described in Materials and Methods, and apparent pK_a values are listed in Table 3.3. The fitted profile for the WT enzyme (dashed lines) is characterized by a pH optimum of 5.7 and follows pK_a values of 4.6 and 6.7 (McIntosh *et al.*, 1996). Note the different ordinate scales for the WT (right) and mutant enzymes (left).

apparent pK_a value of Glu172 from 6.7 to 7.8, combined with a smaller shift of pK_a from 4.6 to 4.8 for Glu78.

The two substitutions at position 127, Q127A and Q127E, resulted in similar reductions in k_{cat}/K_m relative to WT BCX, but different pH-dependent activity profiles. The profile of Q127A followed apparent pK_a values of 4.1 and 7.3 for the acidic and basic limbs respectively. Thus, while its pH optimum did not change relative to WT BCX, its activity profile was broadened. The Q127E BCX mutant was different from the other mutants discussed so far in that it was a substitution where a negatively charged residue was introduced into the active-site. This resulted in a shift of the pH optimum of Q127E from 5.7 to a more acidic value of 5.1. Most notable was the decrease in the apparent pK_a value of the acidic limb, corresponding to the ionization of Glu78, by 1 pH unit from 4.6 to 3.6, combined with a smaller decrease of 0.3 units for basic limb (Glu172). Other studies have shown that the substitution of Asn35 by a negatively charged Asp also shifts the pH optimum of BCX to a more acidic value of 4.6 (Chapter 4 ; Joshi *et al.*, 2000a).

In summary, the active-site substitutions altered the pH-activity profile of BCX, both in terms of pH optima and/or the apparent pK_a values of the acidic and basic limbs. In particular, the mutations Y80F and R112N led to a small elevation in the pH optimum, due primarily to an increase in the pK_a assignable to Glu172. The reverse trend occurred with Q127E, with the pK_a of Glu78 being most influenced. Since the pH optima of the mutant enzymes are shifted relative to WT BCX, Table 3.3 also provides a comparison of their maximum k_{cat}/K_m values at 40 °C. These relative activities were comparable to those discussed previously for measurements made at a fixed pH of 6.0, and indicated that, with the exception of N35A, mutation of active-site residues generally impaired the catalytic ability of BCX under all pH conditions.

iii) Pre-Steady State Kinetics

Each of the xylanases was analyzed by rapid stopped-flow methods to determine if the rate-determining step had changed from glycosylation to deglycosylation as a result of mutation. Using $ONPX_2$ as a substrate, none of the proteins analyzed showed the presence of a diagnostic pre-steady state burst phase (data not shown). Hence, it appears that glycosylation is the rate-limiting step for WT BCX and all mutants examined towards $ONPX_2$ and that the values listed for k_{cat} in Table 3.3 correspond to the k_2 rate constant in Scheme 3.1.

In addition to $ONPX_2$, the substrate 2,5-$DNPX_2$ was tested because its better leaving group (pK_a 7.22 *versus* 5.15, respectively) (Tull and Withers, 1994) would allow deglycosylation, if rate-limiting, to become more dominant and thus kinetically visible (Namchuk and Withers, 1995). In the case of Y80F BCX, stopped-flow kinetic studies clearly indicated a pre-steady state burst with this readily hydrolyzable substrate (Figure 3.5). Thus with this system, k_2 (glycosylation) > k_3 (deglycosylation), and the formation and accumulation of the enzyme-intermediate is kinetically observable. This result is consistent with the low K_m value (0.060 mM) (Zechel *et al.*, 1998) observed for this substrate compared to WT (2.2 mM) (Lawson *et al.*, 1997). Fitting of the first-order rate constants (k_{obs}) determined at each substrate concentration to equation 3.8, yielded a value of k_2/K_d of 0.72 mM^{-1} s^{-1}. This closely matches the previously measured value of 0.70 mM^{-1} s^{-1} for the corresponding second-order rate constant k_{cat}/K_m of Y80F BCX reacting with 2,5-$DNPX_2$ (Zechel *et al.*, 1998), indicating a rapid binding equilibrium before catalysis (k_{-1} > k_2) in Scheme 3.1. The results obtained for Y80F were, therefore, in excellent overall agreement with those obtained previously by Zechel *et al.*, (1998)
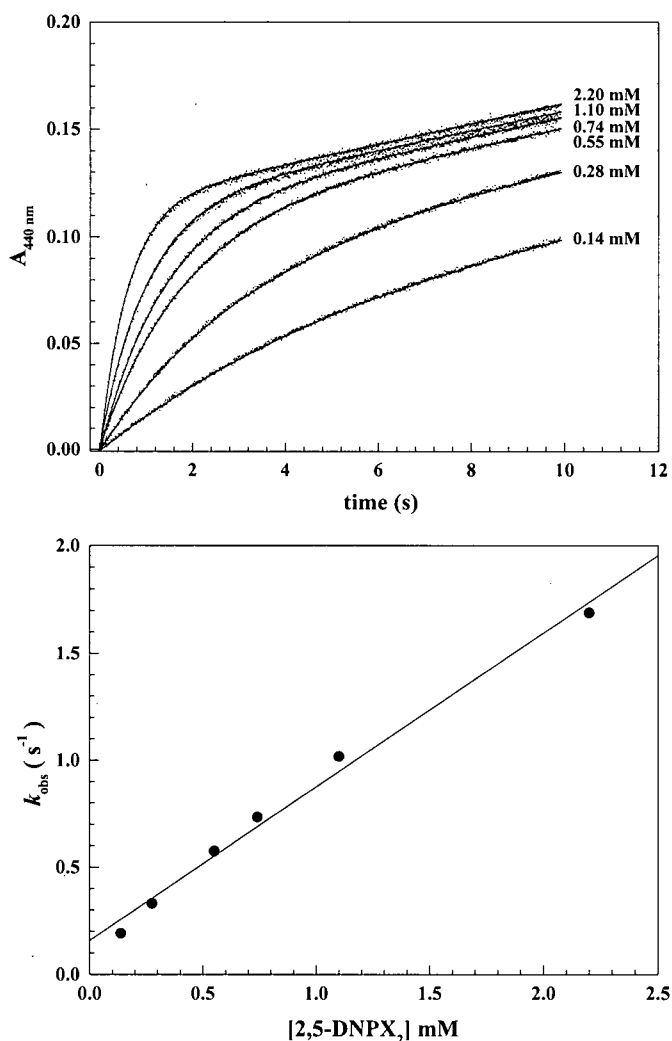
Figure 3.5. Pre-steady state kinetic analysis of the hydrolysis of 2,5-DNPX$_2$ by Y80F BCX at 25 °C and pH 6.0 monitored by stopped-flow UV-vis spectroscopy. This system showed an initial exponential pre-steady state burst phase, indicating the accumulation of a glycosyl-enzyme intermediate, followed by a linear steady state phase due to its subsequent turnover (upper plot). First-order rate constants for the exponential pre-steady state phase (k_{obs}) were determined at each substrate concentration by fitting the experimental data in the upper plot, indicated by minute solid circles, to an expression with an exponential and linear term (—). Values of k_{obs} (●) were then plotted as a function of 2,5-DNPX$_2$ concentration in order to determine the second-order rate constant k_2/K_d of 0.72 mM^{-1} s^{-1} (lower plot).

in their founding study of the use of time-resolved electrospray ionization mass spectrometry for the accurate determination of pre-steady state kinetic parameters.

3.3.2 Direct Measurement of the pK$_a$ Values of Glu78 and Glu172 by ^{13}C-NMR

To correlate the pH-activity profiles with the ionizations of the catalytic residues, ^{13}C-NMR was utilized to measure directly the pK$_a$ values of Glu78 and Glu172 in each of the mutant proteins. Specifically, the carbonyl ^{13}C chemical shifts of the Glu and Gln sidechains were monitored in selectively isotopically labelled proteins over the course of a pH titration (Figure 3.6). The assignments of these resonances were based upon previous studies of WT BCX (McIntosh *et al.*, 1996), and were confirmed by the notable exchange broadening of the resonance of Glu172 centered at its pK$_a$ value. As seen previously for WT BCX, the titration curves of Glu78 and Glu172 were multiphasic in the case of each mutant xylanase (McIntosh *et al.*, 1996). Note that two or more ionizable groups may show coupled or biphasic titration curves if either the microscopic pK$_a$ or the chemical shift of one is dependent upon the ionization state of the other (Appendix I ; Shrager *et al.*, 1972). The first case is analogous to the classic case of a dibasic acid in which each carboxyl has two microscopic pK$_a$ values corresponding to the neutral and charged states of its interacting partner. The second case reflects the possibility that the chemical shift of one residue can be sensitive to the ionization state of another, for example, through electric field effects or structural perturbations. As previously (Joshi *et al.*, 2000a; Joshi *et al.*, 2000c), I fitted the titration curves measured for each mutant to simple equations describing sequential ionization equilibria in order to extract apparent or macroscopic pK$_a$ values. The apparent pK$_a$ value that corresponded to the largest positive chemical shift change (ionized *versus* neutral) of each Glu residue was attributed to reflect its own ionization, while

those that contributed to smaller chemical shift changes were assigned to the ionization equilibria of neighboring residues. In parallel, these titration data were also analyzed according to a model of microscopic pK_a values (Appendix I).

The pH-titration of N35A BCX showed that both Glu78 and Glu172 exhibited biphasic titration behaviour (Figure 3.6 and Table 3.4). Two apparent pK_a values were observed for Glu78. The first, with a major chemical shift change of +3.09 ppm, followed a pK_a value of 4.5 and was assigned to the ionization of Glu78 itself. The second, with a minor chemical shift change of +0.12 ppm, followed a pK_a value of 6.8 and reflected the ionization of Glu172. Similarly, the titration curve of Glu172 followed two apparent pK_a values. The first, with a minor chemical shift change of +0.44 ppm followed a pK_a value of 4.9 and thus reflected the ionization of Glu78. The second, with a major chemical shift change of +2.81 ppm at a pK_a value of 6.9, represented the ionization of Glu172 itself. The pH-dependent spectra of other mutants (Y69F, Y80F, Q127A and R112N BCX) were assigned and analyzed in a similar manner to N35A. In each case, the titration curves for Glu78 and Glu172 were consistently biphasic. Although the magnitudes of the spectral changes varied between mutants, a major positive chemical shift could always be identified as reflecting the protonation equilibrium of the glutamate whose resonance was being followed. Thus, the mutation of Tyr80 to Phe (Y80F BCX) yielded predominant pK_a values of 5.0 for Glu78 and 7.9 for Glu172. In R112N BCX, Glu78 and Glu172 titrated with pK_a values of 5.0 and 7.6 respectively. The titration of Q127A BCX yielded a pK_a value of 4.2 for Glu78 and a pK_a value of 7.3 for Glu172. Finally, although the pK_a values of Y69F BCX could not be determined from kinetic pH-rate profiles due to the inactivity of the protein, they were readily measured to be 4.9 (Glu78) and 8.3 (Glu172) by ^{13}C-NMR methods.
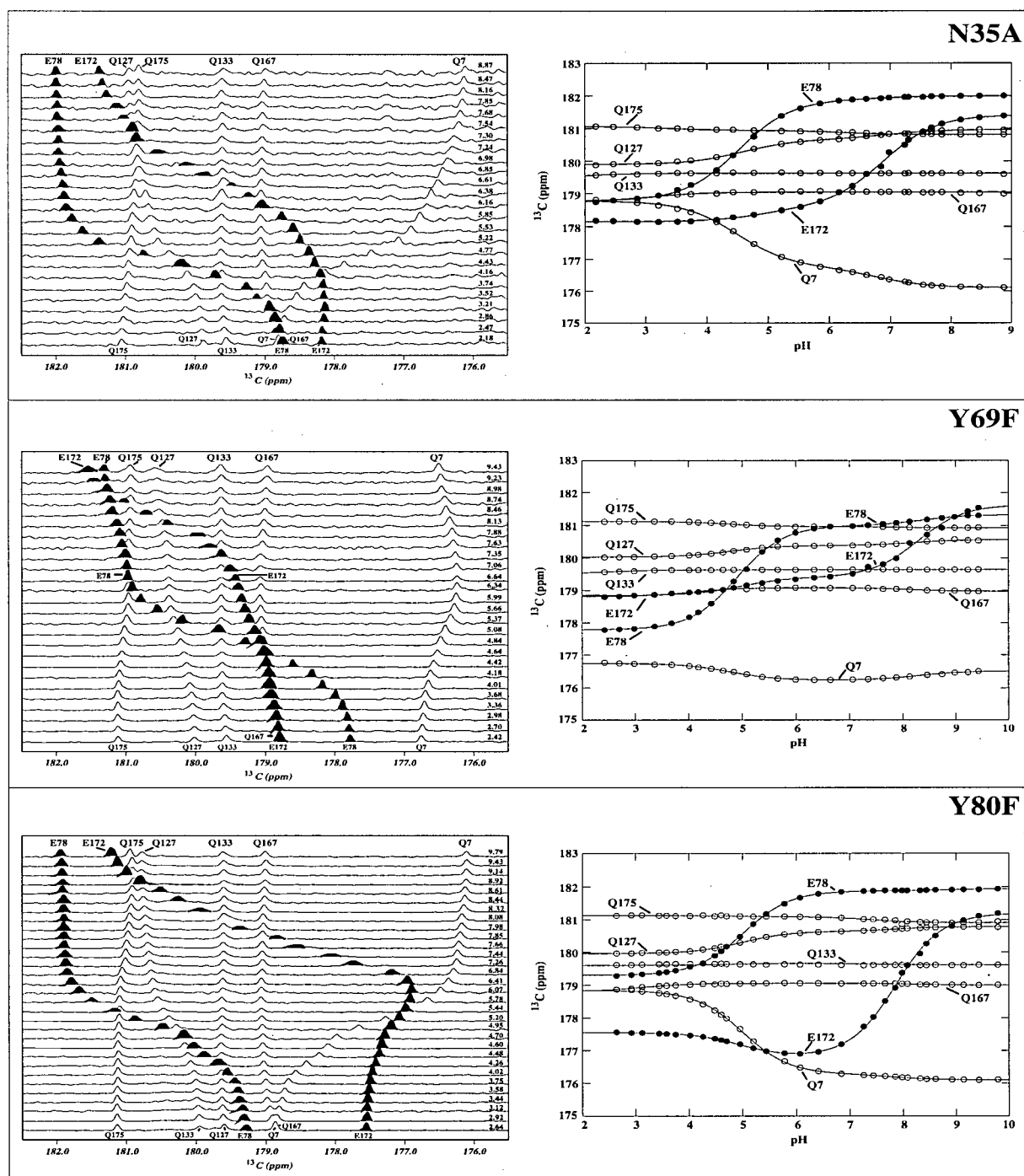
Figure 3.6. ^{13}C-NMR spectra of mutant BCX proteins recorded as a function of pH at 25 °C. The peaks corresponding to Glu78, Glu172 and, in the case of Q127E BCX, Glu127 are shaded in black or grey, respectively, for emphasis. Spectral assignments are based on a previous analysis of WT BCX (McIntosh *et al.*, 1996) and pH values are listed above each spectrum (right-hand side). Apparent pK_a values were determined by fitting the data for the two catalytic Glu (●) and five Gln (○) carbonyl groups to an equation describing the pH-dependence of the chemical shift of a residue to one or more sequential ionization events. Data used for the fitting of Glu127 in Q127E BCX are also indicated by an open-circle (○) symbol (continued on next page).

Figure 3.6. ^{13}C-NMR spectra of mutant BCX proteins recorded as a function of pH at 25 °C. The peaks corresponding to Glu78, Glu172 and, in the case of Q127E BCX, Glu127 are shaded in black or grey, respectively, for emphasis. Spectral assignments are based on a previous analysis of WT BCX (McIntosh *et al.*, 1996) and pH values are listed above each spectrum (right-hand side). Apparent pK_a values were determined by fitting the data for the two catalytic Glu (●) and five Gln (O) carbonyl groups to an equation describing the pH-dependence of the chemical shift of a residue to one or more sequential ionization events. Data used for the fitting of Glu127 in Q127E BCX are also indicated by an open-circle (O) symbol (continued from previous page).

Table 3.4. Experimentally measured apparent pK_a values of WT and mutant BCX proteins obtained from ^{13}C-NMR pH titrations.[a]

Protein	pK_{aGlu78}	$\delta\Delta^c$	$pK_{aGlu172}$	$\delta\Delta^c$	$\Delta pK_{aGlu78}{}^d$	$\Delta pK_{aGlu172}{}^d$
WT[b]	<u>4.6</u>	+2.80 ppm	4.6	+0.44 ppm	0	0
	6.5	+0.33 ppm	<u>6.7</u>	+2.78 ppm		
N35A	<u>4.5</u>	+3.09 ppm	4.9	+0.44 ppm	-0.1	
	6.8	+ 0.12 ppm	<u>6.9</u>	+2.81 ppm		+0.2
Y69F	<u>4.9</u>	+3.21 ppm	5.0	+0.55 ppm	+0.3	
	8.9	+0.33 ppm	<u>8.3</u>	+2.22 ppm		+1.6
Y80F	<u>5.0</u>	+2.58 ppm	4.9	-0.75 ppm	+0.4	
	8.8	+0.06 ppm	<u>7.9</u>	+4.40 ppm		+1.2
R112N	<u>5.0</u>	+3.96 ppm	4.8	-0.16 ppm	+0.4	
	7.5	-0.71 ppm	<u>7.6</u>	+3.67 ppm		+0.9
Q127A	<u>4.2</u>	+3.52 ppm	4.5	+0.42 ppm	-0.4	
	7.6	-0.06 ppm	<u>7.3</u>	+3.03 ppm		+0.6
Q127E[e]	<u>3.8</u>	+2.88 ppm	3.8	-0.25 ppm	-0.8	
	6.6	+0.34 ppm	<u>6.5</u>[f]	+3.08 ppm		-0.2
	8.6[g]	+0.21 ppm	9.0	+1.74 ppm		
N35D[h]	4.2	+0.96 ppm	4.0	+0.76 ppm		
	<u>5.7</u>	+2.69 ppm	5.5	-0.32 ppm	+1.1	
	8.4	-0.39 ppm	<u>8.4</u>	+3.09 ppm		+1.7
N35D-2FXb[h]	2.9[j]	-0.03 ppm	<u>1.9</u>[i]	+1.63 ppm	[j]	
	9.3[j]	-0.18 ppm	<u>3.4</u>[i]	+0.48 ppm		< -5.0[i]
			9.0	+0.10 ppm		
WT-2FXb[b]	[k]	[k]	<u>4.2</u>	+1.58 ppm	[k]	-2.5
E172Q[b,l]	<u>5.1</u>	+3.93 ppm	5.1[j]	-0.48 ppm[j]	+0.5	[i]
E78Q[b,l]	[k]	[k]	<u>4.2</u>	+3.81 ppm	[k]	-2.5

[a]The major apparent pK_a, assigned to the ionization of the given residue is underlined. An error in the pK_a value of ± 0.1 pH units is estimated from the error in pH measurements.
[b]Data were taken from McIntosh *et al.*, (1996).

[c]The δΔ value refers to the magnitude and direction of the chemical shift change upon deprotonation of the listed residue. The error in chemical shift is estimated to be ± 0.015 ppm.

[d]$\Delta pK_a = pK_a$ mutant - pK_a WT (Differences are calculated using the major pK_a values of the mutant and WT).

[e]Data for Glu127 were fit to give pK_a values of 3.7 (δΔ = +0.74 ppm), 6.4 (δΔ = +1.10 ppm) and 8.4 (δΔ = +1.52 ppm).

[f]The assignment of the major pK_a for Glu172 in Q127E BCX is tentative. Simultaneous fitting of the titration curves measured for Glu172 and Glu127 yields microscopic pK_a values of 6.5 and 8.5 for Glu172 and 6.8 and 8.7 for Glu127 (corresponding to ionization in the presence of neutral or charged partner).

[g]The third and minor pK_a value of 8.6 for Glu78 was determined from fitting the data from pH 5-10 only.

[h]Data were taken from Chapter 4 and Joshi *et al.*, (2000a). Asp35 yielded pK_a values of 3.7 (δΔ = +2.13 ppm), assigned to its titration, and 5.6 (δΔ = +1.07 ppm), attributed to the ionization of Glu78.

[i]Glu172 and Asp35 are assigned to titrate as a coupled pair, with the first pK_a ~ 1.9-3.4 and the second > 9. $\Delta pK_{aGlu172}$ is relative to the unmodified N35D BCX Chapter 4 and Joshi *et al.*, (2000a).

[j]Change in chemical shift does not reflect ionization of the residue itself since it is has either been substituted with a residue with an unionizable side chain or because it has been modified by covalent attachment to the inhibitor.

[k]No observable pH-dependent change in chemical shift.

[l]E78Q and E172Q are in the background of *Bacillus subtilis* xylanase, which differs from BCX by the non-perturbing substitution of T147S on the surface of the protein (McIntosh *et al.*, 1996).

Interestingly, with Y80F and R112N BCX, minor chemical shift changes due to the protonation of the adjacent glutamate were negative in sign.

The titration behaviour of Q127E BCX was markedly different than the other proteins analyzed due to the presence of an additional Glu residue in the active-site. Note that this new Glu replaces Gln127, which is directly hydrogen bonded to Glu78 in WT BCX. The resonance assignment of Glu78 was straightforward based on its chemical shift at neutral pH and its titration behaviour. Although the resonance assignments of Glu172 and Glu127 were difficult to make from chemical shift and titration behaviour alone, the exchange-broadening observed in all BCX variants for Glu172 was used to distinquish the signals from these two glutamic acids. The titration curve of Glu78 was triphasic and followed three pK_a values. The first, with a major change in chemical shift change of +2.88 ppm, fitted to a pK_a value of 3.8 and was assigned to the ionization of Glu78 itself. The second, with a minor change in chemical shift of +0.34 ppm followed a pK_a value of 6.6 and was tentatively attributed to the ionization of Glu172. The third,

with a minor change in chemical shift of +0.21 ppm, followed a pK_a value of 8.4 and was

tentatively ascribed to be due to the ionization of Glu127. The titration curve of Glu172 was

triphasic in nature and reflected three ionizations. The first, corresponding to a minor change in

chemical shift of -0.25 ppm, followed a pK_a value of 3.8, and likely reflected the ionization of

Glu78. The second, corresponding to the largest change in chemical shift of +3.08 ppm, followed

a pK_a of 6.5 and was assigned tentatively to the ionization of Glu172 itself. The third,

corresponding to a change in chemical shift of +1.74 ppm, followed a pK_a value of 9.0 and was

attributed to Glu127. The titration curve of Glu127 in Q127E BCX was also triphasic and

followed three apparent pK_a values. The first pK_a value of 3.7, accompanied by a minor change

in chemical shift of +0.74 ppm, likely corresponded to the ionization of Glu78. The second pK_a

value of 6.4 was accompanied by a chemical shift change of +1.10 ppm and was assigned to an

indirect perturbation due to Glu172. Finally, the third pK_a value of 8.4, accompanied by the

largest change in chemical shift of +1.52 ppm, likely corresponded to the ionization of Glu127

itself. The pK_a value for Glu127 of either 9.0, from the titration curve of Glu172, or the pK_a

value of 8.4, from the titration curve of Glu127 may be underestimated since no distinct titration

plateau or baseline was observed in the basic pH range of the titration. We could not

unambiguously assign the pK_a values of Glu127 and Glu172 from these NMR data as both

showed titrations near pH 6.5 and > 8 with pronounced chemical shift changes. However, in

support of these tentative assignments, the pH-activity profile of Q127E showed apparent pK_a

values of 3.6 and 6.5 that, by comparison to all other mutants studied herein, can be attributed to

Glu78 and Glu172, respectively.

The ^{13}C-NMR resonances of the side chain δ carbonyls of all Gln residues were also

detected in the ^{13}C-NMR spectra of all of the proteins analyzed. Their presence is due to the

metabolic interconversion of glutamic acid to glutamine in *Escherichia coli*. The ^{13}C chemical shifts of the non-ionizable Gln residues are pH-dependent due to the influence of other titratable side chains within the protein. Thus these served as reporter groups to further verify the pK_a values measured for the glutamic acid residues. For example, in Q127E BCX the pH-dependent chemical shift of Gln7 followed three pK_a values, namely 3.51 ($\delta\Delta = 0.67$ ppm), 6.40 ($\delta\Delta = 1.06$ ppm), and 9.04 ($\delta\Delta = 0.27$ ppm). These were assigned to reflect the ionizations of Glu78, Glu172, and Glu127, respectively. Similarly, in R112N BCX, the pH-dependent chemical shift of Gln7 predominantly followed two pK_a values; namely a pK_a of 4.9 ($\delta\Delta = 1.90$ ppm) due to the ionization of Glu78, and a pK_a of 7.4 ($\delta\Delta = 0.20$ ppm) due to the ionization of Glu172. In the WT protein, the resonance of Gln7 followed the titrations of Glu78 (pK_a 4.5, $\delta\Delta = 2.09$ ppm) and Glu172 (pK_a 6.6, $\delta\Delta = 0.47$ ppm) (McIntosh *et al.*, 1996).

In general, the pK_a values of Glu78 and Glu172 determined from the pH-dependence of k_{cat}/K_m are in close agreement to those directly measured by ^{13}C-NMR (Table 3.3). This indicates that the ionization states of Glu78 and Glu172 (free enzyme) primarily dictate the pH-dependence of activity in all of the mutant proteins analyzed. In the case of R112N, there is a small discrepancy of 0.5 units between the kinetically and NMR determined pK_a values of Glu78, which may reflect the scatter in the kinetic data. Nevertheless, the fact that both methods yield very comparable results allows for detailed interpretation of the pH-dependent mechanism of BCX and the electrostatic interplay of Glu78 and Glu172 in catalysis.

3.3.3 Structures of Mutant BCX Proteins

The crystal structure of Y69F BCX was solved previously at pH 7.5 to a resolution of 1.5 Å with an R-factor of 18.8 % (Sidhu *et al.*, 1999). The structure was found to be very similar to

WT BCX with an overall r.m.s. deviation of 0.09 Å for main chain atoms. Hence, the substitution at position 69 had little effect upon the three-dimensional structure of this protein (Figures 3.7 and 3.8, Table 3.5). Of the minor changes in the active-site of this mutant, a notable case is the shift of Wat A to within hydrogen bonding distance to Asn35 $O^{\delta 1}$. Wat A and Wat B (arbitrarily named) are solvent atoms observed in the active-site of BCX, proposed to play a role in catalysis (Sidhu *et al.*, 1999).

The crystal structure of Y80F BCX was determined at pH 7.5 to a resolution of 1.6 Å with an R-factor of 18.1 %. The structure showed an overall r.m.s difference of only 0.12 Å and 0.29 Å for main chain and side chain atoms, respectively, when compared to WT BCX. Most of the changes observed for side chain atoms involved residues located on the surface of the protein. In the active-site of the enzyme, the phenyl ring of the newly introduced Phe80 is shifted relative to Tyr80 in the WT protein as a result of 4° and 9° rotations in the χ_2 and χ_3 angles of the side chain, respectively. Other minor changes in the Y80F BCX structure include small rotations in the side chains of Glu172 ($\Delta\chi_1 = 3°$) and Asn35 ($\Delta\chi_2 = 7°$) compared to the WT protein. More notably, Wat B, which is held in place in the free WT enzyme by hydrogen bonding interactions with Tyr80 O^{η} and Gln127 $N^{\epsilon 2}$ (Sidhu *et al.*, 1999; Wakarchuk *et al.*, 1994a), is no longer detected in the structure of Y80F BCX. Upon formation of the glycosyl-enzyme intermediate in WT BCX, this water moves to within hydrogen bonding distance of the general base Glu172 $O^{\epsilon 2}$, and thus appears to acts as a nucleophile in the deglycosylation step of the reaction (Sidhu *et al.*, 1999). The absence of a corresponding crystallographically-identifiable water molecule in Y80F BCX provides a simple explanation for the change in the rate-determining step from glycosylation to deglycosylation with 2,5-DNPX$_2$ as a substrate for this
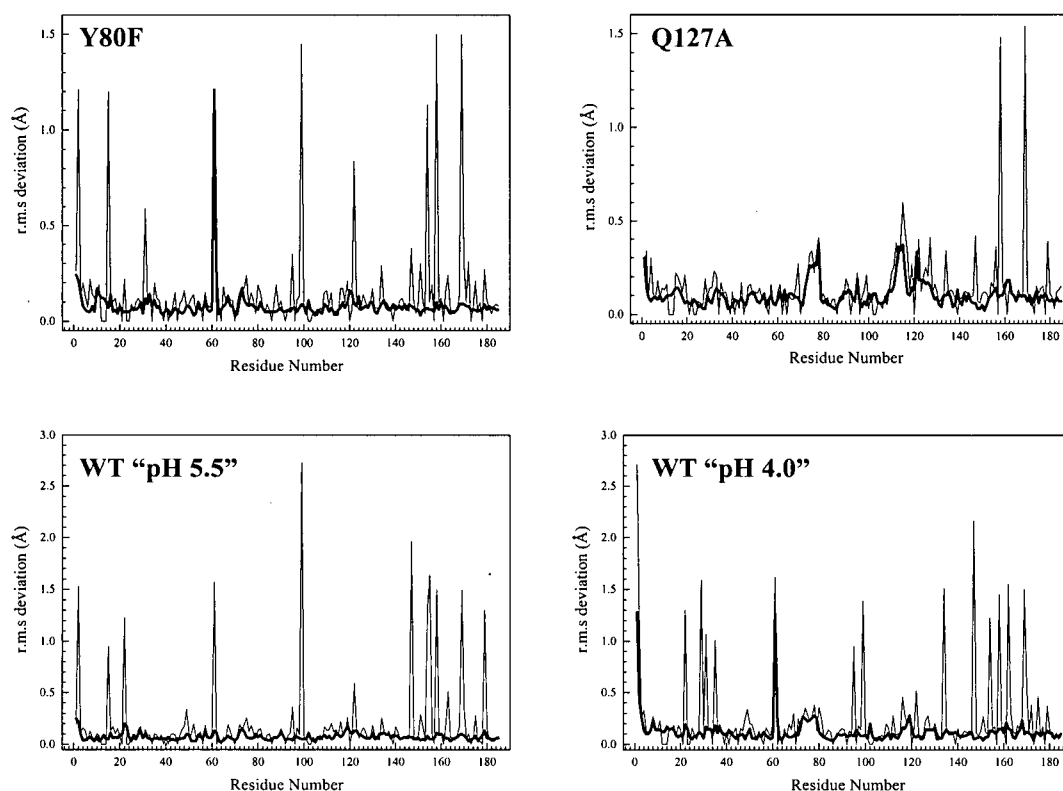
Figure 3.7. The r.m.s deviations of main chain (thick line) and side chain (thin line) heavy atoms of Y80F, Q127A, and WT BCX at apparent pH values of "5.5" and "4.0", compared to the WT species at pH 7.5. Structures were superimposed by a least-square fitting of the main chain and side chain atoms of all residues. The site of mutation was excluded from the plot of each respective mutant. A large majority of the observed side chain deviations, as well as that of the backbone at the peptide of Asn61/Gly62, are attributed to alternate conformations of surface residues. Any relevant structural deviations are discussed with the text. The main chain and side chain r.m.s deviations are respectively: 0.12 Å and 0.29 Å for Y80F BCX; 0.12 Å and 0.23 Å for Q127A BCX; 0.08 Å and 0.41 Å for WT "pH 5.5" BCX; 0.18 Å and 0.42 Å for WT "pH 4.0" BCX.
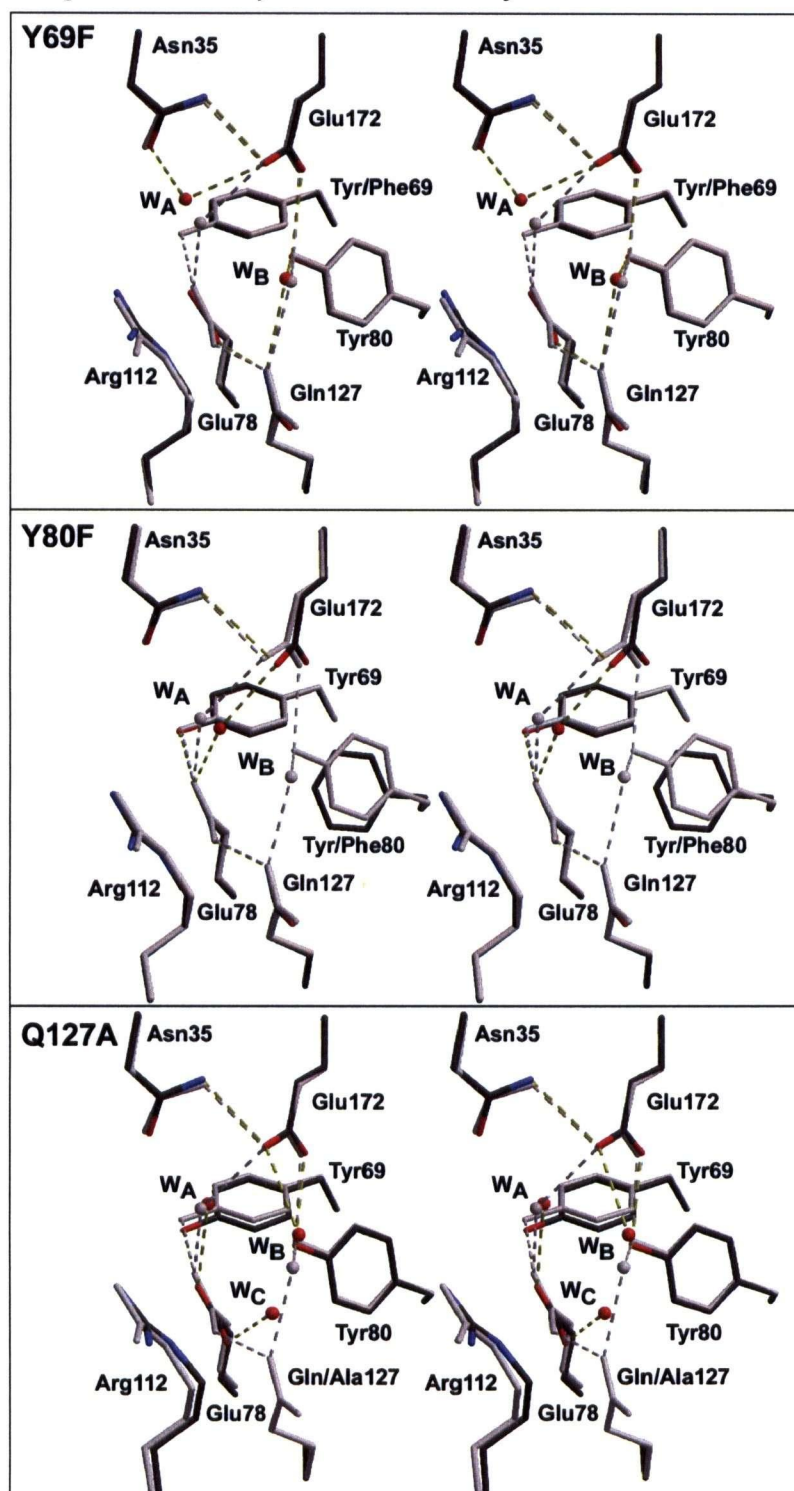
Figure 3.8. Stereo-illustrations of the structural conformations of key active-site residues of BCX mutants superimposed upon those of the WT protein at pH 7.5. The mutant structures are shown in dark gray, with potential hydrogen bonds indicated by broken yellow lines, protein and water oxygen atoms in red, and nitrogen atoms in blue. The WT reference structure, including all atoms and potential hydrogen bonds, is off-white. See Table 3.5 and Figure 3.7 for interatomic distances and r.m.s.d plots, respectively. Data for Y69F BCX is from Sidhu *et al.*, (1999).

Table 3.5. Interatomic distances within the active-site of WT and mutant BCX proteins.

Interaction	Distances (Å)			
Active-site residues	WT[a]	Y69F[a]	Y80F[b]	Q127A[b]
Glu78 $O^{\varepsilon2}$ – Asn35 $O^{\delta1}$	6.4	6.9	6.6	6.8
Glu78 $O^{\varepsilon1}$ – Gln127 $N^{\varepsilon2}$ (Ala127 C^{β})	2.7	2.7	2.7	(4.0)
Glu78 $O^{\varepsilon2}$ – Tyr69 O^{η} (Phe69 C^{ζ})	2.6	(3.1)	2.6	2.6
Glu78 $O^{\varepsilon2}$ – Arg112 N^{ε}	6.2	6.3	6.2	5.7
Glu78 $O^{\varepsilon2}$ – Glu172 $O^{\varepsilon2}$	5.6	6.2	5.6	5.9
Glu172 $O^{\varepsilon2}$ – Asn35 $N^{\delta2}$	3.1	3.2	3.8	3.2
Glu172 $O^{\varepsilon1}$ – Tyr80 O^{η} (Phe80 C^{ζ})	2.7	2.8	(4.1)	2.9
Glu172 $O^{\varepsilon2}$ – Arg112 N^{ε}	7.1	6.9	7.2	6.9
Asn35 $N^{\delta2}$ – Asp11 $O^{\delta2}$	6.1	6.0	5.5	5.4
Asn35 $N^{\delta2}$ – Arg112 N^{ε}	7.8	7.8	7.9	7.9
Water molecules				
Glu78 $O^{\varepsilon2}$ – Wat A	2.9	3.9	2.8	3.2
Glu78 $O^{\varepsilon1}$ – Wat B	4.4	4.5	c	5.3
Glu172 $O^{\varepsilon2}$ – Wat A	3.0	3.1	2.9	2.9
Glu172 $O^{\varepsilon2}$ – Wat B	3.8	3.7	c	3.1
Tyr80 O^{η} (Phe80 C^{ζ}) – Wat A	3.2	3.9	(3.9)	3.1
Tyr80 O^{η} (Phe80 C^{ζ}) – Wat B	2.8	2.9	c	3.1
Asn35 $O^{\delta1}$ – Wat A	3.8	3.2	4.4	4.0
Asn35 $N^{\delta2}$ – Wat A	4.7	4.4	5.3	4.8
Tyr69 O^{η} (Phe69 C^{ζ}) – Wat A	4.0	(4.7)	4.0	3.8
Gln127 $N^{\varepsilon2}$ (Ala127 C^{β}) – Wat A	5.2	6.0	4.7	(4.9)
Gln127 $N^{\varepsilon2}$ (Ala127 C^{β}) – Wat B	3.1	3.2	c	7.3

[a]Structural coordinates used for distance measurements were obtained from the RCSB Protein Data Bank (Bernstein *et al.*, 1977), PDB identification number 1XNB for WT BCX (Wakarchuk *et al.*, 1994a) and 2BVV for Y69F BCX (Sidhu *et al.*, 1999).
[b]Structural coordinates will be deposited in the RCSB Protein Data Bank.
[c]Wat B was not present in the crystal structure of Y80F BCX.

mutant enzyme (discussed later). Wat A, which does not play a role in the second step of the reaction in BCX, is, however, present.

The structure of Q127A BCX was also determined at pH 7.5 to a resolution of 1.8 Å with an R-factor of 16.4 %. The overall three-dimensional fold of the protein was retained upon substitution as was evident from a main chain and side chain r.m.s deviation of 0.12 Å and 0.23 Å, repectively, between Q127A and WT BCX. Changes in the active-site of this mutant were confined mostly to the region surrounding the substitution. The position of Glu78 was perturbed as a result of the loss of its interaction with Gln127. Changes of 5° and 7° in χ_1 and χ_2 respectively were primarily responsible for the movement of Glu78 in towards the cavity created by the alanine substitution at position 127. Also as a consequence of the mutation, a new solvent molecule (Wat C) was found to reside within hydrogen bonding distance of Glu78 $O^{\varepsilon 1}$ (3.1 Å). The loss of a hydrogen bonding interaction between Gln127 $N^{\varepsilon 2}$ and Wat B led to the distance between this water molecule and Glu172 being decreased by 0.7 Å. Another change that surrounded the mutation was a rotation of 10° in the χ_3 angle of Arg112, bringing the positive charge of its N^{ε} atom 0.5 Å closer to Glu78 $O^{\varepsilon 2}$.

Crystallization trials were performed under a variety of conditions with N35A, R112N and Q127E BCX, yet were largely unsuccessful. Should the structures of these proteins be obtained at a later date, their coordinates will be deposited in the RCSB Protein Data Bank.

3.3.4 Structures of WT BCX as a Function of pH

The structure of WT BCX was solved at apparent pH values of "5.5" and "4.0" to assess the possibility of pH-dependent structural changes within the active-site of the enyzme. To perform these studies, crystals were grown at pH 7.5 and transferred to a new buffer at reduced

pH. After allowing approximately four hours for equilibration, data were collected for each xylanase sample. Thus the exact pH within the crystal was not measured, but assumed to reflect that of the final buffer. This assumption is denoted by the use of quotation marks. The "pH 5.5" structure was determined at a resolution of 1.6 Å with an R-factor of 18.4 %. The "pH 4.0" structure was determined at a resolution of 1.9 Å with an R-factor of 18.0 %.

At an apparent pH of 5.5, corresponding to the pH optimum of BCX, virtually no structural changes were present in the active-site as evident by a main chain r.m.s difference of 0.08 Å relative to the pH 7.5 WT BCX structure. (Figures 3.7 and 3.9, Table 3.6). This is somewhat surprising as the ionization state of Glu172 (pK_a 6.7) should differ in the two crystalline states. However, when the pH was lowered further to 4.0, the main chain r.m.s difference versus the WT increased to 0.15 Å, and the active-site showed a number of structural perturbations. In particular, the Asn35 side chain was rotated almost 22° (χ_1) such that it was no longer able to hydrogen bond to Glu172 ($\Delta\chi_2 = 5°$) since the distance between these two residues increased by 0.8 Å to 3.9 Å. The position of the Tyr80 side chain also changed, albeit not so dramatically, such that the hydrogen bonding distance to the side chain of Glu172 increased from 2.7 Å to 3.4 Å. Interestingly, the catalytic water (Wat B) proposed to function in the second step of hydrolysis moved almost 2 Å such that it formed stronger hydrogen bonds with both Glu78 (2.6 Å) and Glu172 (2.9 Å). Note that these changes involve primarily Glu172, rather than Glu78 (pK_a 4.6). This suggests that the pH values of the crystals may have been slightly higher than expected such that Glu172 becomes fully protonated in the lowest pH form while Glu78 remains ionized. In the crystal structure of a family 11 xylanase from *Trichoderma reesei* (XYNII), a notable conformational change is observed for the acid/base catalyst Glu177 when the pH of the crystal is lowered from 6.5 to 4.0 (Torronen and Rouvinen, 1995). The Glu177 side chain flips
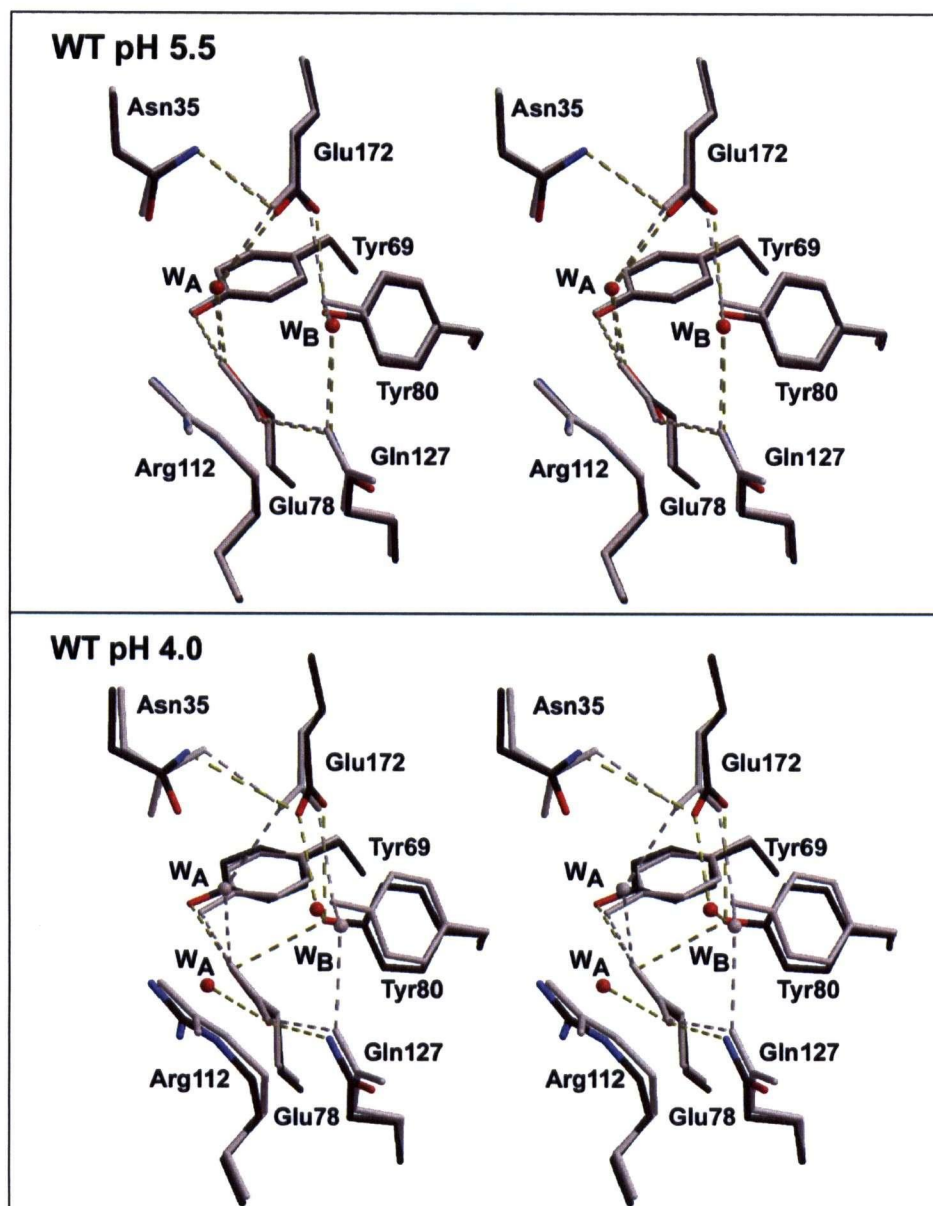
Figure 3.9. Stereo-diagrams of the structural conformations of active-site residues of WT BCX at apparent pH values of "5.5" and "4.0" superimposed upon those of WT BCX at pH 7.5. The low pH structures are shown in dark gray, with potential hydrogen bonds indicated by broken yellow lines, protein and water oxygen atoms in red, and nitrogen atoms in blue. The pH 7.5 WT reference structure, including all atoms and potential hydrogen bonds, is off-white. See Table 3.6 and Figure 3.7 for interatomic distances and r.m.s.d plots.

Table 3.6. Interatomic distances within the active-site of WT BCX at different pH values.

Interaction	Distances (Å)		
Active-site residues	pH 7.5[a]	"pH 5.5"[b]	"pH 4.0"[b]
Glu78 $O^{\epsilon 2}$ – Asn35 $O^{\delta 1}$	6.4	6.6	8.0
Glu78 $O^{\epsilon 1}$ – Gln127 $N^{\epsilon 2}$	2.7	2.7	2.7
Glu78 $O^{\epsilon 2}$ – Tyr69 O^{η}	2.6	2.5	2.9
Glu78 $O^{\epsilon 2}$ – Arg112 N^{ϵ}	6.2	6.2	6.6
Glu78 $O^{\epsilon 2}$ – Glu172 $O^{\epsilon 2}$	5.6	5.5	5.8
Glu172 $O^{\epsilon 2}$ – Asn35 $N^{\delta 2}$	3.1	3.3	3.9
Glu172 $O^{\epsilon 1}$ – Tyr80 O^{η}	2.7	3.0	3.4
Glu172 $O^{\epsilon 2}$ – Arg112 N^{ϵ}	7.1	7.0	7.2
Asn35 $N^{\delta 2}$ – Asp11 $O^{\delta 2}$	6.1	6.0	5.9
Asn35 $N^{\delta 2}$ – Arg112 N^{ϵ}	7.8	7.8	7.9
Water molecules			
Glu172 $O^{\epsilon 2}$ – Wat A	3.0	2.8	5.4
Glu172 $O^{\epsilon 2}$ – Wat B	3.8	3.7	2.9
Tyr80 O^{η} – Wat A	3.2	3.3	4.3
Tyr80 O^{η} – Wat B	2.8	2.9	2.9
Asn35 $O^{\delta 1}$ – Wat A	3.8	3.6	5.7
Asn35 $N^{\delta 2}$ – Wat A	4.7	4.5	6.6
Glu78 $O^{\epsilon 2}$ – Wat A	2.9	3.1	3.5
Glu78 $O^{\epsilon 1}$ – Wat B	4.4	4.5	2.6
Tyr69 O^{η} – Wat A	4.0	4.0	5.6
Gln127 $N^{\epsilon 2}$ – Wat A	5.2	5.2	3.8
Gln127 $N^{\epsilon 2}$ – Wat B	3.1	3.2	3.8

[a]Structural coordinates used for distance measurements were obtained from the RCSB Protein Data Bank (Bernstein *et al.*, 1977), PDB identification number 1XNB for WT BCX at pH 7.5 (Wakarchuk *et al.*, 1994a).
[b]pH values of the buffer into which protein was transferred for four hours after crystallization at pH 7.5.

outward in the same manner that Asn35 does in BCX. Tyr88 (analogous to Tyr80 in BCX) also changes position such that it can hydrogen bond to the nucleophile Glu86.

3.3.5 Theoretical pKₐ Calculations

In addition to the catalytic glutamic acids, the pK_a values of all remaining carboxyl and imadazole groups in BCX have also been measured (Chapter 2; Joshi *et al.*, 1997). Using this reference data, a variety of protocols for theoretical pK_a calculations were examined. Overall, the best agreement with experimental results was obtained using uniform dielectric constants of 8 and 80 for the protein and solvent, respectively. Values calculated (measured in Chapter 2) were Glu78: 2.9 (4.6); Glu172: 5.9 (6.7); Asp 4: 3.5 (3.0); Asp 11: 2.5 (2.5); Asp 83: < 0 (< 2); Asp 101: 0.2 (< 2); Asp 119: 3.0 (3.2); Asp121: 3.9 (3.6); His149: 3.8 (< 2.3); His156 5.0 (~ 6.5); and the C-terminal W185: 0.9 (~ 2.7). Reducing the protein dielectric to 4 yielded a more accurate theoretical pK_a value of 7.2 for Glu172, yet a poorer value of 2.7 for Glu78; increasing the protein dielectric to 12 had the opposite effect, giving predicted values of 5.3 for Glu172 and 3.0 for Glu78. The use of a dielectric of 8 for well-ordered residues and 16 for those involved in crystal contacts or with B-values higher than 20 (Nielsen *et al.*, 2000) produced poorer values for the two glutamic acids, as did explicit inclusion of crystallographically-bound waters. Increasing the theoretical ionic strength of the solvent from 0 to 150 mM changed the pK_a value of Glu78 from 2.4 to 3.4 due to reduced screening of favorable interactions with the positively charged residues in BCX; the increases in the pK_a values calculated for Glu172 were about half as large due to its titration at higher pH values where the net charge of the protein is less positive.

Although not quantitatively exact, the theoretical and measured pK_a values for BCX generally agree qualitatively. Notably, abnormally low pK_a values for Asp83 and Asp101 are

predicted. Both residues have pK_a values below the practical limit of the NMR titrations, indicating that each is always charged within the context of the native enzyme. Structurally, Asp83 is involved in a buried ion pair with Arg136, whereas Asp101 is stabilized in its ionized state by a network of neutral hydrogen-bonding interactions. In contrast, one discrepancy is seen with His149, which remains in a neutral state ($pK_a < 2.3$) under all experimental conditions examined. The pK_a value of this buried residue proved difficult to calculate using an automated protocol as it is hydrogen bonded to an internal water molecule. Inclusion of the water, combined with manual correction of the tautomerization state of His149 reduced the theoretical pK_a value from 3.8 to < 0, thus emphasizing the importance of correctly defining hydrogen-bonding networks with a protein for electrostatic calculations. The pK_a values calculated for the catalytic glutamic acids in the WT and mutant xylanases are summarized in Table 3.9 and will be referred to within the discussion section.

3.4 DISCUSSION

3.4.1 Structural Roles of Active-Site Residues

Several highly conserved active-site residues are important for the hydrolysis of xylosidic substrates by BCX. Although synthetic substrates with aryl leaving groups that lack interactions with the +1 subsite and beyond were used in this study, the results and trends presented here are consistent with those initially reported in the first major mutational analysis of BCX where the natural substrate xylan was used (Wakarchuk et al., 1994a). (According to the nomenclature suggested by Davies et al., (1997), cleavage is defined to occur between the −1 and +1 subsites). While natural and synthetic substrates can both form potential interactions with the −2 and −1 subsites on the enzyme, the synthetic substrate does not contain the same interaction in the +1 subsite and beyond due to the presence of a single aryl leaving group instead of a chain of xylose subunits). For example, Y69F BCX shows no detectable activity on both xylan and ONPX$_2$, whereas R112N and Y80F BCX show somewhat different results towards natural and synthetic substrates. Specifically, R112N and Y80F BCX hydrolyze xylan at 12 % and ~ 0.01 % of WT levels, respectively, whereas their activities towards the synthetic substrate ONPX$_2$ are reduced by 4 % and 3 %, respectively. This difference may reflect additional important interactions between Tyr80 and xylose subunits occurring beyond the site of cleavage (or experimental difficulties in performing assays with less characterizable substrates such as xylan). The nature of such interactions remains to be established as no xylanase structure solved to date contains substrates occupying these subsites (Joshi et al., 2000a; Sidhu et al., 1999; Wakarchuk et al., 1994a). Nevertheless, the reductions in activity seen for the series of mutants on both substrates, except at position 35 (discussed later), emphasize the importance of these residues in hydrolysis and the necessity for their absolute conservation amongst the family 11 xylanases.

Kinetic analyses of mutants of BCX using well-characterized synthetic substrates, combined with crystallographic structures of these proteins, allows for delineation of the individual functions of the active-site residues in this xylanase. The availability of the structure of a catalytically compromised acid/base mutant of BCX reacted with xylobiose (E172C-Xb) (Wakarchuk *et al.*, 1994a) provides information regarding potential ground state interactions between protein and substrate. In parallel, the more recently solved structure of WT BCX bound to the mechanism-based inhibitor DNP2FXb (WT-2FXb) (Sidhu *et al.*, 1999) yields information regarding the glycosyl enzyme-intermediate, including an unusual distortion of the sugar ring in the -1 position that may facilitate formation of an oxocarbenium ion-like transition state (Figure 3.10). A comparison of these complexes reveals potential structural interactions that may occur in the transition states for glycosylation and deglycosylation. To a first approximation, changes in K_m resulting from the mutations studied herein should reflect perturbations more akin to ground state interactions while changes in k_{cat} would be more related to altered interactions occurring in the transition state. This generalization is not without pitfalls in the case of BCX, however, since the mechanism by which it hydrolyzes xylosidic substrates involves multiple steps.

The side chain of Tyr69 is hydrogen bonded to Glu78. Based on the complete inactivity of the Y69F BCX variant, it was initially concluded that Tyr69 might play a role in positioning this nucleophilic glutamate (Wakarchuk *et al.*, 1994a). Subsequent elucidation of the crystal structure of Y69F BCX, however, showed nearly exact superposition of active-site residues, thus excluding this possibility (Sidhu *et al.*, 1999) (Figure 3.8). However, close structural contacts observed in the WT glycosyl-enzyme intermediate, WT-2FXb, between Tyr69 O^η and both Glu78 $O^{\varepsilon 2}$ and the endocyclic oxygen (O5) of the proximal xylose residue in the −1 subsite,

indicated a more direct catalytic role for Tyr69 (Figure 3.10 and Table 3.6). It was proposed that

through specific charge rearrangement, Tyr69 considerably stabilizes the oxocarbenium-ion like

transition state via a direct dipolar interaction between its O^η and the partially positively charged

O5 atom of the proximal xylose residue. Absence of this crucial interaction in Y69F BCX results

in severe crippling of the mutant enzyme.

Tyr80 O^η is involved in a hydrogen bonding interaction with both Glu172 $O^{\epsilon 1}$ and Wat B

(Figure 3.8 and Table 3.5). Furthermore, inspection of the crystal structures of WT-2FXb and

E172C-Xb shows that Tyr80 O^η may interact weakly with the O5 atom of the proximal xylose

subunit in the former (*distance* = 3.6 Å) but not in the latter (*distance* = 4.6 Å) (Figure 3.8 and

Table 3.6). Given this difference, Tyr80 may selectively stabilize the proximal saccharide in the

transition state and glycosyl-enzyme intermediate relative to the enyzme-substrate complex.

Perhaps more importantly, previous studies of WT-2FXb have also revealed that the side chain

of Tyr80 helps position the catalytic water (Wat B) proposed to function as a displacing

nucleophile in the deglycosylation step of the hydrolytic reaction. Indeed, an analogous water

molecule is not detected in the crystallographic structure of Y80F BCX (Sidhu *et al.*, 1999). The

apparent absence of this water is consistent with the observation that deglycosylation is the rate-

limiting step for hydrolysis of the reactive 2,5-DNPX$_2$ substrate by this variant xylanase (Figure

3.5).

In addition to Tyr69, the sidechain of Glu78 is hydrogen bonded to the primary amide of

Gn127 (O^ϵ-$N^{\epsilon 2}$ distance = 2.7 Å) in the WT enzyme (Figure 3.8 and Table 3.5). To probe the

role of this interaction, Gln127 was mutated to an alanine and a glutamic acid. The former

mutation, Q127A, resulted in the movement of the side chain of Glu78 in towards the cavity

formed at the site of substitution. This is the only structure where the side chain of Glu78

experiences a positional change, albeit small. An additional bound solvent molecule (Wat C) is also found, satisfying the hydrogen bonding requirements of the Glu78 carboxylate. Examination of both liganded structures indicates a potential hydrogen bonding interaction between Gln127 $N^{\varepsilon 2}$ and the O3 atom of the proximal xylose unit (Figure 3.10 and Table 3.6). These interactions are weaker (3.5 Å in WT-2FXb and 3.7 Å in E172C-Xb) than those observed for some of the other residues and therefore may not contribute as much to catalysis. However, when combined with the change in position of Glu78, these could account for the reduction in activity of Q127A to 11 % of WT.

Changing the residue at position 127 to a glutamic acid led to a similar overall reduction in activity to that observed for Q127A BCX. Given that the apparent pK_a value of Glu127 is > 6.5 (Table 3.4), it must be protonated near the pH optimum of 5.1 measured for this mutant and should resemble the WT glutamine in conformation and hydrogen-bonding potential. No crystal structure was solved, but any structural perturbations of the nucleophile Glu78, which may lead to the observed reductions in k_{cat} and K_m due the amino acid substitution, are likely to be subtle. Alternatively, as discussed below, electrostatic coupling between Glu127 and Glu172 results in a perturbation of the pK_a of the latter. This in turn may also lead to a change in the activity of the protein, either by altering the ability of Glu172 to serve as a general acid/base catalyst or by changing the population of protein with this residue in its active protonated form.

The primary amide of Asn35 is involved in a hydrogen bonding interaction with the carboxyl group of the acid/base catalyst Glu172 (Figure 3.9 and Table 3.6). This interaction
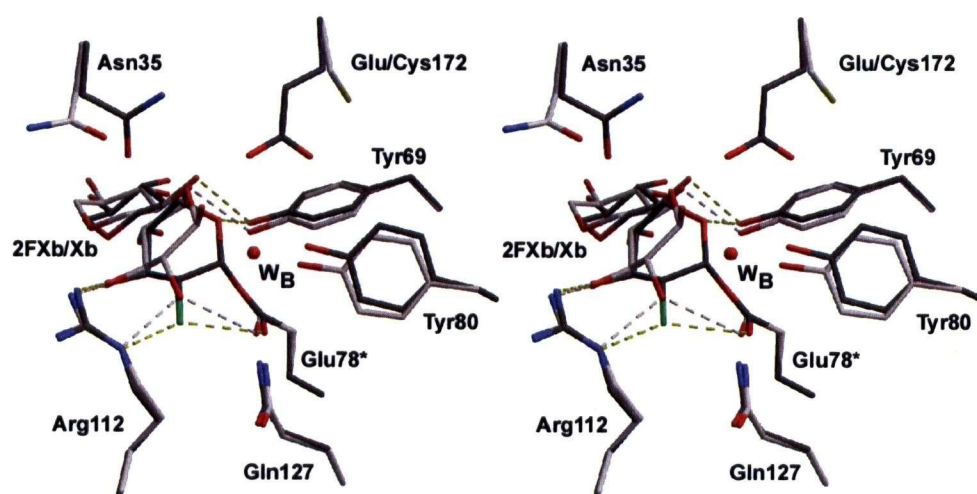
Figure 3.10. A stereo-illustration of active-site residues of WT-2FXb BCX (dark grey) superimposed upon those of the non-covalent enzyme-substrate complex E172C-Xb BCX (off-white). The former is a trapped colvalent glycosyl-enyzme intermediate, whereas the latter is a non-covalent complex of xylotetraose with a catalytically inactive form of the enzyme. Potential hydrogen bonds between the enzyme and the saccharide (2FXb or Xb) are indicated by yellow broken lines for WT-2FXb and broken off-white lines for E172C-Xb. Oxygen atoms are shown in red, nitrogen atoms in blue, fluorine atoms in green and sulfur atoms in yellow. The catalytic water (W_B) is shown only for WT-2FXb. See Table 3.7 for specific interatomic distances.

Table 3.7. Protein-saccharide distances within the active-sites of WT-2FXb[a] and E172C-Xb[a] BCX.

Interaction	Distances (Å)	
	WT-2FXb	E172C-Xb
Tyr69 O^{η} – proximal xylose O5	3.0	4.0
Tyr69 O^{η} – distal xylose O2	2.8	2.9
Arg112 N^{ε} – proximal xylose O2 (F2)	3.2	3.0
Arg112 $N^{\eta 2}$ – proximal xylose O3	3.3	3.2
Gln127 $N^{\varepsilon 2}$ – proximal xylose O2 (F2)	3.5	3.7
Tyr80 O^{η} – proximal xylose O5	3.6	4.6
Asn35 $O^{\delta 1}$ – proximal xylose O5	4.5	5.3
Glu78 $O^{\varepsilon 1}$ – proximal xylose O2 (F2)	2.9	3.4

[a]Structural coordinates used for distance measurements were obtained from the RCSB Protein Data Bank (Bernstein *et al.*, 1977) identification numbers 1BVV for WT-2FXb BCX and 1BCX for E172C-Xb (Wakarchuk *et al.*, 1994a).
[b]Atoms that are substituted at the 2-position in the DNP2FXb ligand are indicated in parenthesis.

appears modest, however, as judged both structurally (3.1 Å) and by the lack of a significant

perturbation in the pK_a value of Glu172 upon its removal by mutation (Table 3.4). Strikingly,

replacement of Asn35 with an Ala leads to a doubling of overall activity of N35A BCX

compared to WT as judged by k_{cat}/K_m. Substitution of an Asp at this site also leads to a 20%

increase in activity (Chapter 4; Joshi *et al.*, 2000a). Thus, these mutations at position 35 are

distinct in that they do not impair the catalytic ability of BCX. A possible explanation at least for

the reduced K_m and k_{cat} values of N35A BCX towards $ONPX_2$ comes from a comparison of the

crystal structures of WT-2FXb and E172C-Xb (Figure 3.10). In the former (a glycosyl-enzyme

intermediate with a distorted proximal sugar) no direct interactions between Asn35 and the

xylose subunits are observed, while in the latter (an inactive enzyme-substrate complex), the side

chain of Asn35 is displaced outwards. This displacement may be due to the loss of the glutamic

acid hydrogen-bonding partner at position 172 and/or to the avoidance of an unfavourable van

der Waals contact with the bound sugar. That is, when the structure of WT BCX is superimposed

upon that of E172C-Xb, the distance between Asn35 $O^{\delta 1}$ in the former and the O5 atom of the

proximal xylose residue in the latter is 3.2 Å. Thus, in the catalytically competent enzyme-

substrate complex, a potentially destabilizing interaction may exist between Asn35 and the

bound substrate. This distance increases to 4.5 Å in WT-2FXb as a result of the proximal sugar

adopting a boat conformation. Substitution of an alanine at position 35 would eliminate this

contact, thus improving substrate binding to N35A BCX. This would lead to a favorable decrease

in K_m yet an unfavorable reduction in k_{cat}; predominance of the latter results in the overall

increase in k_{cat}/K_m relative to the WT enzyme.

Arg112 is positioned approximately equidistant from both Glu78 and Glu172 in the

unliganded WT structure and does not make direct contacts with either catalytic residue (Figure

3.9 and Table 3.6). In the structures of WT-2FXb and E172C-Xb, however, the side chain of Arg112 is observed to make potential hydrogen-bonding interactions with the O2 (or F2) and O3 atoms of the proximal xylose saccharide (Figure 3.10). Since these interactions are comparable in the enzyme-substrate complex and glycosyl-enzyme intermediate, I speculate that the significant reduction in the k_{cat} value of R112N BCX mutant results from the loss of preferential transition state interactions between Arg112 N^ε and the exocyclic oxygens of the proximal saccharide. Interactions of this magnitude are reasonable, since an in depth study of *Agrobacterium faecalis* β-glucosidase has shown that the 2-position of a dinitrophenyl glycoside substrate can contribute almost 4.3 kcal mol^{-1} and 5.3 kcal mol^{-1} of transition-state binding energy for the glycosylation and deglycosylation steps respectively (Namchuk and Withers, 1995), while interactions at the 3-position can contribute another 2.2 kcal mol^{-1} at both transition-states.

3.4.2 pH-Dependent Activity

The pH optima of BCX proteins are set by the pK_a values of the nucleophile Glu78 and the acid/base catalyst Glu172. With the exception of N35D BCX (Chapter 4; Joshi *et al.*, 2000a) the pK_a values determined from the activity profiles matched those determined site-specifically for Glu78 and Glu172 by NMR (Table 3.3). Hence, the factors that determine the pK_a values of Glu78 and Glu172 primarily dictate the pH-dependent activity of BCX. Any modifications to the local and global environments of residues 78 and 172 therefore result in changes in the pH optimum of the enzyme.

i) Roles of Ionizable Residues

The presence of ionizable groups in the active-site of BCX influences the pK_a values of both Glu78 and Glu172. Removal of a positive charge contributed by Arg112 resulted in an increase in the pH optimum of the enzyme from 5.7 to 6.2. NMR measurements showed that this shift came about as a result of increases in the pK_a values of Glu78 and Glu172 by 0.4 and 0.9 units, respectively (Table 3.4). This was expected as the positive charge on Arg112 could electrostatically stabilize the conjugate base forms of both Glu residues, thereby serving to lower their pK_a values. What is less obvious, however, is the greater effect that this mutation has upon the pK_a of Glu172 compared to Glu78 in spite of it being closer to Glu78 by ~ 1 Å (Table 3.5).

In the case of Q127E BCX, introduction of a negatively charged Glu residue (Glu127) adjacent to Glu78 serves to decrease the pH optimum of this protein from 5.7 to 5.1 units. This reflects the decrease in pK_a value of Glu78 by almost one unit (the largest observed decrease amongst the series of active-site residue mutants studied here) while the apparent pK_a of Glu172 remains essentially unchanged. Since the pK_a of Glu78 is significantly lower than that of Glu127, at its pH optimum a majority of the BCX population is in a state where Glu78 is ionized yet Glu127 is neutral. Hence, Glu127 is protonated and, similar to WT Gln127, can donate a charge stabilizing hydrogen bond to Glu78. The observation that the pK_a value of Glu78 is 3.8 in the mutant versus 4.6 in the WT enzyme suggests that a neutral glutamic acid provides a more stabilizing hydrogen bond than does glutamine. This behaviour is, however, difficult to examine further in light of the complexities associated with analyzing the coupled ionization equilibria of three interacting groups (Chapter 4; Appendix I; Joshi *et al.*, 2000a). Nevertheless, the decrease in the pK_a of Glu78 most likely arises from the donation of a charge-stabilizing hydrogen bond from the side chain of Glu127, conversely the high pK_a value of ~ 8.4 reported for this newly

introduced Glu residue must reflect the unfavourable juxtaposition of two negatively charged

residues.

In Chapter 4 and in Joshi *et al.*, (2000a) I report that the analogous mutation of Q127E

BCX, namely N35D BCX (i.e. carboxyl adjacent to 172), has a profound influence upon the pK_a

values of both the nucleophile and the acid/base catalyst. Instead of placing a negatively charged

residue near the nucleophile, a negatively charged Asp residue was placed beside the acid/base

catalyst Glu172. This resulted in an increase in the pK_a values of both Glu78 and Glu172 to 5.7

and 8.4, respectively. Counter-intuitively, however, the pH optimum had decreased to 4.6 instead

of increasing to the expected value of ~ 7. The pH-dependent activity of N35D BCX followed

the pK_a values of the newly introduced Asp residue (pK_a 3.7) and Glu78 (pK_a 5.7) instead of

Glu78 and Glu172 as in WT BCX. After extensive analysis, it was determined that Glu78 was

still the nucleophile and that Asp35 and Glu172 were functioning together to perform the role of

the acid/base catalyst using a "reverse protonation" mechanism.

ii) Roles of Neutral Polar Residues

The mechanisms by which neutral polar residues (e.g. those which do not ionize within

the pH range studied) influence the pH-dependent activity of BCX appear to be more subtly

manifested. Removal of a hydrogen bond to Glu172 contributed by Asn35 was achieved through

mutation of this residue to an Ala. The mutation resulted in no change in the pH optimum of the

enzyme nor any perturbations in the pK_a values of Glu78 and Glu172. While this observation is

somewhat surprising, it is possible that a new solvent molecule occupies the cavity created by the

mutation and provides a hydrogen bond to Glu172. Nevertheless, this indicates that the hydrogen

bonding interaction contributed by Asn35 is not essential in establishing and maintaining the pK_a

values of Glu78 and Glu172. The position of Asn35 also varies in some of the BCX structures solved (Y80F, WT pH 4.0, E172C-Xb BCX). This may indicate a certain degree of structural flexibility and suggests that the interaction between Asn35 and Glu172 is relatively weak.

Surprisingly, removal of the hydrogen bond contributed by Gln127 to the nucleophile Glu78 influenced the pK_a values of both catalytic residues in opposite directions instead of only affecting Glu78 as expected. The pK_a value of Glu78 decreased from 4.6 to 4.2 while that of Glu172 increased from 6.7 to 7.3 when Gln127 was mutated to an Ala. This resulted in the pH optimum remaining the same as WT. The lower pK_a observed for Glu78 was somewhat unexpected as a hydrogen bond to Glu78 should serve to stabilize preferentially the conjugate base form of the acid. Removal of this stabilizing interaction should lead to either no change or an increase in the pK_a value of Glu78. It is possible that a new solvent molecule (Wat C in Figure 3.8), observed in the structure of Q127A to occupy the position corresponding to the Gln127 side chain in WT BCX, serves to better stabilize the ionized form of Glu78. Alternatively, removal of the glutamine side chain may expose Glu78 to the higher dielectric constant of the ionic solvent and thus reduces the unfavourable (Born energy) partial burial of this residue. Although there was a minor perturbation in the positioning of Glu78, the precise nature by which the mutation leads to an increase in the pK_a value of Glu172 is difficult to rationalize given the numerous potential interactions that exist within the active-site of this xylanase.

The side chain of Tyr80 is positioned such that it can donate a hydrogen bond to Glu172 at pH 7.5. Removal of this hydrogen bond by mutation to a Phe results in an increase in the pH optimum from 5.7 to 6.3 and increases in the pK_a values of Glu78 and Glu172 from 4.6 to 5.0 and 6.7 to 7.9, respectively. As expected from the structure of BCX, the side chain of Tyr80 clearly contributes a charge stabilizing hydrogen bond to Glu172. The smaller increase in the pK_a

value of Glu78 upon mutation of Tyr80 to Phe can be rationalized by examination of the structure of WT BCX at "pH 4". At this lowered pH, the side chain of Tyr80 shifts slightly such that it can weakly hydrogen bond with either Glu78 $O^{\epsilon 1}$ or $O^{\epsilon 2}$ (*distance* Tyr80 O^{η} to Glu78 $O^{\epsilon 1}$ or $O^{\epsilon 2}$ = 3.4 Å), while still interacting with Glu172 $O^{\epsilon 1}$. This shift may result from protonation of Glu172. In this manner, Tyr80 can provide a charge-stabilizing hydrogen bond to both Glu78 and Glu172 when required. The dynamic hydrogen bonding ability of Tyr80 is further enhanced by its ability to function as either a hydrogen bond acceptor, donor, or both. This residue can hence adapt to accommodate pH-dependent changes that occur in the active-site of BCX.

The side chain of Tyr69 forms a strong hydrogen bond to the side chain of Glu78. When this interaction is removed through mutation of Tyr69 to Phe, the pK_a of Glu78 rises by 0.4 units to 4.9 and the pK_a of Glu172 increases by 1.6 units to a value of 8.3. The pH optimum of the enzyme was not measurable, since the Y69F mutant was inactive. As seen for other BCX mutants, the pK_a value of Glu172 is far more sensitive to changes in the active-site than is the pK_a of Glu78. It is clear that the hydrogen bond between Tyr69 and Glu78 can serve to lower the pK_a of Glu78 through direct structural interaction. However, the mode by which Tyr69 lowers the pK_a of Glu172 is less obvious since the O^{η} atom of Tyr69 is > 5 Å away from either Glu172 $O^{\epsilon 2}$ or $O^{\epsilon 1}$. Unlike Tyr80, the position of the side chain of Tyr69 does not change with pH such that it can form a hydrogen bond with Glu172. As mentioned previously, however, the ionizations of Glu78 and Glu172 are electrostatically coupled and the changes in the pK_a of one partner can influence the ionization of the other via this linkage. Interestingly, Tyr69 and Tyr80 are involved in a π-stacking interaction with each other. They stack in a typical T-shaped arrangement with their closest inter-side-chain distance being 3.6 Å (*distance* Tyr69 $C^{\delta 1}$ to Tyr80 $C^{\epsilon 2}$), which is well within the prescribed range for aromatic-aromatic interactions (McGaughey

et al., 1998). This interaction therefore provides an additional avenue by which Glu78 and Glu172 can be structurally and hence electrostatically linked.

iii) Hydrogen Bonding

The degree to which a specific hydrogen bond can influence the pK_a values of Glu78 and Glu172 is generally dependent on the length of the bond and the identity of the donor (Table 3.8). Removal of hydrogen bonds generally serves to raise the pK_a values of the catalytic residues and the pH optimum of the enzyme, with mutation of residues that donate shorter and stronger hydrogen bonds to Glu78 and Glu172 resulting in larger perturbations in pK_a values. No trend was however observed between the ideality of the hydrogen bond donor angle and its influence on pK_a value.

The chemical identity of the hydrogen bond donor is also a factor that can dictate the relative perturbation of the pK_a value of residues 78 and 172. Energies of hydrogen bonds between uncharged donors and uncharged acceptors range from $1.0 - 1.4$ kcal mol^{-1}, whereas, those involving one charged group in the pair are slightly larger at $1.5 - 2.8$ kcal mol^{-1} (Jeffrey and Saenger, 1991). Hydrogen bonds where both donor and acceptor are charged are yet higher in energy at ~ 4 kcal mol^{-1} (Fersht *et al.*, 1985). Based on simple electrostatic models, the energy of a hydrogen bond reaches a maximum value when $\Delta pK_a = 0$ between donor and acceptor (Shan *et al.*, 1996). In nonprotic solvents, it is estimated that each pH unit of mismatch between donor and acceptor weakens the hydrogen bond by a factor of five (Cleland and Northrop, 1999; Shan and Herschlag, 1996). Using pK_a values determined from model compounds (Kyte, 1994), the order

Table 3.8. Average hydrogen bonding distances and acceptor angle deviations observed for Glu78 and Glu172 in all BCX proteins.

Interaction	Donor Type	Average Distance[a]	Average Acceptor Angle Deviation[a,b]	ΔpK_{aGlu78}[c]	$\Delta pK_{aGlu172}$[c]
Glu78 $O^{\varepsilon 1}$ – Gln127 $N^{\varepsilon 2}$	NH_2	2.7 Å	33°	-0.4	+0.6
Glu172 $O^{\varepsilon 2}$ – Asn35 $N^{\delta 2}$	NH_2	3.4 Å	4°	-0.1	+0.2
Glu78 $O^{\varepsilon 2}$ – Tyr69 O^{η}	OH	2.7 Å	15°	+0.3	+1.6
Glu172 $O^{\varepsilon 1}$ – Tyr80 O^{η}	OH	2.9 Å	4°	+0.4	+1.2

[a]Structural coordinates used for average value of distance/angle measurements were obtained from the RCSB Protein Data Bank (Bernstein *et al.*, 1977), PDB identification number 1XNB for WT BCX at pH 7.5 (Wakarchuk *et al.*, 1994a), 1BVV for WT-2FXB BCX at pH 7.5 (Sidhu *et al.*, 1999) and 2BVV for Y69F BCX (Sidhu *et al.*, 1999). Structures that were used from this study include WT BCX at "pH 5.5", WT BCX at "pH 4.0", Y80F BCX (accession number) and Q127A BCX (accession number).

[b]Hydrogen bond acceptor angles ($C^{\delta}-O^{\varepsilon 1/2} \cdots X$) and distances of Glu78 and Glu172 were measured using heavy atom positions. Ideal acceptor angle for a Glu/Asp side chain carboxyl group is 120° (Jeffrey and Saenger, 1991). Deviations (absolute values) were calculated by subtracting the ideal angle from the measured angle.

[c]$\Delta pK_a = pK_a$ mutant - pK_a WT (Differences were calculated using the major pK_a values of the respective mutant and WT; e.g. for the Glu78 $O^{\varepsilon 1}$ – Gln127 $N^{\varepsilon 2}$ interaction, the ΔpK_a value listed is for Q127A BCX where Gln127 is removed).

of the strengths of hydrogen bonds should, to a first approximation, follow the trend Glu-Glu/Asp (COOH) > Glu-Tyr (OH) > Glu-Gln/Asn (NH_2). According to this criterion, if there is a correlation between hydrogen bond strength and charge stabilization, then hydrogen bonds donated by neutral Glu/Asp residues (Glu127 in Q127E) should lower the pK_a values of Glu78 and Glu172 the most followed next by Tyr residues (Tyr69 and Tyr 80 in WT BCX) and finally by Gln/Asn residues (Asn35 and Gln127 in WT BCX). This trend is generally followed in the active-site of BCX with respect to the ionizations of Glu78 and Glu172.

As mentioned above, the pK_a of Glu172 is markedly more sensitive to active-site substitution compared to that of Glu78 (Figure 3.11). Inspection of Table 3.8 shows that Glu78 is flanked by two very well seated residues (Tyr69 and Gln127) whose hydrogen bonding distance remains short (2.7 Å) in all proteins studied. This stands in contrast to Glu172, whose hydrogen bond donors are not as sturdily placed (Asn35 and Tyr80), as judged by the variation in interatomic distances for the series of mutant structures. This may also account for the greater degree of charge stabilization afforded to Glu78 and contribute to its intrinsic pK_a (discussed below) being lower compared to that of Glu172. Normalized isotropic thermal factors are also consistently higher for Glu172 and the residues surrounding it when all of the BCX structures examined in this study are considered. This can be rationalized by considering the functions of Glu78 and Glu172. Glu78 must be held rigidly in position in a negatively charged state for the first crucial step of hydrolysis, while the acid/base catalyst Glu172 performs dual functions and must be accommodated in the active-site in either a protonated or deprotonated state. It must be positioned such that it can protonate the leaving aglycone in the first step and be held in proximity to a water molecule for the second step. The flexible nature of its environment thus complements its dynamic role from an electrostatic as well as structural viewpoint.
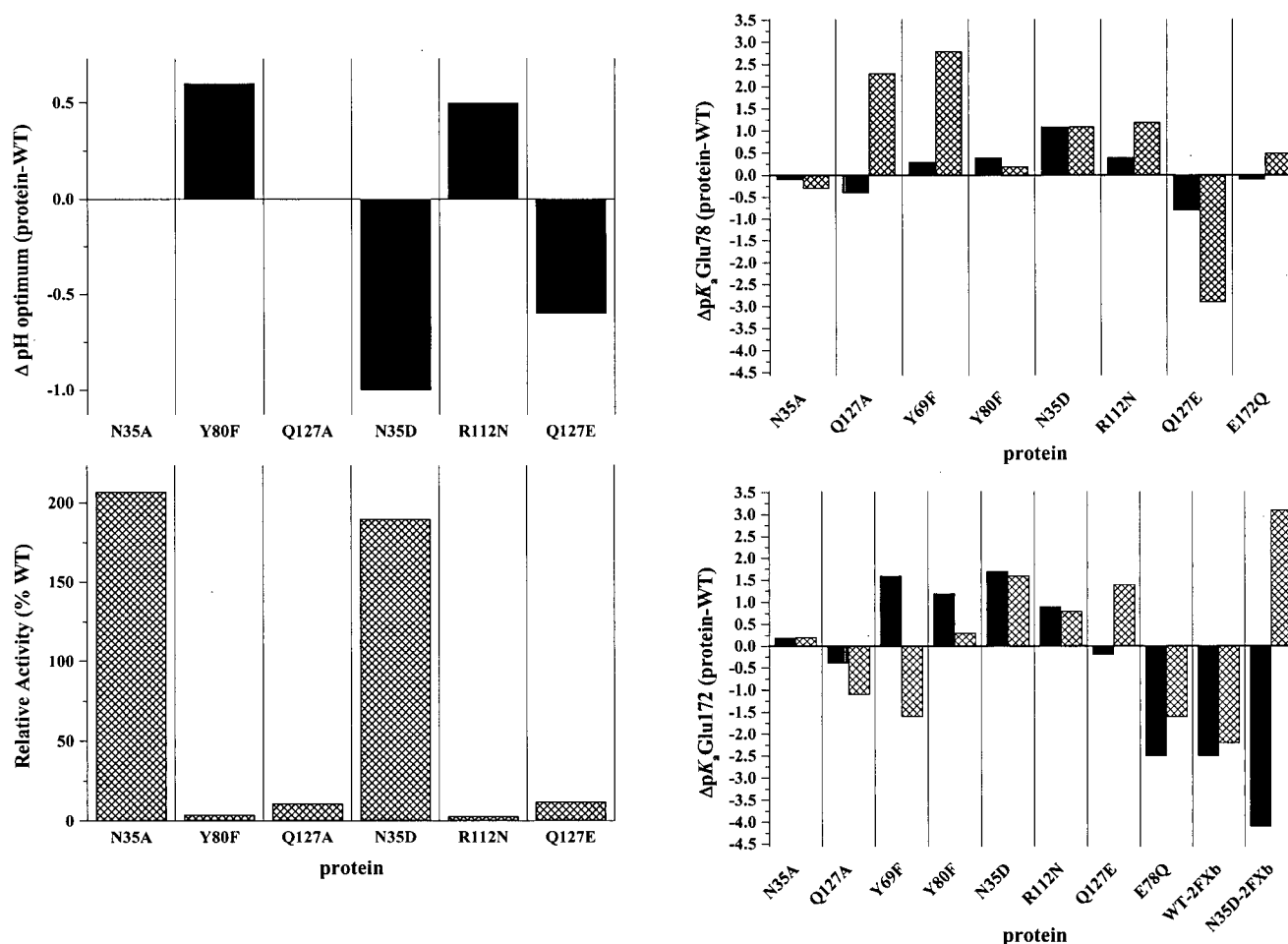
Figure 3.11. Summary of the effects of active-site substitution. Changes in pH optimum (upper left) are indicated relative to the WT value of 5.7 using data obtained from activity profiles (Table 3.3). Activity levels (lower left) are shown relative to WT (100 %) and were determined based on the parameter k_{cat}/K_m (Table 3.3). Changes in pK_a values for Glu78 (upper right) and Glu172 (lower right) are shown for those determined directly using NMR (solid bars) and for those calculated theoretically (hatched bars). Differences are plotted using only NMR data (solid = NMR pK_a protein- NMR pK_a WT) or only calculated data (hatched = calculated pK_a protein − calculated pK_a WT) (Table 3.9).

iv) Theoretical pK$_a$ Calculations

Within the context of this study, we were particularly interested in the calculated pK$_a$ values for Glu78 and Glu172 in the free WT enzyme. These two catalytic glutamic acids are in very similar hydrogen bonding environments with comparable degrees of solvent exposure. This requires a detailed analysis to explain their different ionization behaviours. As summarized in Table 3.9, electrostatic calculations indicate that Glu78 has a slightly less unfavourable desolvation energy than Glu172 (+2.0 *vs.* +2.3 pK$_a$ units), combined with more favourable background interactions involving the permanent partial charges of the protein (-2.0 *vs.* -1.5 pK$_a$ units). Together, these shift the "intrinsic" pK$_a$ (that is, the pK$_a$ in the absence of interactions with any titratable groups; (Yang and Honig, 1993)) of Glu78 below that of Glu172. Consideration of favourable interactions with ionizable groups reduces the pK$_a$ of Glu78 by a further -1.5 units to a final calculated value of 2.9. These interactions involve primarily Arg112 (-1.2 units, as indicated by the effects of removing this positive charge in the R112N mutant), compounded by contributions from the net positive charge of BCX at acidic pH values. The reason why the calculated pK$_a$ of 2.9 for Glu78 differs from the measured value of 4.6 is not clear, although this may reflect an inadequate description of the microscopic environment (solvation and dielectric constant) along the surface of the active-site or subtle differences between the structure of the protein in solution and in a crystalline environment due to side chain and backbone mobility (Connelly *et al.*, 2000).

Combined with the calculation of a lower "intrinsic" pK$_a$ for Glu78 relative to Glu172, the most salient aspect of the electrostatic calculations is that the glutamic acids are strongly coupled with an unfavourable charge-charge interaction of 1.6 units. Thus, with rising pH, Glu78 predominantly deprotonates first, thereby disfavouring the ionization of Glu172 and forcing its

pK_a to a calculated value of 5.9. *Thus, the difference in the pK$_a$ values of Glu78 and Glu172 results intrinsically from their electrostatic juxtaposition within the active-site of the enzyme.* This key conclusion is supported both experimentally (McIntosh *et al.*, 1996) and theoretically (Joshi *et al.*, 2000c) by the observation and prediction, respectively, of biphasic titration curves reflecting the coupled microscopic ionization behaviour of these two residues. In addition, paralleling that observed experimentally, the calculated pK_a of Glu172 in the E78Q mutant decreases by 1.6 units to 4.3 due to removal of the negative charge at position 78. (Conversely, the pK_a of Glu78 in E172Q BCX is essentially unperturbed relative to the WT enyzme since, in both cases, it corresponds to ionization in the presence of a neutral residue at 172). Covalent modification of Glu78 to form the glycosyl-enzyme intermediate, WT-2FXb BCX, also results in a similar decrease in the predicted pK_a value of Glu172 to 3.7 due to the removal of charge repulsion, as well as to smaller changes in desolvation and background interaction energies. This supports the previous conclusion that *"cycling" of the pK$_a$ value of Glu172 to match its role as a general acid and then base during the two-step double displacement reaction results intrinsically from the cycling of the nucleophile between its charged free, and neutral glycosylated states* (McIntosh *et al.*, 1996).

Calculations performed on the active-site mutants also showed some interesting trends (Figure 3.11). The direction and magnitude of the change in pK_a upon mutation is more accurately predicted for the removal/addition of ionizable residues (N35D, R112N, Q127E, E78Q, E172Q, and WT-2FXb) in proximity to Glu78 and Glu172 than it is for the mutation of non-ionizable residues that donate hydrogen bonds (N35A, Q127A, Y69F and Y80F) to the catalytic pair. The theoretical calculations also do not predict the marked sensitivity of the pK_a of Glu172 to active-site substitution compared to Glu78. The differences between the

Table 3.9. Theoretical and experimental pK_a values in BCX proteins.

Protein	Residue	pK_a calc./obs.[a]	ΔpK_a calc./obs.[b]	desolvation[c]	background[c]	ionizable[c]
WT	Glu78	2.9 / 4.6	-	+2.0	-2.0	-1.5
	Glu172	5.9 / 6.7	-	+2.3	-1.5	+0.8
E78Q	Glu172	4.3 / 4.2	-1.6 / -2.5	+2.3	-1.5	-0.9
E172Q	Glu78	2.8 / 5.1	-0.1 / +0.5	+2.0	-2.0	-1.5
Y69F	Glu78	5.7 / 4.9 (4.0, 5.9)[d] /	+2.8 / +0.3 (+1.1)[d]	+2.1	-1.0	+0.2
	Glu172	4.3 / 8.3 (3.7, 5.6)[d] /	-1.6 / +1.6 (-0.3)[d]	+2.0	-1.4	-0.7
Y80F	Glu78	3.1 / 5.0	+0.2 / +0.4	+1.9	-1.7	-1.5
	Glu172	6.2 / 7.9	+0.3 / +1.2	+2.0	-1.0	+0.9
N35A	Glu78	2.6 / 4.5	-0.3 / -0.1	+2.0	-2.2	-1.6
	Glu172	6.1 / 6.9	+0.2 / +0.2	+2.1	-1.2	+0.8
N35D	Glu78	4.0 / 5.7	+1.1 / +1.1	+2.3	-2.4	-0.3
	Glu172	7.5 / 8.4	+1.6 / +1.7	+1.6	-0.9	+2.4
	Asp35	1.0 / 3.7		+1.7	-3.0	-1.7
Q127A	Glu78	5.2 / 4.2 (3.8, 5.6)[e] /	+2.3 / -0.4 (+0.9)[e]	+2.0	-1.1	-0.1
	Glu172	4.8 / 7.3 (3.8, 5.6)[e] /	-1.1 / +0.6 (-0.3)[e]	+2.1	-1.5	-0.2
Q127E	Glu78	<0 / 3.8	> -2.9 / -0.8	+2.2	-4.8	> -1.8
	Glu172	7.3 / 6.5 (6.1,7.4) / (6.5,8.5)[f]	+1.4 / -0.2 (+0.2,+1.5) / (-0.2,+1.8)[f]	+2.3	-1.4	+2.0
	Glu127	5.8 / 8.4 (5.6, 6.9) / (6.8,8.7)[f]		+1.6	-0.9	+0.7
R112N	Glu78	4.1 / 5.0	+1.2 / +0.4	+1.9	-2.2	-0.1
	Glu172	6.7 / 7.6	+0.8 / +0.9	+2.2	-1.6	+1.7
WT-2FXb	Glu172	3.7 / 4.2	-2.2 / -2.5	+1.3	-1.2	-0.9
N35D-2FXb	Glu172	9.0 / 1.9-3.4[g]	+3.1 / > -5.0[g]	+2.3	-1.5	+3.8
	Asp35	0.2 /		+2.3	-4.2	-1.9

[a]Calculated pK_a values correspond to the pH at which a given residue is 50% ionized (dielectric constants of 8 and 80 for protein and water, respectively; ionic strength of 50 mM; 25 °C)

[b]ΔpK_a values are determined by comparison to the corresponding calculated and observed pK_a values for WT BCX.

[c]Contributions to the calculated pK_a values due to desolvation, interaction with permanent background (partial) charges, and interactions with titratable groups (at pH = pK_a), respectively.

[d]The calculated titration curves of Glu78 and Glu172 in Y69F are highly biphasic. Fitting to a model of two coupled ionizable groups gives microscopic pK_a values of ~ 4.0 and ~ 5.9 for Glu78 in the presence of neutral or charged Glu172, respectively, and values of ~ 3.7 and ~ 5.6 for the Glu172 in the presence of neutral or charged Glu78, respectively. For comparison to WT, the corresponding calculated ΔpK_a values are for the first microscopic pK_a of Glu78 and the 2nd of Glu172.

[e]The calculated titration curves of Glu78 and Glu172 in Q127A are highly biphasic and are treated similarly to Y69F (footnote d).

[f]The calculated titration curves of Glu127 and Glu172 in E127Q are highly biphasic and are treated similarly to Y69F (footnote d).

[g]Due to strong hydrogen-bonding in the covalently modified protein, Asp35-Glu172 titrate as a tightly coupled system with a first pK_a value in the range of 1.9-3.4 and the second > 9 (Chapter 4; Joshi *et al.*, 2000a).

---

experimentally measured and theoretically predicted pK_a values in this regard reflect the need to accurately define the precise geometry of hydrogen bond networks and proton placement. (This is certainly not a trivial task). Furthermore, as discussed previously, many additional factors, which may not be accounted for by computational methods can also serve to influence the ability of a donated hydrogen bond to stabilize/destabilize the pK_a of an ionizable group.

v) Catalysis

At this point in the discussion it would be useful to discuss the microscopic pK_a values of Glu78 and Glu172 (See Appendix I for a description of microscopic/macroscopic pK_a analyses) (McIntosh *et al.*, 1996). Two ionizable groups may show coupled or biphasic spectral changes during a pH tiration if (i) the chemical shift or (ii) the microscopic pK_a of one group is dependent upon the ionization state of the other (Shrager *et al.*, 1972). In the first case, the chemical shift of the carboxyl may be influenced directly by electric fields that perturb the shielding of the ^{13}C nucleus or indirectly through conformational changes that, for example, alter hydrogen-bonding interactions. In the absence of detailed structural information, the expected magnitudes and directions of these possible pH-dependent chemical shift perturbations are difficult to predict (Batchelor *et al.*, 1975; Gu *et al.*, 1994). However, inspection of the crystallographic structure of

BCX reveals that the α-carbons of the two catalytic residues are separated by 6.5 Å, and thus, these glutamates should interact electrostatically, as in the classical example of a dibasic acid (Edsall and Wyman, 1958). This corresponds to case (ii), in which the microscopic pK_a of one glutamic residue is dependent upon the ionization state of the other, such that the full chemical shift change due to protonation occurs only upon the neutralization of both groups. An analysis of the pH dependence of the ^{13}C-NMR spectra of the wild type enzyme using a model of two coupled ionization equilibria, yet independent chemical shifts for Glu78 and Glu172, yields the microscopic pK_a values summarized in Scheme 3.2. From a simultaneous fitting of the two titration curves, the pK_a of Glu78 is 4.63 when Glu172 is neutral and 5.79 when it is negatively charged. Similarly, the pK_a of Glu172 is 5.50 when Glu78 is neutral and 6.66 when it is charged. Therefore, in this model, the mutual electrostatic repulsion between the carboxylate groups elevates each pK_a by ~ 1.2 units. The lower ionization pathway in Scheme 3.2 is favoured significantly, and thus, the microscopic pK_a values of 4.63 (Glu78) and 6.66 (Glu172) are essentially equal to the macroscopic or apparent pK_a values assignable to these two groups.
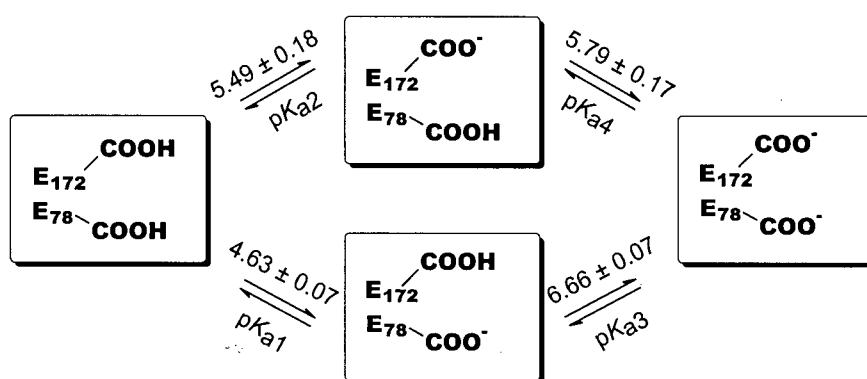
Scheme 3.2

More specifically, the value of the pK_a of Glu172 in the presence of a neutral Glu78 (5.5) is not as low as the pK_a value of Glu172 in the glycosyl-enzyme intermediate (4.2) or in the

E78Q mutant (4.2). This implies that there must be other structural interactions, in addition to electrostatic, that help to lower the pK_a of Glu172 by an additional 1.3 units (McIntosh *et al.*, 1996). Nevertheless, the results obtained from microscopic pK_a analyses still predict a lower pK_a for Glu172 when Glu78 is neutral, and thus support the concept of pK_a cycling for Glu172.

While the pK_a values of the nucleophile and the general acid/base catalyst determine the classic bell-shaped pH-dependent activity profile of retaining glycosidases such as BCX, electrostatic linkage of their ionization equilibria is crucial to achieving efficient catalysis. A glycosidase can be engineered such that the pK_a values of the nucleophile and the acid/base catalyst in the free enzyme span a broad range of pH; however, these are not the only pH-dependent factors that influence catalysis. The pK_a value of the general acid/base catalyst must be able to cycle to match its catalytic function as a general acid and as a general base. If the pK_a values of the nucleophile and the general acid/base catalyst are too far apart (ΔpK_a is large), then the intrinsic cycling mechanism, driven significantly by the charged/neutral state of the nucleophile, may not function properly. For example, at the pH optimum of BCX (5.7), the acid/base catalyst Glu172 cycles its pK_a value from 6.7 where it is protonated and can function as a general acid to a value of 4.2 where it is deprotonated and can function as a general base. If the pK_a value of Glu172 was raised high enough (by some factor other than the repulsive charge of the nucleophile) such that it was only able to shift in the glycosyl-enzyme intermediate to a value above its pH optimum instead of below as required, then its function as a general base would be compromised, since the fraction of enzyme that is protonated at residue 172 would be greater.

As discussed above, microscopic pK_a analyses of the titration curves of Glu78 and Glu172 in WT BCX indicate that the pK_a value of the acid/base catalyst should be ~ 5.5 instead of the observed value of 4.2 if protonation/deprotonation of the nucleophile is the sole driving

force for pK_a cycling. At the pH optimum of 5.7, a pK_a value of 5.5 for Glu172 will impair its general base function in the second step of hydrolysis. Hence, while elimination of the negative charge of the nucleophile is a significant factor in driving pK_a cycling, its impact is limited by simple electrostatic constraints. Given these limitations, retaining glycosidases, and by inference other enzymes that use a similar mechanism, must evolve structurally to be able to lower further the pK_a of the acid/base catalyst if a broad pH profile is desired. Furthermore, since the chemical step of covalent glycosyl-enzyme intermediate formation is closely coupled to the ionization behaviour of the key active-site residues, the observed downward shift in the pK_a value of the general acid/base catalyst as it cycles drives the glycosylation step of the reaction by enhancing proton transfer to the glycosidic bond oxygen (Joshi *et al.*, 2000a; McIntosh *et al.*, 1996; Richard, 1998). It is difficult to determine what effects many of the active-site mutations have upon the efficiency of acid/base catalysis, since most of the residues that were mutated in this study are involved in putative transition and ground-state binding interactions with the substrate. Given that reductions in activity were accompanied by changes in the pK_a value of Glu172 in the free enzyme, it is possible that mutation affects the ability of the acid/base catalyst to cycle its pK_a value and has hence adversely affected the efficiency of proton transfer. However, without direct measurements of the pK_a of Glu172 in the glycosyl-enzyme intermediates of these mutants, it is difficult to assess the magnitude of the effect of the mutation on pK_a cycling. A prime example of an extremely efficient mutant is N35D BCX, where the enhanced ability of the acid/base catalyst contributes to making the mutant inherently 100-fold more efficient than WT (Chapter 4; Joshi *et al.*, 2000a). While the pK_a shift of the acid/base catalyst of 2.5 units in WT BCX corresponds to an energy difference of 3.5 kcal mol^{-1}, the significantly higher pK_a shift of 5.8 units in N35D BCX provides ~ 8 kcal mol^{-1} of energy at 25 °C ($2.303RT \Delta$pK_a). In the N35D

BCX protein, the large decrease in the pK_a of Glu172 is attributed to the formation of a short and strong hydrogen bond in the glycosyl-enzyme intermediate, which strongly favours deprotonation of the acid catalyst. As shall be discussed in Chapter 4, only a small fraction of the enzyme ($\sim 1\%$) is in the correct ionization state, yet is so efficient that it can achieve WT levels of activity.

What about situations where the fraction of the enzyme in the correct ionization state is reduced but catalysis is not as efficient? Q127E BCX is a possible example of this. Although there is no structure available for this mutant, there is no reason to expect that substitution of a glutamic acid for a glutamine would cause significant structural perturbations. Furthermore, it is also unlikely, judging by the WT-2FXb and E172C-Xb structures, that Gln127 makes critical interactions with the substrate. The activity is reduced significantly, however, in the Q127E BCX mutant. The answer to its reduced activity may lie in an examination of the microscopic pK_a values and electrostatic linkage of Glu127 and Glu172. Fitting of the titration data, in a similar manner to Scheme 3.2, in the pH range from 6-11 to extract microscopic pK_a values yields a rather revealing result (Scheme 3.3):
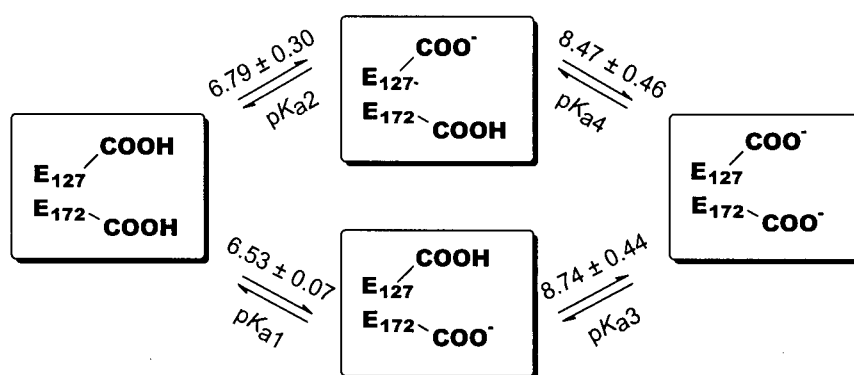
In the lower ionization pathway Glu172 ionizes first with a pK_a of 6.53, which is identical to the value observed in the basic limb of the pH-dependent activity profile (Table 3.3). Since Glu172

is well positioned to be the acid catalyst, it must be the group whose deprotonation dictates the alkaline limb of the profile. However, according to Scheme 3.2, this pathway is followed only ~ 50 % of the time given the similar values of pK_{a1} and pK_{a2}. The other half of the enzyme population is in a state where Glu127 ionizes before Glu172. (In WT BCX, $pK_{a1} > pK_{a2}$ and the lower ionization pathway, corresponding to the correct ionization states for catalysis, is dominant). This reduces the fraction of the enzyme that is in the correct protonation state for the first step of the reaction. Further reductions in activity may also occur as a result of Glu172 being compromised in its ability to cycle or be able to donate a proton to the leaving group. Coincidently, the value of k_{cat}/K_m for Q127E BCX is similar to the value obtained for E172Q BCX, in which the acid catalyst is removed (Table 3.3), emphasizing the possibility of compromised proton donation.

Therefore, the factors that establish and maintain the pK_a values of the acid/base catalyst in both the free enzyme and the glycosyl-enzyme intermediate are of importance to not only defining the pH optimum of the enzyme but also the efficiency of acid/base catalysis. These intricacies are often overlooked when attempting to engineer glycosidases to function over a variety of pH optima. Furthermore, the effects that these changes have upon the pK_a values of the catalytic groups and other active-site residues in the transition state(s) are even less well understood.

3.5 CONCLUSION

The three-dimensional structure of BCX has been finely tuned at the local and global levels to not only maintain the correct ionization states of the catalytic glutamic acids, but also to position active-site residues for catalytically optimal protein-substrate interactions. The active-site residues act concertedly in setting the pK_a values of Glu78 and Glu172, with no particular residue being singly more important than any of the others. As a result of the intricate network of hydrogen bonds, van der Waals interactions and electrostatic interactions, both catalytic glutamic acid residues are perturbed in complex ways with active-site substitution (i.e. mutation of the environment of one affected the other). In general, positively charged groups serve to lower pK_a values as do residues that contribute hydrogen bonds. The length of the hydrogen bond and the chemical identity of the donor are also factors dictating the degree of charge stablization afforded to the ionizable acceptor. Groups that donate shorter hydrogen bonds are more effective in lowering pK_a values than those that contribute longer hydrogen bonds. In contrast, the mechanism by which adjacently positioned acidic residues lower pK_a values is more complex and is dependent upon the microscopic pK_a values and electrostatic linkage of the groups involved in the interaction. In the case of BCX, both acidic substitutions resulted in lower pH optima; however, the apparent pK_a lowering effect was accomplished via different mechanisms in these two cases. Theoretical pK_a calculations provide qualitative insights into electrostatic interactions occurring in BCX in certain cases. The key conclusion from these studies is that Glu78 inherently has a lower pK_a than Glu172 due to a number of electrostatic interactions that result from interplay with both the global and local environments surrounding it, in addition to the dominant, yet unfavourable charge-charge interaction it has with Glu172. However, a challenge is to correctly account for the effects of hydrogen bonding to ionizable groups.

Mutations of active-site residues also lead to significant reductions of activity in many cases. This is not surprising since many of these groups are involved in ground and/or transition state binding of the saccharide. Active-site substitution generally leads to small structural perturbations, yet can significantly alter activity, including the rate-determining step and the pH-dependence of hydrolysis. The pH optimum of BCX can be modified from −1.0 to +0.6 pH units, albeit at the expense of activity in some cases. Strategies for engineering pH optima can involve mutations of key active-site residues, although more general approaches would be to change residues outside the core of the active-site to avoid perturbing the exquisitely balanced network of complex interactions that surround the catalytic glutamates. Longer-range electrostatic interactions could be taken advantage of in this manner. Mechanistic considerations are also central to successful engineering of glycosidases. Further studies should probe the effects that alterations have upon intrinsic phenomena such as pK_a cycling as well as the values of ionization constants of key residues in the transition states.

Rational approaches can result in the production of glycosidases with altered pH optima. However, activity is compromised in many cases. In nature, xylanases have a wide range of activities and pH optima. What lesson can be learned from these naturally occurring examples that reflect eons of evolutionary selection? In the next chapter I describe a remarkable example in which nature has changed pH optima within a family of glycosidases.

Chapter 4

A Novel Mechanism for Regulating the pH-Dependent Activity of Glycosidases: Lessons from Nature

ABSTRACT

The pH optima of family 11 xylanases are well correlated with the nature of the residue adjacent to the acid/base catalyst. In xylanases that function optimally under acidic conditions, this residue is an aspartic acid, whereas it is an asparagine in those that function under more alkaline conditions. Previous studies of wild type *Bacillus circulans* xylanase (BCX), with an asparagine at position 35, demonstrated that its pH-dependent activity follows the ionization states of the nucleophile Glu78 (pK_a 4.6) and the acid/base catalyst Glu172 (pK_a 6.7). As predicted from sequence comparisons, substitution of this asparagine with an aspartic acid (N35D BCX) shifts its pH optimum from 5.7 to 4.6, with an ~ 20% increase in activity. The bell-shaped pH-activity profile of this mutant enzyme follows apparent pK_a values of 3.5 and 5.8. Based on ^{13}C-NMR titrations, the predominant pK_a values of its active-site carboxyls are 3.7 (Asp35), 5.7 (Glu78) and 8.4 (Glu172). Thus, in contrast to the wild type enzyme, the pH-activity profile of N35D BCX appears to be set by Asp35 and Glu78. Mutational, kinetic, and structural studies of N35D BCX, both in its native and covalently modified 2-fluoro-xylobiosyl glycosyl-enzyme intermediate states, reveal that the xylanase still follows a double-displacement mechanism with Glu78 serving as the nucleophile. It is proposed, therefore, that Asp35 and Glu172 function together as the general acid/base catalyst, and that N35D BCX exhibits a

"reverse protonation" mechanism in which it is catalytically active when Asp35, with the lower pK_a, is protonated, while Glu78, with the higher pK_a, is deprotonated. This implies that the mutant enzyme must have an inherent catalytic efficiency at least 100 fold higher than that of the parental wild type because only ~ 1% of its population is in the correct ionization state for catalysis at its pH optimum. The increased efficiency of N35D BCX, and by inference all "acidic" family 11 xylanases, is attributed to the formation of a short (2.7 Å) hydrogen bond between Asp35 and Glu172, observed in the crystal structure of the glycosyl-enzyme intermediate of this enzyme, that can substantially stabilize the transition state for glycosyl transfer. Such a mechanism may be much more commonly employed than is generally realized, necessitating careful analysis of the pH-dependence of enzymatic catalysis.

4.1 INTRODUCTION

The low molecular weight xylanases (Gilkes *et al.*, 1991) provide a fascinating example of how the pH-dependence of enzymatic catalysis can be modulated within a family of retaining glycosidases. Members of the family 11 endo-β-(1,4)-glycosidases derive from both eukaryotic and bacterial species and share sequence identity varying from 40-90 % (Torronen *et al.*, 1993; Torronen and Rouvinen, 1997). All members of this family studied to date have strikingly similar three-dimensional structures and active-site geometries (Torronen and Rouvinen, 1997). In particular, they all contain two catalytically essential glutamic acid residues that are involved in an intricate network of hydrogen bonds contributed by highly conserved neighboring residues (Torronen and Rouvinen, 1997; Wakarchuk *et al.*, 1994a). One catalytic glutamic acid residue functions as a nucleophile and the other as a general acid/base catalyst in a double-displacement mechanism whereby hydrolysis of xylosidic substrates proceeds with retention of anomeric configuration (Gebler *et al.*, 1992; Koshland, 1953; Sinnott, 1990). In spite of all these similarities, the pH optima of family 11 xylanases vary widely from acidic values of < 2 to alkaline values > 7 (Table 4.1).

A comparison of the sequences of these low molecular weight endo-β-(1,4)-glycosidases reveals a striking correlation in that the residue hydrogen bonded to the general acid/base catalyst is an asparagine in so-called "alkaline" xylanases, whereas it is an aspartic acid in those with a more "acidic" pH optimum (Torronen and Rouvinen, 1997). This seems counter-intuitive since it might be expected that placement of a negatively-charged residue next to the acid/base catalyst should electrostatically elevate its pK_a and *raise* the pH optimum of the enzyme to a more alkaline value. Nevertheless, this correlation has been confirmed by mutational analysis of *Aspergillus kawachii* xylanase C in which the single substitution of an Asn for an Asp at this key

Table 4.1. Properties of family 11 xylanases.

Xylanase	pH optimum	pI[i]	Residue at Position 35[j]	Distances (Å)[j] Asx35 $N^{\delta2}/O^{\delta2}$-Glu172 $O^{\epsilon2}$
B.agaradhaerens (Xyl11)[a]	7.1[a]	8.8	Asn	[k]
T.lanuginosus[b]	6.5[a]	4.7	Asn	3.0[l]
B.circulans (BCX)[c]	5.7[b]	9.1	Asn	3.1
T.reesei (XYNII)[d]	5.3[c]	8.7	Asn	3.6
B.circulans (N35D)[e]	4.6[d]	8.8	Asp	3.2
T.reesei (XYNI)[f]	3.5[e]	4.6	Asp	2.9
A.niger (xylanase I)[g]	3.0[f]	4.0	Asp	2.8
A.kawachii (XynC)[h]	2.0[g]	3.9	Asp	2.8

[a]*Bacillus agaradhaerens* xylanase (Xyl11) structure was solved at pH 5.0, PDB code 1QH7 (Sabini *et al.*, 1999).

[b]*Thermomyces lanuginosus* xylanase structure was solved at pH 4.0, PDB code 1YNA (Gruber *et al.*, 1998).

[c]*Bacillus circulans* xylanase (BCX) structure was solved at pH 7.5, PDB code 1XNB (Wakarchuk *et al.*, 1994a).

[d]*Trichoderma reesei* xylanase II (XYNII) structure was solved at pH 6.5, PDB code 1XYP (Torronen *et al.*, 1994).

[e]*Bacillus circulans* xylanase variant N35D structure was solved at pH 7.5, PDB code 1C5H.

[f]*Trichoderma reesei* xylanase I (XYNI) structure was solved at pH 8.0, PDB code 1XYN (Torronen and Rouvinen, 1995).

[g]*Aspergillus niger* xylanase I structure was solved at pH 4.7, PDB code 1UKR (Krengel and Dijkstra, 1996).

[h]*Aspergillus kawachii* xylanase C (XynC) structure was solved at pH 6.5, PDB code 1BK1 (Fushinobu *et al.*, 1998).

[i]Theoretical pI was calculated using the "Compute pI/Mw tool" resource located on the ExPASy server (Wilkins *et al.*, 1998).

[j]Residue numbering and atom labelling is based on the sequence and structure of BCX.

[k]Coordinates not released from the Brookhaven Protein Data Bank at time of submission.

[l]Measured distances are based on a structure in which the acid/base catalyst, Glu178, is in an unfavourable conformation and points away from the nucleophile, Glu86 (Gruber *et al.*, 1998).

position dramatically elevates its pH optimum from ~ 2 to 5 (Fushinobu *et al.*, 1998). Several studies of these family 11 xylanases have led to proposed mechanisms by which this paradoxical effect is manifested (Fushinobu *et al.*, 1998; Krengel and Dijkstra, 1996), though none of these explanations has been entirely satisfactory.

In order to understand how the substitution of a single amino acid can modulate the pH optimum of an enzyme, we have focused our attention on the "alkaline" xylanase from *Bacillus circulans* (BCX) (Sung *et al.*, 1993; Wakarchuk *et al.*, 1992). As discussed in Chapter 3, the pK_a values of Glu78 and Glu172, measured directly using ^{13}C-NMR spectroscopy, are 4.6 and 6.7, respectively. These are in close agreement with those determined from the bell-shaped pH activity profile of this enzyme and thereby provide a straightforward explanation for its observed pH optimum near 5.7. Likewise, the pH-dependent activities of the mutants (N35A, Y80F, R112N, Q127A and Q127E) presented in Chapter 3 all directly follow the ionization states of Glu78 and Glu172, which dictate the pH optima of the enzymes. An asparagine residue (Asn35), adjacent to the general acid/base catalyst Glu172 in BCX, was substituted with an aspartic acid. As predicted by sequence comparisons, this substitution led to a pronounced decrease in the pH optimum of the enyzme to 4.6. We have thoroughly investigated this phenomenon, combining kinetic studies using synthetic aryl β-xylobioside substrates, site-specific measurements of the pK_a values of catalytic groups by ^{13}C-NMR spectroscopy, electrospray mass spectrometry (ESMS), and X-ray crystallographic structure determination. Integrating these analyses, we propose a detailed mechanism to explain the dependence of the pH optima of family 11 xylanases on the nature of the group adjacent (Asn or Asp) to the acid/base catalyst.

This work has been published in Joshi *et al.*, (2000a) and was the result of a collaboration with two groups. In the laboratory of Dr. Stephen G. Withers, the substrates were synthesized by

Timothy Hiebert, Lloyld Mackenzie and David Zechel and the mass spectrometry data was collected by Dr. Shouming He. In the laboratory of Dr. Gary D. Brayer, the structures of N35D BCX and the N35D BCX glycosyl-enzyme intermediate were solved by Gary Sidhu. All other experiments and procedures were performed by me.

4.2   *MATERIALS AND METHODS*

4.2.1   *Cloning, Mutagenesis and Protein Expression*

The synthetic gene encoding BCX was cloned into the pCW plasmid system under control of an inducible *tac* promoter, as described previously (McIntosh *et al.*, 1996; Sung *et al.*, 1993; Wakarchuk *et al.*, 1994a). To create the genes encoding N35D, N35D/E78Q and N35D/E172Q, site-directed mutagenesis was performed using a QuickChange™ Site-Directed Mutagenesis Kit (Stratagene Cloning Systems, La Jolla, CA). The following oligonucleotide primers were used in the mutagenesis of WT BCX to N35D BCX [based on complementarity to the synthetic BCX gene (Sung *et al.*, 1993)]: 5' GG TCT AAT ACT GGG **GAC** TTC GTA GTC GG 3' and 5' CC GAC TAC GAA **GTC** CCC AGT ATT AGA CC 3'. The double mutants, N35D/E78Q and N35D/E172Q BCX, were made by performing further site-directed mutagenesis on the N35D BCX gene using the following oligonucleotide primer pairs: for N35D/E78Q, 5' G CGT TCG CCA CTG ATT **CAA** TAT TAC GTT GTC G 3' and 5' C GAC AAC GTA ATA **TTG** AAT CAG TGG CGA ACG C 3'; for N35D/E172Q, 5' GTA ATG GCG ACC **CAA** GGC TAC CAG AGC 3' and 5' GCT CTG GTA GCC **TTG** GGT CGC CAT TAC 3'. All other recombinant DNA procedures, such as plasmid isolation and purification, were performed as recommended by the manufacturers. After the sequences were confirmed by automated DNA sequencing, the mutagenized plasmids were transformed into bacterial *E. coli* strain BL21 (λDE3) using electroporation or calcium chloride-heat shock.

Proteins used for kinetic studies were expressed in *E. coli* strain BL21 grown in TYP medium at 37 °C until the time of induction (OD$_{600}$ = 0.5 - 0.6) and thereafter at 30 °C until the cells were harvested 16 hours later. Protein expression was induced by addition of IPTG to a final concentration of 0.75 mM. Purification was performed as described previously using SP-

Sepharose™ ion-exchange chromatography followed by Sephacryl S-100™ HR size exclusion chromatography (Pharmacia Biotech, Inc.) (Sung *et al.*, 1993). Fresh column material was used for different proteins to prevent any possible cross contamination. Proteins were purified to > 95% homogeneity as judged by SDS-PAGE with Coomassie staining. Further characterization was performed using a Perkin Elmer Sciex API 300 electrospray mass spectrometer with the following results: N35D, observed 20 402 ± 3.5 Da, expected 20 402 Da; N35D/E78Q, observed 20 400 ± 3.5 Da, expected 20 401 Da; N35D/E172Q, observed 20 401 ± 3.5 Da, expected 20 401 Da.

N35D BCX, ^{13}C-enriched in the side chain δ-carbonyl of the glutamate and glutamine residues, was expressed as described previously (McIntosh *et al.*, 1996). Bacteria were grown in a synthetic medium (Anderson *et al.*, 1993; McIntosh *et al.*, 1996; Muchmore *et al.*, 1989) containing 275-325 mg/L 99% L-[δ-^{13}C]-glutamate (Tracer Technology, Cambridge, MA). The isotopically labelled proteins were expressed and purified as above, except that the size-exclusion chromatography step was not performed. The [δ-^{13}C]-Glu and -Gln enriched xylanases were purified to > 90% homogeneity as judged by SDS-PAGE and Coomassie Blue staining. Further characterization was performed using electrospray mass spectrometry, yielding an observed mass of 20 406 ± 3.5 Da (expected 20 409 Da) for isotopically labelled N35D BCX. The expected mass value was calculated assuming ~ 100% ^{13}C enrichment of seven residues. Deviations from observed and expected molecular masses reflects isotopic dilution of the [δ-^{13}C]-Glutamate.

4.2.2 Enzyme Kinetics

(i) Steady State Kinetics

Several aryl β-xylobiosides were used as substrates in the assays described below: 2,5-dinitrophenyl β-xylobioside (2,5-DNPX$_2$), $\Delta\varepsilon_{400nm,pH6.0}$ = 3.57 mM^{-1} cm^{-1} (where $\Delta\varepsilon$ is the difference in molar absorptivity between the phenol and its corresponding xylobioside); 3,4-dinitrophenyl β-xylobioside (3,4-DNPX$_2$), $\Delta\varepsilon_{400nm,pH6.0}$ = 11.71 mM^{-1} cm^{-1}; orthonitrophenyl β-xylobioside (ONPX$_2$), $\Delta\varepsilon_{400nm,pH6.0}$ = 1.07 mM^{-1} cm^{-1}; and phenyl β-xylobioside (PhX$_2$), $\Delta\varepsilon_{288nm,pH12.2}$ = 2.17 mM^{-1} cm^{-1}. Inhibition studies were performed using 2,4-dinitrophenyl 2-deoxy-2-fluoro-β-xylobioside (DNP2FXb) as a mechanism-based inhibitor. All substrates and inhibitors were synthesized and characterized according to previously published procedures (Lawson *et al.*, 1997; Ziser *et al.*, 1995). All other materials, unless otherwise stated, were obtained from the Sigma Chemical Company. Spectrophotometric assays were performed on either a Pye Unicam 8700 or UV4 UV/Vis spectrophotometer, both equipped with a circulating water bath for temperature control. Assays were carried out in 200 μL micro black-walled quartz cuvettes with a 1 cm path length, according to methods described previously (Lawson *et al.*, 1997). The pH values of assay solutions were measured using a Corning G-P Micro Combo™ electrode. Steady-state kinetic data were fitted using the programs PlotData (TRIUMF, University of British Columbia) and GraFit (Leatherbarrow, 1998).

Assays used to determine the Michaelis-Menten steady state parameters, k_{cat} and K_m, utilized the appropriate aryl β-xylobioside substrate in 20 mM MES, 50 mM NaCl, 0.1 % BSA buffer (pH 6.0). Typically, substrate concentrations were varied from 0.2K_m to 5K_m. After a 15 minute preincubation time at 40 °C, 10 μL of enzyme at an appropriate concentration (2.0 × 10^{-4} mM to 7.0 × 10^{-2} mM final) was added to 190 μL of the assay solution. The rates of enzymatic

hydrolysis of the aryl β-xylobiosides were determined by monitoring the rate of phenol release at the appropriate wavelength in a continuous assay at 40 °C. Enzyme concentrations and reaction times were chosen such that less than 10 % of the total substrate was hydrolyzed over the course of the measurement. In the case of PhX$_2$, a stopped assay was used to measure enzymatic hydrolysis rates. After an appropriate time, 600 μL of 200 mM Na$_3$PO$_4$ (pH 12.3) buffer was added to terminate the reaction. The absorbance of the released phenol was measured at 288 nm and corrected for both the spontaneous hydrolysis of PhX$_2$ and the background absorbance of the enzyme. All other conditions were identical to those listed above for assays containing the other aryl β-xylobiosides. Experimental rates measured at each given substrate concentration were fitted to the standard Michaelis-Menten expression to determine the parameters k_{cat} and K_m. Values of k_{cat}/K_m were determined from the slope of a Lineweaver-Burke plot. Brønsted plots were constructed by plotting the log of the rate constant against the pK_a of the leaving group, according to the Brønsted equation:

$$\log k = A + \beta_{lg} pK_a \quad (4.1)$$

The Brønsted coefficient, β$_{lg}$, was obtained from the slope of the plot determined by a linear least squares fitting of the data using the program Grafit (Leatherbarrow, 1998).

Assays used to determine the pH-dependence of k_{cat}/K_m employed low concentrations of ONPX$_2$ substrate (0.35 mM), 50 mM NaCl, 0.1 % BSA, and the appropriate buffer for a given pH range (pH 2-5: 20 mM succinate; pH 5-7: 20 mM MES; pH 7-8: 20 mM HEPES; pH 8-11: 20 mM CHES). After a 15 minute preincubation time at 25 °C, the enzymatic reaction was initiated by addition of 10 μL of enzyme (3.0×10^{-3} mM final) to 190 μL of the assay solution. Progress curves were followed by measuring the release of *o*-nitrophenolate at 400 nm *versus* time until at least 80 % substrate depletion was observed. The pH of each assay solution was

measured after completion of the reaction. An aliquot of the assay mix was then re-assayed at pH 6.0 to confirm the stability of the enzyme compared to an aliquot of unassayed enzyme which had not been exposed to assay conditions. Experimental data were fitted to a pseudo-first-order expression, which upon division by the enzyme concentration yielded k_{cat}/K_m values. This method obviated the need to correct for the variation of extinction coefficient of ONPX$_2$ with pH and eliminated any errors associated with the determination of substrate concentrations. The k_{cat}/K_m data were then plotted as a function of pH and fitted to a bell-shaped activity profile, described in equation 4.2, from which apparent pK_a values were determined.

$$\left(\frac{k_{cat}}{K_m}\right)_{obs} = \left(\frac{k_{cat}}{K_m}\right)_{max}\left(\frac{1}{1+\dfrac{10^{-pH}}{10^{-pK_a}}+\dfrac{10^{-pK_{a2}}}{10^{-pH}}}\right) \quad (4.2)$$

(ii) Pre-Steady State Kinetics

Pre-steady state kinetic measurements were taken for mutant BCX proteins using a stopped-flow spectrophotometer (Olis RSM-1000) with a 2 cm cell path length and a circulating water bath, as described previously (Zechel *et al.*, 1998). The dead-time of the instrument was 2.5 ms. Data were collected at a rate of 1000 spectra/s over a 10 s time period. Assays consisted of various amounts of 2,5-DNPX$_2$ substrate (0.30 mM to 2.20 mM) and enzyme (1.0×10^{-3} mM to 2.0×10^{-3} mM) in 10 mM MES, 25 mM NaCl, buffer (pH 6.0) at 25 °C. The limited solubility of 2,5-DNPX$_2$ under the conditions described precluded assays containing higher concentrations of substrate. Since no pre-steady state burst was observed with N35D, N35D/E78Q or N35D/E172Q BCX, further data analysis was not necessary.

(iii) Kinetics of Covalent Inhibition

Inhibition studies of N35D BCX were performed using previously described methods (Miao *et al.*, 1994). Enzyme (1.5×10^{-3} mM) was incubated at 40 °C in a buffer (pH 4.1) containing 20 mM succinate, 50 mM NaCl and 0.1 % BSA in the presence of DNP2FXb inhibitor at concentrations of 1.70 mM, 1.00 mM, 0.65 mM or 0.40 mM. A control in which no inhibitor was added was also performed. Residual enzymatic activity was determined by removing 5 μL aliquots of the reaction mixture at various times and assaying in a solution of 2.89 mM ONPX$_2$ in 20 mM MES, 20 mM NaCl, 0.1 % BSA, pH 6.0 buffer by monitoring the release of *o*-nitrophenolate at 400 nm. Pseudo-first-order rate constants (k_{obs}) at each inhibitor concentration were determined by fitting the residual activity (v/v$_o$) *versus* time data directly to a first-order equation as described previously (Miao *et al.*, 1994). Values of k_i (inhibition rate constant) and K_i (dissociation constant for the inhibitor) were determined by fitting values of k_{obs} to equation 4.3. The second-order rate constant, k_i/K_i, was determined from the slope of a reciprocal plot.

$$k_{obs} = \frac{k_i[\text{DNP2FXb}]}{K_i + [\text{DNP2FXb}]} \qquad (4.3)$$

4.2.3 NMR

All NMR spectra were recorded using a Varian Unity™ spectrometer operating at 500 MHz for protons.

(i) Titration curves

The [δ-^{13}C]-Glu and -Gln enriched N35D BCX protein was dialyzed or exchanged, using a microconcentration device, into 10 mM sodium phosphate, 10% D$_2$O/90% H$_2$O, at pH* ~ 6.0.

The sample contained 1.20 mM of selectively labelled N35D BCX in a final volume of 2.0 mL. One dimensional ^{13}C-NMR spectra were recorded as a function of pH* at 25 °C and processed as described previously (McIntosh *et al.*, 1996). Chemical shifts were referenced to an external sample of DSS at 0.00 ppm.

The ^{13}C-NMR spectra of [δ-^{13}C]-Glu and -Gln enriched N35D BCX, covalently modified with DNP2FXb, were recorded and processed as described above for the uninhibited protein. Solid DNP2FXb (2.00 mM final) was added directly to the ^{13}C-labelled protein, initially at 1.20 mM in 2.0 mL of 10 mM sodium phosphate, 10 % D_2O/90% H_2O at pH* 6.21. The protein was completely modified within 30 minutes, as judged by ^{13}C-NMR measurements, and was stable for the period over which the measurements were taken. The inhibition was also confirmed by mass spectrometry (observed 20 677 ± 2 Da, expected 20 675 Da).

Titration curves were generated by recording ^{13}C-NMR spectra of [δ-^{13}C]-Glu and -Gln labelled xylanases as a function of pH* at 25 °C. Proteins were titrated using microlitre aliquots of either 0.25-0.50 M HCl or NaOH. The pH* of the sample was determined using a Corning G-P Micro Combo™ electrode. After measuring the acidic limb of the titration curve, the protein was exchanged into neutral buffer, using a micro concentrating device, to remove any excess salt and to avoid aggregation resulting from the addition of a large quantity of base. Titration of the basic limb was then carried out in a similar manner to that used for the acidic limb. The sample was also centrifuged periodically to remove any precipitate that formed during the titration. Individual δ-carbon resonances of glutamate and glutamine side chains of mutant xylanase proteins were assigned based on previous analysis of the WT spectra (McIntosh *et al.*, 1996; Plesniak *et al.*, 1996b). pK_a values were determined by nonlinear least squares fitting of the observed data to models involving one, two, or three sequential ionizations (equations 4.4, 4.5,

and 4.6) (Shrager *et al.*, 1972) using the program, PlotData (TRIUMF, University of British Columbia). The inherent error of the pH measurements is estimated to be $\pm$ 0.1 pH unit.

NMR-derived titration curves characterized by one, two, or three apparent or macroscopic pK_a values are described by equation 3, 4, and 5, respectively (Appendix I). δ_{obs} is the chemical shift of the residue being monitored, and δ_i represents the chemical shift of the residue in each ionization state of the enzyme:

$$\delta_{obs} = \frac{\delta_a 10^{-pH} + \delta_b 10^{-pK_a}}{10^{-pH} + 10^{-pK_a}} \qquad (4.4)$$

$$\delta_{obs} = \frac{\delta_a 10^{-2pH} + \delta_b 10^{-(pH+pK_{a1})} + \delta_c 10^{-(pK_{a1}+pK_{a2})}}{10^{-2pH} + 10^{-(pH+pK_{a1})} + 10^{-(pK_{a1}+pK_{a2})}} \qquad (4.5)$$

$$\delta_{obs} = \frac{\delta_a 10^{-(3pH)} + \delta_b 10^{-(pK_{a3}+2pH)} + \delta_c 10^{-(pK_{a2}+pK_{a3}+pH)} + \delta_d 10^{-(pK_{a1}+pK_{a2}+pK_{a3})}}{10^{-(3pH)} + 10^{-(pK_{a3}+2pH)} + 10^{-(pK_{a2}+pK_{a3}+pH)} + 10^{-(pK_{a1}+pK_{a2}+pK_{a3})}} \qquad (4.6)$$

Selection of the appropriate model was based on the criterion of using the minimal number of ionization events to adequately fit the observed titration data.

(ii) Deuterium Isotope Shifts

Deuterium isotope shifts of the $[\delta-^{13}C]$-Glu and -Gln side chains of isotopically labelled N35D BCX were measured for both free and inhibited proteins. Spectra were recorded at 25 $^\circ$C and processed as described above. The initial sample conditions for the free protein were 10 mM sodium phosphate, 10 % D_2O at pH* 6.32, 0.72 mM N35D, while for the inhibited protein the initial conditions were 10 mM sodium phosphate, 10 % D_2O at pH* 5.90, 1.20 mM N35D. After recording the initial spectra of these proteins in 10 % D_2O, samples were exchanged into 90 %

D_2O using a microconcentration device, and the pH* was readjusted to the same value as in the respective 10 % D_2O sample by addition of 0.1 M HCl.

(iii) Stereochemistry

The stereochemical course of hydrolysis of N35D BCX was determined by adding 60 μL of enzyme (0.015 mM N35D final) directly to a 5 mm NMR tube containing 5.4 mM $ONPX_2$, 10 mM sodium phosphate, 50 mM NaCl, 99.9 % D_2O at pH* 4.8 (Lawson *et al.*, 1996). One-dimensional ^1H spectra were recorded at 25 °C as a function of time (t = 5, 10, 20, 25, 210 minutes) after addition of enzyme in order to monitor the hydrolysis and subsequent mutarotation of the anomeric proton of the xylobiose unit proximal to the departing phenolate group.

4.2.4 Electrospray Mass Spectrometry

Labelling and identification of the active-site nucleophile was performed as described previously (Lawson *et al.*, 1996; Miao *et al.*, 1994). N35D BCX (0.50 mM final) was inhibited at 40 °C in a buffer (pH 4.1) containing 20 mM succinate, 50 mM NaCl, and DNP2FXb (1.50 mM final). After 8 hours of inhibition, an aliquot of the inhibited sample was analyzed using a Perkin Elmer Sciex API 300 LC-ESMS system. A major peak corresponding to the mass of the covalently labelled protein was observed (20 666 ± 2 Da) and a relatively minor peak corresponding to the mass of the unlabelled protein were observed (20 401 ± 2 Da). After heat-denaturing by boiling in a water bath for 2 minutes and subsequent cooling to room temperature, the covalently modified N35D protein (0.1 mM final) was subject to proteolytic digestion for 7 hours using a solution containing 0.5 mg/mL pepsin and 200 mM sodium phosphate (pH 2.0). A

control experiment in which no DNP2FXb inhibitor was added was performed in parallel. Neutral loss MS/MS studies on the labelled peptide were performed as described previously for WT BCX (Miao *et al.*, 1994). The triple quadrupole neutral loss scan mode was set to detect a mass loss of m/z 133.5, corresponding to the loss of 2FXb from a peptide ion in the doubly charged state.

4.2.5 X-ray Crystallography

Crystals of N35D BCX were grown and soaked with DNP2FXb at pH 7.5 as previously described for the WT enzyme (Sidhu *et al.*, 1999). Diffraction data were collected from a single N35D BCX crystal and a single crystal of N35D-2FXb BCX on a Rigaku R-AXIS IIC imaging plate area detector system using CuK_α radiation supplied by a Rigaku RU300 rotating anode generator operating at 50 kV and 100 mA. Each diffraction data frame was exposed for 20 minutes during which time the crystal was oscillated through 1.2°. Intensity data were integrated, scaled, and reduced to structure factor amplitudes with the HKL suite of programs (Otwinowski and Minor, 1997) (Table 4.2). Because both types of crystals retained unit cells isomorphous to WT BCX, the WT model, with residue 35 truncated to alanine was used as the starting model in each case. These models were subjected to rigid body, simulated annealing, positional, and individual isotropic thermal factor refinement using X-PLOR (Brunger, 1992) and the CCP4 Suite (Collaborative Computational Project Number 4, 1994). At this point F_o-F_c difference electron density maps were calculated and both Asp35 and the 2FXb saccharide were built into observed density with the program O (Jones *et al.*, 1991). The models were then refined further with X-PLOR. A standard carbohydrate topology and parameter library was used in the refinement of the glycosyl-enzyme intermediate (Sidhu *et al.*, 1999). The structural models were

examined periodically during refinement with F_o-F_c, $2F_o$-F_c, and fragment-deleted difference electron density maps. Manual adjustments were made as necessary and solvent molecules were identified. The validity of solvent molecules was assessed based on both hydrogen bonding potential to appropriate protein atoms and refinement of a thermal factor of less than 75 Å^2 (Table 4.3). The coordinate error estimated from a Luzzati plot (Luzzati, 1952) is 0.18 Å for N35D BCX and 0.19 Å for N35D-2FXb BCX (plots not shown). Atomic coordinates and related structure factors have been deposited in the Brookhaven Protein Data Bank (Bernstein *et al.*, 1977) with identification codes 1C5H for N35D BCX and 1C5I for N35D-2FXb BCX. (Structural illustrations using atomic coordinates were generated using the programs Bobscript (Kraulis, 1991) and Raster3d (Merrit and Murphy, 1994).

Table 4.2. X-ray crystallographic data collection parameters.

Parameters	N35D BCX	N35D-2FXb BCX
Space group	$P2_12_12_1$	$P2_12_12_1$
Cell dimensions (Å)		
a	44.05	43.83
b	52.69	52.74
c	78.61	78.80
Number of measurements	150984	99311
Number of unique reflections	27301	17579
Mean $I/\sigma I^{\dagger}$	21.1 (7.0)	25.8 (11.1)
Merging R-factor (%)[a,b]	5.7 (15.2)	5.7 (14.2)
Resolution range (Å)	∞ - 1.55	∞ - 1.8

[a]Values in parentheses are for data in the highest resolution shell (1.61 – 1.55 Å for N35D BCX and 1.86 – 1.80 for N35D-2FXb BCX).

$$^bR_{merge} = \frac{\sum_{hkl}\sum_{i=0}^{n}\left|I_i - \bar{I}_{hkl}\right|}{\sum_{hkl}\sum_{i=0}^{n}I_{hkl}}$$

Table 4.3. X-ray crystallographic refinement statistics.

Parameters	N35D-BCX	N35D-2FXb BCX
Number of reflections	25023	16559
Resolution range (Å)	10 – 1.55	10 – 1.8
Completeness within range (%)	91.8	94.5
Number of non-hydrogen protein atoms	1448	1448
Number of non-hydrogen ligand atoms		18
Number of solvent atoms	146	129
Average thermal factors (Å^2)		
Protein	13.2	12.3
Ligand		23.2
Solvent	36.6	34.0
Final refinement R-factor (%)[a]	19.4	19.3

Stereochemistry	r.m.s. deviations	
bonds (Å)	0.007	0.007
angles (°)	1.210	1.136

$$^{a}\text{R-factor} = \frac{\sum_{hkl}|F_{o,hkl} - F_{c,hkl}|}{\sum_{hkl}|F_{o,hkl}|}$$

4.3 RESULTS

4.3.1 pH-dependent Activity of N35D BCX

Comparison of the pH-dependence of the second-order rate constant, k_{cat}/K_m, for the hydrolysis of orthonitrophenyl β-xylobioside (ONPX$_2$) by WT and N35D BCX reveals that the point mutation causes a pronounced shift in the pH optimum of this enzyme from 5.7 to 4.6 and an increase in its activity by ~ 20 % (Figure 4.1). Therefore, a single substitution at position 35 leads to a decrease in pH optimum by 1.1 units. This is consistent with previous studies of Family 11 xylanases where there is an Asp at position 35 for those with an "acidic" pH optimum, and an Asn for those functioning with an "alkaline" pH optimum (Fushinobu *et al.*, 1998; Krengel and Dijkstra, 1996; Torronen and Rouvinen, 1995).

The activity profile of N35D BCX is characterized by an acidic limb that follows an apparent pK_a of 3.5 and a basic limb that follows a pK_a of 5.8 when fitted to a model involving two ionizable sites. This is noticeably different from the pH-dependent activity of WT BCX whose profile is characterized by two ionizations with apparent pK_a values of 4.6 and 6.7 for the acidic and basic limbs, respectively. Previous studies of WT BCX have shown that the group that ionizes with a pK_a of 4.6 is the nucleophile, Glu78, while that with a pK_a of 6.7 is the general acid catalyst, Glu172 (McIntosh *et al.*, 1996; Miao *et al.*, 1994; Wakarchuk *et al.*, 1994a). Extrapolation to N35D BCX would lead to the erroneous prediction that Glu78 has a pK_a of 3.5 and Glu172 has a pK_a of 5.8 in this mutant protein (discussed later). However, on the basis of the structure, this is counter-intuitive. The presence of Asp35 might be expected to either not change (in the case of a neutral aspartic acid), or to elevate (a negatively charged aspartate) the pK_a of the neighboring Glu172, relative to that found in the WT protein with Asn35, and thus shift the pH optimum to a more basic rather than a more acidic value.
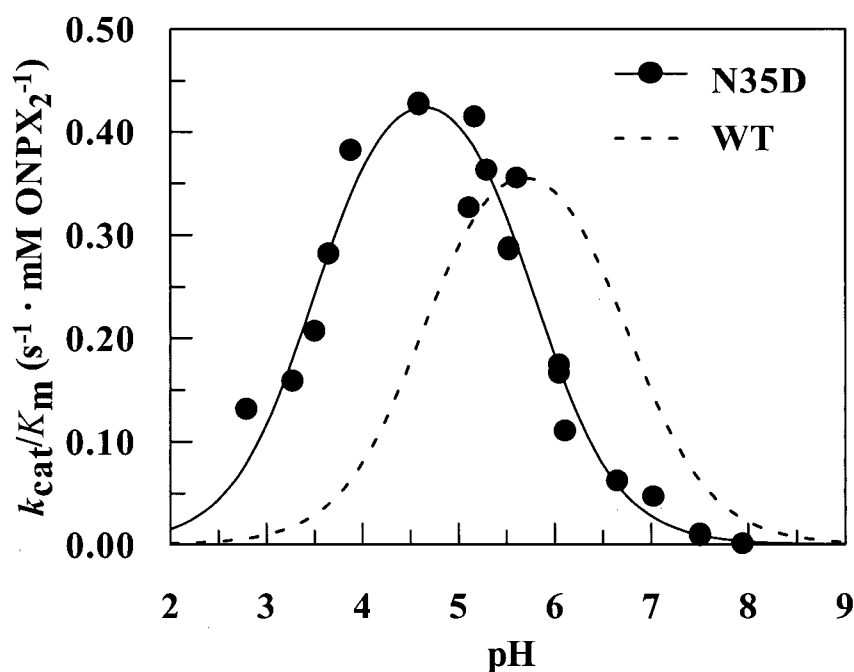
Figure 4.1. pH-dependence of k_{cat}/K_m for N35D BCX (●) at 25 °C towards the synthetic substrate orthonitrophenyl β-xylobioside (ONPX₂). Substitution of an Asp residue at position 35 shifts the pH optimum from 5.7 for the WT protein to 4.6 for the N35D mutant. The activity profile follows ionizations with pK_a values of 3.5 and 5.8 in the N35D enzyme (—) and 4.6 and 6.7 in the WT enzyme (---) (McIntosh *et al.*, 1996). The data points, shown only for N35D BCX, were fitted as described in the "Materials and Methods" section.

4.3.2 Structure of N35D BCX

The crystal structure of N35D BCX was determined at pH 7.5 to a resolution of 1.55 Å with an R-factor of 19.4% (Figure 4.2). This structure is highly similar to that of WT BCX (Wakarchuk *et al.*, 1994a), with an overall r.m.s. deviation of only 0.23 Å for all atoms between these two models. Upon detailed inspection, it is seen that the side chain of Asp35 adopts approximately the same conformation as that of the WT Asn35, differing only in the χ_2 dihedral angle by a rotation of ~ 16°. A small rotation in χ_3 (~ 8°) of Glu172 is also observed. Correspondingly, the distance between Asn35 $N^{\delta2}$/Asp35 $O^{\delta2}$ and Glu172 $O^{\epsilon2}$ increases very slightly from 3.1 Å in WT BCX to 3.2 Å in N35D BCX due to the amino acid substitution at position 35 (Table 4.4) (Note: as shown below, at pH 7.5, Asp35 is negatively charged and Glu172 is neutral in N35D BCX, whereas in the WT protein, Asn35 is neutral and Glu172 is negatively charged). Asp35 $O^{\delta2}$ in the variant structure also forms an additional, albeit bent, hydrogen bond with the amide nitrogen of Phe36 (bond angle $O^{\delta2}\cdots HN = 120°$). This interaction is not possible in the WT enzyme as Asn35 $N^{\delta2}$ and Phe36 N are unable to hydrogen bond to one another. The exchange of asparagine for aspartate at position 35 appears to increase the thermal motion of both residues 35 and 172, as determined from normalized isotropic thermal factors. The average thermal factor for residue 35 increases from 11 $Å^2$ to 17 $Å^2$, while for residue 172 this parameter increases from 11 $Å^2$ to 14 $Å^2$. No significant change in the position of Glu78 is observed. The only other noteworthy perturbations are small (~ 0.5-0.7 Å) shifts in the positions of the guanido groups of Arg112, which is within the binding cleft of BCX, and Arg122, which is exposed on the surface of protein. In summary, only subtle structural perturbations accompany the substitution of Asp for Asn35. Thus, there is no apparent conformational basis for the shift in pH optimum of N35D BCX to a more acidic value compared to the WT enzyme.
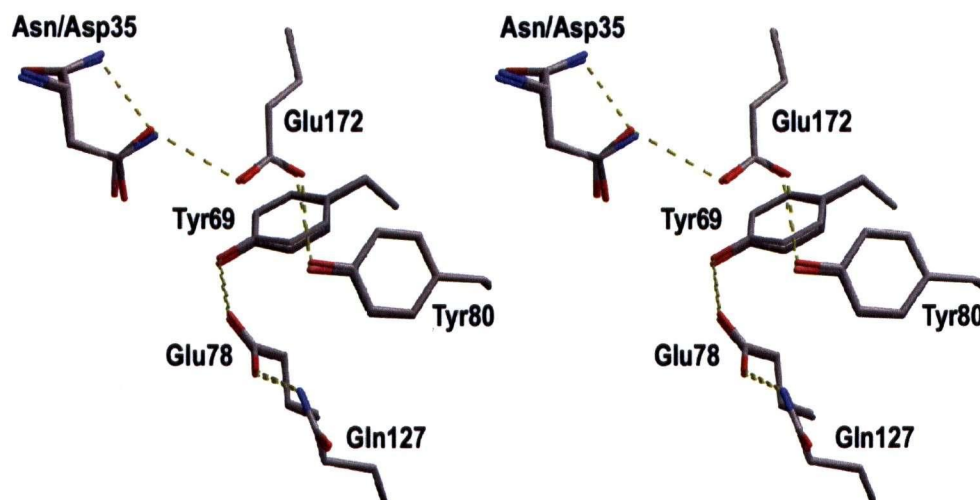
Figure 4.2. A stereo-drawing of the structural conformations of key active-site residues of N35D BCX (dark grey) superimposed upon those of WT BCX residues (light grey) (pH 7.5). Potential hydrogen bonds are indicated by yellow dashed lines, oxygen atoms are shown in red and nitrogen atoms in blue. The structures are highly similar with an overall r.m.s deviation of only 0.23 Å. See Table 4.4 for a listing of selected interatomic distances.

Table 4.4. Selected interatomic distances within the active-site of WT and N35D BCX.

Interaction	Distances (Å)			
	N35D	N35D-2FXb	WT[a]	WT-2FXb[a]
Asn/Asp35 $N^{\delta 2}/O^{\delta 2}$ – Glu172 $O^{\varepsilon 2}$	3.2	2.7	3.1	3.3
Glu78 $O^{\varepsilon 2}$ – Asn/Asp35 $O^{\delta 1}$	6.6	6.2	6.4	6.5
Glu78 $O^{\varepsilon 2}$ – Glu172 $O^{\varepsilon 2}$	5.6	5.5	5.6	5.8
Asn/Asp35 $N^{\delta 2}/O^{\delta 2}$ – Phe36 N	2.9	2.9	3.2	3.0
Glu172 $O^{\varepsilon 2}$ – Wat[b]	3.7	3.9	3.8	3.1
Glu172 $O^{\varepsilon 1}$ – Tyr80 O^{η}	2.9	2.9	2.7	2.8
Tyr80 O^{η} – Wat[b]	2.9	2.8	2.8	2.7
Glu78 $O^{\varepsilon 2}$ – Tyr69 O^{η}	2.5	2.9	2.6	3.0
Glu78 $O^{\varepsilon 2}$ – Gln127 $N^{\varepsilon 2}$	2.7	2.6	2.7	2.6
Glu172 $O^{\varepsilon 2}$ – Arg112 N^{ε}	7.0	7.2	7.1	7.2
Asn/Asp35 $N^{\delta 2}/O^{\delta 2}$ – Asp11 $O^{\delta 2}$	6.1	5.9	6.1	6.0
Glu78 $O^{\varepsilon 2}$ – Arg112 N^{ε}	5.9	5.9	6.2	6.0
Asn/Asp35 $N^{\delta 2}/O^{\delta 2}$ – Arg112 N^{ε}	8.1	7.9	7.8	7.9

[a]Structural coordinates used for distance measurements were obtained from the Protein Data Bank (Bernstein *et al.*, 1977), PDB identification number 1XNB for WT BCX (Wakarchuk *et al.*, 1994a) and 1BVV for WT-2FXb BCX (Sidhu *et al.*, 1999).
[b]See text for discussion.

4.3.3 Direct Measurement of the pK_a values of the Catalytic Residues of N35D BCX

To ascertain which groups are responsible for the activity profile of N35D BCX, the pK_a values of the catalytic residues were measured directly by monitoring the pH-dependence of the carbonyl ^{13}C-NMR chemical shifts of the Glu and Gln sidechains. Analysis of the titration curves of [δ-^{13}C]-glutamic acid labelled N35D BCX protein shows a noteworthy difference when compared to WT BCX (McIntosh *et al.*, 1996) (Figure 4.3). That is, the titration curves of Glu78 and Glu172 are triphasic instead of biphasic, indicating the presence of an additional ionizable group in the active-site. As discussed later, this third titrating group is assigned as Asp35.

The biphasic nature of the titration curves measured previously for Glu78 and Glu172 in WT BCX has been attributed to electrostatic and/or structural coupling of the ionization equilibria of these two catalytic residues. As discussed in detail by Shrager *et al.*, (1972), two or more ionizable groups may show coupled or biphasic titration curves if either the microscopic pK_a or the chemical shift of one is dependent upon the ionization state of the other. The first case is analogous to the classic branched equilibria of a dibasic acid in which each carboxyl has two microscopic pK_a values corresponding to the neutral and charged states of its interacting partner. The second case reflects the fact that the chemical shifts of one residue may be dependent upon the ionization state of the second, for example, through electric field effects or structural perturbations. (An example of this case is when the chemical shift of a non-ionizable group is dependent upon the protonation states of nearby titratable groups). Fitting of the titration data for WT BCX to either model reveals that the predominant pK_a values of Glu78 and Glu172 are 4.6 and 6.7, respectively. These arguments also hold for triphasic titration curves involving three coupled protonatable groups. However, with eight possible ionization states, the data cannot be
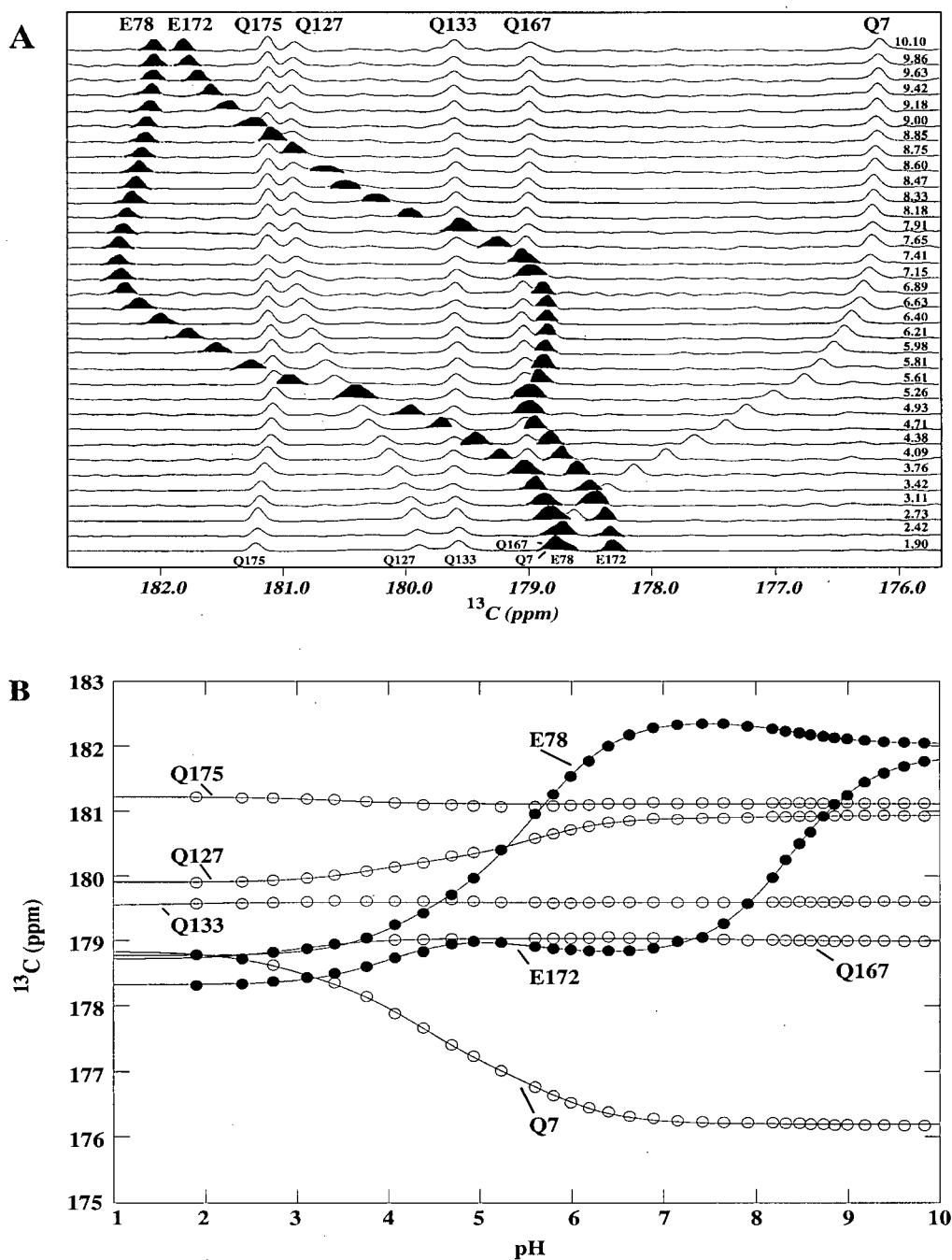
Figure 4.3. (A) ^{13}C-NMR spectra of N35D BCX recorded as a function of pH at 25 °C. The peaks corresponding to Glu78 and Glu172 are shaded in black for emphasis. Spectral assignments were based on previous analysis of WT BCX (McIntosh *et al.*, 1996) and pH values are listed above each spectrum. (B) Apparent pK_a values were determined by fitting the data for the two Glu (●) and five Gln (○) carbonyls to an equation describing the pH-dependence of the chemical shift of a residue to one or more sequential ionization events.

readily fitted to extract the desired microscopic pK_a values (Scheme 4.1, Discussion). I therefore chose to fit the titration curves measured for N35D BCX to simple equations describing sequential ionization equilibria in order to extract apparent pK_a values. We attribute the apparent pK_a value corresponding to the largest positive chemical shift change (ionized *versus* neutral) of each Glu or Asp residue to reflect its own ionization, and those corresponding to smaller chemical shift changes to the ionization equilibria of neighboring residues.

In the case of N35D BCX, the titration curve of Glu78 has three apparent pK_a values (Table 4.5). The first, with a minor chemical shift change of +0.96 ppm, follows a macroscopic pK_a of 4.2 and is attributed to the ionization of Asp35. The second, with a major chemical shift change of +2.69 ppm, follows a pK_a of 5.7 and is assigned to the ionization of Glu78 itself. Finally a third, with a minor chemical shift change of -0.39 ppm, follows a pK_a of 8.4 and reflects the ionization of Glu172. Similarly, in the titration curve of Glu172, three apparent pK_a values can be observed. The first minor chemical shift change of +0.76 ppm follows a pK_a of 4.0 and is due to the ionization of Asp35. The second minor chemical shift change of -0.32 ppm follows a pK_a of 5.5 and is due to the ionization of Glu78. Finally, a third and major chemical shift change of +3.09 ppm follows a pK_a of 8.4 and is assigned to the ionization of Glu172 itself. In a similar manner, the ionization of Asp35 was monitored directly in a ^{13}C-γ-Asp labelled N35D protein (data not shown). The titration curve of Asp35 is biphasic in nature and reflects two pK_a values: the first major chemical shift change of +2.13 ppm follows a pK_a of 3.7 and is attributed to the ionization of Asp35 itself, whereas the second minor change in chemical shift of +1.07 ppm follows a pK_a of 5.6 and is due to the ionization of Glu78. The pK_a of Glu172 was not apparent in the titration curve of Asp35 because the data used to directly measure the pK_a of Asp35 did not extend beyond pH 8.3.

Table 4.5. Experimentally measured apparent pK_a values of N35D and WT BCX obtained from ^{13}C-NMR pH titrations.[a]

Residue	N35D BCX		WT BCX[c]	
	pK_a	$\delta\Delta^b$	pK_a	$\delta\Delta^b$
Glu78	4.2	+0.96 ppm	<u>4.6</u>	+2.80 ppm
	<u>5.7</u>	+2.69 ppm	6.5	+0.33 ppm
	8.4	-0.39 ppm		
Glu172	4.0	+0.76 ppm	<u>6.7</u>	+2.78 ppm
	5.5	-0.32 ppm	4.6	+0.44 ppm
	<u>8.4</u>	+3.09 ppm		
Asp35	<u>3.7</u>	+2.13 ppm		
	5.6	+1.07 ppm		

	N35D-2FXb BCX		WT-2FXb BCX[c]	
Glu78-2FXb	(2.9^d)	-0.03 ppm	e	e
	(9.3^d)	-0.18 ppm		
Glu172	<u>1.9^f</u>	+1.63 ppm	<u>4.2</u>	+1.58 ppm
	<u>3.4^f</u>	+0.48 ppm		
	9.0	+0.10 ppm		

[a]The major apparent pK_a, assigned to the ionization of the given residue, is underlined. An error in the pK_a value of ± 0.1 pH units is estimated from the error in pH measurements.
[b]The $\delta\Delta$ value refers to the magnitude and direction of the chemical shift change upon deprotonation of the listed residue. The error in chemical shift is estimated to be ± 0.015 ppm.
[c]Data taken from McIntosh et al., (1996).
[d]Change in chemical shift does not reflect ionization of the residue itself since it is covalently attached to the inhibitor.
[e]No observable pH-dependent change in chemical shift.
[f]See text for discussion.

The resonances of the side chain δ carbonyls of all Gln residues are also detected in the ^{13}C-NMR spectra of N35D BCX (Figure 4.3). Their presence is due to the metabolic interconversion of glutamic acid to glutamine in *Escherichia coli*. The ^{13}C chemical shifts of the non-ionizable Gln residues are pH-dependent due to the influence of other titratable side chains within the protein; thus these serve as reporter groups to further verify the pK_a values measured for residues 35, 78 and 172. In particular, in N35D BCX the pH-dependent chemical shift of Gln7 predominantly follows two pK_a values; namely a pK_a of 3.9 ($\delta\Delta$ =1.37 ppm) due to the ionization of Asp35, and a pK_a of 5.6 ($\delta\Delta$ =1.17 ppm) due to the ionization of Glu78. In the WT protein, the resonance of Gln7 follows the titrations of Glu78 (pK_a 4.5, $\delta\Delta$ = 2.09 ppm) and Glu172 (pK_a 6.5, $\delta\Delta$ = 0.47 ppm) (McIntosh *et al.*, 1996). Similarly, the resonance of Gln127 is also pH-dependent, following the ionizations of Glu172 (pK_a 8.4, $\delta\Delta$ = 0.03 ppm), Glu78 (pK_a 5.6, $\delta\Delta$ = 0.65 ppm) and Asp35 (pK_a 3.8, $\delta\Delta$ = 0.65 ppm) in N35D BCX and of Glu172 (pK_a 6.6, $\delta\Delta$ = 0.32 ppm) and Glu78 (pK_a 4.5, $\delta\Delta$ = 0.76 ppm) in the WT protein (McIntosh *et al.*, 1996).

The analyses of the ionization behaviour of Asp35, Glu78 and Glu172 are further supported by deuterium isotope shift measurements (Joshi *et al.*, 1997; Ladner *et al.*, 1975; Yamazaki *et al.*, 1994). An estimate of the protonation state of a carboxyl group can be made by observing the difference in its ^{13}C chemical shift in H_2O *versus* D_2O solutions. A neutral carboxylic acid group is expected to show an isotope shift of ~ -0.25 ppm between its protonated and deuterated forms, whereas a carboxylate would show no such effect. Measurement of the deuterium isotope shift of the δ sidechain carbons of Glu78 and Glu172 in N35D BCX protein reveals that at pH* 6.32, Glu78 is deprotonated (no apparent isotope shift), whereas Glu172 is protonated (isotope shift of -0.29 ppm). These data are consistent with the measured pK_a values of the three active-site carboxyl groups in N35D BCX.

Based on both titration curves and isotope shifts, we conclude that the pK_a values corresponding primarily to the ionizations of Asp35, Glu78 and Glu172 in N35D BCX are 3.7, 5.7 and 8.4, respectively. The small differences in the corresponding pK_a values measured from the multiphasic titration curves of the Asp, Glu and Gln residues (Table 4.5) are attributed to difficulties in accurately fitting these data and the complex nature of the structural or electrostatic interactions in this highly coupled network of ionizable sidechains. Regardless, these data clearly differ from the pK_a values of 4.6 and 6.8 measured for Glu78 and Glu172 in the WT enzyme and confirm the expectation that the substitution of Asn35 by Asp elevates the pK_a values of the nearby catalytic glutamic acid residues.

4.3.4 Determining the Catalytic Roles of Asp35, Glu78 and Glu172

The directly measured pK_a values of Asp35, Glu78, and Glu172 indicate that the pH-dependent activity of N35D BCX appears to follow the ionization of Asp35 (pK_a 3.7) and Glu78 (pK_a 5.7). The pK_a of Glu172 (8.4) is not apparent in the activity profile. This presents an interesting problem as the acidic limb of the activity profile, which reflects the deprotonation of the nucleophile Glu78 in WT BCX, now appears to follow the ionization of Asp35, while the basic limb of the activity profile, which reflects the need to have the acid catalyst Glu172 protonated in WT BCX, now appears to follow the ionization of Glu78. These observations begged the question of whether or not the mechanism of BCX had changed due to the substitution of Asn35 by Asp.

To address this question, several experimental approaches were utilized. First, determination of the stereochemical course of hydrolysis using 2,5-DNPX$_2$ as a substrate indicated that, as with the WT enzyme, the initial product released was the β anomer of the

xylobiose (Figure 4.4). Hence, both WT and N35D BCX utilize a double-displacement retaining mechanism to hydrolyze aryl β-xylobiosides.

Second, the role of Glu78 as the nucleophile was ascertained by three methods. The essential function of Glu78 was confirmed by the observation that the N35D/E78Q double mutant has no detectable activity on $ONPX_2$ (Table 4.6). Similarly, the single (nucleophile) mutant E78Q BCX is completely inactive. Using electrospray mass spectrometry (ESMS), we also demonstrated that a mechanism-based inhibitor, 2,4-dinitrophenyl 2-deoxy-2-fluoro-β-xylobioside (DNP2FXb), covalently attaches to Glu78. In particular, peptic digestion of inhibited N35D BCX yielded the same doubly charged covalently modified peptide containing Glu78 (m/z of 826 in neutral loss mode) as observed in a previous analysis of WT BCX (Miao *et al.*, 1994) (data not shown). Finally, the crystal structure of the N35D BCX glycosyl-enzyme intermediate (N35D-2FXb) clearly shows covalent modification at Glu78 by the DNP2FXb inhibitor (details discussed subsequently).

Third, the role of Glu172 was also probed by site-directed mutagenesis. Analysis of the activity of the double mutant protein, N35D/E172Q, indicated that Glu172 still plays a primary role in functioning as the general acid/base catalyst in N35D BCX. This is not surprising given the structural similarity of the mutant and WT enzymes (Figure 4.2), and thus the conserved positioning of the side chain of Glu172 with respect to the binding site for xylosic substrates. Specifically, similar values of k_{cat}/K_m for hydrolysis of $ONPX_2$ were found for both the N35D/E172Q double mutant protein (0.021 s^{-1} mM^{-1}) and the E172Q single mutant protein (0.075 s^{-1} mM^{-1}) (Table 4.6). Note that this synthetic substrate has an activated leaving group that needs less general acid catalytic assistance for departure. Therefore, activity is observed, albeit at a substantially reduced rate, even with BCX variants lacking their general acid catalyst.
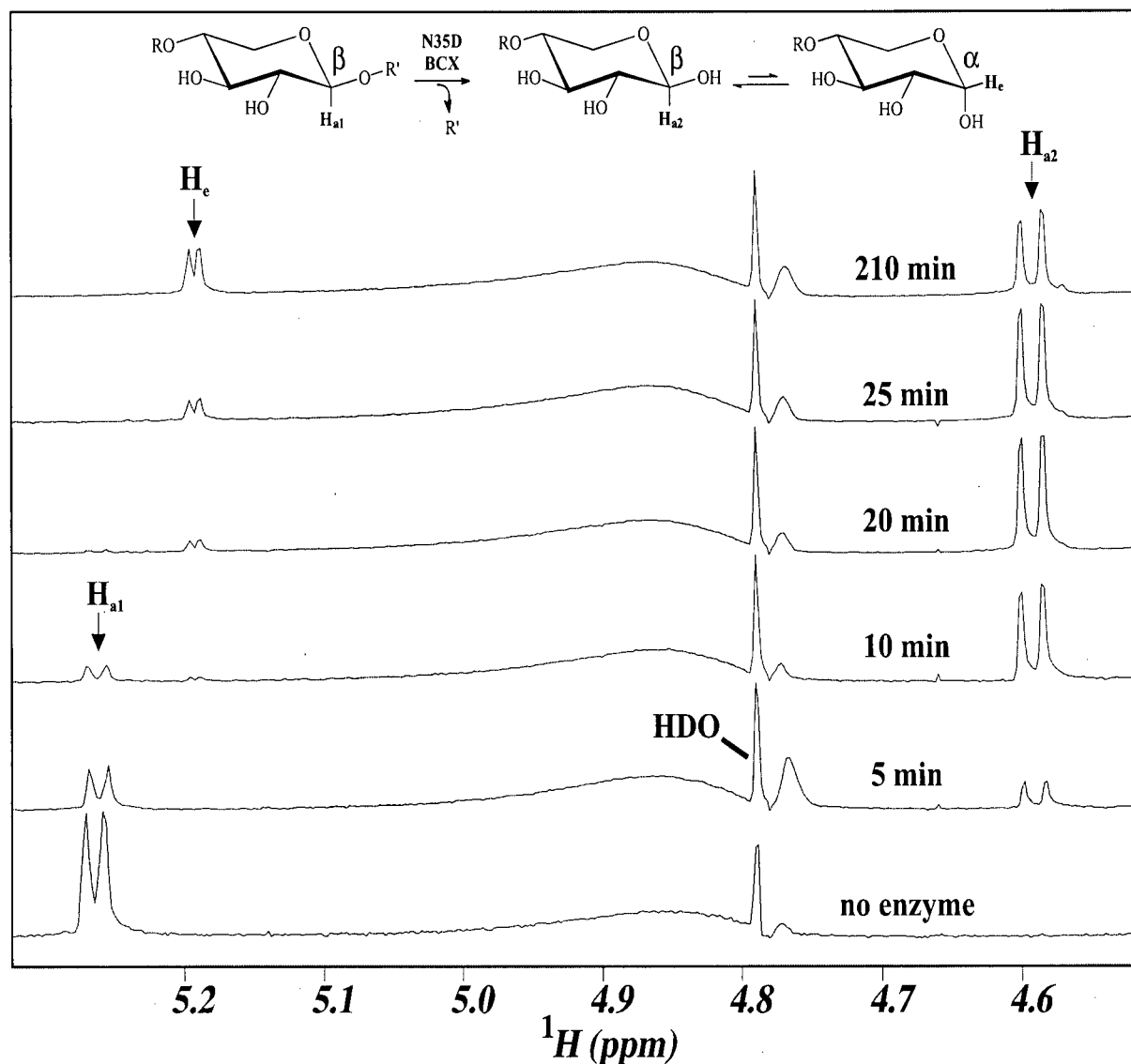
Figure 4.4. Stereochemical course of hydrolysis of ONPX$_2$ by N35D BCX at 25 °C, 99.9 % D$_2$O and pH* 4.8. ^{1}H-NMR spectra were recorded as a function of time after addition of ONPX$_2$ substrate (R = xylose, R' = 2' dinitrophenyl). The control spectrum of ONPX$_2$ with no enzyme (bottom) shows a doublet at 5.26 ppm (J = 7.0 H$_z$) corresponding to the axial anomeric proton of the xylose residue nearest to the aryl leaving group (R'), H$_{a1}$, that is present in the β-anomer of the unhydrolyzed substrate. Initially (t < 10 min) after the addition of N35D enzyme, the doublet at 5.26 ppm disappears while a new doublet at 4.59 ppm (J = 7.9 H$_z$) appears. This is due to the axial proton, H$_{a2}$, of the initial β-anomeric product released and demonstrates that the mechanism of N35D BCX involves stereochemical retention of anomeric configuration of the product. As time proceeds (t = 20-210 min) mutarotation of the initial product occurs as is evident by the appearance of a second peak at 5.19 ppm (J = 3.5 H$_z$) due to the presence of the α-anomer at the reducing end of the xylobioside. The distorted peak near 4.8 ppm is due to the residual signal of HDO.

Table 4.6. Steady state kinetic parameters for the hydrolysis of aryl β-xylobiosides for N35D and WT BCX.[a]

Phenol Substituent	pK_a[b]	Protein	k_{cat}[c] (s^{-1})	K_m[c] (mM)	k_{cat}/K_m[c] (s^{-1} mM^{-1})
2,5-dinitro (2,5-DNPX$_2$)	5.15	**N35D**	**14.8**	**5.7**	**2.6**
		WT[d]	76	2.2	35
3,4-dinitro (3,4-DNPX$_2$)	5.36	**N35D**	**8.2**	**48.1**	**0.18**
		WT[d]	8.3	3.4	2.7
2-nitro (ONPX$_2$)	7.22	**N35D**	**14.5**	**25.6**	**0.56**
		WT[e]	9.6	14	0.66
		N35D/E172Q	0.72	33.3	0.021
		E172Q[f]	0.62	8.3	0.075
		N35D/E78Q	g	g	g
		E78Q	g	g	g
unsubstituted (PhX$_2$)	9.99	**N35D**	**0.14**	**20.1**	**0.0070**
		WT[e]	0.051	8.7	0.0050

[a]Assays were carried out at pH 6.0 and 40 °C.
[b]Phenol pK_a values were taken from Tull and Withers, (1994).
[c]Values of k_{cat}/K_m were taken from the slope of the Lineweaver-Burk plot, whereas values of k_{cat} and K_m were determined from a non-linear fit of the Michaelis-Menten equation.
[d]Data taken from Ziser *et al.*, (1995).
[e]Data taken from Lawson *et al.*, (1996).
[f]Data taken from Lawson *et al.*, (1997).
[g]No detectable enzymatic hydrolysis (data not shown).

4.3.5 Brønsted Analysis of the Activity of N35D BCX Towards Aryl β-Xylobiosides

The enzymatic activity of N35D BCX was measured using a number of different synthetic aryl β-xylobiosides of varying leaving group ability (Table 4.6). ONPX$_2$ was chosen as a reference substrate to compare the activities of all the BCX variants considered in this study. As summarized in Table 4.6, at pH 6, N35D BCX has similar hydrolytic activity toward ONPX$_2$ (k_{cat}/K_m = 0.56 s^{-1} mM^{-1}) compared to the WT enzyme (k_{cat}/K_m = 0.66 s^{-1} mM^{-1}). Note, however, that the activity of N35D BCX is underestimated in this case because measurements of k_{cat} and K_m were performed above its pH optimum of 4.6 and closer to the pH optimum of the WT protein.

Brønsted plots illustrating the dependence of log k_{cat} and log k_{cat}/K_m *versus* pK_a of the leaving group showed a similar dependence of rate on the pK_a of the departing phenol for both WT (β_{lg} = -0.5, correlation coefficient = 0.88 (Lawson *et al.*, 1997)) and N35D BCX (β_{lg} = -0.4, correlation coefficient = 0.88) (Figure 4.5). The data unfortunately exhibit substantial scatter, perhaps due to the placement of the nitro substituent, which may differentially influence the binding of the substrate in the two cases and obscure the electronic effects of interest. However, the trend is clear and the general dependence of k_{cat} on the leaving group pK_a indicates that the glycosylation step is rate-limiting in the hydrolysis of aryl β-xylobiosides, since only the glycosylation step is influenced by the nature of the leaving group. Also, within the limits to which we can trust these Brønsted coefficients, there is a similar extent of negative charge development on the departing phenolate oxygen atom for the two proteins. Pre-steady state kinetic studies of N35D BCX further confirmed that glycosylation is the rate limiting step, since no observable burst phase was detected under a variety of conditions (data not shown). That is,
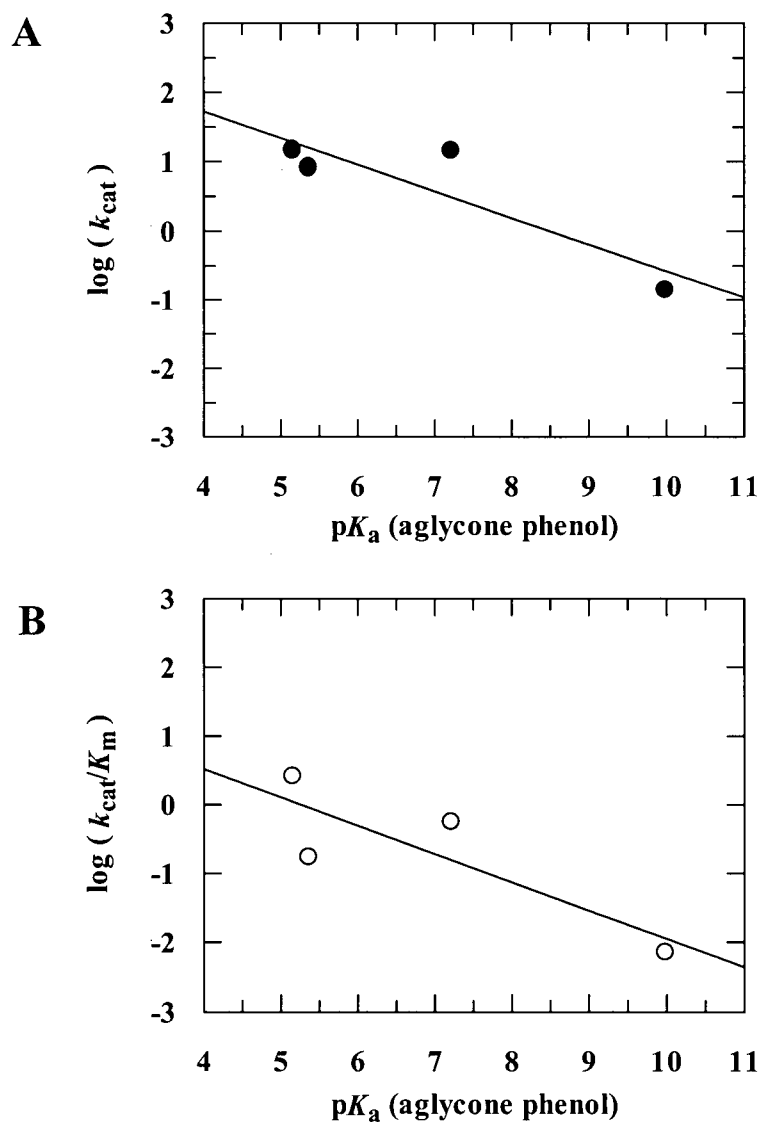
Figure 4.5. Brønsted plots of N35D BCX activity towards aryl β-xylobiosides. Values of the Brønsted coefficient (β_{lg}) for general acid catalysis were determined for k_{cat} (●) (β_{lg} = -0.4, correlation coefficient = 0.88) and k_{cat}/K_m (○) (β_{lg} = -0.4, correlation coefficient = 0.85).

no enzyme intermediate accumulated since the initial glycosylation step was slower than the subsequent deglycosylation step. Together, these data reveal that the rate-limiting step for hydrolysis of aryl xyloside substrates has not changed as a result of a substitution of Asp for Asn35.

4.3.6 Studies of the N35D BCX Glycosyl-Enzyme Intermediate

Use of the mechanism-based inhibitor or "slow substrate", DNP2FXb, has allowed for trapping and subsequent analysis of the WT BCX glycosyl-enzyme intermediate (WT-2FXb) by ESMS, X-ray crystallography and NMR spectroscopy (McIntosh *et al.*, 1996; Miao *et al.*, 1994; Sidhu *et al.*, 1999). N35D BCX is also readily inhibited in a time-dependent manner by DNP2FXb (Figure 4.6). The kinetics of inhibition followed a pseudo-first order scheme with values of the inhibition rate constant, $k_i = 0.68$ min^{-1}, and of the inhibitor dissociation constant, $K_i = 10.5$ mM, at pH 4.1 and 40 °C. Since the DNP2FXb inhibitor has limited solubility under the conditions employed, saturation of the enzyme could not be achieved, thus, the values of k_i and K_i are only estimates. However, as has been previously noted, the value of the second-order rate constant for the reaction of inhibitor and enzyme, k_i/K_i, is reasonably accurate (Miao *et al.*, 1994). The value of k_i/K_i for N35D was determined from the slope of the reciprocal plot and found to be 0.065 min^{-1} mM^{-1}. This is reduced by only 5-fold compared to the value obtained for the WT protein ($k_i/K_i = 0.34$ min^{-1} mM^{-1}, $k_i = 2.2$ min^{-1}, $K_i = 6.4$ mM at pH 6.0 and 40°C) (Miao *et al.*, 1994).
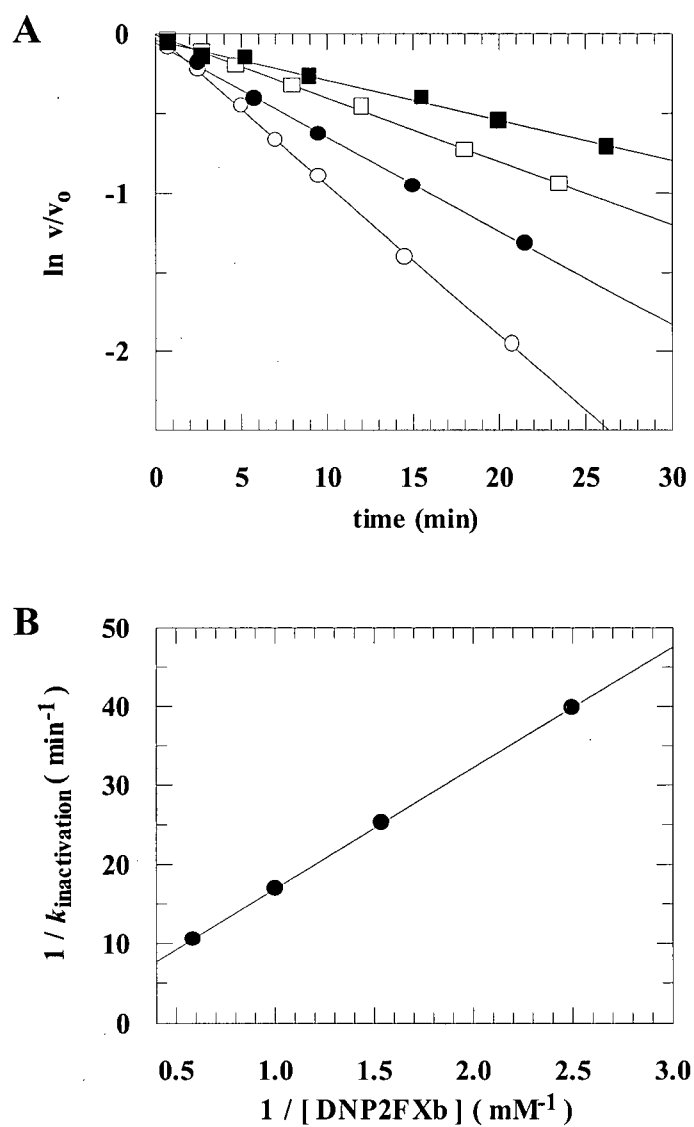
Figure 4.6. Time-dependent inhibition of N35D BCX by DNP2FXb at pH 4.1 and 40 °C. (A) Semi-logarithmic plot of residual activity (v/v_0) *versus* time at various concentrations of DNP2FXb: ■, 0.40 mM; □, 0.65 mM; ●, 1.00 mM; and ○, 1.70 mM. (B) Inverse plot of the pseudo-first order rates measured in (A) *versus* inhibitor concentration yielded a value of 0.065 min^{-1} mM^{-1} for the second order rate constant, k_i/K_I, determined from the slope of the plot.

4.3.7 Structure of the N35D BCX Glycosyl-Enzyme Intermediate

The structure of the N35D BCX glycosyl-enzyme intermediate (N35D-2FXb) was determined at pH 7.5 to a resolution of 1.8 Å with an R-factor of 19.3 %. As seen with WT BCX, no significant changes occur in the backbone structure of N35D BCX upon formation of the covalent intermediate, except for a small displacement of the loop region (residues 111-125) over the active-site cleft (Connelly et al., 2000; Sidhu et al., 1999). The most pronounced change is the covalent attachment of a 2-fluoro-xylobiosyl (2FXb) moiety to the $O^{\varepsilon 2}$ atom of Glu78 via an α-anomeric linkage with the C1 atom of the proximal saccharide (Figure 4.7). The presence of this covalent attachment confirms that Glu78 functions as the nucleophile in N35D BCX and that hydrolysis proceeds through a double-displacement mechanism. In addition, the side chain carboxyl of Glu172 remains positioned to serve as a general acid and donate a proton to the oxygen of the aglycone leaving group during formation of the glycosyl-enzyme intermediate, and in turn, as a general base to facilitate deglycosylation by a nucleophilic water molecule. This provides strong support for the role of Glu172, at least in part (see Discussion), as a general acid/base catalyst in both the WT and mutant enzymes. Furthermore, the interactions between the protein side chains and the 2FXb moiety in the N35D intermediate are also almost identical to those occurring in the WT intermediate, as discussed extensively by Sidhu *et al.*, (1999). Most notably, the distal xylose is stacked against Trp9 and forms hydrogen bonds to Tyr166 and Tyr69, whereas the proximal distorted xylose residue extensively hydrogen bonds to Tyr69, Arg112 and Pro116. Finally, the proximal saccharide is distorted to a $^{2,5}B$ (boat) conformation whereas the distal saccharide is maintained in the conventional $^4C_1$ (chair) conformation in the glycosyl-enzyme intermediate of both WT (Sidhu *et al.*, 1999) and N35D BCX.
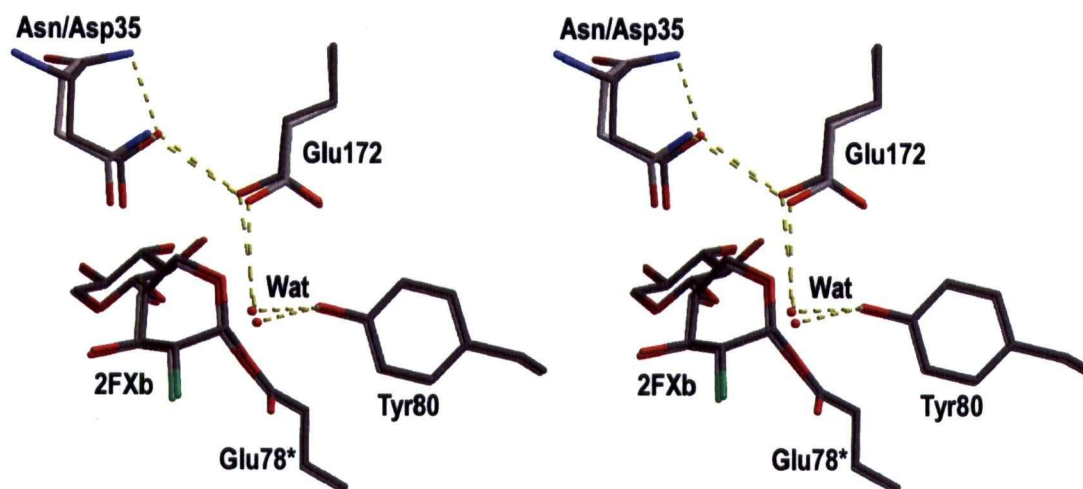
Figure 4.7. A stereo-illustration of the structural conformations of key active-site residues of the N35D BCX glycosyl-enzyme intermediate (N35D-2FXb) (dark grey) superimposed upon those of the WT glycosyl-enzyme intermediate (WT-2FXb) (light grey) (pH 7.5). Potential hydrogen bonds are indicated by yellow dashed lines, oxygen atoms are shown in red and nitrogen atoms in blue. Modified Glu78-2FXb (Glu78*) is covalently attached to a 2-fluoroxylobiosyl (2FXb) moiety where the proximal saccharide is distorted to a $^{2,5}B$ conformation in both N35D-2FXb and WT-2FXb. A crystallographically identifiable water (Wat) molecule that is proposed to function in the deglycosylation step of the reaction is indicated by a red sphere. The most notable change is a reduction in the distance between Asn35 $N^{\delta 2}$/Asp35 $O^{\delta 2}$ and Glu172 from 3.3 Å in WT-2FXb to 2.7 Å in N35D-2FXb. See Table 4.4 for a listing of additional interatomic distances.

A comparison of the structures of the covalent intermediates of WT and N35D BCX reveals only two notable differences. Firstly, the distance between Glu172 $O^{\epsilon 1}$ and a water molecule, that has been proposed to function as the nucleophile in the deglycosylation step (Sidhu *et al.*, 1999), is increased by ~ 0.7 Å in the N35D complex compared to the WT complex (Table 4.4). Second, and most significantly, the distance between Asn35 $N^{\delta 2}$/Asp35 $O^{\delta 2}$ and Glu172 decreases from 3.3 Å in WT-2FXb to 2.7 Å in N35D-2FXb. A small rotation of ~ 15° (χ_3) also increases the co-planarity of the two carboxyl groups. This is suggestive of a strong hydrogen bonding interaction between the side chains of Asp35 and Glu172 in the N35D BCX glycosyl-enzyme intermediate at pH 7.5.

4.3.8 *pK$_a$ Measurements of the N35D BCX Glycosyl-Enzyme Intermediate*

The pK_a of Glu172 in N35D BCX inhibited with DNP2FXb was also directly measured by NMR spectroscopy (Figure 4.8). The ^{13}C-NMR spectra of N35D-2FXb BCX are very similar to those of WT-2FXb BCX (McIntosh *et al.*, 1996), allowing the carbonyl resonances to be readily assigned. Comparison to the data in Figure 4.3 reveals that N35D-2FXb and unmodified N35D BCX are markedly different in both chemical shift and titration behaviour. Upon formation of the glycosyl-enzyme intermediate in N35D BCX, the δ-^{13}C resonance of Glu172 moves downfield by 1.4 ppm to 180.41 ppm while the resonance of Glu78 moves upfield by almost 6.4 ppm to 175.94 ppm at neutral pH. The carbonyl resonance of Glu78 is essentially invariant with pH and shows no deuterium isotope shift (data not shown), as would be expected due to its covalent attachment to the 2-deoxy-2-fluoro-β-xylobiose. A minor shift with an apparent pK_a of 9.3 ($\Delta\delta$ = 0.18 ppm) is observed for Glu78, which probably reflects a pH-dependent change occurring at another site on the protein (Table 4.5). In contrast to the situation
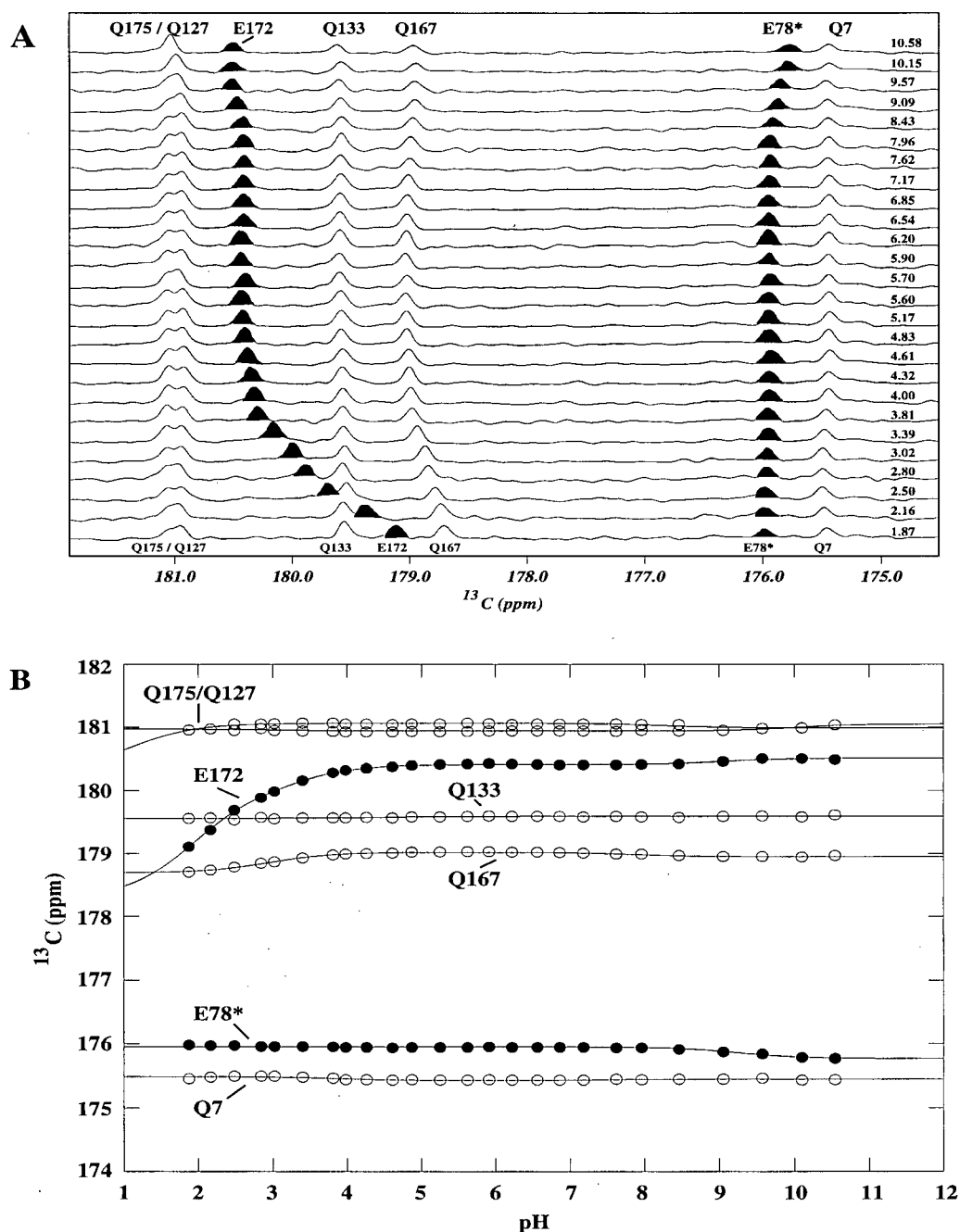
Figure 4.8. (A) pH-dependence of the ^{13}C-NMR spectra of N35D BCX covalently inhibited at Glu78 with 2FXb (25 °C). Resonance assignments were based on previously collected data for inhibited WT BCX (McIntosh *et al.*, 1996) and the spectra displayed as in Figure 4.3A. The resonance of modified Glu78-2FXb (E78*) was distinguished from that of Gln7 by a lack of a hydrogen-deuterium isotope shift (not shown). The peaks corresponding to Glu172 and modified Glu78-2FXb are highlighted in black for emphasis. (B) Apparent pK_a values were determined for the two Glu residues (●) (Table 4.5) and the five Gln residues (○) by fitting to equations describing one or more sequential ionization equilibria.

with unmodified N35D BCX, Gln7 and Gln127 no longer show pH-dependent shifts, thus confirming the dependence of their resonance frequencies on the charge state of Glu78. After covalent modification of Glu78, Glu172 is the only titratable glutamic acid in N35D-2FXb BCX and thus its ^{13}C-NMR resonance is readily identifiable in the spectra shown in Figure 4.8. However, the pK_a of this residue is difficult to estimate from these data since no titration baseline is observed in the acidic range, and thus a lower chemical shift limit could not be established. Nevertheless, fitting the data to a model involving three ionizations yielded very approximate apparent pK_a values of 1.9 ($\Delta\delta$ = 1.63 ppm), 3.4 ($\Delta\delta$ = 0.48 ppm) and 9.0 ($\Delta\delta$ = 0.10 ppm). A single pK_a of ~2.6 is obtained when these data are analyzed assuming one ionization event in the acidic range, although the fit is less satisfactory.

To further investigate the ionization behaviour of Glu172 in the glycosyl-enzyme intermediate of N35D BCX, deuterium isotope shift measurements were carried out. Comparison of the spectra of the covalently modified protein in 10% D_2O and 90 % D_2O buffer at pH* 5.90 unambiguously shows that the carbonyl of Glu172 has an isotope shift of -0.16 ppm. This value is midway between that of 0 ppm measured for deprotonated Glu78 in the uninhibited form of N35D BCX and -0.29 ppm for protonated Glu172. Possible interpretations of this result are that, in the glycosyl-enzyme intermediate, Glu172 is either ~ 50% protonated at pH 5.9 or is fully protonated yet with significantly reduced O-H covalent bond character. This observation poses an interesting problem, given that Glu172 should be fully deprotonated at pH 5.9 if its pK_a value is indeed less than 3.4, as suggested by the titration data of Figure 4.8. One plausible explanation of this behaviour is that, upon formation of the glycosyl-enzyme intermediate, the microscopic pK_a of Glu172 drops to a value in the range of 1.9 to 3.4 such that it is approximately equal to that of Asp35. Although I did not measure the pK_a of residue 35 in this system, due to the large

number of aspartic acids and asparagines in N35D-2FXb BCX (and thus the need to reassign the δ-carbonyl resonances in the modified protein), it is reasonable to assume that its pK_a would not increase significantly from the value of 3.7 found in the uninhibited form of N35D BCX. Given that these two residues have intimately associated carboxyl groups, as shown crystallographically (Figure 4.7), as well as comparable pK_a values, they may in effect behave as a single coupled unit. The first proton of the pair can be lost in the titration event corresponding to the apparent pK_a value of 1.9 or 3.4 measured from the pH-dependent chemical shift of Glu172, or to a single pK_a of 2.6 obtained when these data are fitted to one ionization event in the acidic range. (This argument recognizes the difficulty in differentiating the effects of the ionization of Glu172 or Asp35 on the chemical shift of the carbonyl of Glu172, and thus the ambiguity in the interpretation of the fitted pK_a values). Consistent with the observed separation of only 2.7 Å between the O^δ of Asp35 and the O^ϵ of Glu172 (Figure 4.7), this leaves a single proton shared in an ionic hydrogen bond between two residues at neutral pH values. Thus the deuterium isotope effect of -0.16 ppm would be attributed to the effects of strong hydrogen bonding, rather than partial protonation *per se*. This is reminiscent of the description of a so-called low barrier hydrogen bond (LBHB). However, we did not observe the signal from an unusually downfield shifted proton in the ^{1}H-NMR spectrum of N35D-2FXb BCX at pH* 6.1 and 25°C that is often attributed to a hydrogen in a LBHB.

To complete this argument, we must define the pK_a for the loss of the second proton from the Asp35-Glu172 pair of N35D-2FXb BCX. From the titration data shown in Figure 4.8, the carbonyl chemical shift of Glu172 remains approximately constant in the alkaline pH range up to a pH of 10.6. Only a small change of 0.1 ppm, fitting an apparent pK_a of 9.0, was observed. Although not impossible, it seems unlikely that this small shift reflects the deprotonation of

Glu172, suggesting that the actual pK_a value for the loss of the second proton must be > 11. However, based on this uncertainty, we conservatively conclude that the pK_a for the second ionization of Asp35-Glu172 is > 9. This represents a perturbation of at least 5.5 units from the value of the first ionization, or an energetic interaction of > 9 kcal mol^{-1} disfavouring the juxtaposition of Asp35 and Glu172 in their negatively charged forms.

The low pK_a of the Asp35-Glu172 pair in the glycosyl-enzyme intermediate of N35D is consistent with the phenomenon of pK_a cycling which occurs in retaining glycosidases (McIntosh *et al.*, 1996). In a retaining glycosidase, the pK_a of the general acid/base cycles to match its catalytic role as a general acid in the glycosylation step (higher pK_a) or a general base in the deglycosylation step (lower pK_a). Previous studies of BCX using DNP2FXb to trap the glycosyl-enzyme intermediate have shown that the pK_a of Glu172 cycles from 6.7 in the free WT enzyme when it functions as a general acid to 4.2 in the enzyme intermediate when it functions as a general base (McIntosh *et al.*, 1996). Hence, a lower pK_a measured for the Asp35-Glu172 pair in the glycosyl-enzyme intermediate of N35D BCX indicates that this carboxyl pair can play a dual catalytic role as a general acid and as a general base in the double-displacement hydrolysis reaction.

4.4 DISCUSSION

4.4.1 pK$_a$ Values of the Catalytic Residues

Previous NMR studies of WT BCX revealed that Glu78 and Glu172 have coupled ionization equilibria. Consistent with their catalytic roles, the major pK$_a$ values for these two residues are 4.6 and 6.7, respectively. However, when their biphasic titration curves were fitted to a model describing the interaction of two ionizable groups, the microscopic pK$_a$ of Glu172 in the presence of a neutral Glu78 was found to be 5.5, and that of Glu78 in the presence of a charged Glu172 was 5.8 (Chapter 3: Scheme 3.1, p112). Therefore, the electrostatic interaction between the two nearby carboxyl groups (C$^{\delta}$ separation = 6.5 Å) perturbs their pK$_a$ values by ~ 1.2 units. This is supported by the observation that upon substitution of Glu78 with Gln, the pK$_a$ of Glu172 drops to 4.2, whereas the reciprocal mutation of Glu172 leads to a slight elevation of the pK$_a$ of Glu78 to 5.0. In both cases, the titration curves become monophasic. The differences between the pK$_a$ values measured for the mutant proteins and those determined from an analysis of the biphasic titration curves of WT BCX suggest that the coupling between the two glutamic acids is not purely electrostatic. Conformational changes in the active-site upon ionization or mutation may also influence the titration behaviour of Glu78 and Glu172.

Substitution of Asn35 to an aspartic acid residue leads to a dramatic change in the ionization properties of BCX. Most notably, the apparent pK$_a$ values of Glu78 and Glu172 are elevated to 5.7 and 8.4, respectively, and both residues show triphasic titration curves. This undoubtedly arises from an additional electrostatic interaction with Asp35, which has an apparent pK$_a$ of 3.7 and thus is predominantly in a negatively charged state at pH values when Glu78 and Glu172 undergo deprotonation. The greater perturbation of the pK$_a$ value of Glu172 is consistent with the crystal structure of N35D BCX, determined at pH 7.5. That is, the carboxyl

carbons of Asp35 and Glu172 are separated by 4.8 Å, whereas those of Asp35 and Glu78 are 8.5 Å apart (Figure 4.2 and Table 4.4).

The multiphasic titration curves recorded for Asp35, Glu78, and Glu172 clearly indicate a complex network of electrostatic and possibly structural interactions between these three residues. As outlined in the Results section, the apparent pK_a values listed in Table 4.5 were determined by fitting the NMR-detected titration curves of the active-site carboxyl groups to a simple model of sequential ionization events. However, to gain further insight into the electrostatic interactions between Asp35, Glu78, and Glu172, it is also useful to analyze their titration data to extract microscopic pK_a values. Unfortunately, with eight possible ionization states, it is difficult to carry out this analysis in full. Using only data recorded in acidic solutions (e.g. with Glu172 protonated), a simultaneous fit of the titration curves for Asp35 and Glu78 to a model of two coupled ionization equilibria yields the microscopic pK_a values shown in Scheme 4.1:
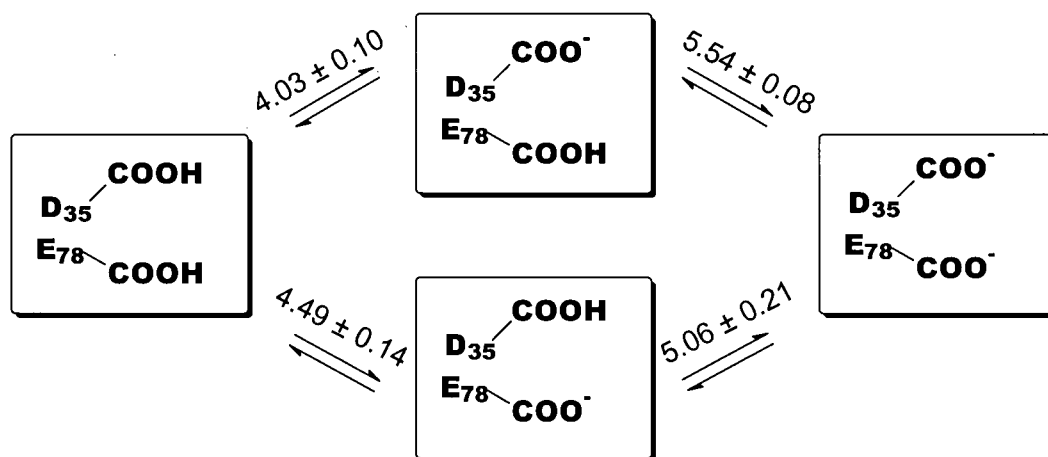
The upper limb of this scheme shows the predominant ionization pathway of N35D BCX in which Asp35 deprotonates with increasing pH before Glu78, whereas the lower corresponds to

the minor population of protein in which Glu78 is negatively charged and Asp35 neutral. Note that the microscopic pK_a of 5.54 for Glu78 along the upper limb of this coupled equilibrium curve is similar to the apparent pK_a value of 5.7 listed in Table 4.5, whereas that of 4.03 for Asp35 is somewhat higher that the corresponding value of 3.7 determined from a sequential ionization model. This reflects the difficulty in extracting pK_a values for complex binding equilibria in proteins, as the chemical shifts of involved residues are exquisitely sensitive to both structural and electrostatic factors. Thus, the equations describing their NMR behaviour are underdetermined experimentally. However, support for Scheme 4.1 follows from the observation that the microscopic pK_a of 4.49 fitted for Glu78 in the presence of a neutral Asp35 is very similar to that of 4.6 measured for this catalytic residue in WT BCX, which contains a neutral asparagine at position 35. Recognizing that the accuracy of these fits is uncertain, Scheme 1 suggests that the ionization of Asp35 elevates the pK_a of Glu78 by ~ 1 unit, and vice versa, due to charge repulsion, with an energetic coupling of $2.303RT\Delta pK_a \cong 1.4$ kcal mol^{-1}. The implications of this analysis for understanding the catalytic mechanism of N35D BCX will be discussed below.

Unfortunately, we were unable to extract microscopic pK_a values for the coupling of Glu172 with Glu78 or Asp35 for the following two reasons. First, in contrast to the case of the WT protein, upon addition of acid, the $^{13}C^\delta$ nuclei of Glu78 and Glu172 in N35D BCX show small downfield shifts (i.e. opposite to that expected for protonation of a carboxylate) at pH values corresponding to each other's pK_a values. Therefore, it is not possible to fit these data to the equation describing the pH-dependence of the chemical shifts of two residues with coupled ionization equilibria (Shrager *et al.*, 1972). Second, NMR data were not recorded above pH 8.3 for $^{13}C^\gamma$ Asp labelled N35D BCX, thus precluding a mutual fit of the titration curves of Asp35

and Glu172 for microscopic pK_a values. However, due to the large difference in their apparent pK_a values, the population of protein with Asp35 protonated and Glu172 deprotonated must be negligible.

Upon formation of a long-lived glycosyl-enzyme intermediate, the pK_a value of Glu172 in WT-2FXb BCX drops from 6.7 to 4.2 (McIntosh *et al.*, 1996). This pK_a cycling allows the glutamate residue to perform its dual role as a general acid for the glycosylation step and general base for deglycosylation. The reduction in the pK_a value of Glu172 by 2.5 units is attributed to the elimination of charge repulsion from Glu78, due to formation of a covalent linkage to the 2-fluoro-xylobiose, as well as to possible changes in the structure and hydration of BCX (McIntosh *et al.*, 1996). In a similar fashion, formation of the N35D BCX glycosyl-enzyme intermediate leads to a dramatic change in the titration behaviour of Glu172. As seen in Figure 4.8, the pH-dependence of the δ-^{13}C resonance of Glu172 follows apparent pK_a values of 1.9 or 3.4 when fitted to two sequential titrations or 2.6 when fitted to one ionization event in the acidic range. The observation of an isotope shift of -0.16 ppm at pH* 5.90 for Glu172 indicates that this residue is at least partially protonated at pH's above these pK_a values.

Based on this measured titration and deuterium isotope shift data, we conclude that Asp35 and Glu172 are behaving as a highly coupled dicarboxylic acid system in N35D-2FXb BCX, with a first pK_a in the range of 1.9 - 3.4 and a second estimated to be > 9. This is remarkable for two reasons. First, in the case of the WT enzyme, the pK_a of Glu172 drops by only 2.5 units upon covalent modification of Glu78, whereas in N35D BCX, the pK_a value associated with Glu172 falls by ~ 5.8 units from 8.4 to ~ 2.6. Second, assuming that the pK_a values for the first and second deprotonation steps of the Asp35-Glu172 pair are ~ 2.6 and > 9, this represents an energetic interaction of > 9 kcal mol^{-1} disfavouring the juxtaposition of the two

carboxylates in their negatively charged forms. A possible explanation for this behaviour is seen from a comparison of the crystal structures of N35D BCX in its free and modified forms, determined at pH 7.5. In the free enzyme, the distance between Asp35 $O^{\delta 2}$ and Glu172 $O^{\epsilon 2}$ is 3.2 Å, whereas in the glycosyl-enzyme intermediate, the separation is reduced to 2.7 Å (Table 4.4). The corresponding values for the WT protein are 3.1 Å and 3.3 Å. This suggests that a relatively strong hydrogen bond exists between Asp35 and Glu172 in N35D-2FXb BCX, such that one proton is shared between the two carboxyls with a net charge of -1. As mentioned previously, this interaction shares many similarities to a LBHB in that a proton is partitioned somewhat equally between the two carboxylates with first ionization pK_a values that are approximately matched. However, the signature proton with a downfield shifted resonance commonly attributed to the presence of an LBHB is not detected. Also, although comparable to the ~ 2.8 Å oxygen-oxygen hydrogen bonding distance observed in water, the Asp35-Glu172 separation is somewhat longer than the value of < 2.55 Å often cited for such a LBHB in model compounds (Cleland *et al.*, 1998). Regardless, this close interaction between these two active-site residues, which is not observed in WT-2FXb BCX, could account for the distinct pK_a values measured for Glu172 in the mutant enzyme. By way of comparison, in a study of the ionization of symmetric dicarboxylic acids, McDaniel and Brown, (1953) reported that the pK_a values for cis-caronic acid were 2.3 and 8.2. This strong energetic coupling was attributed to a highly favourable hydrogen bond between a carboxylic acid and a carboxylate in this constrained ring system.

4.4.2 Reverse Protonation Mechanism

Based upon the pK_a values of Glu78 (5.7) and Glu172 (8.4) determined by ^{13}C-NMR, and by analogy to the WT enzyme, the pH optimum of N35D BCX is expected to be ~ 7.0. However,

in marked contrast, the observed pH-dependence of k_{cat}/K_m, which reflects ionizations in the free enzyme, yields a pH optimum of 4.6 and a bell-shaped activity profile with apparent pK_a values of 3.5 and 5.8. Therefore, it appears that the pH-dependent activity of N35D BCX is determined by the ionization states of Asp35 and Glu78, rather than Glu172 and Glu78 as seen with the WT protein. However, since Glu78 must still be *deprotonated* to serve as a nucleophile, it follows that Asp35 must be *protonated* in the active enzyme. This situation, in which enzymatic hydrolysis requires that the group with the higher pK_a be deprotonated while the one with the lower pK_a remains protonated, has been termed "reverse protonation" (Mock and Aksamawati, 1994). Although somewhat unintuitive, this reversed ionization scheme will also give rise to a bell-shaped activity profile with apparent pK_a values for the acidic and basic limbs closely matching those of the two ionizable groups (Figure 4.9). However, in contrast to the more frequently observed cases exemplified by WT BCX, only a small percentage of the enzyme is in the correct ionization state for catalysis to occur. This kinetic mechanism has been invoked to explain the pH-dependence of the activities of several enzymes, including thermolysin, urease, and aspartate transcarbamylase (Karplus *et al.*, 1997; Mock and Aksamawati, 1994; Mock and Stanford, 1996; Turnbull *et al.*, 1992).

Upon closer examination, several fundamental questions arise in attempting to explain the activity of N35D BCX, as well as other acidic xylanases, in terms of a reverse protonation mechanism. First, as is clearly shown in Figure 4.9, based on their spectroscopically-measured
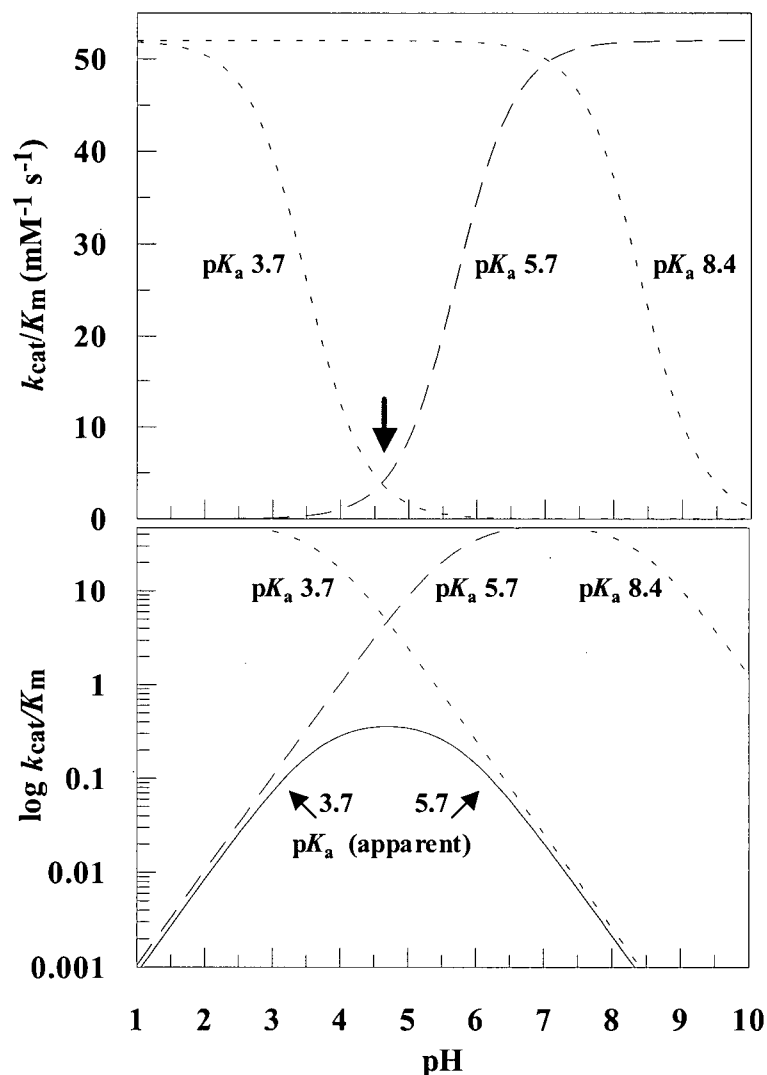
Figure 4.9. Simulated activity profiles for the proposed reverse protonation mechanism of N35D BCX. In the upper panel, titration curves are generated for the deprotonation of Glu78 (pK_a 5.7, — — —) and the protonation of Asp35 (pK_a 3.7, -----) and Glu172 (pK_a 8.4, -----). If N35D BCX behaved like the WT enzyme, optimal activity would be observed at pH ~ 7, where Glu78 is deprotonated and Glu172 protonated. In contrast, to explain the observed pH optimum of 4.6, we propose that Asp35 is protonated in the active form of the enzyme to function as general acid along with Glu172, while Glu78 is depronated to serve as a nucleophile. Since the pK_a of Glu78, measured by NMR spectroscopy, is greater than that of Asp35, the required combination of ionization states only occurs in the small region of overlap between the titration curves of these two residues (arrow). This is illustrated in the lower panel, where the product of the two titration curves is shown as a solid line and the scale of k_{cat}/K_m is logarithmic. Fitting to the standard equation for a bell-shaped activity profile yields apparent pK_a values of 3.7 and 5.7. This verifies that both normal and reverse protonation mechanisms yield bell-shaped activity curves with apparent pK_a values matching those measured for the two groups whose ionization states dictate the activity of the enzyme. Note, however, with the latter mechanism, N35D BCX has only ~ 1% of the activity that it would have in a theoretical state with Asp35 fully protonated and Glu78 fully deprotonated. The curves in this figure were scaled to match the observed maximum value k_{cat}/K_m of 0.43 s^{-1} mM^{-1} measured with ONPX$_2$ at 25 °C (Figure 4.1).

apparent pK_a values, the fraction of the enzyme with Asp35 and Glu78 in the correct ionization states is only ~ 1%. Since the overall activity of N35D BCX is ~ 20% greater than WT BCX at their respective pH optima, the mutant enzyme in a state with Asp35 neutral and Glu78 deprotonated must have an inherent catalytic efficiency at least 2 orders of magnitude higher than that of the parental WT. Why, then, is this enzyme species such an efficient catalyst? Second, this mechanism implies that N35D BCX is inactive when Asp35 is deprotonated, even though Glu172 (pK_a = 8.4) still bears a proton. Furthermore, Glu172 is positioned structurally to donate a proton to the aglycone oxygen during the glycosylation reaction and to abstract a proton from a water molecule during the subsequent deglycosylation reaction (Figures 4.2 and 4.7). Why can Glu172 not act alone as the acid catalyst under these conditions to allow hydrolysis at elevated pH values?

A possible answer to these two questions lies with the observation of a short hydrogen bond between Asp35 and Glu172 in the glycosyl-enzyme intermediate. A series of elegant model studies carried out by Kirby using small molecule systems to probe intramolecular proton transfer in the acid-catalyzed hydrolysis of acetals revealed that extremely effective intramolecular acid catalysis occurs when a strong hydrogen bond is formed between the departing alcohol and the conjugate base form of the general acid catalyst in systems such as that shown in Scheme 4.2 (Kirby, 1997). This strong hydrogen bond must exist, at least in part, in the transition state leading to the product, thereby stabilizing it and facilitating hydrolysis.
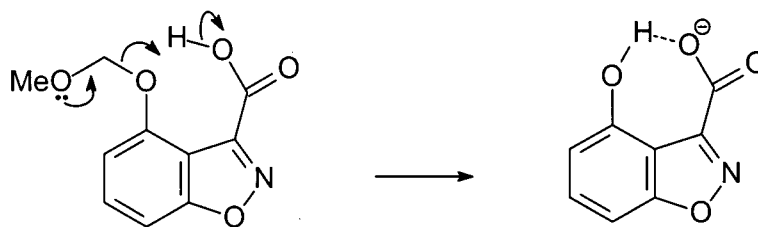
Scheme 4.2

The situation observed with N35D BCX is directly analogous to these model systems, since a strong hydrogen bond is formed between Asp35 and Glu172 in the glycosyl-enzyme intermediate. This hydrogen bond is stronger (shorter) than that in the free enzyme, largely as a consequence of the removal of charge from Glu78 upon formation of the glycosyl-enzyme intermediate. Stated equivalently, elimination of repulsive Coulombic interactions, by formation of an ester on Glu78, lowers the pK_a value of Glu172 to more closely match that of Asp35, thereby allowing Asp35-Glu172 to function together as an efficient general acid. Even though this strong hydrogen bond is not formed between the acid/base catalyst and the departing aglycone oxygen, as in the cases studied by Kirby, the effect is the same since the glycosyl-enzyme intermediate, and therefore the transition states leading to it, are stabilized (Figure 4.10). Indeed, this situation is preferable in a catalytic system since, were the hydrogen bond formed to the aglycone oxygen, product dissociation could be significantly slowed.

The question then arises as to whether the hydrogen bond formed is strong enough to lower the activation energy for glycosyl-enzyme intermediate formation sufficiently to account for the inherently 100-fold more efficient enzyme. An answer to this lies in the observation made previously (Richard, 1998), on the basis of our earlier demonstration of pK_a cycling in BCX (McIntosh *et al.*, 1996), that the chemical step of covalent glycosyl-enzyme formation is closely coupled to the ionization behaviour of the key active-site carboxylic acids. Thus the observed shift in the pK_a value of the acid/base catalyst upon formation of the glycosyl-enzyme intermediate in effect drives its formation. The pK_a shift of 2.5 units in WT BCX corresponds to an energy difference of 3.5 kcal mol^{-1}. In the case of N35D BCX, the very large pK_a shift of 5.8 units from 8.4 to ~ 2.6 for Glu172, which represents an energy difference of ~ 8 kcal mol^{-1}, is indeed sufficient to overcome the fact that only a very small percentage of the enzyme is in the
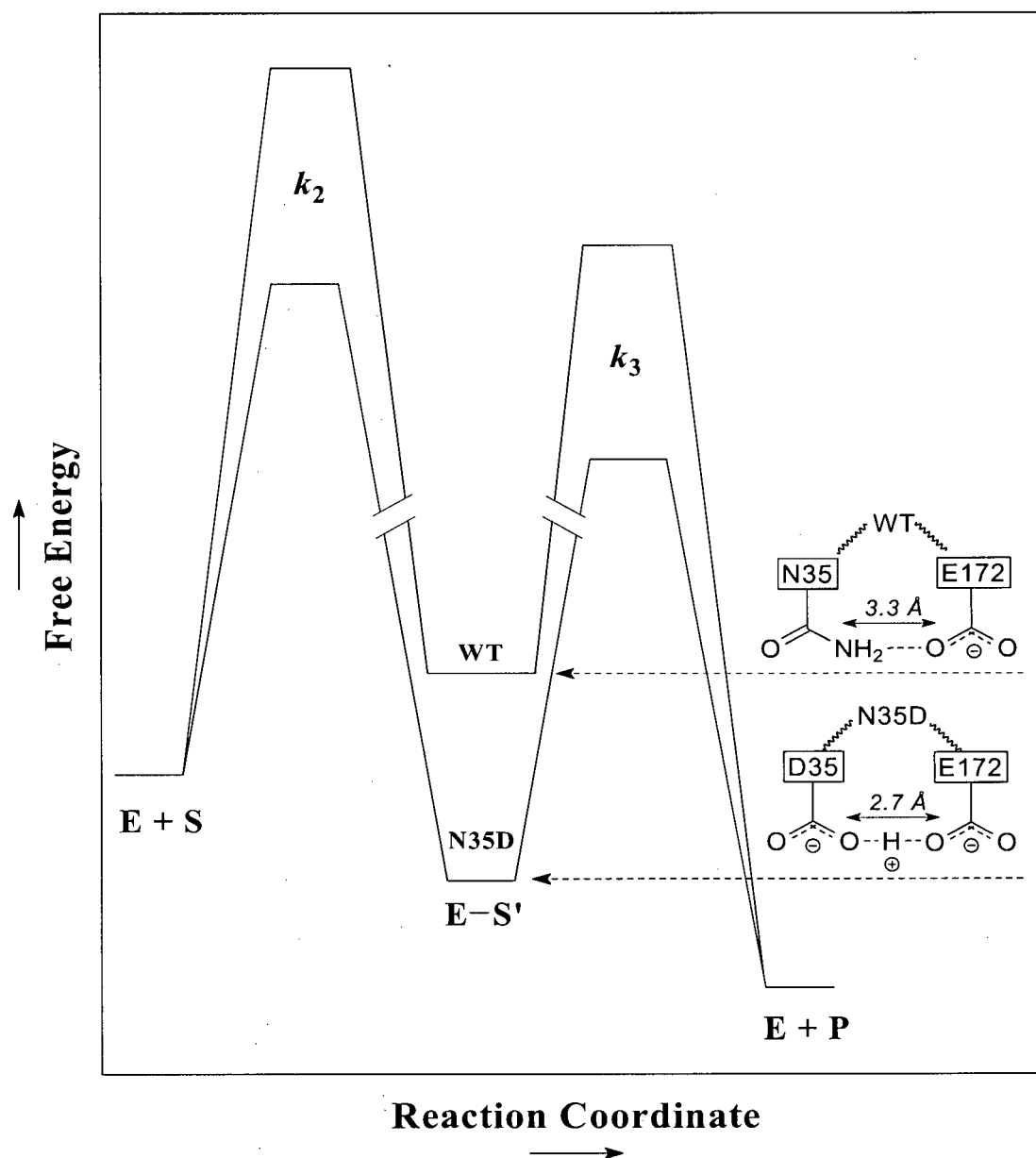
Figure 4.10. A reaction-coordinate diagram illustrating how the formation of the highly favourable N35D BCX glycosyl-enzyme intermediate along the hydrolytic reaction pathway lowers the activation energy for hydrolysis compared to WT BCX. The formation of a relatively strong and short (2.7 Å) hydrogen bond between Asp35 and Glu172 leads to significant stabilization of the N35D BCX glycosyl-enzyme intermediate and the neighboring glycosylation (k_2) and deglycosylation (k_3) transition states (lower trace). In contrast, the longer (3.3 Å) hydrogen bond formed between Asn35 and Glu172 in the glycosyl-enzyme intermediate of WT BCX does not lead to the same degree of stabilization and rate enhancement (upper trace). (Energy levels of the free enzyme and substrate (E + S), the enzyme-intermediate (E–S), and the free enzyme and product (E + P) are relatively indicated).

correct ionization state for catalysis. It is interesting to also note that the first pK_a of the Asp35-Glu172 system drops from 3.7 in the free enzyme to ~ 2.6 in the glycosyl-enzyme intermediate due to the removal of the charge on Glu78. Thus, at each point along the reaction coordinate proton donation becomes *more* effective. The other question concerns why the monoprotonated Asp35-Glu172 system could not act as an effective acid catalyst, despite the pK_a value of 8.4 measured in the free enzyme. This is the consequence of unfavourable coupling of ionization behaviour to glycosyl-enzyme intermediate formation in this system since glycosyl-enzyme intermediate formation results in an increase in the pK_a of Glu172 from 8.4 to > 9. In other words, at each point along the reaction coordinate in this system, proton donation becomes *less* effective.

Although the two questions posed above regarding the catalytic efficiency of a reverse protonation mechanism can be adequately resolved, a rather subtle caveat to this mechanism should be noted. The current proposal of a reverse protonation mechanism follows from the similarities of the pK_a values determined from the activity profile of N35D BCX and the major "apparent" pK_a values of Asp35 and Glu78 measured by ^{13}C-NMR. However, if Asp35 is in a protonated state when the enzyme is catalytically active, we must in fact consider the *microscopic* pK_a values of Asp35 and Glu78, rather than their predominant or apparent pK_a values. According to this model, shown in Scheme 4.1, in the presence of a neutral Asp35, the pK_a of Glu78 is ~ 4.5 rather than ~ 5.5. Similarly, in the presence of a negatively charged Glu78, the pK_a of Asp35 is ~ 5 rather than ~ 4. This implies that the pH-dependent activity profile of N35D BCX should follow apparent pK_a values of ~ 4.5 (Glu78) and ~ 5 (Asp35). Since this is not observed, the analysis of the ^{13}C-NMR titration data according to Scheme 4.1 may not be appropriate for N35D BCX due to the previously mentioned difficulties in interpreting the pH-

dependent changes in the chemical shifts of carboxyl groups. However, irrespective of the details of the analysis, the pK_a values of Glu78 and Glu172 in the presence of a neutral Asp35 are expected to differ from those measured from the major pH-dependent change in their ^{13}C-NMR spectra due to electrostatic interactions between their closely juxtaposed side chain carboxyl groups. Thus, the correspondence between the observed pK_a values of 3.5 and 5.8 from the pH-dependent activity profile of N35D BCX and 3.7 (Asp35) and 5.7 (Glu78) from NMR measurements is somewhat perplexing. Perhaps this expectation is false and the perturbation of the pK_a value of Glu78 due to the N35D substitution does not arise from electrostatic interactions, as implied in Scheme 4.1, but rather from very subtle structural differences between aspartic acid and asparagine sidechains. Thus in the presence of a neutral Asp35, Glu78 may still have a pK_a of ~ 5.7, and in the presence of a charged Glu78, Asp35 may still have a pK_a of ~ 3.7, corresponding to the limbs of the activity profile of N35D BCX. To address this issue, crystallographic studies of WT and N35D BCX at acidic pH values may be necessary.

In summary, a combination of NMR and kinetic studies demonstrate that the pH-dependent activity of N35D BCX, and by inference other "acidic" family 11 xylanases, is dictated by the ionization states of the nucleophile, Glu78, and the Asp35 residue adjacent to the general acid, Glu172. Although not without concerns, this can be explained by a reverse protonation mechanism in which Asp35 and Glu172 act *together* as the general acid and, subsequently, as the general base in the 2-step hydolysis reaction (Figure 4.11).

4.4.3 Comparison to Other Xylanases

The correlation between the presence of an asparagine or an aspartic acid at position 35 (BCX numbering) and the "alkaline" or "acidic" pH optima of family 11 xylanases, repectively,
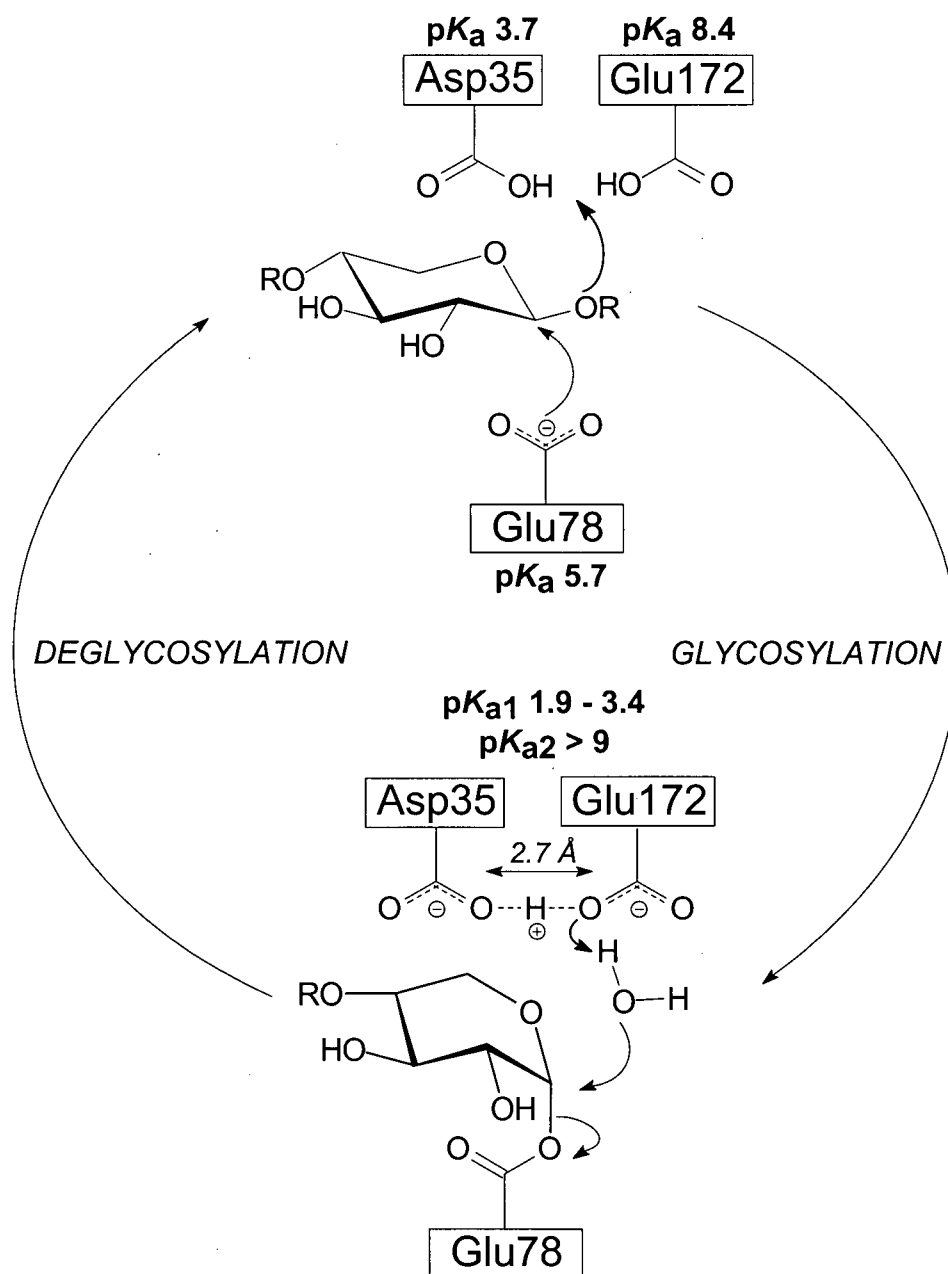
Figure 4.11. The proposed double-displacement retaining mechanism of N35D BCX. In the glycosylation step, Asp35 and Glu172 function together in serving the role of the acid/base catalyst, whereas deprotonated Glu78 is the nucleophile. In the glycosyl-enzyme intermediate, Asp35-Glu172 interact strongly with coupled ionizations, pK_{a1} 1.9-3.4 and $pK_{a2} > 9$. Due to this pK_a cycling, they can now serve as a general base in the deglycosylation step of the reaction

is well recognized. As summarized below, three structural investigations aimed at understanding this phenomenon have been reported.

Torronen and Rouvinen examined two family 11 xylanases from *Trichoderma reesei* (Torronen and Rouvinen, 1995). XYNI is an acidic xylanase with an aspartic acid at position 33 and a pH optimum of 3.5, whereas XYNII is an alkaline xylanase with an asparagine at position 44 and a pH optimum of 5.3 (Table 4.1). In XYNI, Asp33 clearly makes a hydrogen bond (2.9 Å) to the acid/base catalyst (Glu164). In contrast, in XYNII, Asn44 is involved in a weaker interaction (3.4-3.7 Å) with the acid/base catalyst (Glu177). Without information regarding the pK_a values of the catalytic residues, or the ability to directly detect their protonation states by X-ray diffraction, the authors suggested that, in XYNI, Asp33 is neutral and involved in a strong hydrogen bonding interaction that serves to lower the pK_a of Glu164 and thereby reduce the pH optimum of the enzyme. Based on our studies of N35D BCX, it seems likely that Glu164 in XYNI actually has a higher pK_a than Glu177 in XYNII, and that Asp33 is largely deprotonated under the experimental conditions used for this study.

In a crystallographic analysis of the acidic xylanase, *Aspergillus niger* xylanase I, Krengel and Dijkstra found that Asp37 and the acid/base catalyst (Glu170) were within close hydrogen bonding distance (2.8 Å) of each other, as had been observed for the analogous residues in *T.reesei* XYNI (Krengel and Dijkstra, 1996; Torronen and Rouvinen, 1995). Based on its solvent exposure, they proposed that Asp37 is negatively charged at the pH of crystallization (pH 8) and therefore serves to elevate the pK_a of Glu170. To explain the pH optimum of 3 measured for this enzyme, they suggested that xylanase I is active when Asp37 is protonated and inactive when it is deprotonated. At low pH when Asp37 is protonated, the proton of the general acid, Glu170 is available for catalysis. However, at high pH, when Asp37 is

deprotonated, the catalytic proton of Glu170 is suggested to be detained in an ionic hydrogen bond to this residue, thereby preventing hydrolysis at elevated pH values. Thus, according to this mechanism, the ionization state of Asp37 primarily dictates the acidic limb of the pH-dependent activity profile of this xylanase. Although no correlation of activity to the ionization state of the nucleophile (or measurement of its pK_a value) was given, this argument is essentially equivalent to the reverse protonation mechanism proposed herein to explain the activity of N35D BCX.

In a more recent study of the acidic xylanase from *Aspergillus kawachii*, xylanase C, Fushinobu *et al.* (1998) experimentally confirmed the essential role that an aspartic acid residue (Asp37) adjacent to the acid/base catalyst (Glu170) has in lowering the pH optimum of this family 11 xylanase. Xylanase C has a pH optimum of 2, one of the lowest of this family. Mutation of Asp37 to an asparagine dramatically shifts the pH optimum of Xylanase C from 2 to 5, albeit with an 85 % reduction in xylanolytic activity. (This substitution is the reverse of that in N35D BCX). In their structural analysis of the WT enzyme, they also observed the same short distance between Asp37 and Glu170 (2.8 Å) as was reported for the other acidic xylanases (Table 4.1).

A summary of the structural and enzymatic properties of these xylanases, plus those from *Bacillus agaradhaerens* and *Thermomyces lanuginosus*, is presented in Table 4.1. Although each of these enzymes shares a structurally similar arrangement of fully conserved active-site residues surrounding two catalytic glutamic acids, they exhibit pH optima spanning a remarkable range from approximately 2 to 7. While the presence of an aspartic acid or an asparagine at position 35 (BCX numbering) provides a clear division between those with "acidic" (< 5) or "alkaline" (> 5) optima, additional factors must also contribute to defining their pH-dependent activity profiles. One trend, evident from Table 4.1, is that, for the "acidic" enzymes, the shorter the distance

between the acid/base catalyst and the adjacent aspartic acid residue, the lower the pH optimum of the xylanase. It is plausible that this reflects increasingly stronger hydrogen bonding between these residues, which would correlate with a reduction in the pK_a of the Asp and hence a shift in the acidic limb of the activity profile of these enzymes to lower pH values. It would be particularly interesting to extend this analysis to the measurement of the same distances in the glycosyl-enzyme intermediates of these xylanases to see if the stabilization of the "Asp-Glu" general base is also correspondingly greater.

A second, albeit imperfect, trend seen in Table 4.1 is that naturally-occuring "acidic" xylanases have low pI values, whereas "alkaline" xylanases tend to have high pI values. This is also somewhat counter-intuitive as, for example, a low pI indicates an excess of glutamic acid and aspartic acid residues, which by charge repulsion, should disfavour low pK_a values for the active-site catalytic groups. However, with further inspection, we see that xylanases with pH optima below ~ 6 have theoretical pI values such that they should actually carry a net positive charge at their respective pH optima (e.g. pI > pH optimum). This may help lower the pK_a values of the catalytic carboxylic acid side chains, and thereby allow activity under acidic conditions. In contrast, the *T.lanuginosus* xylanase with a pH optimum of 6.5 has a pI value less than its pH optimum, indicating that it will carry a net negative charge when maximally active. This may serve to elevate the pK_a values of the catalytic glutamic acids, as required for activity near neutral conditions. The qualitative nature of these arguments clearly highlights the need to experimentally and theoretically dissect the role of global and local electrostatic interactions in establishing the pK_a values and hence pH optima of enzymes. In closing, we also note that the observed trends in the pI values of the family 11 xylanases could simply reflect requirements for

stability or solubility in the environmental conditions under which these enzymes have evolved to be active.

4.4.4 Comparison to Other Glycosidases

A similar triad of carboxylates, as present in N35D BCX or acidic xylanases, is seen in other glycosidases. However, in contrast to the family 11 xylanases, a negatively charged aspartic acid residue near the acid/base catalyst is proposed to raise the pH optimum (pH 6.0) (Knegtel *et al.*, 1995) of cyclodextrin glycosyl transferases (CGTase) (Klein *et al.*, 1992; Strokopytov *et al.*, 1995). In *Bacillus circulans* strain 251 CGTase, the nucleophile, Asp229, the acid/base catalyst, Glu257, and the aspartic acid group adjacent to it, Asp328, all occupy a very similar geometrical arrangement to that found in BCX. The interaction between these residues is strong in the unliganded structure (2.7 Å separation between Glu257 $O^{\varepsilon 2}$ and Asp328 $O^{\delta 2}$) and weaker when the substrate is bound (3.6 Å) (Strokopytov *et al.*, 1995). In their analysis of *Aspergillus niger* xylanase I, Krengel and Dijkstra suggest a reason for the opposite effect of a negatively charged aspartate near the acid/base catalyst in lowering the pH optimum of xylanases while raising it in the CGTases (Krengel and Dijkstra, 1996). Upon substrate binding, Asp328 moves to form a new hydrogen bond with the substrate instead of with Glu257. In this manner, the proton on Glu257 is available for catalysis at higher pH values because it is no longer bound by Asp328 (Krengel and Dijkstra, 1996).

A similar arrangement of catalytic residues is also observed in the α-amylases. Functioning at a neutral pH optimum, pig pancreatic α-amylase (PPA) (Qian *et al.*, 1994) contains the three residues analogous to those found in both the CGTases (Strokopytov *et al.*, 1995) and the acidic family 11 xylanases. In PPA, Glu233 is the proposed acid/base catalyst,

with Asp300 adjacent to it, while Asp197 functions as the nucleophile. Asp300 is fully

conserved amongst α-amylases (Brayer *et al.*, 1995) and, along with a chloride ion (Qian *et al.*,

1994) that is situated 4.8 Å away from Glu233 in the unliganded structure (Machius *et al.*, 1996),

is proposed to play a role in elevating the pK_a of the acid/base catalyst (Glu233). In contrast to

the family 11 xylanases, however, the distances between the acid/base catalyst and the adjacent

aspartic acid residue are greater in the α-amylases, being 6.2 Å between Glu233 O$^{\varepsilon2}$ and Asp300

O$^{\delta2}$ in PPA, and 3.9 Å in human pancreatic α-amylase (HPA) (Brayer *et al.*, 1995).

Distinct from PPA and HPA, the acidic α-amylase from *Aspergillus niger* exhibits

maximal activity at pH ~ 3-4, yet also contains an adjacent aspartic acid residue, Asp297, 3.8 Å

away from the acid/base catalyst, Glu230 (Boel *et al.*, 1990). Interestingly, however, fungal α-

amylases do not bind chloride ions in the active-site whereas animal α-amylases do (Brayer *et

al.*, 1995). This may further implicate the evolutionary role of the negatively charged chloride

ion in shifting the pH optimum of animal α-amylases to neutral pH by elevating the pK_a of the

acid/base catalyst. It remains to be seen, however, if the fungal α-amylases from *Aspergillus

niger* use the same mechanism as the xylanases in lowering the pH optimum of the enzyme

through an aspartic acid residue adjacent to the acid/base catalyst.

4.5 CONCLUSION

The residue at position 35 plays a significant role in determining the pH optima of the family 11 xylanases. Using site-directed mutagenesis, we were able to confirm what was known from nature and modify BCX, an "alkaline" xylanase, to function under more acidic conditions without any reduction in its net activity. Counter-intuitively, the presence of an aspartic acid residue adjacent to the acid/base catalyst serves to lower the pH optimum of N35D BCX, instead of raising it as would be predicted from simple electrostatic considerations. Furthermore, we demonstrated with ^{13}C-NMR that Asp35 indeed elevates the pK_a of the acid/base catalyst, Glu172, significantly from 6.7 to 8.4.

To explain this paradox, we propose that N35D BCX and, by inference, all "acidic" family 11 xylanases, functions using a reverse protonation mechanism. In this catalytic scheme, Asp35 ($pK_a = 3.7$) and Glu172 act together to fulfil the role of the acid/base catalyst, donating a proton to the glycosidic oxygen, while Glu78 ($pK_a = 5.7$) still serves as the nucleophile. Only a small percentage of the enzyme (~ 1 %) is in the requisite ionization state at this optimal pH. However, this form functions as a highly effective catalyst since a strong hydrogen bond, formed between Asp35 and Glu172 in the glycosyl-enzyme intermediate, substantially stabilizes the transition state for glycosyl transfer. The enzyme becomes inactive at higher pH since loss of the second proton from the Asp35-Glu172 pair would remove this strong hydrogen bonding interaction and result in substantial charge repulsion between these active-site residues. This study highlights the complexity of possible electrostatic interactions within a protein and the diverse mechanisms by which the pH optima of enzymes can be set.

Chapter 5

Concluding Remarks

The primary goals of this thesis were focused on examining the pH-dependent mechanism and stability of BCX. Achievement of the goals outlined in this thesis was made possible because a multidisciplinary approach was used in solving the problems at hand. X-ray crystallography made it possible to rapidly determine the structures of many proteins, NMR studies allowed us to site-specifically measure the pK_a values and get to the heart of electrostatic interactions, while enzymology allowed for an assessment of the actual function of the enzymes. Each technique complemented the other and allowed for conclusions to be made at the fundamental level of the atom. In reading this thesis, I hope that the reader will have gained an appreciation for the overwhelming advantage of not being confined to using one technique. In my perception of the work presented here, significant insight was gained through the use of pK_a measurements made by NMR, albeit, the data would have had little meaning had structural and enzymological information not been available. The largest value of this work to the scientific community is that it provides a comprehensive database of information that will aid substantially to many fields: computational chemistry, by providing a test set to refine algorithms used in electrostatic calculations, and protein engineering and enzymology, by providing information regarding the roles that electrostatic interactions play in defining pH optima and overall activities of enzymes. Structures, site-specific pK_a values for the catalytic carboxyl groups, and functional

correlations are all now available for many BCX proteins. No other protein existing in the literature has been characterized in all of these ways to the extent that BCX has.

In the first part of this thesis (Chapter 2), I described the roles that ionizable groups (acidic) had upon the structural stability of the enzyme. The ones that were the most conserved, the most buried and most perturbed in pK_a value contributed the most to the pH-dependent stability of the enzyme and were stabilized extensively by either hydrogen bonds or salt bridges. I was able to estimate the contributions to the stability of the enzyme without mutating residues and without observing the protein under non-native conditions. The most fundamental problem in mutating an ionizable residue to examine its effects upon stability is that the properties of a protein are a function of the entire system, and not the sum of its parts. Hence, the effect of the mutation can reflect the loss of numerous interactions and not just those due to the substituted residue itself. Furthermore, double mutant-cycle analysis, used to circumvent this problem, is not without pitfalls either (Albeck *et al.*, 2000). The pK_a value of a given residue is the result of interactions that occur within the entire protein, hence is representative of many local and global interactions. Since little is actually known about the roles of buried salt bridges in protein stability (Tissot *et al.*, 1996; Yang and Honig, 1993), this work further contributes to our understanding of this type of interaction. Our results on BCX are further supported by computational studies that show a significant correlation between conserved salt-bridges and solvent accessibility (Schueler and Margalit, 1995) and substantiate the role of electrostatics in the protein interior. It is interesting to also note that while conserved buried salt bridges may not be critical for protein folding, they can stabilize evolutionarily conserved elements of secondary stucture formed early in the folding pathway, such as in the small ribonuclease, barnase, and limit the number of available conformations thus accelerating the folding of the protein (Tissot *et*

al., 1996). Since the buried salt bridge in BCX is highly conserved, it may also contribute to facilitating folding in all family 11 xylanases.

In the second major section of this thesis (Chapters 3 and 4), I provided a thorough examination of the pH-dependent mechanism and activity of BCX. I first determined the factors that set the pK_a values of nucleophile Glu78 and the acid/base catalyst Glu172 and gave rise to the bell-shaped pH-activity profile. I found that a number of conserved active-site residues acted concertedly in maintaining the ionization states of residues 78 and 172. Positively charged groups and hydrogen bonds served to lower pK_a values and decrease pH optima as expected. Furthermore, the degree to which hydrogen bonded groups contributed to lowering pK_a values was largely dependent on the length of the hydrogen bond and the chemical nature of the donor. Shorter hydrogen bonds provided more charge stabilization as did interactions where the difference in pK_a between donor and acceptor was smaller. Examination of a number of BCX structures revealed that Glu78 was preferentially stabilized over Glu172 by shorter and stronger hydrogen bonds in addition to favourable electrostatic interactions occurring in the protein, which were determined from electrostatic calculations. The calculations predicted the effects of charge removal/addition more accurately than they did for mutations involving hydrogen bonded residues, signifying the need to develop methods to adequately account for complex hydrogen bonding patterns that exist within proteins.

The results from this work have a number of implications for engineering pH optima in glycosidases as well as other enzymes. While active-site mutations resulted in changes in pH optima, activity was lost in many instances. In some cases important ground and/or transition state interactions were lost, whereas in others the population of the enzyme that was in the correct ionization state was reduced and thus leading to an apparent decrease in activity. This

highlights the importance of microscopic pK_a values and the wealth of information that can be derived from them. Analyses of BCX proteins using this method provided insights into not only determining the fraction of the enzyme in the correct ionization state, but also the phenomenon of pK_a cycling that drives both steps of glycosyl hydrolysis. Microscopic pK_a analysis has never been used in assessing the effects of mutations on pH-dependent activities and therefore provides a new perspective in the way we think about and approach engineering pH optima.

The N35D BCX mutant brings all of these studies together and teaches us a in important lesson in how nature has devised beautifully intricate, yet highly effective methods for successfully adjusting pH optima. The work described in Chapter 4 provides a solution to the well-documented enigma of the mechanism by which family 11 xylanases lower pH optima and shows how the formation of a single short, strong hydrogen bond can improve catalysis by almost two orders of magnitude. The reverse protonation mechanism proposed in our solution, in which a small percentage (1 %) of the enzyme carries all of the catalytic responsibilities, has never been invoked to explain the pH-dependence of activity of any glycosidase and is probably much more prevalent than expected, since most analyses do not included site-specific pK_a values of individual residues.

Future studies on engineering pH optima and activity should focus on a number of factors. More knowledge is required regarding the features that establish the pK_a values of the catalytic groups in both the free and glycosyl-enzyme intermediate states, since the ΔpK_a value of the acid/base catalyst as it cycles between its dual roles provides a significant portion of the driving force for catalysis. Mutations which modify the pK_a values of catalytic groups in the free enzyme and lead to a change in the pH optimum may in fact be adversely affecting ionization properties in the glycosyl-enzyme intermediate such that catalysis is impaired by the inability of

the acid/base catalyst to cycle its pK_a. Finally, the future of this work should lead in a direction that will enable us to decipher pK_a values of the enzyme and substrate in the transition states of catalysis—where the most important chemistry is occurring!

Appendix I

## *NMR pH-Titration Curve Fitting*

Various types of site-specific pH-titration curves of the acidic residues of BCX proteins require that specific ionization models be used in order to adequately fit the titration data and extract pK_a values. The ionization models used in fitting the data for BCX are described in detail in this Appendix. Although many cases are discussed, particular emphasis is placed on models describing pair-wise interactions between ionizable groups, such as those that describe the linked titration behaviour of Glu78 and Glu172.

Ionization Models

The analysis of the NMR titration curves for a system of two ionizable groups follows the formalism of Edsall and Wyman, (1958) and Shrager *et al.*, (1972). Note that one rarely detects the ionizable proton directly, but rather observes a non-exchangeable nucleus, usually within a given residue, whose chemical shift is dependent upon the protonation state of that residue. Thus, in specific reference to this study, we discuss the case of two glutamic (or aspartic) acids whose titrations are monitored by their side chain carboxyl δ- (or γ-) ^{13}C chemical shifts. However, this is general for any pair of ionizable groups, as well as for non-ionizable side chains whose chemical shifts are dependent upon the protonation state of two ionizable groups. The carboxyl groups may interact either "directly", whereby the ionization constant of one depends on the ionization state of the other, or "indirectly" in that the chemical shift of one side chain is perturbed (e.g. through changes in the protein structure or via electric field-induced shielding

effects) by the ionization of the other. The equations can be extended to binding phenomenon in general, although the requirement of knowing the free rather than total ligand concentration (which is readily provided for pH studies by a proton-sensitive glass electrode) often introduces additional complications into the data fitting procedures (Johnson, 1994; Li *et al.*, 1995).

Consider the general Scheme 1 for acidic groups at sites 1 and 2 in a protein P:
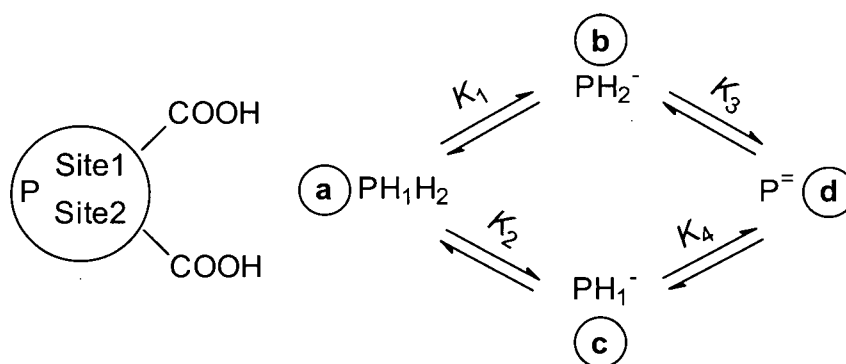
Protonation at site 1 is denoted as H_1 and site 2 as H_2. The microscopic or site-specific acid dissociation constants are defined relationships of the form $K_1 = [PH_2^-][H^+] / [PH_1H_2]$, with K_1 and K_4 corresponding to the loss of a proton from site 1 and K_2 and K_3 from site 2. (Note that the microscopic ionization constants are indicated by lower case characters, whereas macroscopic ionization constants, defined subsequently, are indicated in upper case letters). Molar concentrations are assumed to accurately reflect thermodynamic activities. Overall $K_1K_3 = K_2K_4$. In the absence of any interaction between the two sites, $K_1 = K_4$ and $K_2 = K_3$. Otherwise, if the ionization constant for one carboxyl group is influenced by the ionization state of the other, then $K_4 = \alpha K_1$ and $K_3 = \alpha K_2$, where a is an interaction or cooperativity factor ($\alpha < 1$ for electrostatic repulsion). This may arise from direct electrostatic interactions or indirectly via conformational changes. The fraction of the protein in states a, b, c, and d is given by:

$$f_a = [H^+]^2 / \Sigma$$

$$f_b = K_1[H^+] / \Sigma$$

$$f_c = K_2[H^+] / \Sigma$$
$$f_d = K_1 K_3 / \Sigma$$

where,

$$\Sigma = [H^+]^2 + K_1[H^+] + K_2[H+] + K_1 K_3 \quad (1)$$

Under the commonly observed conditions of fast exchange, the measured chemical shift of the carboxyl group at site 1, δ_1, is the weighted average of the chemical shifts of this group (δ_{a1}, δ_{b1}, δ_{c1}, δ_{d1}) in the four possible states of the enzyme shown in Scheme 1:

$$\delta_1 = f_a \delta_{a1} + f_b \delta_{b1} + f_c \delta_{c1} + f_d \delta_{d1} \quad (2a)$$

The change in chemical shift, ($\delta_{b1} - \delta_{a1}$) and ($\delta_{d1} - \delta_{c1}$), of the site 1 carboxyl is attributed directly to its own ionization. The "indirect" effect of the ionization of the carboxyl at site 2 on the chemical shift of the group at site 1 results in the changes ($\delta_{c1} - \delta_{a1}$) and ($\delta_{d1} - \delta_{b1}$). Similarly, for the carboxyl at site 2:

$$\delta_2 = f_a \delta_{a2} + f_b \delta_{b2} + f_c \delta_{c2} + f_d \delta_{d2} \quad (2b)$$

The pH-dependence of the chemical shift of each carboxyl is potentially a function of 4 chemical shifts and 3 independent microscopic dissociation constants. However, as noted by Shrager *et al.* (1972), titration curves for Scheme 1 can be completely defined by five variables (e.g. two baselines, one intermediate chemical shift, and two apparent pK values corresponding to inflection points), and thus equations (2) are experimentally underdetermined. Since the titrations of sites 1 and 2 share common pK values, simultaneous analysis can improved the accuracy of

the fit parameters, but does not fully resolve this problem (e.g. eight shifts and three pK values *versus* ten measurable parameters). Accordingly, several limiting cases must be considered in order to extract the desired ionization constants from pH-dependent NMR spectra by non-linear least squares analysis (Shrager *et al.*, 1972).

Case 1: Independent, non-interacting sites.

In the simplest case where the two carboxyl groups titrate independently ($\alpha = 1$) and the chemical shift of each is independent of the other, then for site 1, $K_1 = K_4$, $\delta_{a1} = \delta_{c1}$, $\delta_{b1} = \delta_{d1}$. In terms of the measured sample pH, equation (2) becomes the familiar expression for the titration curve of a single ionizable group:

$$\delta_1 = \frac{\delta_{a1}10^{-pH} + \delta_{b1}10^{-pK_1}}{10^{-pH} + 10^{-pK_1}} \quad (3)$$

A similar expression can be written for site 2, with $K_2 = K_3$, $\delta_{a2} = \delta_{b2}$, $\delta_{c2} = \delta_{d2}$.

Case 2: Coupled titrations: Inter-dependent microscopic pK values with chemical shifts depending only on the individual ionization state of a carboxyl group.

In the case where the two carboxyl groups interact such that the microscopic acid dissociation constant of each residue depends on the ionization state of the other, then $\alpha \neq 1$, and $K_1 \neq K_4$ and $K_2 \neq K_3$. However, if the chemical shift changes exhibited by each carboxyl result only from its own ionization, then for site 1, $\delta_{a1} = \delta_{c1}$ and $\delta_{b1} = \delta_{d1}$, and for site 2, $\delta_{a2} = \delta_{b2}$ and $\delta_{c2} = \delta_{d2}$. The pH dependence of the chemical shift of the carboxyl at site 1 is given by:

$$\delta_1 = \frac{\delta_{a1}([H^+]^2 + K_2[H^+]) + \delta_{b1}(K_1[H^+] + K_1K_3)}{\Sigma} \quad (4)$$

From a non-linear least squares fit of the observed chemical shift δ_1 versus pH to this equation in the form:

$$\delta_1 = \frac{\delta_{a1}(10^{-2pH} + 10^{-(pH+pK_2)}) + \delta_{b1}(10^{-(pH+pK_1)} + 10^{-(pK_1+pK_3)})}{10^{-2pH} + 10^{-(pH+pK_2)} + 10^{-(pH+pK_1)} + 10^{-(pK_1+pK_3)}} \quad (5a)$$

two baseline chemical shifts and three microscopic pK values are extracted. The fourth is obtained from the relationship $K_1K_3 = K_2K_4$. Similarly for site 2:

$$\delta_2 = \frac{\delta_{a2}(10^{-2pH} + 10^{-(pH+pK_1)}) + \delta_{c2}(10^{-(pH+pK_2)} + 10^{-(pk_2+pK_4)})}{10^{-2pH} + 10^{-(pH+pK_1)} + 10^{-(pH+pK_2)} + 10^{-(pK_2+pK_4)}} \quad (5b)$$

Although deriving two chemical shifts and three pK values from a biphasic or apparent 2-step titration curve may seem non-intuitive, note that the "plateaus" correspond to fractional chemical shift changes of:

$$\delta_1 - \delta_{a1} = (\delta_{b1} - \delta_{a1})\left(\frac{K_1}{K_1 + K_2}\right) \quad \text{(site 1)} \quad (6a)$$

$$\delta_2 - \delta_{a2} = (\delta_{c2} - \delta_{a2})\left(\frac{K_2}{K_1 + K_2}\right) \quad \text{(site 2)} \quad (6b)$$

Thus the fit is exactly equivalent that obtained using three chemical shifts and two pK values, as for cases 3 and 4 below.

Case 3: Sequential titrations: Independent microscopic pk values with chemical shifts depending on the ionization states of both carboxyl groups.

In the case where the two carboxyl groups titrate independently ($\alpha = 1$), $K_1 = K_4$ and $K_2 = K_3$. This can be described as a sequential titration of non-interacting groups. However, if the chemical shift of each carboxyl depends upon not only its own ionization state, but also on that of the second carboxyl, then for site 1, $\delta_{a1} \neq \delta_{c1}$ and $\delta_{b1} \neq \delta_{d1}$, and for site 2, $\delta_{a2} \neq \delta_{b2}$ and $\delta_{c2} \neq \delta_{d2}$. The pH-dependent chemical shift of site 1 is given by:

$$\delta_1 = \frac{(\delta_{a1} 10^{-2pH} + \delta_{b1} 10^{-(pH+pK_1)} + \delta_{c1} 10^{-(pH+pK_2)} + \delta_{d1} 10^{-(pK_1+pK_2)})}{\Sigma} \quad (7)$$

This equation is still underdetermined with six variables and generally cannot be fitted robustly, unless additional restraints are included. These include independent knowledge of the chemical shifts of the carboxyl in the various ionization states of the protein, or by assuming additive chemical shift effects, e.g. $\delta_{c1} = \delta_{a1} + (\delta_{d1} - \delta_{b1})$. However, if one titration pathway in above scheme is preferred significantly, for example with p$K_2 >$ pK_1, then the equations for sites 1 and 2 reduce to the commonly used expressions for the analysis of "sequential" titration curves:

$$\delta_1 = \frac{\delta_{a1} 10^{-2pH} + \delta_{b1} 10^{-(pH+pK_1)} + \delta_{c1} 10^{-(pH+pK_2)} + \delta_{d1} 10^{-(pK_1+pK_2)}}{10^{-2pH} + 10^{-(pH+pK_1)} + 10^{-(pH+pK_2)} + 10^{-(pK_1+pK_2)}} \quad (8a)$$

$$\delta_2 = \frac{\delta_{a2}10^{-2pH} + \delta_{b2}10^{-(pH+pK_1)} + \delta_{c2}10^{-(pH+pK_2)} + \delta_{d2}10^{-(pK_1+pK_2)}}{10^{-2pH} + 10^{-(pH+pK_1)} + 10^{-(pH+pK_2)} + 10^{-(pK_1+pK_2)}} \quad (8b)$$

Non-linear least squares fitting of the observed titrations to these equations yield three limiting chemical shifts for each carboxyl groups and the two ionization constants. "Plateaus" in these titration curves occurs at δ_{b1} and δ_{b2} for this pathway. However, as shown below, the acid dissociation constants derived from fitting to equation (8) are in fact macroscopic pK values.

Case 4: Macroscopic Model.

The most general approach to fitting multiphasic titration curves is to consider macroscopic or net ionization constants, which describe the overall behavior of a system. For the titration of the two carboxyl groups, K_A corresponds to the net dissociation of the first proton and K_B to the second. In terms of the previously defined microscopic ionization constants,

$$K_A = (K_1 + K_2) \quad (9a)$$

and

$$(K_B)^{-1} = [(K_3)^{-1} + (K_4)^{-1}] \quad (9b)$$

Clearly $K_A K_B = K_1 K_3 = K_2 K_4$, regardless of whether the groups interact ($\alpha \neq 1$) or not ($\alpha = 1$). If we define state i as that corresponding to a net single deprotonation of the enzyme, then:

$$f_i = (K_1 + K_2)[H^+] / \Sigma = K_A [H+] / \Sigma' \quad (10a)$$

where,

$$\Sigma' = [H^+]^2 + K_A[H^+] + K_A K_B \quad (10b)$$

The pH-dependence of the chemical shifts of sites 1 and 2 are given by the expressions:

$$\delta_1 = \frac{\delta_{a1}10^{-2pH} + \delta_{i1}10^{-(pH+pK_A)} + \delta_{d1}10^{-(pK_A+pK_B)}}{10^{-2pH} + 10^{-(pH+pK_A)} + 10^{-(pK_A+pK_B)}} \quad (11a)$$

$$\delta_2 = \frac{\delta_{a2}10^{-2pH} + \delta_{i2}10^{-(pH+pK_A)} + \delta_{d2}10^{-(pK_A+pK_B)}}{10^{-2pH} + 10^{-(pH+pK_A)} + 10^{-(pK_A+pK_B)}} \quad (11b)$$

Here, δ_{i1} and δ_{i2} correspond to the chemical shifts of the two residues after the first net titration step. With five variables, these equations will accurately describe the titration curve of one ionizable group in the presence of another. In addition to K_A and K_B each being composites of two microscopic dissociation constants, from a comparison to the expanded form of equation (2), we see that δ_{i1} and δ_{i2} are weighted chemical shifts of the two possible singly protonated species, e.g. for site 1 (cf. equation 6):

$$\delta_{i1}\ (K_1+K_2) = \delta_{b1}K_1 + \delta_{c1}K_2 \quad (12)$$

Intuitively, this means that changes in the chemical shift of a carboxyl can depend upon both ionization events, and thus in the most general case, we measure the macroscopic or averaged properties of the system by NMR spectroscopy. As noted above, expressions (11) have the identical form as for the simplified versions of Case 3 (equations 8), which were derived assuming a significant difference in microscopic pK values and hence sequential ionization of one carboxyl before the second (e.g. pK_1 ~ pK_A and pK_2 ~ pK_B). The difference between the two equations is one of physical interpretation, with (11) applying macroscopically to all cases of Scheme 1 and (8) to a selected microscopic example.

The utility of fitting titration curves to macroscopic equilibria can be seen in the easy extension of equations (11) to systems involving more than two ionizable groups. For example, with three carboxyls, one can describe the pH-dependence of the chemical shift of site 1 as:

$$\delta_1 = \frac{\delta_{3,1}10^{-3pH} + \delta_{2,1}10^{-(2pH+pK_A)} + \delta_{1,1}10^{-(pH+pK_A+pK_B)} + \delta_{0,1}10^{-(pK_A+pK_B+pK_C)}}{10^{-3pH} + 10^{-(2pH+pK_A)} + 10^{-(pH+pK_A+pK_B)} + 10^{-(pK_A+pK_B+pK_C)}} \quad (14)$$

where K_A is the sum of the three microscopic K values governing the net dissociation of the first proton, K_c is the inverse of the sum of the inverses of the three microscopic K for net dissociation of the third proton, and $K_A K_B$ is the sum of the products of the first and second dissociation constants for the three pathways leading to net loss of two protons. $\delta_{3,1}$, $\delta_{2,1}$, $\delta_{1,1}$, and $\delta_{0,1}$ are weighted values of the chemical shifts of site 1 in the triple, double, single and zero protonated form of the protein, respectively. Although straightforward in form, the physical interpretation of these macroscopic pK values and chemical shifts in terms of specific or microscopic events can be difficult, except for simple cases such as a single predominant ionization pathway with sequential loss of protons from carboxyls at well separated pH values.

BIBLIOGRAPHY

Albeck, S., Unger, R. and Schreiber, G. (2000). Evaluation of direct and cooperative contributions towards the strength of buried hydrogen bonds and salt bridges. *J Mol Biol* **298**(3), 503-20.

Anderson, D. E., Becktel, W. J. and Dahlquist, F. W. (1990). pH-induced denaturation of proteins: a single salt bridge contributes 3-5 kcal/mol to the free energy of folding of T4 lysozyme. *Biochemistry* **29**(9), 2403-8.

Anderson, D. E., Lu, J., McIntosh, L. P. and Dahlquist, F. W., Eds. (1993). The folding, stability and dynamics of T4 lysozyme: a perspective using nuclear magnetic resonance. Edited by Clore, G. M., Gronenborn, A.M. London: McMillian Press.

Antosiewicz, J., McCammon, J. A. and Gilson, M. K. (1996). The determinants of pK_as in proteins. *Biochemistry* **35**, 7819-7833.

Ash, E. L., Sudmeier, J. L., De Fabo, E. C. and Bachovchin, W. W. (1997). A low-barrier hydrogen bond in the catalytic triad of serine proteases? Theory versus experiment. *Science* **278**, 1128-1132.

Bachovchin, W. W., Kaiser, R., Richards, J. H. and Roberts, J. D. (1981). Catalytic mechanism of serine proteases: reexamination of the pH dependence of the histidyl $^{1}J^{13}C$ 2-H coupling constant in the catalytic triad of α-lytic protease. *Proc Natl Acad Sci USA* **78**, 7323-7326.

Bashford, D. and Karplus, M. (1990). pK_a's of Ionizable Groups in Proteins: Atomic detail from a continuum electrostatic model. *Biochemistry* **29**, 10219-10225.

Batchelor, J. G., Feeney, J. and Roberts, G. C. K. (1975). Carbon-13 NMR Protonation Shifts of Amines, Carboxylic Acids and Amino Acids. *J. Magn. Reson.* **20**, 19-38.

Bernstein, F. C., Koetzle, T. F., Williams, G. J., Meyer, E. E., Jr., Brice, M. D., Rodgers, J. R., Kennard, O., Shimanouchi, T. and Tasumi, M. (1977). The Protein Data Bank: a computer-based archival file for macromolecular structures. *J Mol Biol* **112**(3), 535-42.

Boel, E., Brady, L., Brzozowski, A. M., Derewenda, Z., Dodson, G. G., Jensen, V. J., Peterson, S. B., Swift, H., Thim, L. and Woldike, H. F. (1990). Calcium binding in α-amylases: an X-ray diffraction study at 2.1 Å resolution of two enzymes from *Aspergillus.* *Biochemistry* **29**, 6244-6249.

Brayer, G. D., Luo, Y. and Withers, S. G. (1995). The structure of human pancreatic alpha-amylase at 1.8 Å resolution and comparisons with related enzymes. *Protein Sci* **4**(9), 1730-42.

Brunger, A. T. (1992). *X-PLOR version 3.1: A system for x-ray crystallography and NMR*, Yale University Press, New Haven.

Bundi, A. and Wuthrich, K. (1979). Use of amide ^{1}H-NMR titration shifts for studies of polypeptide conformation. *Biopolymers* **18**(299-311).

Cleland, W. W., Frey, P. A. and Gerlt, J. A. (1998). The low barrier hydrogen bond in enzymatic catalysis. *Journal of Biological Chemistry* **273**(40), 25529-25532.

Cleland, W. W. and Northrop, D. B. (1999). Energetics of substrate binding, catalysis, and product release. *Methods Enzymol* **308**, 3-27.

Collaborative Computational Project Number 4. (1994). The CCP4 suite: programs for protein crystallography. *Acta. Crystallogr.* **D50**, 760-763.

Connelly, G. P. and McIntosh, L. P. (1998). Characterization of a buried neutral histidine in *Bacillus circulans* xylanase: internal dynamics and interaction with a bound water molecule. *Biochemistry* **37**(7), 1810-8.

Connelly, G. P., Withers, S. G. and McIntosh, L. P. (2000). Analysis of the dynamic properties of *Bacillus circulans* xylanase upon formation of a covalent glycosyl-enzyme intermediate. *Protein Sci* **9**, 512-524.

Creighton, T. E. (1993). *Proteins: structures and molecular properties*. 2nd edit, W.H. Freeman and Co., New York.

Dao-pin, S., Sauer, U., Nicholson, H. and Matthews, B. W. (1991). Contributions of engineered surface salt bridges to the stability of T4 lysozyme determined by site-directed mutagenesis. *Biochemistry* **30**, 7142-7153.

Darvill, A., Augur, C., Bergmann, C., Carlson, R. W., Cheong , J. J., Eberhard, S., Hahn, M. G., Lo, V. M., Marfa, V. and Meyer, B. (1992). Oligosaccharins--oligosaccharides that regulate growth, development and defence responses in plants. *Glycobiology* **2**, 181-98.

Davies, G. and Henrissat, B. (1995). Structures and mechanisms of glycosyl hydrolases. *Structure* **3**(9), 853-859.

Davies, G. J., Wilson, K. S. and Henrissat, B. (1997). Nomenclature for sugar-binding subsites in glycosyl hydrolases. *Biochem J* **321**, 557-559.

Davoodi, J., Wakarchuk, W. W., Campbell, R. L., Carey, P. R. and Surewicz, W. K. (1995). Abnormally high pK_a of an active-site glutamic acid residue in *Bacillus circulans* xylanase. The role of electrostatic interactions. *Eur J Biochem* **232**(3), 839-43.

Davoodi, J., Wakarchuk, W. W., Surewicz, W. K. and Carey, P. R. (1998). Scan-rate dependence in protein calorimetry: the reversible transitions of *Bacillus circulans* xylanase and a disulfide-bridge mutant. *Protein Sci* **7**(7), 1538-44.

Edsall, J. T. and Wyman, J. (1958). *Biophysical Chemistry*, Academic Press, New York.

Elcock, A. H. (1999). Realistic modeling of the denatured states of proteins allows accurate calculations of the pH dependence of protein stability. *J Mol Biol* **294**, 1051-1062.

Fersht, A. (1998). *Structure and mechanism in protein science: a guide to enzyme catalysis and protein folding* (Julet, M. R. and Hadler, G. L., Eds.), W.H. Freeman and Company, New York.

Fersht, A. R., Shi, J. P., Knill-Jones, J., Lowe, D. M., Wilkinson, A. J., Blow, D. M., Brick, P., Carter, P., Waye, M. M. and Winter, G. (1985). Hydrogen bonding and biological specificity analysed by protein engineering. *Nature* **314**, 235-238.

Forsyth, W. R., Gilson, M. K., Antosiewicz, J., Jaren, O. R. and Robertson, A. D. (1998). Theoretical and experimental analysis of ionization equilibria in ovomucoid third domain. *Biochemistry* **37**(24), 8643-52.

Fushinobu, S., Ito, K., Konno, M., Wakagi, T. and Matsuzawa, H. (1998). Crystallographic and mutational analyses of an extremely acidophilic and acid-stable xylanase: biased distribution of acidic residues and importance of Asp37 for catalysis at low pH. *Protein Eng* **11**(12), 1121-8.

Gebler, J., Gilkes, N. R., Claeyssens, M., Wilson, D. B., Beguin, P., Wakarchuk, W. W., Kilburn, D. G., Miller, R. C., Jr., Warren, R. A. and Withers, S. G. (1992). Stereoselective hydrolysis catalyzed by related β-1,4-glucanases and β-1,4-xylanases. *J Biol Chem* **267**(18), 12559-61.

Gilkes, N. R., Henrissat, B., Kilburn, D. G., Miller, R. C., Jr. and Warren, R. A. J. (1991). Domains in microbial β-1,4-glycanases: sequence conservation, function, and enzyme families. *Microbiol. Rev.* **55**(303), 303-315.

Gilson, M. K., Rashin, A., Fine, R. and Honig, B. (1985). On the calculation of electrostatic interactions in proteins. *J Mol Biol* **183**, 503-516.

Ginsberg, V. and Robbins, P. W., Eds. (1981). Biology of Carbohydrates. Vol. 1. 3 vols. New York: John Wiley and Sons.

Gruber, K., Klintschar, G., Hayn, M., Schlacher, A., Steiner, W. and Kratky, C. (1998). Thermophilic xylanase from *Thermomyces lanuginosus*: high-resolution X-ray structure and modeling studies. *Biochemistry* **37**(39), 13475-85.

Gu, Z., Zambrano, R. and McDermott, A. (1994). Hydrogen Bonding of Carboxyl Groups in Solid-State Amino Acids and Peptides: Comparision of Carbon Chemical Shielding, Infrared Frequencies, and Structures. *J. Am. Chem. Soc.* **116**, 6368-6372.

Henrissat, B. (1998). Glycosidase families. *Biochemical Society Transactions* **26**, 153-156.

Henrissat, B. and Bairoch, A. (1993). New families in the classification of glycosyl hydrolases based on amino acid sequence similarities. *Biochem. J.* **293**(781), 781-788.

Higgins, D. G. (1994). CLUSTAL V: multiple alignment of DNA and protein sequences. *Methods Mol Biol* **25**, 307-318.

Hiromi, K. (1979). *Kinetics of fast enzyme reactions*, John Wiley and Sons, New York.

Hooft, R. W. W., Sander, C. and Vriend, G. (1996). Positioning hydrogen atoms by optimizing hydrogen-bond networks in protein structures. *Proteins* **26**, 363-376.

Jacobson, R. H., Zhang, X. J., DuBose, R. F. and Matthews, B. W. (1994). Three-dimensional structure of β-galactosidase from *E. coli*. *Nature* **369**, 761-766.

Jeffrey, G. A. and Saenger, W. (1991). *Hydrogen bonding in biological structures*, Springer-Verlag, Berlin.

Johnson, M. L. (1994). Use of least-squares techniques in biochemistry. *Methods in Enzymology* **240**, 1-22.

Jones, T. A., Zhou, J. Y., Cowan, S. W. and Kjeldgaard, M. (1991). Improved methods for building protein molecules in electron density maps and the location of errors in these maps. *Acta. Crystallogr.* **A47**, 110-119.

Joshi, M. D., Hedberg, A. and McIntosh, L. P. (1997). Complete measurement of the pK_a values of the carboxyl and imidazole groups in *Bacillus circulans* xylanase. *Protein Sci* **6**(12), 2667-70.

Joshi, M. D., Nielsen, J. E. and McIntosh, L. P. (2000c). pK_a measurements by NMR revisited: dissecting electrostatic interactions in *Bacillus circulans* xylanase. *In preparation*.

Joshi, M. D., Sidhu, G., Pot, I., Brayer, G. D., Withers, S. G. and McIntosh, L. P. (2000a). Hydrogen bonding and catalysis: a novel explanation for how a single amino acid substitution can change the pH optimum of a glycosidase. *J Mol Biol* **299**(1), 255-279.

Joshi, M. D., Sidhu, G., Wakarchuk, W., Brayer, G. D. and McIntosh, L. P. (2000b). Functional electrostatic interactions throughout a catalytic cycle: ^{13}C-NMR, X-ray crystallographic and Enzymological Characterization of a Glycosidase. *In Preparation*.

Karplus, P. A., Pearson, M. A. and Hausinger, R. P. (1997). 70 Years of Crystalline Urease: What Have We Learned? *Acc. Chem. Res.* **30**, 330-337.

Kirby, A. J. (1997). Efficiency of proton transfer catalysis in models and enzymes. *Acc. Chem. Res.* **30**(7), 290-296.

Klein, C., Hollender, J., Bender, H. and Schulz, G. E. (1992). Catalytic center of cyclodextrin glycosyltransferase derived from X-ray structure analysis combined with site-directed mutagenesis. *Biochemistry* **31**, 8740-8746.

Knegtel, R. M. A., Strokopytov, B., Penninga, D., Faber, O. G., Rozeboom, H. J., Kalk, K. H., Dijkhuizen, L. and Dijkstra, B. W. (1995). Crystallographic studies of the interaction of cyclodextrin glycosyltransferase from *Bacillus circulans* strain 251 with natural substrates and products. *J Biol Chem* **270**(49), 29256-29264.

Koshland, D. E. (1953). Stereochemistry and mechanism of enzymatic reactions. *Biol. Rev.* **28**, 416-436.

Kraulis, P. J. (1991). MOLSCRIPT: a program to produce both detailed and schematic plots of proteinstructures. *J Appl Cryst* **24**, 946-950.

Krengel, U. and Dijkstra, B. W. (1996). Three-dimensional structure of endo-1,4-beta-xylanase I from *Aspergillus niger*: molecular basis for its low pH optimum. *J Mol Biol* **263**(1), 70-8.

Kunkel, T. A., Roberts, J. D. and Zakour, J. (1983). Rapid and efficient site-specific mutagenesis without phenotypic selection. *Methods Enzymol.* **154**, 367-382.

Kuroki, R., Weaver, L. H. and Matthews, B. W. (1995). Structure-based design of a lysozyme with altered catalytic activity. *Nat Struct Biol* **2**, 1007-1011.

Kyte, J. (1994). *Structure in protein chemistry*, Garland Publishing, New York and London.

Ladner, H. K., Led, J. J. and Grant, D. M. (1975). Deuterium isotope effects on ^{13}C chemical shifts in amino acids and dipeptides. *J Magn Reson* **20**, 530-534.

Lawson, S. L., Wakarchuk, W. W. and Withers, S. G. (1996). Effects of both shortening and lengthening the active site nucleophile of *Bacillus circulans* xylanase on catalytic activity. *Biochemistry* **35**(31), 10110-8.

Lawson, S. L., Wakarchuk, W. W. and Withers, S. G. (1997). Positioning the acid/base catalyst in a glycosidase: studies with *Bacillus circulans* xylanase. *Biochemistry* **36**(8), 2257-65.

Leatherbarrow, R. J. (1998). *Gra-Fit, Version 4.0, Erithacus Software Ltd., Staines, U.K.*

Li, M. X., Gagne, S. M., Tsuda, S., Kay, C. M., Smillie, L. B. and Sykes, B. D. (1995). Calcium binding to the regulatory N-domain of skeletal muscle troponin C occurs in a stepwise manner. *Biochemistry* **34**, 8330-8340.

Lin, J., Westler, W. W., Cleland, W. W., Markley, J. L. and Frey, P. A. (1998). Fractionation factors and activation energies for exchange of the low barrier hydrogen bonding proton in peptidyl trifluoromethyl ketone complexes of chymotrypsin. *Proc Natl Acad Sci USA* **95**, 14664-14668.

Linderstorm-Lang, K. (1924). The ionization of proteins. *Compt Rend Trav Lab Carlsberg* **29**, 15--70.

Luzzati, P. V. (1952). Traitment statistique des erreurs dans la determination des structures cristallines. *Acta. Crystallogr.* **A50**, 803-810.

Machius, M., Vertesy, L., Huber, R. and Wiegand, G. (1996). Carbohydrate and protein-based inhibitors of porcine pancreatic α-amylase: structure analysis and comparison of their binding characteristics. *J Mol Biol* **260**, 409-421.

Matthew, J. B. (1985). Electrostatic effects in proteins. *Ann Rev Biophys Biophys Chem* **14**, 387-417.

McCarter, J. D. and Withers, S. G. (1994). Mechanisms of enzymatic glycoside hydrolysis. *Curr Opin Struct Biol* **4**(6), 885-92.

McDaniel, D. H. and Brown, H. C. (1953). Hydrogen bonding as a factor in the ionization of dicarboxylic acids. *Science* **118**, 370-372.

McDonald, I. K. and Thornton, J. M. (1994). Satisfying Hydrogen Bonding Potential in Proteins. *Journal of Molecular Biology* **238**, 777-793.

McGaughey, G. B., Gagne, G. and Rappe, A. K. (1998). π-Stacking interactions. *J Biol Chem* **273**(25), 15458-15463.

McIntosh, L. P., Hand, G., Johnson, P. E., Joshi, M. D., Korner, M., Plesniak, L. A., Ziser, L., Wakarchuk, W. W. and Withers, S. G. (1996). The pK_a of the general acid/base carboxyl group of a glycosidase cycles during catalysis: a ^{13}C-NMR study of *Bacillus circulans* xylanase. *Biochemistry* **35**(31), 9958-66.

Merrit, E. A. and Murphy, M. E. (1994). Raster3D version 2.0: a program for photorealistic molecular graphics. *Acta Cryst* **D50**, 869-873.

Miao, S., Ziser, L., Aebersold, R. and Withers, S. G. (1994). Identification of glutamic acid 78 as the active site nucleophile in *Bacillus subtilis* xylanase using electrospray tandem mass spectrometry. *Biochemistry* **33**(23), 7027-32.

Mikami, B., Hehre, E. J., Sato, M., Katsube, Y., Hirose, M., Morita, Y. and Sacchettini, J. C. (1993). The 2.0-Å resolution structure of soybean beta-amylase complexed with α-cyclodextrin. *Biochemistry* **32**, 6836-6845.

Mock, W. L. and Aksamawati, M. (1994). Binding to thermolysin of phenolate-containing inhibitors necessitates a revised mechanism of catalysis. *Biochem J* **302**, 57-68.

Mock, W. L. and Stanford, D. J. (1996). Arazoformyl dipeptide substrates for thermolysin. confirmation of a reverse protonation catalytic mechanism. *Biochemistry* **35**, 7369-7377.

Muchmore, D. C., McIntosh, L. P., Russell, C. B., Anderson, D. E. and Dahlquist, F. W. (1989). Expression and nitrogen-15 labeling of proteins for proton and nitrogen-15 nuclear magnetic resonance. *Methods Enzymol* **177**, 44-73.

Namchuk, M. N. and Withers, S. G. (1995). Mechanism of Agrobacterium beta-glucosidase: kinetic analysis of the role of noncovalent enzyme/substrate interactions. *Biochemistry* **34**(49), 16194-202.

Nicholls, A., Sharp, K. A. and Honig, B. (1991). Protein folding and association: insights from the interfacial and thermodynamic properties of hydrocarbons. *Proteins* **11**(4), 281-96.

Nielsen, J. E., Beier, L., Otzen, D., Borchert, T. V., Frantzen, H. B., Andersen, K. V. and Svendsen, A. (1999). Electrostatics in the active site of an α-amylase. *Eur J Biochem* **264**, 816-824.

Nielsen, J. E., Borchert, T. V. and Vriend, G. (2000). The determinants of α-amylase pH-activity profiles. *submitted.*

Oda, Y., Yamazaki, T., Nagayama, K., Kanaya, S., Kuroda, Y. and Nakamura, H. (1994). Individual ionization constants of all the carboxyl groups in Ribonuclease HI from *Escherichia coli* determined by NMR. *Biochemistry* **33**, 5275-5284.

Oliveberg, M., Arcus, V. L. and Fersht, A. R. (1995). pK_A values of carboxyl groups in the native and denatured states of barnase: the pK_A values of the denatured state are on average 0.4 units lower than those of model compounds. *Biochemistry* **34**, 9424-9433.

Otwinowski, Z. and Minor, W. (1997). Processing of X-ray diffraction data collected in oscillation mode. *Methods Enzymol* **276**, 307-326.

Pace, C. N., Laurents, D. V. and Thomson, J. A. (1990). pH dependence of the urea and guanidine hydrochloride denaturation of ribonuclease A and ribonuclease T1. *Biochemistry* **29**, 2564--2572.

Plesniak, L. A., Connelly, G. P., Wakarchuk, W. W. and McIntosh, L. P. (1996a). Characterization of a buried neutral histidine residue in *Bacillus circulans* xylanase: NMR assignments, pH titration, and hydrogen exchange. *Protein Sci* **5**(11), 2319-28.

Plesniak, L. A., Wakarchuk, W. W. and McIntosh, L. P. (1996b). Secondary structure and NMR assignments of *Bacillus circulans* xylanase. *Protein Sci* **5**(6), 1118-35.

Pome, J. (1996). Signalling events elicited in plants by defined oligosaccharide structures. *Curr Opin Struct Biol* **6**(5), 671-8.

Prade, R. A. (1996). Xylanases: from biology to biotechnology. *Biotechnol Genet Eng Rev* **13**, 101-31.

Qian, M., Haser, R., Buisson, G., Duee, E. and Payan, F. (1994). The active center of a mammalian α-amylase. Structure of the complex of a pancreatic α-amylase with a carbohydrate inhibitor refined to 2.2 Å resolution. *Biochemistry* **33**, 6284-6294.

Richard, J. P. (1998). The enhancement of enzymatic rate accelerations by Brønsted acid-base catalysis. *Biochemistry* **37**, 4305-4309.

Richarz, R. and Wuthrich, K. (1978). Carbon-13 NMR chemical shifts of the common amino acid residues measured in aqueous solutions of the linear tetrapeptides H-Gly-Gly-X-L-Ala-OH. *Biopolymers* **17**, 2133-2141.

Rudd, P. M., Morgan, B. P., Wormald, M. R., Harvey, D. J., van den Berg, C. W., Davis, S. J., Fergusson, M. A. J. and Dwek, R. A. (1997). The glycosylation of the complement regulatory protein, human erythrocyte CD59. *J Biol Chem* **272**, 7229-7244.

Sabini, E., Sulzenbacher, G., Dauter, M., Dauter, Z., Jorgensen, P. L., Schulein, M., Dupont, C., Davies, G. J. and Wilson, K. S. (1999). Catalysis and specificity in enzymatic glycoside hydrolysis: a $^{2,5}B$ conformation for the glycosyl-enzyme intermediate revealed by the structure of the *Bacillus agaradhaerens* family 11 xylanase. *Chem Biol* 6(7), 483-92.

Schoellman, G. and Shaw, E. (1963). *Biochemistry* 2, 252.

Schueler, O. and Margalit, H. (1995). Conservation of salt bridges in protein families. *J Mol Biol* 248(1), 125-35.

Shan, S. and Herschlag, D. (1996). The change in hydrogen bond strength accompanying charge rearrangement: implications for enzymatic catalysis. *Proc Natl Sci USA* 93, 14474-14479.

Shan, S. O., Loh, S. and Herschlag, D. (1996). The energetics of hydrogen bonds in model systems: implications for enzymatic catalysis. *Science* 272(5258), 97-101.

Sharp, K. A. and Honig, B. (1990). Electrostatic interactions in macromolecules: theory and applications. *Annu Rev Biophys Biophys Chem* 19, 301-32.

Shrager, R. I., Cohen, J. S., Heller, S. R., Sachs, D. H. and Schechter, A. N. (1972). Mathematical models for interacting groups in nuclear magnetic resonance titration curves. *Biochemistry* 11(4), 541-547.

Sidhu, G., Withers, S. G., Nguyen, N. T., McIntosh, L. P., Ziser, L. and Brayer, G. D. (1999). Sugar ring distortion in the glycosyl-enzyme intermediate of a family G/11 xylanase. *Biochemistry* 38(17), 5346-5354.

Sinnott, M. L. (1990). Catalytic mechanisms of enzymic glycosyl transfer. *Chem. Rev.* 90(1171), 1171-1202.

Sridharan, S., Nicholls, A. and Sharp, K. A. (1995). A rapid method for calculating derivatives of solvent accessible surface areas of molecules. *Journal of Computational Chemistry* **16**, 1038-1044.

Stoesz, J. D., Malinowski, D. P. and Redfield, A. G. (1979). Nuclear magnetic resonance study of solvent exchange and nuclear Overhauser effect of the histidine protons of bovine superoxide dismutase. *Biochemistry* **18**(21), 4669-4675.

Strokopytov, B., Penninga, D., Rozeboom, H. J., Kalk, K. H., Dijkhuizen, L. and Dijkstra, B. W. (1995). X-ray structure of cyclodextrin glycosyltransferase complexed with acarbose. Implications for the catalytic mechanism of glycosidases. *Biochemistry* **34**, 2234-2240.

Sung, W. L., Luk, C. K., Zahab, D. M. and Wakarchuk, W. (1993). Overexpression of the *Bacillus subtilis* and *circulans* xylanases in *Escherichia coli*. *Protein Expr Purif* **4**(3), 200-6.

Tanford, C. (1961). *Physical chemistry of macromolecules*, J. Wiley and Sons, New York.

Tishmack, P. A., Bashford, D. A., Harms, E. and Van Etten, R. L. (1997). Use of ^{1}H NMR spectroscopy and computer simulations to analyze histidine pK_a changes in a protein tyrosine phosphatase: experimental and theoretical determination of electrostatic properties in a small protein. *Biochemistry* **36**(11984-11994).

Tissot, A. C., Vuilleumier, S. and Fersht, A. R. (1996). Importance of two buried salt bridges in the stability and folding pathway of barnase. *Biochemistry* **35**(21), 6786-94.

Torronen, A., Harkki, A. and Rouvinen, J. (1994). Three-dimensional structure of endo-1,4-β-xylanase II from *Trichoderma reesei*: two conformational states in the active site. *Embo J* **13**(11), 2493-501.

Torronen, A., Kubicek, C. P. and Henrissat, B. (1993). Amino acid sequence similarities between low molecular weight endo-1,4-β-xylanases and family H cellulases revealed by clustering analysis. *FEBS Lett* **321**(2-3), 135-9.

Torronen, A. and Rouvinen, J. (1995). Structural comparison of two major endo-1,4-xylanases from *Trichoderma reesei*. *Biochemistry* **34**(3), 847-56.

Torronen, A. and Rouvinen, J. (1997). Structural and functional properties of low molecular weight endo-1,4- beta-xylanases. *J Biotechnol* **57**(1-3), 137-49.

Tull, D. and Withers, S. G. (1994). Mechanisms of cellulases and xylanases: a detailed kinetic study of the exo-beta-1,4-glycanase from *Cellulomonas fimi*. *Biochemistry* **33**(20), 6363-70.

Turnbull, J. L., Waldrop, G. L. and Schachman, H. K. (1992). Ionization of amino acid residues involved in the catalytic mechanism of aspartate transcarbamoylase. *Biochemistry* **31**(28), 1285-1294.

van Holde, K. E., Johnson, W. C. and Ho, P. S. (1998). *Principles of physical biochemistry*, Prentice-Hall, New Jersey.

van Vlijmen, H. W., Schaefer, M. and Karplus, M. (1998). Improving the accuracy of protein pKa calculations: conformational averaging versus the average structure. *Proteins* **33**(2), 145-58.

Wakarchuk, W., Methot, N., Lanthier, P., Sung, W., Seligy, V., Yaguchi, M., To, R., Campbell, R. and Rose, D. (1992). The 20 kD xylanase of *Bacillus subtilis*: A structure/function analysis. In *Xylan and xylanases* (Visor, J., *et al.*, ed.), pp. 439-442. Elsevier Science B. V., Amsterdam.

Wakarchuk, W. W., Campbell, R. L., Sung, W. L., Davoodi, J. and Yaguchi, M. (1994a). Mutational and crystallographic analyses of the active site residues of the *Bacillus circulans* xylanase. *Protein Sci* **3**(3), 467-75.

Wakarchuk, W. W., Sung, W. L., Campbell, R. L., Cunningham, A., Watson, D. C. and Yaguchi, M. (1994b). Thermostabilization of the *Bacillus circulans* xylanase by the introduction of disulfide bonds. *Protein Eng* **7**(11), 1379-86.

Wilkins, M. R., Gasteiger, E., Bairoch, A., Sanchez, J. C., Williams, K. L., Appel, R. D. and Hochstrasser, D. F. (1998). Protein Identification and Analysis Tools in the ExPASy Server. In *2-D Proteome Analysis Protocols* (Link, A. J., ed.). Humana Press, New Jersey.

Wishart, D. S., Willard, L. and Sykes, B. D. (1995). VADAR-Volume, area and dihedral angle reporter. University of Alberta, Edmonton.

Yamazaki, T., Nicholson, L. K., Torchia, D. A., Wingfield, P., Stahl, S. J., Kaufman, J. D., Eyermann, C. J., Hodge, C. N., Lam, P. Y. S., Ru, Y., Jadhav, P. K., Chang, C. and Weber, P. C. (1994). NMR and X-ray evidence that the HIV protease catalytic aspartyl groups are protonated in the complex formed by the protease and a non-peptide cyclic urea-based inhibitor. *J Am Chem Soc* **116**, 10791-10792.

Yang, A. and Honig, B. (1993). On the pH dependence of protein stability. *J Mol Biol* **231**, 459-474.

Zechel, D. L., Konermann, L., Withers, S. G. and Douglas, D. J. (1998). Pre-steady state kinetic analysis of an enzymatic reaction monitored by time-resolved electrospray ionization mass spectrometry. *Biochemistry* **37**(21), 7664-9.

Ziser, L., Setyawati, I. and Withers, S. G. (1995). Syntheses and testing of substrates and mechanism-based inactivators for xylanases. *Carbohydr Res* **274**, 137-53.